C of A Report 7805

Cranfield

College of Aeronautics

SOME ASPECTS OF THE FLOW NEAR A SWEPT ATTACHMENT LINE WITH PARTICULAR REFERENCE TO BOUNDARY LAYER TRANSITION.

D I A Poll

August 1978

CoA Report No. 7805

CRANFIELD INSTITUTE OF TECHNOLOGY

COLLEGE OF AERONAUTICS

SOME ASPECTS OF THE FLOW NEAR A SWEPT ATTACHMENT LINE WITH PARTICULAR REFERENCE TO BOUNDARY LAYER TRANSITION

by

D.I.A. POLL, B.Sc.(Eng.) Hons., ACGI

SUMMARY

The general properties of the flow at an infinite swept attachment line have been investigated theoretically and experimentally. By using the concepts of reference temperature and Reynolds analogy it has been possible to produce a simple, semi-empirical calculation technique for skin friction and heat transfer rate which is valid for free stream Mach numbers up to eight both with and without heat transfer to the body surface. A consideration of the predictions made by this method shows that an understanding of the transition phenomenon is particularly important and therefore the response of the incompressible attachment line boundary layer to two-dimensional trip wires and turbulent boundary layers generated on bounding end plates has been investigated experimentally. A sufficiently wide range of parameters has been covered to ensure that the results are typical of full scale flight situations and simple prediction criteria have been derived. By re-evaluating existing data from several different sources it has been possible to extend the validity of some of the principal results to include flight at hypersonic speeds. In addition the mechanism of transition via cross flow instability has been studied experimentally for incompressible flow conditions and prediction criteria which are compatible with advanced boundary layer calculation methods, have been developed with the aid of linear stability theory and results obtained from the re-evaluation of several early experimental investigations. In all cases sample calculations have been performed for typical flight situations and the practical implications of the various predictions have been discussed.

ACKNOWLEDGEMENTS

The author wishes to express his thanks to Professor J.L.Stollery for all his help and encouragement whilst supervising this project, to Dr.L.F.East and Mr.J.H.B.Smith of the Royal Aircraft Establishment for their guidance whilst monitoring the work and to the Procurement Executive of the Ministry of Defence who provided the financial support.

Grateful thanks are also due to Dr.M.R.Head and Dr.N.A.Cumpsty (Cambridge University) who loaned the swept wing model and provided details of their experimental work; to Mr.J.A.Beasley (RAE) who provided a copy of his computer programme for laminar boundary layer calculations; to Dr.M.Gaster (NPL) for several illuminating discussions and also for providing some references; to M.C.Champion and M.V.Rivron (SUPAERO) who wrote the computer programme for the solution of the Orr-Sommerfeld equation; to Mr.K.G.Winter (RAE) and Dr.E.H.Hirschel (DFVLR) who provided useful references; to Mr.S.W.Clark, Mr.D.Sibley, Mr.W.Munn, Mr.J.Baylis, Mr.T.Atkins and Mr.J.Churchill for contributing to the success of the experimental work through their wealth of skill and experience; to Mrs.P.Forrest-Holden who painstakingly typed the manuscript and Mr.M.F.Goodridge who drafted the figures and finally to my wife Elizabeth who has provided the kind of encouragement which makes all things possible.

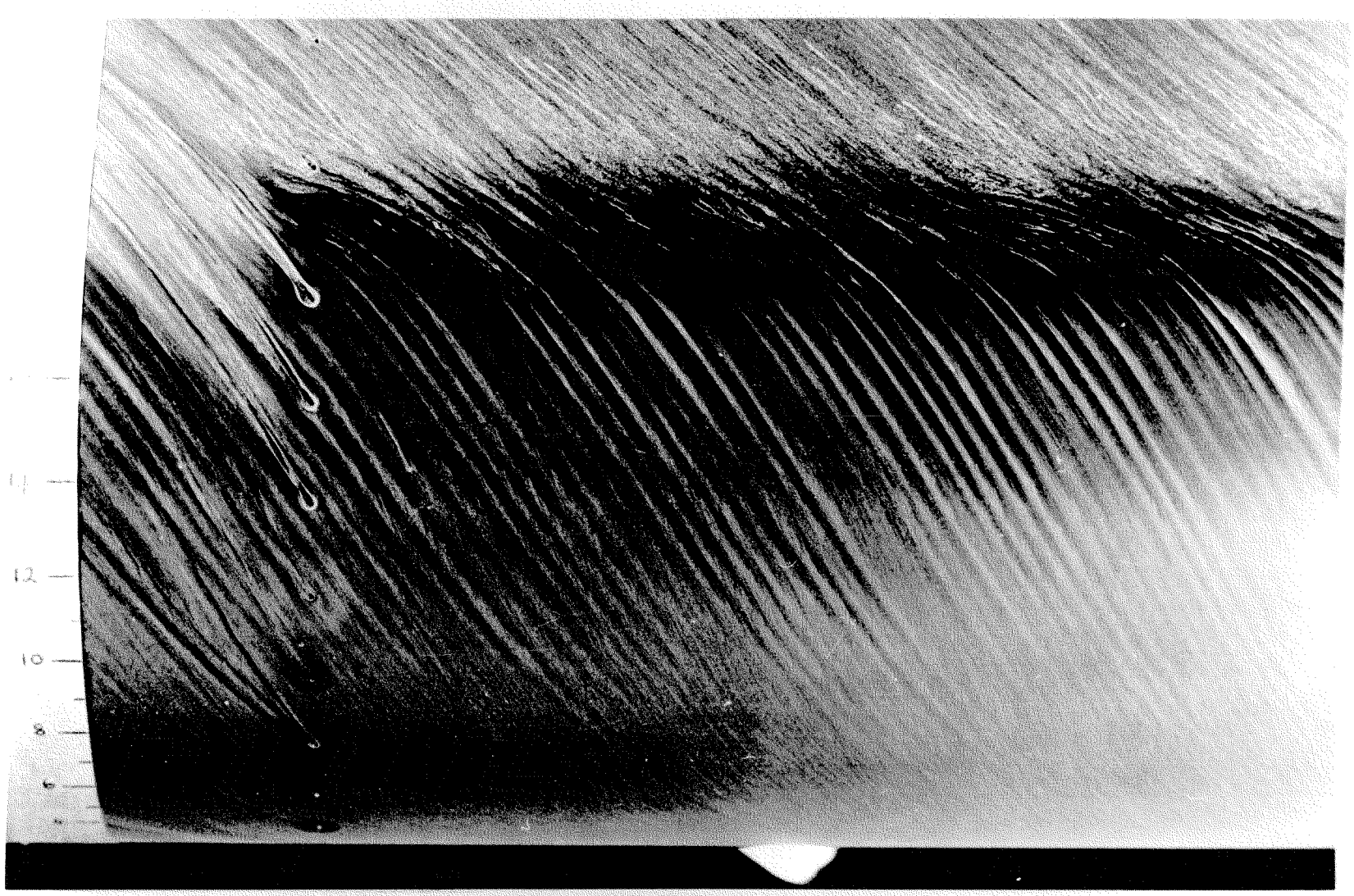

Frontispiece – A surface oil flow pattern showing a transition to turbulence which is produced by a sweep induced instability of the laminar boundary layer.

CONTENTS

FIGURES

NOTATION

A	amplitude
a	radial coordinate for rotating disc
Cf	skin friction coefficient
Cg	group velocity for travelling wave
Co	chord measured normal to leading edge
Cp	pressure coefficient
c	velocity component in the n direction
D	leading edge diameter or pipe diameter
d	trip wire diameter
f	frequency (Hz)
Gr	Grashof number
H	total enthalpy
h	heat transfer coefficient
K	acceleration parameter $(\nu/We)(dWe/d\ell)$
k	thermal conductivity
ℓ	coordinate direction (see figure 62)
M	Mach number
Nu	Nusselt number
n	coordinate normal to the external stream direction
p	pressure
Pr	Prandtl number
Q	Resultant velocity $(U^2 + V^2)^{\frac{1}{2}}$
R	Reynolds number
$\mathcal{R}$	gas constant
r	recovery factor or radius of curvature
S	constant in Sutherlands viscosity/temperature law.
s	distance from trip wire measured along attachment line or velocity in the t direction.
St	Stanton number
t	coordinate aligned with the external stream direction
T	temperature
Tu	turbulence level = $(((U^1)^2 + (V^1)^2 + (W^1)^2)/(3Q^2))^{\frac{1}{2}}$
U	velocity components in inviscid flow in the
V	x, y, z directions.
W	

u	
v	velocity components in boundary layer in x,y,z,directions
w	
U_1	attachment line velocity gradient $\frac{d(Ue/U_\infty)}{d(x/Co)}_{x=0}$
x	
y	orthogonal surface coordinates
z	
α	angle of incidence
α_i	imaginary part of the x component of the complex wavenumber - the x component of the spatial amplification rate.
α_r	real part of the x component of the complex wave number
β_i	imaginary part of the y component of the complex wave number - the y component of the spatial amplification rate
β_r	real part of the y component of the complex wave number
Γ	intermittency factor
γ	ratio of specific heats
$\delta_{.99}$	0.99% boundary layer thickness
δ_1	displacement thickness
δ_2	momentum thickness
ε	angle between the streamwise coordinate t and the alternative coordinate t'
η	boundary layer length scale $(\frac{\nu x}{Ue})^{\frac{1}{2}}$
Θ	wedge semi-angle
θ	streamline inclination to the x axis
Λ	wing sweep angle
λ	disturbance wave length
μ	viscosity
ν	kinematic viscosity
ρ	density or leading edge radius
σ	amplitude function
τ	shear stress
Φ	velocity potential
ϕ	attachment line similarity variable
χ	cross flow Reynolds number
Ψ	stream function
ψ	attachment line length scale or vector direction (see figure 62)
Ω	angular velocity for rotating disc (rads/sec).

ω_i	imaginary part of the complex disturbance frequency - the temporal amplification rate
ω_r	real part of the complex disturbance frequency.

Subscripts

a	at the attachment line
B	according to Beasley definition (ref.70)
c	compressible flow
CT	complete turbulence
e	at the boundary layer edge
ε	coordinate inclined at an angle ε to the t or n direction
FB	first bursts of turbulence
I	quantities refered to that coordinate direction which gives a velocity profile with a stationary inflection point.
i	at the point of first instability
L	laminar flow
o	stagnation conditions
r	recovery conditions
T	at the beginning of transition
w	wall conditions
∞	free stream conditions
*	reference conditions
-	dimensional quantity

Superscripts

1	fluctuating term
-	time averaged value of a fluctuating quantity.
'	differential operator $\frac{d}{d\eta}$

INTRODUCTION

The advent of the jet engine in the mid-1940's meant that typical military flight envelopes were quickly extended to include conditions at which the effects of compressibility were posing serious design problems notably with the shock stall phenomenon. However, it was soon realised that these effects could be delayed by the use of wing sweep back and consequently this became a standard feature in the layout of any high performance aircraft. Early theoretical investigations showed that for laminar boundary layers the flow normal to the leading edge was unaffected by the sweep angle - the so called Independence Principle, and it was argued that transition to turbulence would also remain unaffected by sweep. At that time the small scale wind tunnel tests supported this view and therefore it was believed that in flight there would always be a region of purely laminar flow in the vicinity of the leading edge and that the chordwise location of the transition front could be estimated from two-dimensional results.

However, during flight tests on swept wing aircraft conducted at the R.A.E. between 1951 and 1952 Gray (ref.1 and 2) found that under certain conditions the transition front associated with the wing boundary layer moved forward in a way which could not be explained in terms of two-dimensional experience. Using sublimation techniques he observed that transition could occur at, or very close to, the leading edge if a 'critical' speed was exceeded. This critical speed appeared to be a function of the leading edge radius and the leading edge sweep. In addition, some of the sublimation patterns indicated the presence of streamwise vortices within the laminar part of the boundary layer. It was assumed at the time that these vortices were produced by an instability in the laminar flow. Theoretical investigations conducted by Squire (unpublished),Owen and Randall (refs.3 and 4) and Stuart (ref.5) showed that an instability, the 'cross flow instability' could exist, whilst experiments performed by Anscombe and Illingworth (ref.6) and Gregory and Walker (ref. 5) showed that it did exist. Moreover, the theory gave quantitative results which were in broad agreement with the observations of both flight and wind tunnel experiments.

The problem of transition near the leading edge was considered to be essentially solved until 1963. At this time Handley Page Limited in Great Britain and Northrop Norair in the United States attempted to produce swept wings which would have completely laminar boundary layers in full scale flight conditions. These wings were designed with suction systems which were intended to delay the development of the cross-flow instability. However, during the early test stages it was found that at the design conditions laminar flow was restricted to small regions near the tips. The two groups working independently, discovered that the source of the trouble was turbulence which was propagating from the wing/body junction and travelling along the leading edge producing a turbulent boundary layer on the attachment line and at all chordwise stations. Having found that the attachment line boundary layer was becoming turbulent it was clear that transition could not be explained in terms of a de-stabilised cross flow alone and so a number of wind tunnel investigations were undertaken. Experiments were carried out by Pfenninger at Norair, by Gregory at the National Physical Laboratory and by Gaster at the College of Aeronautics but despite the fact that the contamination mechanism was of obvious practical

significance the work ceased when the respective laminar flow projects were cancelled and the physics of the transition process was never completely investigated.

Recently, however, the increasing use of variable sweep wings for high performance military aircraft and detailed studies for special advanced technology projects such as Space Shuttle and the NASA laminar flow aircraft has highlighted both the importance of the swept wing leading edge region and the general lack of understanding of the underlying physics particularly when the flow is turbulent. At subsonic speeds the boundary layer in the vicinity of the attachment line may influence the stalling characteristics and hence the maximum lift coefficient generated by a wing whilst the design of a successful laminar flow wing depends critically upon an understanding of the various transition mechanisms. The problems are more serious at hypersonic speeds where the heat transfer rates generated at the attachment line are amongst the highest experienced anywhere on the vehicle and consequently an accurate prediction method is vital if adequate thermal protection is to be provided with the minimum of extra weight. In addition to these special cases a more complete understanding of the sweep dependent boundary layer transition mechanisms is an important element in the general problem of the reliable prediction of the behaviour of high performance wings at flight Reynolds numbers and Mach numbers. Modern boundary layer calculation methods have reached a degree of sophistication which is not matched by the currently available transition prediction criteria. The deficiency in the state of the art has been emphasised by the decision to adopt the swept wing problem as the focal point of coordinated effort by the Eurovisc Working Party on Transition in Boundary Layers (see Hirschel - ref.7.)

The present work seeks to investigate the flow in the vicinity of the attachment line and aims to improve the physical understanding of the boundary layer characteristics and transition behaviour. For the attachment line itself emphasis will be placed upon the development, via experiment and theory, of simple prediction techniques for skin friction and heat transfer rate over a wide range of operating conditions together with transition prediction criteria which are compatible with advanced boundary layer calculation methods. In addition the mechanism of cross flow instability will be studied experimentally as well as theoretically and accurate criteria established. Finally, wherever possible the implications of the various prediction methods will be assessed and compared at flight scale.

1. THE ATTACHMENT LINE BOUNDARY LAYER

Figure 1 shows a sketch of the streamline pattern for the flow near the leading edge of a swept cylinder. It is apparent that the flow in this region is highly three-dimensional and that the attachment line boundary layer, which lies along A-A, is strongly influenced by the divergence of the external stream. The large number of independent variables which are present in the completely general case produces a problem of great complexity. However, practical experience with high aspect ratio untapered swept cylinders has shown that in those regions where the external inviscid flow is effectively independent of the spanwise coordinate, y, the boundary layer is also approximately independent of y - (see for example Cumpsty and Head - reference 13). In addition heat transfer measurements made in the vicinity of an unswept attachment line have shown that the free stream turbulence level, Tu, is only important if it is greater than 0.8%*. Therefore by limiting the discussion to situations with low free stream turbulence levels and in which there are no geometrical variations in the spanwise direction i.e. infinite swept cylinder conditions, it is possible to reduce the number of independent variables whilst still retaining a physically realistic problem.

If no spanwise variation occurs the attachment line boundary layer must have constant properties i.e. constant thickness, constant skin friction, etc., and this is achieved by a balance between the fluid which enters the layer from the free stream and that which is removed by the divergence. This may be compared with the boundary layer formed on a flat plate with uniform suction at the wall. At sufficiently large distances from the leading edge, the boundary layer reaches a state in which the growth due to skin friction is just cancelled by the removal of fluid through the surface. Therefore the attachment line boundary layer is more akin to this asymptotic suction layer or fully developed pipe flow than the more conventional flat plate boundary layer. Moreover the fluid which is withdrawn from the attachment line forms part of the developing chordwise boundary layer flow and, consequently if the attachment line is turbulent then the whole cylinder boundary layer will be turbulent unless there is re-laminarisation in the favourable pressure gradient downstream of A-A.

In the present context of infinite swept cylinder conditions and low free stream turbulence level the steady compressible boundary layer flow along the attachment line may be completely specified by the parameters -

$$Me, \quad Pr, \gamma, \quad {}^{T_w}/_{T_e} \text{ and } \phi$$

where ϕ is a Reynolds number based upon Ve, ρe, μe and a characteristic length scale ψ which must depend upon $(dUe/dx)_{x=0}$ (the variable which characterises the flow divergence). Moreover, it is convenient to define ψ in such a way that the numerical values produced are comparable with the boundary layer thickness. Therefore, by analogy to the Blasius length-scale for the flat plate boundary layer, a suitable length may be defined by -

$$\psi = \left(\frac{\nu e}{dUe/dx)_{x=0}} \right)^{\frac{1}{2}} \qquad 1.1$$

* See - A survey of some recent research investigations on boundary layers and heat transfer - H.Schlichting
Journal of Applied Mechanics, June 1971, pp.289-300

Hence

$$\phi = \frac{V_e\psi}{\nu_e} = \left(\frac{Ve^2}{\nu e . dUe/dx)_{x=0}} \right)^{\frac{1}{2}} = (C^*)^{\frac{1}{2}} \qquad 1.2$$

where C* is the similarity parameter first introduced by Cumpsty and Head (ref.8). When the problem is extended to include the response of the boundary layer to the presence of two-dimensional trip wires then two more independent variables are introduced. These are the trip wire diameter, d and the separation, s, between the trip and the turbulence detector. This means that the number of non-dimensional parameters is increased to seven by the addition of

$$d/\psi \quad \text{and} \quad s/\psi$$

Although the choice of these non-dimensional groups is essentially arbitrary the above have been adopted since the boundary layer has constant thickness. Consequently, they have an immediate and unambiguous physical significance which is not apparent in those groups which are more commonly used in connection with flat plate studies i.e. (Ved/νe) and (VeS/νe). However, it should be noted that these groups are readily available since

$$\frac{V_e d}{\nu_e} = \phi . \frac{d}{\psi} \quad \text{and} \quad \frac{V_e s}{\nu_e} = \phi . \frac{s}{\psi}$$

For incompressible flow there is an exact solution for the attachment line laminar boundary layer equations and the velocity profile is tabulated in most standard boundary layer texts e.g. Rosenhead (ref 9). Figure 2 shows the attachment line velocity profile in comparison with the Blasius flat plate and the flat plate asymptotic suction profiles (all taken from reference 9). From the tabulated data it is possible to calculate the various boundary layer characteristic lengths in terms of ψ -

$$\begin{aligned} \delta_{.99} &= 3.055 \ \psi \\ \delta_1 &= 1.026 \ \psi \\ \delta_2 &= 0.404 \ \psi \end{aligned} \qquad 1.3$$

In previous experimental investigations by Gregory (ref.10), Gaster (ref.11) and Pfenninger (ref.12) the characteristic Reynolds number has been taken to be the incompressible laminar momentum thickness Reynolds number $R_{\delta_{2_L}}$. For the purpose of comparison it can be seen from equations 1.1, 1.2 and 1.3 that

$$R_{\delta_{2_L}} = \frac{Ve\delta_2}{\nu} = 0.404 \frac{Ve\psi}{\nu} = 0.404 \ \phi \qquad 1.4$$

Clearly ϕ and C* are equally suitable for the characteristic Reynolds number and both are to be prefered to $R_{\delta_{2_L}}$ which loses its physical significance in turbulent flow. However in the present work C* has been rejected since the associated length scale $(Ve/(dU_e/dx)_{x=0})$ is not representative of the boundary layer thickness.

Since the present experiments were conducted at low speed (Q_∞ < 200 ft/sec) the list of parameters necessary for the complete specification of the problem is reduced to three - namely ϕ, d/ψ and s/ψ. In a general flow the properties of the boundary layer would be expected to be functions of all three parameters, for example in the case of the flat plate boundary layer the measured momentum thickness at a distance x from the leading edge and s from a trip wire, diameter d, would be a function of the parameters

$$\frac{xU_\infty}{\nu}\ ,\quad {}^{d}/_{(\frac{x\nu}{U_\infty})^{\frac{1}{2}}}\quad \text{and}\quad {}^{s}/_{(\frac{x\nu}{U_\infty})^{\frac{1}{2}}}$$

since the drag of the wire increases the momentum defect in the layer. However, at the attachment line, fluid particles which are disturbed by the roughness elements do not travel along the leading edge but are rapidly carried away in the developing chordwise flow. Figure 3 presents a series of photographs which illustrate the effect of a trip wire on the leading edge of a swept wing. In photograph (a) there is no trip wire attached, the wing was swept at 63° and the wind speed was 90 ft/sec. Flow visualisation fluid was applied near the leading edge only and this has flowed back along the chord until a line of laminar separation is reached. In addition the pattern contains the streak lines which are characteristic of the mechanism of cross flow instability see section (6.1) although this is not causing transition at this Reynolds number. Photograph (b) shows the same arrangement except that a trip wire of diameter 0.0135" has been placed across the attachment line ($\pm\frac{1}{4}$" either side) and the wind speed has been reduced to 80 ft/sec. The line of laminar separation is still distinct although it has been broken by a turbulent wedge which originates at the trip. In photograph (c) the wind speed has been raised to 90 ft/sec and it can be seen that downstream of the trip the flow is completely turbulent from the attachment line since the laminar separation line and the streak pattern have disappeared.

Both Cumpsty and Head (ref.13) and Gaster (ref.11) present measurements which show that for both laminar and turbulent flows the diameter of a distant upstream trip wire has no effect upon the velocity profiles (as would be expected forinfinite swept conditions). In addition, Gaster gives velocity contours for the flow in the vicinity of a very large trip wire ($d/\delta_{.99} \simeq 7$) for conditions which are not sufficient for transition to turbulence and these show that the laminar boundary layer recovers its infinite swept form about 70 boundary layer thicknesses downstream of the trip. It may be concluded that except in regions close to the trip the boundary layer properties are functions of ϕ alone. By way of an example figure 4 presents the variation of incompressible momentum thickness Reynolds number with the similarity parameter ϕ for laminar (equation 1.4) and turbulent flow (Cumpsty and Head (ref.13)).

2. A SIMPLE CALCULATION METHOD FOR THE SKIN FRICTION AND HEAT TRANSFER RATE AT THE ATTACHMENT LINE.

2.1 The Reference Temperature Method

In the past many simple and successful methods for the prediction of skin friction and heat transfer have been based upon the reference temperature concept (see Eckert ref.14). Simply stated, the idea suggests that the incompressible relationship between skin friction coefficient and Reynolds number is valid for compressible flow provided that the temperature dependent flow properties are evaluated at some intermediate or average temperature within the boundary layer, i.e.

$$\tau_c = \frac{1}{2}\cdot\rho_* \cdot Ve^2 . A . \frac{1}{(\phi_*)^B}$$

or

$$Cf_* = \frac{A}{(\phi_*)^B} \qquad 2.1.1$$

where A and B are determined for incompressible flow. When equation (2.1.1) is used in conjunction with an equation of state e.g.

$$p = \rho \mathcal{R} T \qquad 2.1.2$$

and a viscosity law of the form

$$\mu = f_3(T) \qquad 2.1.3$$

where the function, f_3, is chosen according to the gas and temperature range under consideration, then a skin friction coefficient may be expressed in a form which is a function of ϕ and temperature alone -

$$Cf_e = \frac{\tau_c}{\frac{1}{2}\rho_e V_e^2} = A.\left(\frac{Te}{T_*}\right)^{(2-B)/2} . \left(\frac{f_3(T_*)}{f_3(Te)}\right)^{B/2} . \frac{1}{(\phi)^B} \qquad 2.1.4$$

In common with previous investigations (see refs.14,15,16 and 17) the reference temperature T_* will be assumed to be of the form

$$T_* = Te + K1(Tw - Te) + K2(Tr - Te)$$

or

$$\frac{T_*}{Te} = 1 + K1\left(\frac{Tw}{Te} - 1\right) + K2.r.\left(\frac{\gamma-1}{2}\right).Me^2 \qquad 2.1.5$$

where K1 and K2 are constants determined by comparison with experimental data and/or accurate calculation methods.

2.2 Reynolds Analogy

A detailed study of the equations governing the laminar attachment line flow reveals that for a Prandtl number of unity the spanwise momentum equation (governing Cf_e) and the energy equation (governing Ste) are of the same form and, hence, the velocity (v/Ve) and total enthalpy $\left(\frac{H - H_w}{H_e - H_w}\right)$ profiles are geometrically similar. It follows that there is a simple relationship between skin friction coefficient and Stanton number i.e.

$$St_e = \frac{Cf_e}{2}$$

Experience with boundary layers formed on flat plates and cones (see refs 14 and 18) has shown that small variations in the Prandtl number may be accounted for by introducing the following correction to the simple analogy -

$$St_e \simeq Pr^{-2/3} \cdot \frac{Cf_e}{2} \qquad 2.2.1$$

In the present context equation (2.2.1) is assumed to hold for both laminar and turbulent flows.

2.3 Laminar Flow

Skin Friction

Comprehensive results for the exact solution of the equations for the compressible laminar boundary layer on an infinite swept cylinder are tabulated by Beckwith (ref.19) where the spanwise shear stress is given by -

$$\tau_w = \mu_w \cdot \left(\frac{\partial v}{\partial z}\right)_w = \mu_w . V_\infty . g_w' . (\zeta)^{\frac{1}{2}}$$

where $g_w' = f_4(Me, {}^{Tw}/_{Te}, Pr, \gamma)$

$$\zeta = \frac{{}^{Te}/_{To}}{{}^{Te}/_{To} - \left(\frac{\gamma-1}{2}\right)\left(\frac{Ue}{a_o}\right)^2} \cdot \frac{1}{\nu_w} \cdot \frac{dUe}{dx} \qquad 2.3.1$$

Cp = constant

Pr = constant

At the attachment line x = 0 and Ue = 0 therefore

$$Cf_e = 2g_w' \cdot \left(\frac{\mu_w \rho_w}{\mu_e \rho_e}\right)^{\frac{1}{2}} \cdot (\phi)^{-1} \qquad 2.3.2$$

which in conjunction with equations (2.1.2) and (2.1.3) becomes

$$Cf_e = 2g_w' \cdot \left(\frac{f_3(Tw)}{f_3(Te)} \cdot \frac{Te}{Tw}\right)^{\frac{1}{2}} \cdot (\phi)^{-1} \qquad 2.3.3.$$

For the case of incompressible flow with no heat transfer equation (2.3.3.) reduces to the familiar result

$$Cf_e = \frac{1.141}{\phi} \qquad 2.3.4$$

see Rosenhead (ref.9). Therefore the form of the reference temperature equation for skin friction (see equation (2.1.4)) is -

$$Cf_e = 1.141 \left(\frac{Te}{T*}\right)^{\frac{1}{2}} \left(\frac{f_3(T*)}{f_3(Te)}\right)^{\frac{1}{2}} \frac{1}{\phi} \qquad 2.3.5$$

The combination of equations (2.3.3) and (2.3.5) produces an implicit expression for T_* -

$$\frac{T*}{Tw} \cdot \frac{f\,(Tw)}{f\,(T*)} = \left(\frac{1.141}{2g_w'}\right)^2 \qquad 2.3.6$$

which may be solved directly for some of the results presented in reference 19. The values of T_* calculated in this way show that a good correlation may be obtained if the reference temperature is taken to be the temperature at the edge of the boundary layer, Te, i.e. K1 and K2 of equation (2.1.5) are set to zero. Figure 5 shows the area covered by the exact solution for sweep angles in the range 0 to 70^o and free stream static temperatures greater than 50^oK. It can be seen that, subject to these limitations, the adoption of Te as the reference temperature produces an approximation to Cfe where deviation from the exact value always lies between +7% and -14%.

Heat Transfer Rate

Having obtained expression for skin friction the heat transfer rate may be obtained directly from equation (2.2.1).

$$St_e = \frac{\dot{q}_w}{Cp.\rho_e.V_e(Tr - Tw)} = \frac{h}{Cp.\rho_e.V_e} = Pr^{-2/3}.\frac{Cfe}{2}$$

$$\text{i.e.} \quad St_e = \frac{1.141}{2.Pr^{2/3}.\phi} \qquad 2.3.7$$

Measured heat transfer rates taken from references 20, 21, 22, 23, 24 and 28 and plotted in figure 6 show that the predictions made by equation (2.3.7) are in good agreement with the available experimental data.

In order to compare the results of equation (2.3.7) with the exact solutions of reference 19 it is necessary to introduce alternative non-dimensional groups -

$$Nu_x = \frac{hx}{k_w} \quad , \quad R_x = \frac{Ue.\,x}{\nu_w} \qquad 2.3.8.$$

and $$Nu_{D_\infty} = \frac{hD}{k_\infty} \quad , \quad R_{D_\infty} = \frac{Q_\infty D}{\nu_\infty} \qquad 2.3.9$$

Taking equations (2.3.8) first -

In a region close to the attachment line

$$Ue = \left(\frac{dUe}{dx}\right)_{x=0} \cdot x$$

from which it follows that

$$\frac{Nux}{(Rx)^{\frac{1}{2}}} = \frac{h}{k_w}\left(\frac{\nu_w}{dUe/dx)x=0}\right)^{\frac{1}{2}}$$

$$= St_e \cdot Pr \cdot \left(\frac{\mu_e \cdot \rho_e}{\mu_w \cdot \rho_w}\right)^{\frac{1}{2}} \cdot \phi$$

combining this with equation (2.3.7) yields

$$\frac{Nux}{(Rx)^{\frac{1}{2}}} = \frac{1.141}{2} \cdot Pr^{1/3} \cdot \left(\frac{\mu_e \cdot \rho_e}{\mu_w \cdot \rho_w}\right)^{\frac{1}{2}}$$

which for a Prandtl number of 0.7 becomes

$$\frac{Nux}{(Rx)^{\frac{1}{2}}} = 0.507 \left(\frac{\mu_e \cdot \rho_e}{\mu_w \cdot \rho_w}\right)^{\frac{1}{2}} \qquad 2.3.10$$

A comparison between equation (2.3.10) and the exact solutions from reference 19 is presented in figure 7. It can be seen that there is good agreement for the range of parameters considered and there is only a small difference between the present result and the correlating function suggested by the author of reference 19 which is

$$\frac{Nux}{(Rx)^{\frac{1}{2}}} \simeq 0.5 \left(\frac{\mu_e \rho_e}{\mu_w \rho_w}\right)^{0.44} \qquad Pr = 0.7$$

Using the definitions contained in equation (2.3.9), equation (2.3.10) becomes

$$\frac{Nu_{D_\infty}}{R_{D_\infty}^{\frac{1}{2}}} \simeq 0.507 \left(\cos \Lambda \cdot \frac{D}{U_\infty} \cdot \frac{dUe}{dx}\right)_{x=0}^{\frac{1}{2}} \left(\frac{\rho e \mu e}{\rho_\infty \mu_\infty}\right)^{\frac{1}{2}} \qquad 2.3.11$$

where the corresponding equation from reference 20 is

$$\frac{Nu_{D_\infty}}{R_{D_\infty}^{\frac{1}{2}}} \simeq 0.5 \left(\cos \Lambda \cdot \frac{D}{U_\infty} \cdot \frac{dUe}{dx}\right)_{x=0}^{\frac{1}{2}} \left(\frac{\rho_e \mu_e}{\rho_\infty \mu_\infty}\right)^{\frac{1}{2}}$$

For the laminar flow case the approximate expressions produced by the present method and that due to Beckwith and Gallagher are virtually indistinguishable.

2.4 Turbulent Flow

In the case of turbulent flow at the attachment line there is no 'exact' solution available for the prediction of the boundary layer properties. Several detailed calculation methods have been produced (refs. 8,20,21 and 25), but each contains some empirical function which is based upon flat plate or two-dimensional boundary layer behaviour and no published method has been compared with all the existing experimental data. For this reason the universal validity of these methods is in some doubt. The present approach to the problem differs in so far as the various free constants are determined by correlation with attachment line boundary layer experimental data only.

Skin Friction

The only experimental measurements of skin friction are those presented by Cumpsty and Head (ref.13) whose studies were limited to incompressible flow. In order to augment these data attachment line skin friction was measured on the same model (described in detail in section 5.2) but covering a wider range of ϕ than the original work. - ϕ_{max} in the present case being 775. The results of extensive boundary layer profile measurements described in reference 13 show that the fully turbulent attachment line flow obeys the 'universal' two-dimensional law of the wall and, hence, it is possible to determine skin friction by the Preston tube technique.

In the present context two tubes of different diameters (0.032 ins and 0.020 ins) were used and the results deduced via the method of Head and Vasanta Ram (ref.26). The use of two tubes provides a means of detecting those flow conditions which do not obey the law of the wall since in such a case each would produce different values of Cf for the same value of ϕ. Figure 8 shows the measured variation of Cf with ϕ together with the results of reference 13 and it can be seen that over the range considered ϕ is an adequate parameter for correlating the effects of tunnel speed and sweep angle. Moreover the variation may be well represented by a power law of the form -

$$Cf = \frac{0.0592}{\phi^{0.4}} \qquad 2.4.1$$

Where the values of the constants have been determined by a 'least squares' fit (product moment correlation coefficient = 0.983, R.M.S.error 1.3%, maximum error 3.5%). Also included in this figure is the corresponding incompressible variation derived from the theory of Beckwith and Gallagher (ref.20) i.e.

$$Cf = \frac{0.0646}{\phi^{0.4}}$$

where the constants were deduced on the basis of simple power law forms for the chordwise and spanwise velocity profiles and the Blasius flat plat skin friction law -

$$Cf = \frac{0.0228}{R_\delta^{0.25}}$$

Over the range of ϕ for which experimental data are available the Beckwith and Gallagher method overestimates the incompressible skin friction coefficient by approximately 9.1%.

Heat Transfer

Since the data discussed in the previous section can only fix the constants A and B in the incompressible skin friction relation (equation (2.1.1)) the constants K1 and K2 in the reference temperature equation (equation (2.1.5)) must be determined by the compressible heat transfer results via the Reynolds analogy of equation (2.2.1).

References 20, 21, 23, 24, 27 and 28 yield 87 data points for the heat transfer rate at a swept attachment line for free stream Mach numbers in the range 2.4 to 8 and wall to stagnation temperature ratios lying between 0.3 and 1.0. In all cases the data are presented in terms of a Nusselt number, Nu_∞, based upon leading edge diameter and free stream conditions. From equations (2.1.4), (2.2.1) and (2.4.1) it follows that

$$St_e = \frac{0.0592}{2.Pr^{2/3}} \cdot \left(\frac{Te}{T*}\right)^{0.8} \cdot \left(\frac{\mu_*}{\mu_e}\right)^{0.2} \cdot \frac{1}{\phi^{0.4}} \qquad 2.4.2$$

moreover if

$$h = \frac{\dot{q}_w}{(Tr-Tw)} = (St.\rho.V.Cp)_e = \frac{Nu_\infty.k_\infty}{D} \text{ and } Pr = \frac{\mu Cp}{k}$$

i.e. $$St_e = \frac{Nu_\infty.\ k_\infty}{\rho_e.V_e.Cp_e.D}$$

and since for the semi-infinite case

$$Ve = Q_\infty.\sin\Lambda$$

then

$$St_e = \frac{Nu_\infty}{R_{D_\infty}} \cdot \frac{\rho_\infty}{\rho_e} \cdot \frac{k_\infty}{k_e} \cdot \frac{\mu_e}{\mu_\infty} \frac{1}{\sin \Lambda . Pr} \qquad 2.4.3.$$

and $$\phi = \left(\frac{Ve^2}{\nu_e \, dUe/dx)x=0} \right)^{\frac{1}{2}} = \left(R_{D_\infty} \frac{\sin \Lambda \tan \Lambda}{\frac{D}{U_\infty} \, dUe/dx)x=0} \cdot \frac{\mu_\infty}{\mu_e} \cdot \frac{\rho_e}{\rho_\infty} \right)^{\frac{1}{2}} \qquad 2.4.4$$

For the purposes of calculation it was assumed that the viscosity/temperature relationship for air is given by the improved 'Sutherland' type formula proposed by Keyes (ref.29) i.e.

$$\mu = \left(\frac{1.488 \times T^{3/2}}{T + 122.1 \times 10^{-5/T}} \right) \times 10^{-6} \quad \frac{kg}{m.sec} \qquad 2.4.5.$$

where T must be given in Kelvins, and that Pr, γ and r had constant values of 0.72, 1.4 and 0.896 respectively. As a first step the data were transformed into values of St_e and ϕ by the use of equations (2.4.3) and (2.4.4.). The 87 results were then compared with the predictions of equation (2.4.2.) for given values of K1 and K2 and the R.M.S. error was determined. By using a criterion of minimum R.M.S.error it was found that the best values for K1 and K2 are

$$K1 = 0.20$$

and $$K2 = 0.40 \qquad 2.4.6.$$

These values gave an R.M.S.error of 6.9% with a maximum error of 18.4% which may be compared with an R.M.S. error of 8% and a maximum error of 20.6% for the Beckwith and Gallagher method (ref.20) i.e. $T* = Te$, for the same 87 data points. Figure 9 shows the comparison between predicted and measured Stanton numbers.

3. EFFECT OF SWEEP ANGLE

The simple formulae developed in sections 2.3 and 2.4 enable the attachment line skin friction and heat transfer rates to be calculated over a wide range of flight conditions. However, whilst cast in terms of local flow parameters, they conceal some interesting and important features which are only revealed when the coefficients are based upon free stream conditions. For the sake of simplicity the investigation into the effect of sweep angle will be restricted to the limiting cases of zero and infinitely large free stream Mach number.

3.1 Laminar Flow

Skin Friction

In section 2.3 it was shown that -

$$Cf_e = \frac{1.141}{\phi}$$

if the skin friction coefficient is based upon undisturbed flow conditions then

$$\frac{\tau}{\frac{1}{2}\rho_\infty Q_\infty^2} = Cf_\infty = 1.141\ (\sin\Lambda.\cos^{\frac{1}{2}}\Lambda)\ \left(\frac{U_1}{R_{D_\infty}}.\frac{D}{C_0}\right)^{\frac{1}{2}}\left(\frac{\rho e}{\rho_\infty}.\frac{\mu e}{\mu_\infty}\right)^{\frac{1}{2}} \qquad 3.1.1$$

In the case of incompressible flow (see Appendix A) -

a) $M_\infty \to 0$

b) $\left(\frac{D}{C_0}\cdot U_1\right) \to$ a constant value (See section 6.6) 3.1.2

c) $\left(\frac{\rho_e}{\rho_\infty}.\frac{\mu_e}{\mu_\infty}\right) \to 1.0$

equation (3.1.1) then becomes

$$Cf_\infty = 1.141\ (\sin\Lambda.\cos^{\frac{1}{2}}\Lambda)\ \left(\frac{U_1}{R_{D_\infty}}.\frac{D}{C_0}\right)^{\frac{1}{2}} \qquad 3.1.3$$

Simple differentiation with respect to Λ reveals that the $Cf \propto \Lambda$ relation exhibits a maximum i.e.

$$Cf_\infty)_{max} = 0.708\ \left(\frac{U_1}{R_{D_\infty}}.\frac{D}{C_0}\right)^{\frac{1}{2}}$$

when $\tan\Lambda = \sqrt{2}$ 3.1.4

or $\Lambda = 54.74^0$

In the case of hypersonic flow of a perfect gas (see Appendix A) -

a) $M_\infty \rightarrow \infty$

b) $(U_1 \cdot \frac{D}{C_0}) \rightarrow 2(\frac{\gamma-1}{\gamma})^{\frac{1}{2}} = 1.07$ for air

c) $\frac{\rho_e}{\rho_\infty} \rightarrow (\frac{\gamma+1}{2})^{(\frac{\gamma+1}{\gamma-1})} \cdot (\frac{1}{\gamma})^{(\frac{1}{\gamma-1})} \frac{2}{(\gamma-1)} \simeq 6.44$ for air 3.1.5

d) if, for algebraic simplicity, $\frac{\mu_e}{\mu_\infty}$ is assumed to be given by Sutherlands law rather than by equation (2.4.5)

$$\frac{\mu_e}{\mu_\infty} \rightarrow (\frac{Te}{T_\infty})^{\frac{1}{2}} \cdot (1 + \frac{S}{T_\infty}) \quad \text{for air } S \simeq 110^0K$$

$$= (\frac{\gamma-1}{2})^{\frac{1}{2}} \cdot M_\infty \cos\Lambda (1+\frac{S}{T_\infty})$$

Where it has been assumed that the resulting bow shock is parallel to the body surface in the vicinity of the attachment line. Applying the results of (3.1.5) to equation (3.1.1) yields

$$Cf_\infty)_{M_\infty \rightarrow \infty} \rightarrow 1.141 \ (\sin\Lambda\cos\Lambda) \left(\frac{2(\frac{\gamma-1}{\gamma})^{\frac{1}{2}}}{R_{D_\infty}} \right) \left((\frac{\gamma+1}{2})^{(\frac{\gamma+1}{\gamma-1})} (\frac{1}{\gamma})^{(\frac{1}{\gamma-1})} (\frac{2}{\gamma-1})^{\frac{1}{2}} \cdot M_\infty (1+ \frac{S}{T_\infty}) \right)^{\frac{1}{2}}$$

which for air becomes

$$Cf_\infty \simeq 2.002 \ (\sin\Lambda\cos\Lambda) \left(\frac{M_\infty}{R_{D_\infty}} \cdot (1 + \frac{110}{T_\infty}) \right)^{\frac{1}{2}} \qquad 3.1.6$$

Once again the variation of Cf_∞ against Λ exhibits a maximum

i.e. $$Cf_\infty)_{max} = 1.001 \left(\frac{M_\infty}{R_{D_\infty}} \cdot (1 + \frac{110}{T_\infty}) \right)^{\frac{1}{2}}$$

when $\tan\Lambda = 1.0$ 3.1.7

or $\Lambda = 45.00^0$

Thus this section shows that for laminar flow the variation of Cf_∞ with Λ exhibits a maximum and that the effect of increasing free stream Mach number is to reduce the angle of sweep at which this maximum occurs from 55^0 for subsonic flow to 45^0 for hypersonic flow. In addition it has been found that for hypersonic flow conditions the skin friction coefficient is proportional to the square root of the free stream Mach number.

Heat Transfer.

Using the definitions of free stream Reynolds number and Nusselt number given in equation (2.3.9) it has been already shown in equation (2.3.11) that the laminar heat transfer rate is given by -

$$Nu_{D_\infty} = \frac{hD}{k_\infty} = 0.5705.Pr^{1/3}.(\cos\Lambda)^{\frac{1}{2}}\left(U_1\frac{D}{C_o}R_{D_\infty}\right)^{\frac{1}{2}}\left(\frac{\rho_e\mu_e}{\rho_\infty\mu_\infty}\right)^{\frac{1}{2}}$$

In the case of incompressible flow where the simplification of equations (3.1.2) are valid the above expression becomes -

$$Nu_{D_\infty} = 0.5705.Pr^{1/3}.\left(U_1\frac{D}{C_o}.R_{D_\infty}\right)^{\frac{1}{2}}(\cos\Lambda)^{\frac{1}{2}} \qquad 3.1.8$$

Clearly the maximum value of heat transfer rate occurs at zero sweep i.e.

$$Nu_{D_\infty})_{max} = 0.5705.Pr^{1/3}.\left(U_1\frac{D}{C_o}.R_{D_\infty}\right)^{\frac{1}{2}} \qquad 3.1.9$$

Equation (3.1.9) may be compared directly with H.B.Squire's two-dimensional incompressible result for heat transfer from a cylinder near the forward stagnation point (ref.30, pages 631-632) which is -

$$Nu_{D_\infty} \simeq 0.570.Pr^{0.4}.\left(U_1\frac{D}{C_o}.R_{D_\infty}\right)^{\frac{1}{2}}$$

It is apparent that for Prandtl numbers in the range 0.6 to 1.0 the two results are in very good agreement.

Taking the hypersonic flow case with the results of equations (3.1.5) equation (2.3.11) may be re-written

$$Nu_{D_\infty} = 0.5705.Pr^{1/3}.\left(2\left(\frac{\gamma-1}{\gamma}\right)^{\frac{1}{2}}.R_{D_\infty}\right)^{\frac{1}{2}}\left(\left(\frac{\gamma+1}{2}\right)^{\left(\frac{\gamma+1}{\gamma-1}\right)}\cdot\left(\frac{1}{\gamma}\right)^{\left(\frac{1}{\gamma-1}\right)}\cdot\left(\frac{2}{\gamma-1}\right)^{\frac{1}{2}}.M_\infty\left(1+\frac{S}{T_\infty}\right)^{\frac{1}{2}}(\cos\Lambda) \qquad 3.1.10$$

Once again the maximum value of heat transfer rate occurs at zero sweep and is given by -

$$Nu_{D_\infty})_{max} = 0.5705.Pr^{1/3}.\left(2\left(\frac{\gamma-1}{\gamma}\right)^{\frac{1}{2}}.R_{D_\infty}\right)^{\frac{1}{2}}\left(\left(\frac{\gamma+1}{2}\right)^{\left(\frac{\gamma+1}{\gamma-1}\right)}\cdot\left(\frac{1}{\gamma}\right)^{\left(\frac{1}{\gamma-1}\right)}\cdot\left(\frac{2}{\gamma-1}\right)^{\frac{1}{2}}.M_\infty\left(1+\frac{S}{T_\infty}\right)^{\frac{1}{2}} \qquad 3.1.11$$

which for air becomes

$$Nu_{D_\infty})_{max} \simeq 0.897 \left(R_{D_\infty} . M_\infty (1 + \frac{110}{T_\infty}) \right)^{\frac{1}{2}} \qquad 3.1.12$$

Hence for the case of a swept attachment line supporting a laminar boundary layer it has been shown that the maximum heat transfer rate occurs at the zero sweep configuration. In these extreme cases the variation of heat transfer rate with sweep angle may be expressed in the simple form -

$$Nu_{D_\infty} = Nu_{D_\infty\ max} . (\cos\Lambda)^N$$

where N tends to 0.5 in the limit as Mach number tends to zero and 1.0 is the limit as Mach number tends to infinity. Once again the Mach number is seen to exert a powerful influence upon the attachment line condition since Nu_{D_∞} increases as the square root of the Mach number for hypersonic flow.

3.2 Turbulent Flow

Skin Friction

From equation (2.4.1) the skin friction coefficient for turbulent flow may be expressed as

$$Cf_e = 0.0592 \left(\frac{Te}{T_*}\right)^{0.8} \left(\frac{\mu_*}{\mu_e}\right)^{0.2} \left(\frac{\mu_e}{\rho_e} . \frac{U_1}{V_e^2} . \frac{D}{C_o} . \frac{U_\infty}{D}\right)^{0.2}$$

which after some algebraic manipulation may be re-written as

$$Cf_\infty = 0.0592 . \left(\frac{\rho_e}{\rho_\infty} . \frac{Te}{T_*}\right)^{0.8} . \left(\frac{\mu_*}{\mu_\infty} . \frac{U_1}{R_{D_\infty}} . \frac{D}{C_o}\right)^{0.2} . \sin^{1.6}\Lambda . \cos^{0.2}\Lambda \qquad 3.2.1$$

where $\frac{T_*}{T_e} = 1 + 0.20 \left(\frac{T_W}{T_e} - 1\right) + 0.40 . r . \left(\frac{\gamma - 1}{2}\right) . Me^2$

For incompressible flow the simplifications of equations (3.1.2) apply with the following additional results.

$$\text{d)} \quad Te = T_\infty$$

$$\text{e)} \quad \frac{T_*}{T_e} \rightarrow 0.80 + 0.20 \frac{T_W}{T_\infty} \qquad 3.2.2.$$

$$\text{f)} \quad \frac{\mu_*}{\mu_\infty} = f\ (T_W \text{ and } T_\infty \text{ only})$$

These may be substituted into equation (3.2.1) to produce -

$$Cf_\infty = 0.0592\left(0.80+0.20\frac{T_w}{T_\infty}\right)^{-0.8}\left(\frac{\mu_*}{\mu_\infty}.\frac{U_1}{R_{D_\infty}}.\frac{D}{C_o}\right)^{0.2}\sin^{1.6}\Lambda\cos^{0.2}\Lambda \qquad 3.2.3$$

It is readily shown that this expression exhibits a maximum as Cf varies with sweep and the corresponding peak conditions are given by -

$$Cf_\infty)max = 0.0432\left(0.80+0.20\frac{T_w}{T_\infty}\right)^{-0.8}\left(\frac{\mu_*}{\mu_\infty}.\frac{U_1}{R_{D_\infty}}.\frac{D}{C_o}\right)^{0.2} \qquad 3.2.4.$$

when $\tan\Lambda = 2.\sqrt{2}$

or $\Lambda = 70.53$

In the case of hypersonic flow the limiting conditions of equations (3.1.5) are approached together with the following -

$$e)\quad \frac{T_*}{T_e} \rightarrow 0.8 + 0.40.r.\tan^2\Lambda \qquad 3.2.5.$$

$$f)\quad \frac{\mu_*}{\mu_\infty} \rightarrow (1+\frac{S}{T_\infty})\left((0.8+0.40.r.\tan^2\Lambda).\frac{(\gamma-1)}{2}\right)^{\frac{1}{2}}.M_\infty\cos\Lambda$$

(Using Sutherlands Law)

and consequently equation (3.2.1) becomes

$$Cf_\infty = 0.0592\left(\frac{(\frac{\gamma+1}{\gamma-1})(\frac{1}{\gamma-1})}{(\frac{\gamma+1}{2})\cdot(\frac{1}{\gamma})\cdot\frac{2}{(\gamma-1)}}\right)^{0.8}\cdot\left((1+\frac{S}{T_\infty}).(\frac{\gamma-1}{2})^{\frac{1}{2}}.2(\frac{\gamma-1}{\gamma}).^{\frac{1}{2}}\frac{M_\infty}{R_{D_\infty}}\right)^{0.2} x$$

$$\frac{\sin^{1.6}\Lambda\cos^{0.4}\Lambda}{(0.80+0.40.r.\tan^2\Lambda)^{0.7}} \qquad 3.2.6$$

If the gas is air then -

$$Cf_\infty = 0.227.\frac{\sin^{1.6}\Lambda.\cos^{0.4}\Lambda}{(0.80+0.36.\tan^2\Lambda)^{0.7}}\left((1+\frac{110}{T_\infty}).\frac{M_\infty}{R_{D_\infty}}\right)^{0.2}$$

for which

$$Cf_e)max = 0.103\left((1+\frac{110}{T_\infty}).\frac{M_\infty}{R_{D_\infty}}\right)^{0.2} \qquad 3.2.7$$

when $\tan\Lambda = 1.1086$

or $\Lambda = 47.95^o$

As in the case of laminar flow the skin friction variation with sweep exhibits a maximum. The value of sweep angle at which this maximum occurs is found to decrease from 70.53^{o} in the limit of Mach number, M_∞, tending to zero to 47.95^{o} in the limit of Mach number tending to infinity. It should be noted that the total reduction in the value of sweep angle for maximum Cf_∞ is 23^{o} for the turbulent boundary layer whereas for the laminar boundary layer it was only 10^{o}. In addition the influence of free stream Mach number is reduced for turbulent flow since Cf_∞ is proportional to $M_\infty^{0.2}$ instead of $M_\infty^{0.5}$

Heat Transfer

Using equations (2.3.9) and (2.4.3.) it can be shown that -

$$Nu_{D_\infty} = 0.0296.Pr^{1/3}.\left(R_{D_\infty}.\frac{\rho*}{\rho_\infty}\right)^{0.8}\left(\frac{\mu*}{\mu_\infty}.U_1.\frac{D}{C_o}.\cos\Lambda\right)^{0.2}\sin^{0.6}\Lambda \qquad 3.2.8$$

For incompressible flow using equations (3.1.2) and (3.2.2)

$$Nu_{D_\infty} = 0.0296.Pr^{1/3}.\left(\frac{R_{D_\infty}}{0.8+0.2\frac{T_w}{T_\infty}}\right)^{0.8}\left(\frac{\mu*}{\mu_\infty}.U_1.\frac{D}{C_o}\right)^{0.2}\sin^{0.6}\Lambda\cos^{0.2}\Lambda \qquad 3.2.9$$

and, therefore -

$$Nu_{D_\infty)max} = 0.0236.Pr^{1/3}.\left(\frac{\mu*}{\mu_\infty}.U_1.\frac{D}{C_o}\right)^{0.2}\left(\frac{R_{D_\infty}}{0.80+0.20\frac{T_w}{T_\infty}}\right)^{0.8} \qquad 3.2.10$$

when $\tan\Lambda = \sqrt{3}$

or $\Lambda = 60.0$

For hypersonic flow -

$$Nu_{D_\infty} = 0.0296.Pr^{1/3}\frac{\sin^{0.6}\Lambda\cos^{0.4}\Lambda}{(0.80+0.40.r.\tan^2\Lambda)^{0.7}}\left(\left(\frac{\gamma-1}{2}\right)^{\frac{1}{2}}.\left(1+\frac{S}{T_\infty}\right)M_\infty.2\left(\frac{\gamma-1}{\gamma}\right)^{\frac{1}{2}}\right)^{0.2} x$$

$$\left(R_{D_\infty}.\left(\frac{\gamma+1}{2}\right)^{\left(\frac{\gamma+1}{\gamma-1}\right)}.\left(\frac{1}{\gamma}\right)^{\left(\frac{1}{\gamma-1}\right)}.\frac{2}{(\gamma-1)}\right)^{0.8} \qquad 3.2.11$$

If the gas is air then

$$Nu_{D_\infty} = 0.102.\frac{\sin^{0.6}\Lambda\cos^{0.4}\Lambda}{(0.80+0.36.\tan^2\Lambda)^{0.7}}\left(\left(1+\frac{110}{T_\infty}\right)M_\infty\right)^{0.2}\left(R_{D_\infty}\right)^{0.8} \qquad 3.2.12$$

consequently,

$$Nu_{D_\infty})_{max} = 0.0683 \left((1+\frac{110}{T_\infty})M_\infty\right)^{0.2} \left(R_{D_\infty}\right)^{0.8} \qquad 3.2.13$$

when $\tan \Lambda = 0.7149$

or $\Lambda = 35.56^o$

The variation of the turbulent Nusselt number with sweep angle is found to be very different from the laminar flow result. Firstly, at zero sweep angle equations (3.2.9) and (3.2.12) both predict zero heat transfer rate whereas the laminar heating rate was a maximum. This is a direct result of the Reynolds analogy (equation 2.2.1) since for laminar flow equation(2.3.7)shows that the heat transfer coefficient, h , is independent of the edge velocity, Ve, whilst for turbulent flow h varies as $Ve^{0.6}$ - see equation(2.4.2). Clearly this limiting case for turbulent flow is physically unrealistic. However, it will be shown in section (5.6) that for a given geometry and free stream condition there exists a certain value of ϕ_* below which turbulent flow cannot be maintained and, consequently, the inconsistency is resolved. Secondly, the turbulent Nusselt number has a peak value at some finite sweep angle. For incompressible flow this angle is 60^o whilst for hypersonic flow it has been shown to be 35.5^o. This result should be compared with the laminar trend of decreasing Nu_∞ with increasing sweep angle. Thirdly, the hypersonic heat transfer rate is proportional to $M_\infty^{0.2}$ as opposed to $M_\infty^{0.5}$ in the laminar case.

Finally in order to gain some idea of the range of Mach number over which these simple formulae are valid the variation of peak heat transfer rate and the corresponding sweep angle have been calculated for the turbulent attachment line boundary layer on a swept circular cylinder travelling through the upper atmosphere ($T_\infty \simeq 216^oK$) at Mach numbers in the range 0 to 8 and wall temperatures between 0 and 1800^oK. A maximum value of 8 has been chosen for M_∞ since real gas effects have not been included in the analysis. The results are presented as figures 10 and 11 together with the variations predicted by equations (3.2.10) and (3.2.13). In the case of maximum heat transfer rate it can be seen that the incompressible approximation gives good predictions for free stream Mach numbers less than unity whilst the hypersonic approximation overpredicts the heating rates by only 10% at a Mach number of 8. Clearly the approximations define upper and lower bounds on the maximum Nusselt numbers. For the prediction of the sweep angle for maximum heating rate the incompressible result is valid up to a free stream Mach number of about 0.5 whereas for M_∞ in excess of 2.0 it is found that the angle is virtually constant and consequently it is well approximated by the hypersonic result.

4. IMPLICATIONS FOR VEHICLE DESIGN

For low speed vehicles the effect of sweep upon skin friction drag is generally a secondary consideration since the sweep angle is usually determined by some other criterion e.g. the need to delay the onset of the compressible drag rise to a particular free stream Mach number. However, if the design calls specifically for laminar boundary layer flow maintained by artificial means,e.g.by suction, then it becomes necessary to assess the implications of a sudden drag rise caused by the failure of the system and therefore detailed knowledge of the attachment line boundary layer properties and its transition behaviour would be required.

When a vehicle is to travel at hypersonic speeds heat transfer becomes a primary design criterion. By taking the ratio of turbulent to laminar maximum Nusselt numbers (from equations (3.1.12) and (3.2.13) it is found that

$$\frac{Nu_{D_\infty})\ \text{max turbulent}}{Nu_{D_\infty})\ \text{max laminar}} = 0.076\left(\frac{R_{D_\infty}}{M_\infty(1+\frac{110}{T_\infty})}\right)^{0.3} \qquad 4.1$$

for free stream Reynolds numbers in the range 10^5 to 10^7 and Mach numbers between 5 and 10 the ratio of heating rates varies from 1.2 to 6. If the vehicle provides no heat sink ($\dot{q}_{net} = 0$) then the wall must achieve a temperature such that the convective heat input is just balanced by the heat output due to radiation i.e.

$$h(T_r - T_w) = \varepsilon.\sigma\ (T_w^4 - T_\infty^4)$$

where ε is the surface emissivity and σ is the Stefan -Boltzman constant. For hypersonic re-entry conditions

$$T_w^4 >> T_\infty^4 \qquad \text{and} \qquad T_r >> T_w$$

and so the 'equilibrium wall temperature' T_w is given approximately by

$$T_w \simeq \left(\frac{T_r.h}{\varepsilon.\sigma}\right)^{\frac{1}{4}}$$

Therefore the increases in heat transfer rate produced by boundary layer transition correspond to increases in wall temperature of between 5 and 60 percent. Moreover, since the attachment line is expected to be one of the hottest areas on the vehicle this may be an unacceptable increase from the point of view of structural integrity. It is, therefore, particularly important to have a reliable criterion for the prediction of attachment line boundary layer transition in hypersonic flow.

5. THE TRANSITION FROM LAMINAR TO TURBULENT FLOW AT THE ATTACHMENT LINE.

5.1 Previous Experimental Work

Transition in the attachment line boundary layer was first discovered in 1963 whilst British and American aircraft companies were attempting to develop flight scale swept wings with full chord laminar boundary layer flow. Since the phenomenon was only isolated after repeated failures at the flight test stage, the experiments carried out were, by necessity, performed hastily and although the basic nature and governing parameters were identified the mechanism was never subjected to a detailed investigation. In retrospect there can be little doubt that the existance of the leading edge contamination effect was largely responsible for the failure and ultimate cancellation of these early laminar flow projects.

The experimental programme conducted by Pfenninger (ref.12) consisted of flight tests on the Northrop X-21A laminar flow aircraft, which was a Douglas 'Destroyer' WB-66D with a suction wing and a specially modified propulsion system, together with model tests in the Northrop 11' x 8' low speed wind tunnel. Using model wings swept at 33° and 45° it was found that, for two and three-dimensional roughness, bursts of turbulence propagated along the attachment line when ϕ was in the range 235 to 260 whilst for ϕ between 260 and 272 the attachment line and the rest of the wing boundary layer was fully turbulent. Attempts to prevent the spread of turbulence by means of a streamwise fence, which was intended to reduce local values of ϕ , left the critical conditions unaltered even when the leading edge was perfectly smooth. However, strong suction at the wing/fence junction did produce laminar flow up to the top speed of the tunnel ($\phi \simeq 350$). Flight test results showed that almost complete laminar flow could be obtained on both upper and lower wing surfaces provided that the value of ϕ was kept below 250.

Gregory (ref.10) performed experiments in the N.P.L. 13' x 9' and 9' x 7' wind tunnels using an aerofoil with an N.P.L. 153 section where transition was detected by means of hot-wires and hot-film gauges situated on the attachment line. He found that for large diameter trip wires first bursts of turbulence were detected 24 inches away (measured along the leading edge) when ϕ lay in the range 220 to 233 and complete turbulence was obtained for ϕ between 235 and 243. By using small trip wires it was found that up to the maximum value of ϕ available i.e. 370,transition to turbulence occured as the trip wire Reynolds number, R_d, increased from approximately 450 to 550 although there was a great deal of scatter in the experimental results. By contaminating the attachment line with a turbulent boundary layer, generated on a small streamwise flat plate, it was found that transition occured as ϕ increased from 230 to 260.

As a result of the problems encountered in the flight testing of the Handley Page laminar flow wing Gaster (ref.11) undertook some experimental work in the 8' x 6' low speed wind tunnel at the College of Aeronautics, Cranfield. Using a model with a circular leading edge of mean radius 2.5" and varying the sweep angle between 40° and 60° he

obtained values of ϕ in the range 100 to 420. By using a stethoscope to detect turbulence and defining critical conditions as those necessary to produce a signal which corresponded to conditions 'halfway' between completely laminar and fully turbulent flow Gaster found that for large trip wires $\phi_{critical}$ was 257 at a station 24" away from the wire. By extending the investigation to wires of smaller diameter and measuring stations closer to the trip he concluded that "in the limit of very rapid decay", i.e. s/ψ tending to zero, the curves for the decay of turbulence tended to a single line which could be represented by -

$$R_d = 47(R_{\delta_{2L}})^{\frac{1}{2}} = 30\ \phi^{\frac{1}{2}} \qquad 5.1.1$$

or $$\phi = 892/(\frac{d}{\psi})^2$$

Equation (5.1.1) is commonly known as the 'Gaster Criterion'. By introducing spark generated turbulent spots into the laminar attachment line flow and observing their passage along the leading edge it was found that for ϕ less than 280 the spots contracted whereas for ϕ greater than 280 they expanded, thus setting a lower limit on the value of ϕ for which fully developed turbulence could exist. In an attempt to determine the upper limit of laminar flow, i.e. the limit of natural stability of the flow to small disturbances, acoustic waves were introduced into the layer. Although the results were somewhat strange it was possible to conclude that all disturbances decayed for all values of ϕ up to the maximum of 420. Finally Gaster showed that the spanwise spread of turbulence could be delayed by the formation of a true stagnation point on a specially shaped small protuberance - the 'Gaster Bump'-which was attached to the leading edge at a station close to the wingroot.

The deficiency in the current state of the art may be summed up in four statements. Firstly, models used to date have been small, this has made boundary layer measurements difficult and, hence, the values of ϕ quoted have been unreliable. Secondly the maximum values of ϕ achieved in wind tunnels are small compared to those possible on civil and military aircraft in flight. Thirdly, the only consistent results concern very large excresences and very large values of s/ψ and, fourthly, the only criterion for the tripping characteristics of small wires is valid in the limit as s/ψ tends to zero which may not be a practically important situation.

5.2 The Present Investigation

The present investigation had three main objectives:-

a) To design an experimental arrangement which would enable leading edge conditions, typical of full scale flight, to be simulated in a wind tunnel.

b) To perform an extensive investigation into the response of the attachment line boundary layer to two-dimensional trip wires and turbulent flat plate boundary layers (wing/body junction simulation).

c) To produce reliable criteria for the prediction of transition in situations of practical importance.

It has already been shown that for an infinite swept wing in incompressible flow the properties of the attachment line layer are functions of ϕ only - see equation (1.2). In order that the practical implications of the variables in equation (1.2) may be appreciated it is convenient to express ϕ as a function of free stream parameters and leading edge sweep .

$$\phi_{incomp} = \left(\frac{Q_\infty . \sin \Lambda . \tan \Lambda . C_0}{\nu . U_1}\right)^{\frac{1}{2}} \qquad 5.2.1$$

This shows that the attachment line velocity gradient U_1 is the only contribution made to ϕ by the cross-sectional geometry of the model and it follows that an accurate determination of ϕ depends upon the availability of an accurate value for U_1. If the velocity gradient is to be estimated from an experimental surface pressure distribution then the section must be chosen so that U_1 is essentially constant over as large a range of x as possible. One of the shapes which fills this basic requirement is the circular cylinder which has the added advantage of being particularly easy to construct. For the velocity distribution over the surface of a circular cylinder the potential flow solution gives

$$U_1 = 2\left(\frac{C_0}{\rho}\right) \quad \text{(where } \rho \text{ is the leading edge radius)} \qquad 5.2.2.$$

$$\phi = \left(\frac{Q_\infty \rho}{\nu} . \frac{\sin \Lambda . \tan \Lambda}{2}\right)^{\frac{1}{2}} \qquad 5.2.3$$

From equation (5.2.3) it can be seen that to achieve large values of ϕ a large leading edge radius is necessary. A wing with a suitably large leading edge radius was loaned to Cranfield by the Cambridge University Engineering Department. This consisted of a pipe with a diameter of 9 ins faired smoothly from the maximum thickness position to the trailing edge to form an aerofoil with a chord of 18".

The model was mounted vertically in a closed return circuit wind tunnel with a closed working section 8' wide, 6' high and approximately 15' long. Figure 12 shows the general arrangement of the model in the tunnel. To avoid contamination of the upstream tip by the turbulent boundary layer on the tunnel roof and at the same time allow the maximum variation in sweep angle the model suspension point was some 10" below the roof. This arrangement allowed the sweep angle to vary between 50^o and 70^o and since the tunnel speed could vary from 15 to 180 ft/sec, the possible values of ϕ ranged from 125 to 740. In order that disturbances from the upstream tip should be kept to a minimum the area around the stagnation point was built up with filler and rubbed down to form a smooth continuous surface. The great weight of the model combined with an extremely rigid suspension kept model vibration to a very low level.

Disturbances were introduced by wrapping circular trip wires around the leading edge at the position shown in figure 12. These

wires were pre-stretched to remove kinks and great care was taken to ensure that they were in contact with the surface as they crossed the attachment line. A constant temperature hot-wire probe was mounted in a simple wire cradle (figure 13) and positioned at a distance, s, from the trip. By sliding the probe along a support tube it was possible to vary the distance from the hot-wire to the surface. This support tube was calibrated so that the hot-wire could be moved through the boundary layer in a series of equal steps thereby enabling boundary layer profile measurements to be made. The cradle itself was secured to the model with adhesive tape and it was found that this produced a rigid arrangement which proved to be entirely satisfactory. When the hot-wire was used to detect turbulence it was fixed 0.010" from the surface and the output signal was supplied to two oscilloscopes. One had a storage tube which wasscanning at 5 secs/cm and could store up to 50 seconds of signal. This was used for the determination of conditions which were necessary to produce spots of turbulence at a regular frequency of approximately one every 15 secs i.e. the 'first bursts' point. The second oscilloscope wasscanning continuously at 5 m secs/cm and was used to detect the completely turbulent situation, this being defined as the point at which no laminar gaps were observed during a period of not less than 2 minutes. Photographs of typical oscilloscope traces are presented in figure 14. When estimates of the intermittency factor, Γ, were required the hot-wire output was supplied to an ultra violet pen recorder so that a permanent record of the time history of the signal could be obtained. The traces produced in this way were subsequently decoded by hand.

In addition surface pressure distributions were measured using the two sets of pressure tappings (see figure 12), which were connected to an inclined manometer bank.

5.3 Preliminary Measurements

Figure 15 shows the results of pressure measurements made at various sweep angles together with the theoretical distribution for the circular cylinder in inviscid flow. It was found that at all the angles of sweep there was a small positive pressure gradient along the attachment line. The maximum pressure difference recorded was equivalent to 2.9% of the free stream dynamic head and this meant that the velocity along the attachment line was always within 1.7% of the spanwise component of the freestream velocity. Moreover, the measured pressure distributions showed that for both upstream and downstream stations the value of $dUe/dx)x = 0$ was always within 3% of the value given by equation (5.2.2). The observed differences in static pressure and chordwise velocity gradient may have been produced by a small positive pressure gradient along the tunnel axis or they may be the result of a variation of the effective sweep angle with spanwise position. In the latter case calculations show that the maximum deviation from the geometric sweep angle was less than $\pm 1.9^{o}$. As a final check the laminar boundary layer velocity profiles were measured with the hot-wire probe at the two extreme stations i.e. the trip wire position (no trip wire attached) and the downstream pressure tapping position. The results are shown in figure 16 together with the theoretical profile based upon the properties of the ideal circular cylinder pressure distribution and it is apparent that there is very close agreement.

Having shown that the assumptions implicit in equation (5.2.3) are essentially correct for this model/wind tunnel combination, this equation has been used to reduce the transition test data.

5.4 Transition Results

As a first step in the experiment the behaviour of the attachment line flow was investigated in the absence of a trip. This enabled the upper limit of the trip wire experiments to be established and, at the same time, it produced some indication of the "upper" critical value of ϕ i.e. the limit of stability to very small disturbances. Results are presented in figure 17 where it can be seen that the values of ϕ for first bursts of turbulence are well correlated by a single function which decreases monotonically with increasing s (s in this instance being measured from the upstream tip of the model). The conditions necessary for complete turbulence could not be fully investigated since they were beyond the capabilities of the tunnel/model combination. However, from the single value obtained it seems that transition from laminar to turbulent flow requires a change in ϕ of about 100.

In practice it was not possible to make measurements at pre-determined values of s/ψ since ψ_{crit} was initially unknown. Therefore in order to obtain the variation of ϕ with d/ψ at constant values of s/ψ it was necessary to interpolate the experimental results. The measuring procedure involved fixing a trip wire to the wing and noting the wind tunnel speeds required for the appropriate hot-wire signals over ranges of s and sweep angle.* Results obtained in this way were plotted as ϕ against s/ψ - typical sets are shown in figure 18. From these plots it was possible to obtain the critical conditions for any value of s/ψ and, hence, from a knowledge of the trip wire diameter the appropriate value of d/ψ was calculated.

Figures 19 and 20 show the results for the production of first bursts and complete turbulence respectively. It can be seen that the variation of ϕ_{crit} with d/ψ and s/ψ naturally divides itself into four regions bounded by fixed values of d/ψ . Firstly for d/ψ greater than 1.9 the value of ϕ for first bursts is strongly dependent upon s/ψ tending to a constant value of 245 for values of s/ψ greater than 4000 whereas for complete turbulence ϕ is virtually independent of both d/ψ and s/ψ taking a value of approximately 300. Secondly when d/ψ lies between 1.5 and 1.9, the critical values of ϕ are strongly dependent upon d/ψ whilst dependence upon s/ψ is very weak for all values of s/ψ . Thirdly for values of d/ψ lying in the range 0.7 to 1.5 the strong influence of d/ψ remains,however, the dependence upon s/ψ returns producing a kink in the ϕ_{crit} - d/ψ relationship when s/ψ is greater than zero. The fourth and final region corresponds to a cross plot of the free transition results of figure 17 and consequently the critical values of ϕ are independent of d/ψ. For all the tests carried out with 2-D trip wires it was found that the turbulence disappeared as conditions were brought below the critical level i.e. the turbulent boundary layer induced by the trip wires showed no sign of hysteresis.

* A complete set of raw data is presented in Appendix G.

In addition to the trip-wire disturbances the attachment line was also contaminated with a turbulent boundary layer generated on a streamwise flat plate. The tunnel arrangement and fixing position are shown in figure 12. A separate flat plate,15" wide, was made for each of the test sweeps (55^o, 60^o, 65^o, 70^o) to ensure a close fit between model and plate and also keep the distance between the plate leading edge and wing a constant 12 ins. Small gaps in the wing/plate junction were sealed with plasticine and an 0.1" diameter trip wire was fixed 3.5" downstream from the plate leading edge. A titanium dioxide/paraffin suspension was used to provide surface flow visualisation which confirmed that the plate boundary layer remained attached after it had been tripped to the turbulent state and also showed that the flow in the wing/plate junction was smooth. The transition results are presented in figure 21, where it can be seen that the values of ϕ required for the detection of first bursts and complete turbulence are well correlated as a single function of s/ψ. Also shown are the asymptotic results for very large trip wires ($d/\psi \rightarrow \infty$). The curves for first bursts tend to the same limit as s/ψ becomes large, but they exhibit slightly different behaviour at low values of s/ψ. This discrepancy is almost certainly due to the fact that the flat plate acts as a reflection plane and hence, there must be an initial development of the attachment line flow during which the semi-infinite assumption used in the data reduction is invalid. In the case of the completely turbulent flow the trends are in very good agreement. Once again the critical values of ϕ did not exhibit any hysteresis.

To complete the investigation the variation of the intermittency factor, Γ with ϕ, d and s was measured at several representative conditions using the technique described in the previous section with sample times of approximately 2 seconds. The results are presented in figure 22 where it can be seen that, although there are differences between the individual distributions, in all cases there is a smooth progression from laminar to turbulent flow with increasing ϕ.

5.5 Discussion

Figure 17 showed the transition characteristics for d/ψ equal to zero in a wind tunnel whose turbulent intensity level, Tu, is approximately constant at 0.12 ±0.03% over the whole speed range. If this 'natural' transition was produced by the amplification of very small disturbances (typically $u^1_{max}/Ue < 0.01$ see Fasel - ref.38) which originate in the free stream (i.e. a Tollmien-Schlichting mechanism) then these results would represent a true upper limit for laminar flow at this turbulence level. However, if transition was being produced by some finite disturbance ($u^1_{max}/Ue > 0.01$) originating at, or near, the upstream tip then laminar flow may be possible at even higher values of ϕ.

At present the available evidence does not support the idea of large disturbances originating at the upstream tip. Pfenninger (ref.31) shows that the development of the attachment line boundary layer is rapid with the asymptotic conditions being attained when s/ψ is of order 1.0 x ϕ and therefore the 'tip region' is very limited in spanwise extent. Moreover the successful operation of the Gaster bump - a device for preventing the spread of turbulence along a swept leading edge

(see ref.11) depends upon the creation of a true stagnation point and so it would seem that the finite upstream tip region tends to eliminate disturbances rather than produce them. Clearly the results of figure 17 should be compared with a model of the transition process which is based upon linear stability theory.

To investigate the stability of a boundary layer flow it is convenient to begin by writing the equation of motion in terms of a mean flow plus a fluctuating component. For a three-dimensional flow with surface and streamline curvature neglected the equations are the familiar Navier-Stokes equations -

$$\frac{\partial(u+u^1)}{\partial t} + (u+u^1)\frac{\partial(u+u^1)}{\partial x} + (v+v^1)\frac{\partial(u+u^1)}{\partial y} + (w+w^1)\frac{\partial(u+u^1)}{\partial z} = \frac{-1}{\rho}\frac{\partial(p+p^1)}{\partial x} + \nu\nabla^2(u+u^1)$$

$$\frac{\partial(v+v^1)}{\partial t} + (u+u^1)\frac{\partial(v+v^1)}{\partial x} + (v+v^1)\frac{\partial(v+v^1)}{\partial y} + (w+w^1)\frac{\partial(v+v^1)}{\partial z} = \frac{-1}{\rho}\frac{\partial(p+p^1)}{\partial y} + \nu\nabla^2(v+v^1)$$

$$\frac{\partial(w+w^1)}{\partial t} + (u+u^1)\frac{\partial(w+w^1)}{\partial x} + (v+v^1)\frac{\partial(w+w^1)}{\partial y} + (w+w^1)\frac{\partial(w+w^1)}{\partial z} = \frac{-1}{\rho}\frac{\partial(p+p^1)}{\partial z} + \nu\nabla^2(w+w^1)$$

$$\frac{\partial(u+u^1)}{\partial x} + \frac{\partial(v+v^1)}{\partial y} + \frac{\partial(w+w^1)}{\partial z} = 0 \qquad 5.5.1$$

In the case of the flow close to an infinite swept attachment line, if there is no spanwise variation then

$$\frac{\partial u}{\partial y} = \frac{\partial v}{\partial y} = \frac{\partial w}{\partial y} = 0$$

Under these conditions the mean flow is obtained as an exact solution of the boundary layer equations (see section 6.2 for details) for which it is found that

$$\frac{\partial u}{\partial x} = f(z), \quad \frac{\partial v}{\partial x} = 0, \quad \frac{\partial w}{\partial x} = 0$$

Therefore, by dropping those mean flow terms which are negligably small in the boundary layer region and subtracting the mean flow boundary layer equations, the disturbance equations are reduced to -

$$\frac{\partial u^1}{\partial t} + u\frac{\partial u^1}{\partial x} + v\frac{\partial u^1}{\partial y} + w^1\frac{\partial u}{\partial z} + u^1\frac{\partial u}{\partial x} + w\frac{\partial u^1}{\partial z} + u^1\frac{\partial u^1}{\partial x} + v^1\frac{\partial u^1}{\partial y} + w^1\frac{\partial u^1}{\partial z}$$

$$= \frac{-1}{\rho}\frac{\partial p^1}{\partial x} + \nu\nabla^2 u^1$$

$$\frac{\partial v^1}{\partial t} + u\frac{\partial v^1}{\partial x} + v\frac{\partial v^1}{\partial y} + w^1\frac{\partial v}{\partial z} + w\frac{\partial v^1}{\partial z} + u^1\frac{\partial v^1}{\partial x} + v^1\frac{\partial v^1}{\partial y} + w^1\frac{\partial v^1}{\partial z}$$

$$= \frac{-1}{\rho}\frac{\partial p^1}{\partial y} + \nu\nabla^2 v^1 \qquad 5.5.2$$

$$\frac{\partial w^1}{\partial t} + u\frac{\partial w^1}{\partial x} + v\frac{\partial w^1}{\partial y} + w^1\frac{\partial w}{\partial z} + w\frac{\partial w^1}{\partial z} + u^1\frac{\partial w^1}{\partial x} + v^1\frac{\partial w^1}{\partial y} + w^1\frac{\partial w^1}{\partial z}$$

$$= \frac{-1}{\rho}\frac{\partial p^1}{\partial z} + \nu\nabla^2 w^1$$

$$\frac{\partial u^1}{\partial x} + \frac{\partial v^1}{\partial y} + \frac{\partial w^1}{\partial z} = 0$$

Finally, if it is assumed that the mean flow streamlines are locally parallel to the surface ($w = 0$) and that the disturbances are sufficiently small for products of the fluctuating components to be negligable in comparison with other terms, then the approximate (linearised) equations of motion are -

$$\frac{\partial u^1}{\partial t} + u\frac{\partial u^1}{\partial x} + v\frac{\partial u^1}{\partial y} + w^1\frac{\partial u}{\partial z} + u^1\frac{\partial u}{\partial x} = \frac{-1}{\rho}\frac{\partial p^1}{\partial x} + \nu\nabla^2 u^1$$

$$\frac{\partial v^1}{\partial t} + u\frac{\partial v^1}{\partial x} + v\frac{\partial v^1}{\partial y} + w^1\frac{\partial v}{\partial z} = \frac{-1}{\rho}\frac{\partial p^1}{\partial y} + \nu\nabla^2 v^1 \qquad 5.5.3$$

$$\frac{\partial w^1}{\partial t} + u\frac{\partial w^1}{\partial x} + v\frac{\partial w^1}{\partial y} = \frac{-1}{\rho}\frac{\partial p^1}{\partial z} + \nu\nabla^2 w^1$$

$$\frac{\partial u^1}{\partial x} + \frac{\partial v^1}{\partial y} + \frac{\partial w^1}{\partial z} = 0$$

Before any further progress may be made it is necessary to specify the disturbances in an explicit mathematical form. In reference (31) Pfenninger presents data from a hot-wire investigation made at the attachment line of a wing swept at 45^o. The results showed that at sufficiently large values of $R_{\delta 2}$ regular sinusoidal oscillations were observed at different spanwise stations with the frequencies lying in the range 100 to 5000 Hz. By placing two hot-wires at the same spanwise location but at different chordwise positions ($x = \pm 0.3$") he

was able to conclude that for small amplitude disturbances there was no phase shift in the chordwise (x) direction i.e. the waves were essentially two-dimensional with the crests, or constant phase lines, travelling in the spanwise direction. Therefore, if it is assumed that the disturbances are periodic in y and t and that the amplitude is a function of z only then the governing equations are -

$$\frac{\partial u^1}{\partial t} + v\frac{\partial u^1}{\partial y} + w^1\frac{\partial u}{\partial z} + u^1\frac{\partial u}{\partial x} = + \nu\nabla^2 u^1$$

$$\frac{\partial v^1}{\partial t} + v\frac{\partial v^1}{\partial y} + w^1\frac{\partial v}{\partial z} = \frac{-1}{\rho}\frac{\partial p^1}{\partial y} + \nu\nabla^2 v^1 \qquad 5.5.4$$

$$\frac{\partial w^1}{\partial t} + v\frac{\partial w^1}{\partial y} = \frac{-1}{\rho}\frac{\partial p^1}{\partial z} + \nu\nabla^2 w^1$$

$$\frac{\partial v^1}{\partial y} + \frac{\partial w^1}{\partial z} = 0$$

It follows that if the disturbances are truly harmonic then the v^1 and w^1 components may be represented by a stream function Ψ of the form

$$\Psi = \sigma(z)e^{i(\underline{\alpha}\, y - \underline{\omega}\, t)} \qquad 5.5.5$$

where $v^1 = \frac{\partial \Psi}{\partial z}$ and $w^1 = \frac{\partial \Psi}{\partial y}$

Therefore the equations (5.5.4) may be reduced to a single fourth order ordinary differential equation -

$$\left(\frac{\dot{V}}{V_\infty} - \frac{\omega}{\alpha}\right)\left(\frac{d^2\sigma}{d(z/L)^2} - \alpha^2\sigma\right) - \frac{d^2(v/V_\infty)}{d(z/L)^2}\cdot\sigma = \frac{-i}{\alpha R}\left(\frac{d^4\sigma}{d(z/L)^4} - 2\alpha^2\frac{d^2\sigma}{d(z/L)^2} + \alpha^4\sigma\right)$$

5.5.6

where all the terms have been non-dimensionalised using V_∞ and a length scale L and the Reynolds number R, is given by $(V_\infty.L/\nu)$. This equation

is commonly called the Orr-Sommerfeld equation. In general the wave number α , and the frequency ω, are complex numbers but there are two special cases which correspond to physically realistic situations. Firstly if α_i is zero then the resulting wave form amplifies or decays in time (temporal) and secondly, if ω_i is zero then the wave amplifies or decays in space (spatial). The former corresponds to the classical Tollmien-Schlichting wave whilst the latter describes the development of a wave introduced at some fixed point in space by an active disturbance e.g. a vibrating ribbon. For the case of natural waves which arise through the selective amplification of random input disturbances it is not clear whether either of these formulations is adequately representative. However, experimental work in boundary layers and particularly separated shear layers has shown that real disturbance waves are predominantly spatial in character and so only this type will be considered in the present analysis.

$$\Psi = \sigma(z).e^{(-\underline{\alpha_i}\ y)}.\ e^{i(\underline{\alpha_r}\ y - \underline{\omega_r}\ t)} \qquad 5.5.7$$

Having developed a theoretical model for calculating the development of a constant frequency disturbance it is necessary to have some criterion for the transition process itself. At the present time the most widely used, but not necessarily the best, method is the Amplitude Ratio method, see for example Jaffe, Okamura and Smith (ref.33). Briefly this approach maintains that first bursts of turbulence are observed when the amplitude of any fixed frequency disturbance exceeds e^n times the amplitude it had when it first became unstable i.e.

$$\left[\log_e\left(\frac{A_T}{A_i}\right) = -\int_{s_i}^{s} \underline{\alpha_i}\ ds = n\right]_{\underline{\omega_r} = \text{constant}} \qquad 5.5.8$$

Equations (5.5.6) and (5.5.7) have been solved numerically in sufficient detail to enable the transition predictions to be made from equation (5.5.8) and complete details of the calculations are presented in Appendix B.

Figure 23 presents the predicted variation of transition location s_T with momentum thickness Reynolds number $R_{\delta 2_L}$. In this case $R_{\delta 2L}$ is used instead of ϕ since transition is clearly governed by the properties of the laminar boundary layer. Also shown in the figure are the results of the present experiment (figure 17) together with the results obtained by Pfenninger (ref.31) on the 45^o swept wing mounted in the Northrop 10' x 7' wind tunnel and a single result from Carlson (ref.34) for a wing with 33^o of sweep mounted in the NASA Ames 12' pressure tunnel. It is apparent that the data from the various sources are consistent and that the theoretical model produces the correct variation of $R_{\delta 2T}$ with s_T although in general the predicted value of $R_{\delta 2T}$ is about 10% greater than that observed in the experiments. In addition it is of interest to note that the attachment line profile is more stable than the Blasius profile ($R_{\delta 1_{crit}}$=520) and that for large values of s_T/δ_2 the results for amplitude ratios e^6, e^{10} and e^{14} lie very close together indicating

that the Reynolds number for transition is not sensitive to the initial disturbance level provided that it is still sufficiently small to maintain the validity of the linearisation approximations implicit in equation (5.5.6). Finally, figure 24 presents a comparison between the observed disturbance frequencies reported by Pfenninger plus a single result* from the present experiment and the theoretical predictions for the most highly amplified frequencies, where the band width at a given Reynolds number was fixed by including those frequencies whose spatial amplification ratio were within $(8 \times 10^{-5})/\delta_{2L}$ of the minimum value, see Appendix B. In the experiments the frequency which is actually observed will depend upon the free stream disturbance energy spectrum and without a knowledge of this a complete comparison between theory and experiment is not possible. However, it is clear from figure 24 that despite the fact that the theory predicts damping for Reynolds numbers less than 268 the predictions for the most unstable frequencies are in reasonable agreement with the experimental results.

The slight discrepancies between theory and experiment may be due to the omission of any curvature effects from the theoretical model but it seems more reasonable to attribute them to the use of an over-simplified form for the input disturbance. Nevertheless the results presented in figures 23 and 24 when supplemented by Gaster's conclusion that all small amplitude disturbances decay up to $R_{\delta 2L}$ of at least 170 strongly suggests that a value of $R_{\delta 2}$ equal to 240 (ϕ = 600) is a true upper limit for completely laminar flow when s/δ_2 is greater than 20,000.

Figure 25 shows the response of the attachment line boundary layer to two-dimensional trip wires in the limit as s/ψ tends to zero i.e. turbulence at the trip wire location. For values of d/ψ in excess of 2.2 complete turbulence is only possible for values of ϕ greater than 260 whilst first bursts are observed at values which decrease with increasing d/ψ . When d/ψ is less than 2.2 the width of the transition region is approximately constant, the functional relationship between ϕ and d/ψ is smooth and the results show no sign of an upper limit on ϕ for laminar flow. Also shown for comparison is the Gaster criterion (equation 5.1.1). Gaster based this curve on experimental values of ϕ in the range 170 - 450 and it is apparent that, over the same ϕ range it is in good agreement with the present results for first bursts of turbulence. However, for values of ϕ in excess of 500 there is an increasing divergence between this criterion and the experimental values. In the case of complete turbulence it is found that for d/ψ less than 2.2 the results show reasonable agreement with the function

$$\frac{Vd.d}{\nu} = \text{constant} = 550 \qquad 5.5.9$$

where Vd is the velocity in the undisturbed boundary layer at a distance d from the surface. Since there is a close similarity between the attachment line and flat plate boundary layer velocity profiles (figure 2) it is interesting to compare equation (5.5.9) with flat plate results where criteria of this form are commonly used for correlating the conditions necessary to produce transition at the trip wire position. Gibbings (ref.35) presents a short review of flat plate tripping criteria from which it is found that the value of the 'constant'

* At suitably large values of $R_{\delta 2}$ the laminar hot-wire signal would exhibit nearly harmonic fluctuations of almost constant frequency - this frequency was estimated from the oscilloscope trace.

lies somewhere between 200 and 400. Therefore it would appear that the attachment line boundary layer is less sensitive to the presence of a trip wire.

The variation of ϕ with d/ψ for very large values of s/ψ is given in figure 26. There are three major differences between these curves and those of figure 25. In the first instance the width of the transition region is substantially constant ($\Delta\phi \simeq 60$) over the whole range of d/ψ . There is also a discontinuity of slope when d/ψ takes a value of 1.55 and, finally, there is an upper limit upon ϕ for completely laminar flow. For d/ψ greater than 2.0 the critical values of ϕ are constant at 245 and 300 for first bursts and complete turbulence respectively. These values may be taken to be a lower limit on the appearance of turbulence at the attachment line in the presence of very large disturbances, the latter being in very good agreement with Gaster's limit ($\phi \simeq 280$) for the development of large turbulent spots which are capable of sustaining themselves indefinitely whilst neither expanding or contracting in the spanwise direction. When d/ψ lies between 0.8 and 2.0 the critical values of ϕ are strongly dependent upon d/ψ and the Gaster criterion is no longer adequate for the prediction of transition. Despite the kink when d/ψ equals 1.55 the variations may be well represented by the linear functions -

$$\phi = 830 - 294\ (d/\psi) \quad \text{- first bursts}$$
$$\phi = 890 - 294\ (d/\psi) \quad \text{- complete turbulence} \qquad 5.5.10$$

Finally, when d/ψ is less than 0.8 ($d/\delta_{2L} < 2$) the transition process is dominated by disturbances originating in the free stream and the value of ϕ necessary to produce transition at very large distances from the trip ($s/\psi > 10{,}000$) is unaffected by the trip wire diameter. This result has particular significance since it may be interpreted as a criterion for the determination of the largest diameter trip wire which may be placed within the boundary layer and yet not affect the transition position. It is shown in Appendix C that the most reliable criterion for the critical roughness height for the flat plate boundary layer is closely approximated by the function

$$\frac{d}{\delta_{2_L}} = 0.77 \qquad \text{when } \left(\frac{U_\infty s}{\nu}\right)_T = 2.6 \times 10^6$$

For a true comparison between this and the attachment line result it is necessary to match the transition Reynolds number. From figure 17 it can be seen that matching takes place when ϕ takes a value of approximately 720 i.e.

$$\left(\frac{V_\infty s}{\nu}\right)_T = \phi.\frac{s}{\psi} = 720 \times 3630 = 2.6 \times 10^6$$

and from figure 19 the corresponding maximum trip wire diameter is given by

$$\frac{d}{\psi} \simeq 0.45 \quad \text{or} \quad \frac{d}{\delta_2} = 1.1 \qquad 5.5.11$$

when $\left(\frac{V_\infty s}{\nu}\right)_T = 2.6 \times 10^6$

Once again the attachment line flow is found to be less sensitive to the presence of two-dimensional trip wires.

In the case of turbulence produced by contaminating the attachment line with a flat plate boundary layer (figure 21) the results show that at large distances from the trip there is no distinction between transition caused by a turbulent boundary layer and transition induced by a very large trip wire. These findings are in good agreement with those of Pfenninger (ref.12) for both wind tunnel and flight and demonstrate that the use of a wing fence alone cannot delay transition since the fence, whilst locally reducing ϕ, also acts as a large source of disturbance.

A consistent explanation of the transition behaviour may be found by the consideration of the role of the trip wire in the transition process. From studies conducted in flat plate boundary layers* it is known that a two-dimensional trip wire attached to a solid surface does not shed eddies in the form of a Karman Street if d/δ_1 is less than about 0.75. Instead a continuous unsteady free shear layer is formed as the flow separates from the wire and this attaches itself to the wall at some distance downstream (typically of order 10 trip diameters) thus forming a closed bubble consisting mainly of a single large eddy. Free shear layers have very low critical Reynolds numbers, typically of order 10 according to linear stability theory (see Lessen and Ko, ref.36) and consequently even though the boundary layer in which the shear layer is embedded may be completely stable to the small amplitude disturbances which are always present in any real flow these disturbances may be amplified considerably by the shear layer itself. The degree of amplification achieved in any given situation will depend upon the local shear layer Reynolds number, the streamwise distance to the attachment point and the local disturbance level. These amplified disturbances are then fed into the host boundary layer at the shear layer/boundary layer flow interface or via the attachment point and are then convected downstream. The trip wire has not introduced disturbances per se, rather it has acted, via the shear layer, as a pre-amplifier for the small ever present disturbances. Experimental verification of this process for two-dimensional trip wires fixed to a flat plate has been provided by Klebanoff and Tidstrom (ref.37). Moreover, it has recently been demonstrated theoretically by Fasel et al.(ref.38) that if disturbances whose magnitude exceeds approximately 1% of the free stream speed are introduced into the flat plate boundary layer (Blasius profile) then they may be amplified at Reynolds numbers where only damping was predicted by linear stability theory. Consequently, it is possible to produce transition by the amplification of disturbances at Reynolds numbers which are lower than the minimum

* See Hama et al. (reference 40)

critical value predicted by linear stability theory even if the mathematical model includes the effects of non-parallel flow. Once again there is flat plate experimental evidence which confirms this result see, for example, Tani (ref.39). Finally at some suitably large combination of roughness height and Reynolds number the shear layer will either become turbulent before attachment or, as Hama (ref.40) has noted in water table experiments and Fasel has found in the theoretical studies for the flat plate, if d is greater than 75% of the displacement thickness, periodic vortex shedding may occur with the vortices becoming prototype turbulent bursts. In either case the host boundary layer would be expected to be turbulent provided that conditions are such that the turbulence is self sustaining.

Refering to figure 26 it may be postulated that for values of d/ψ less than 0.8 the disturbances in the vicinity of the trip wire are either too small to affect transition even after a degree of free shear layer pre-amplification or they may be fed into the host boundary layer at the wrong level since, presumably, the point of introduction of a disturbance can also be a factor in the transition process. For values of d/ψ lying between 0.8 and 1.55 a comparison of figures 25 and 26 shows that there is a region of laminar flow separating the trip wire and the transition front. This suggests that the free shear layer produced by the trip remains laminar to attachment whilst providing disturbance levels which are sufficiently large to undergo non-linear amplification and consequently produce transition at values of ϕ which are smaller than the linear stability limit of 600 ($R_{\delta 2}$ = 240, figure 23). In reference 31 Pfenninger presents hot-wire measurements made at the attachment line of a 45^0 swept wing. In the clean wind tunnel the attachment line boundary layer did not amplify any disturbances until ϕ was in excess of 570 ($R_{\delta 2} > 230$). However when grid turbulence was introduced ahead of the model amplification was observed at lower values of ϕ. Although no details of the disturbance level for the grid turbulence are presented it is clear that the levels could well have exceeded the threshold for non-linear amplification i.e. $u^1/U_e > 1\%$. When d/ψ is greater than 1.55 it appears that the free shear layer is undergoing transition to turbulence before it attaches to the wall. Consequently there is little or no laminar attachment line flow downstream of the trip, the dependence upon s/ψ is reduced and since the mechanism governing transition has changed there is a discontinuity in the functional relationship between ϕ_{crit} and d/ψ i.e. a kink would be expected. Moreover, for d/ψ in excess of 1.55 the fact that local conditions at the trip wire are dominating the transition is reflected in the form of the approximate criterion of equation (5.5.9) (see figure 25).

For values of ϕ below 300 it is found that a trip wire cannot produce a continuously turbulent boundary layer and when ϕ is approximately 245 only isolated bursts propagate indefinitely along the attachment line. This is consistent with the results of Gasters work on the behaviour of spark induced turbulent bursts which were sufficiently long for their leading and trailing edges to be independent of one another. From his observations he was able to conclude that the bursts contracted if ϕ was less than 280 but grew for larger values. The curves presented in figure 19 show that when ϕ is less than 400 relatively short bursts of turbulence originate at the trip wire and decay as they travel along the attachment line. This behaviour strongly suggests that the laminar layer is stable to those disturbances whose amplitudes are typical of those found in the turbulent flows. Moreover, this being the case, if conditions in the turbulent boundary

layer are such that the turbulence can no longer be maintained then the layer will revert to its laminar form. It follows that the lower limit for turbulent flow ($\phi \simeq 300$) may well be caused by the failure of the turbulence, which is introduced directly by the trip wire, to sustain itself by the generation of an adequate turbulence production rate. For the case of contamination by a very large trip wire or a turbulent boundary layer formed on a streamwise flat plate it was found that the critical values of ϕ were the same irrespective of whether the layer was changing from laminar to turbulent flow (speed increasing) or vice versa (speed decreasing). This provides evidence in support of the non self-sustaining turbulence hypothesis since in the first instance the wire or flat plate always feeds turbulence into the laminar layer in the form of bursts and these only expand when the critical conditions are exceeded, whilst in the second instance there is no laminar flow at any point on the attachment line before conditions drop below the critical level. Clearly the turbulence is the common feature in both situations and, consequently, the lower limit for turbulent flow is expected to depend upon turbulent flow properties. However, in the incompressible case covered by the present experiment the use of a criterion based upon ϕ is correct since it has been shown in section 1 that the properties of the turbulent attachment line are functions of ϕ alone. The success of earlier criteria based upon $R\delta_{2L}$ is due to the fact that this parameter too is a function of ϕ alone. In addition it is interesting to note that the phenomenon of non self-sustaining turbulence is not unique to the attachment line.

It has been known since 1883 that fully turbulent pipe flow cannot be maintained below a Reynolds number, R_D, (based on mean flow velocity) of approximately 4000 no matter how rough the walls or disturbed the entry conditions. By defining a pipe momentum thickness as

$$\theta = \int_0^{d/2} \frac{u}{U_{CL}} \left(1 - \frac{u}{U_{CL}}\right) \left(1 - \frac{2z}{d}\right) dz$$

where U_{CL} is the centre line velocity, it follows that for turbulent flow a pipe Reynolds number of 4000 corresponds to a momentum thickness Reynolds number, $R_{\delta 2}$ of 175. Although the flow at this Reynolds number is essentially fully turbulent the velocity profiles do not obey the law of the wall until $R_{\delta 2}$ is greater than 200, see Preston (ref.41). On the basis of the pipe result and a small amount of experimental data Preston has postulated the existence of a minimum value of $R_{\delta 2}$ for fully turbulent flow on a flat plate and has shown that for the law of the wall to be valid $R_{\delta 2}$ must exceed approximately 320. The present results for the attachment line may be expressed in terms of $R_{\delta 2}$ by the use of figure 4 from which it follows that the flow is essentially fully turbulent when $R_{\delta 2}$ is approximately 235 whereas the profile measurements made by Cumpsty and Head (ref.13) show that the flow obeys the law of the wall when $R_{\delta 2}$ is greater than 330.

Finally, although the values of ϕ for the beginning and end of transition are, in general, functions of d and s it was found that the intermittency distributions of figure 22 could be represented by a single function if Γ was plotted against the normalised coordinate ζ_1 where

$$\zeta_1 = \frac{\phi - \phi)_{\Gamma = 0.5}}{\phi)_{\Gamma=0.75} - \phi)_{\Gamma=0.25}} \qquad 5.5.12$$

The results are presented in figure 27 together with the Gaussian probability distribution and the 'universal' flat plate intermittency distribution proposed by Narasimha (ref.42) i.e.

$$\Gamma = 1 - EXP(-0.412\ (\zeta_1 + 1.3)^2)$$

It is apparent that the various distributions possess some statistical similarity in much the same way as they do for the flat plate boundary layer. In addition the form of the intermittency distribution tends to suggest that the breakdown of the laminar flow may be caused by the appearance of point sources of turbulence in the vicinity of some specific value of s, s_1 say,with the rate of source production being a maximum at s_1 and varying around s_1 in some near Gaussian manner. The resulting dependence of Γ upon ϕ is governed by the growth of these sources as they are convected along the attachment line with the growth rate being a function of ϕ and s. Narasimha's distribution is based upon Emmons' theory (ref.43) with the additional assumption that all the point sources appear at s_1 i.e. the source rate density function is approximated by the Dirac delta function and although the present data appear to be better correlated by the Gaussian distribution Narasimha's result has the advantage that it may be re-arranged into a form which is explicitly dependent upon the value of ϕ at the beginning of transition, ϕ_T i.e.

$$\text{if} \qquad \zeta_2 = \frac{\phi - \phi_T}{\phi)_{\Gamma=0.75} - \phi)_{\Gamma=0.25}}$$

$$\text{then} \qquad \Gamma = 1 - EXP\ (-0.412 \cdot \zeta_2^2) \qquad 5.5.13$$

This form is particularly useful since it is easily incorporated into calculation methods for transitional flows

From the measurements of skin friction presented by Cumpsty and Head (ref.13) it is found that for the case of transition produced by a large trip wire ($d/\psi > 2.5$) the value of ϕ at which departure from the laminar variation is observed at large values of s/ψ is in complete agreement with value at which the first regular bursts of turbulence are found. However, the flow does not exhibit fully developed turbulent skin friction levels until ϕ has exceeded a value of 380 whereas the hot-wire signal indicated completely turbulent flow when ϕ is only 300. This rather large discrepancy, which was noted by Cumpsty and Head suggests that the streamwise (along the attachment line) length of the spot varies with distance from the solid surface i.e. it is narrower at the wall than at some point above the wall. Although the present investigation was not sufficiently detailed to define the geometry of the bursts the result is consistent with the shape of turbulent bursts found in flat plate boundary layer transition, see for example Wygnanski et al. (ref.44).

If the difference in the widths of the transition region is due to an intermittency phenomenon and final proof of this can only come from a more detailed experiment, then it should be possible to relate the definition of ζ_2 to the critical values of ϕ given in figures 19 and 20. From the skin friction data of reference 13

$$\phi_T = 240$$

and if $\Gamma(\phi) = \left(\frac{Cf - Cf_{lam}}{Cf_{turb} - Cf_{lam}}\right)_{\phi}$

where Cf laminar is given by equation (2.3.4) and Cf turbulent by equation (2.4.1) then

$$\phi)_{\Gamma=0.75} - \phi)_{\Gamma=0.25} = 37$$

whereas from figures 11 and 12

$$\phi_{FB} = 240$$

$$\phi_{CT} - \phi_{FB} = 60$$

For the calculation of skin friction in the transition zone it is tentatively suggested that the intermittency factor may be calculated from equation (5.5.13) where

$$\zeta_2 \simeq \frac{\phi - \phi_{FB}}{0.6(\phi_{CT} - \phi_{FB})} \qquad 5.5.14$$

5.6 The Influence of Mach Number and Wall Temperature

The experiment described in the previous sections was conducted under essentially incompressible conditions (maximum $M_\infty \simeq 0.15$) and, therefore, before the criteria can be applied to situations for which the effects of compressibility and heat transfer are significant it is necessary to investigate the influence of Mach number and wall temperature.

Firmin and Cook (ref.45) performed experiments on a wing with an R.A.E.100 section and a thickness/chord ratio of 0.25 normal to the leading edge. The tests were carried out in the R.A.E. 8' x 6' transonic wind tunnel with the attachment line contaminated by a single glass sphere. In the presence of large spheres the transition region was found to extend from a ϕ of 238 to a ϕ of 273 where these values were independent of Mach number up to the maximum free stream speed used (M_∞ of 0.7). Moreover, the minimum roughness Reynolds number, R_d, for the 'gross' roughness transition characteristics was found to be in good agreement with Gregory's 'incompressible' result for single conical excrescences (ref.10). These results suggest that for high subsonic free

stream Mach numbers, the main features of figures 25 and 26 remain unchanged provided that transition is still being controlled by the tripping device.

For the case of supersonic free stream Mach number there have been several experimental studies of the local heat transfer rate at the attachment line of a swept circular cylinder which have included measurements taken in the transition region between laminar and turbulent flow. Beckwith and Gallagher (ref.20) recorded local heat transfer rates for various sweep angles with a free stream Mach number of 4.15, free stream Reynolds numbers in the range 1×10^6 to 4×10^6 and a wall to stagnation temperature ratio of approximately 0.8. In addition they measured average heat transfer rates for the front halves of two cylinders of different diameters under similar free stream conditions. The experimental arrangements in each case were such that the attachment line was contaminated with a boundary layer generated on a streamwise end plate. Bushnell (ref.24) performed similar measurements for a swept cylinder mounted at various angles on the surface of a 12^0 wedge which provided the contaminating disturbance. The experiment was conducted at a free stream Mach number of 8.0, free stream Reynolds numbers in the range 7×10^4 to 9×10^5 and wall to stagnation temperature ratio of about 0.4. Finally, Brun, Diep and Le Fur (ref.23) present similar results for a cylinder mounted on a streamwise flat plate with a free stream Mach number of 2.42, free stream Reynolds number of 1×10^5 and a wall to stagnation temperature ratio of approximately 1.

In the previous section it was argued that when transition is induced by a gross disturbance the criterion should depend upon turbulent flow properties and in section (2.4) it was shown that turbulent skin friction and heat transfer rate were functions of the variable ϕ_*. Consequently ϕ_* might be expected to be a useful parameter for the determination of those conditions necessary for transition. As a first step the transition heat transfer results of references 20 and 24 were transformed into intermittency distributions in terms of ϕ_* by means of equations (2.1.5), (2.4.4) and (2.4.6) together with -

$$\Gamma = \left(\frac{Nu - Nu_{lam}}{Nu_{turb} - Nu_{lam}}\right) \quad \begin{array}{l} \phi = \text{constant} \\ Me = \text{constant} \\ \frac{Tw}{Te} = \text{constant} \end{array}$$

The distributions produced in this way were then normalised in terms of the parameter ζ_2 where

$$\zeta_2 = \frac{\phi_* - \phi_{*_\Gamma}}{\phi_*)_{\Gamma=0.75} - \phi_*)_{\Gamma=0.25}}$$

and the results are presented in figure 28 together with the flat plate intermittency distribution due to Narasimha (ref.42). It can be seen that despite the scatter the data is evenly distributed about the theoretical line. Figures 29(a) and 29(b) show the corresponding variation of ϕ_{*_Γ} and $\phi_*)_{0.75} - \phi_*)_{0.25}$ with the Mach number at the edge

of the boundary layer, Me, and the wall to edge temperature ratio Tw/Te. The available transition data show no consistent variation with either Me or Tw/Te and hence conditions in the transition region may be well represented by the following -

For $\phi_* > 250$

$$\Gamma = 1 - EXP\ (-0.412.\zeta_2^2) \qquad 5.6.1$$

when $\zeta_2 = \frac{\phi_* - 250}{40}$

From which it may be deduced that transition begins when ϕ_* is 250 and is essentially complete when ϕ_* reaches a value of 384 ($\Gamma = 0.99$)

This transition criterion may be compared directly to the criterion published by Bushnell in reference 46. Bushnell's criterion is applicable to "configurations having end plates or adjoining surfaces" and is

$$(R_{D_\infty})_{Transition} \simeq 2 \times 10^5 \qquad \text{within } 30\%$$

$$\text{for} \quad \Lambda > 40^0 \qquad 5.6.2$$

$$\text{and} \quad 2.5 < M_\infty < 8$$

This result is based upon a survey of the heat transfer data for swept leading edges much of which is not available in the open literature. Figure 30 presents the results of calculations for the free stream Reynolds number, R_{D_∞} corresponding to $\phi_* = 302$ (Γ=0.5) for sweep angles in the range 40^0 to 75^0, free stream Mach numbers varying from 2.5 to 8.0, wall to total temperature ratios typical of flight through the upper atmosphere $(Tw)_{max} = 1700^0K$ $Tw)_{min} = 288^0K$) and total temperatures typical of both wind tunnel and flight environments. It is found that for wind tunnel conditions the present criterion predicts values of R_{D_∞} which are evenly distributed about 2×10^5 with a maximum deviation of ±50%. For flight conditions the present criteria produces values of Rd_∞ which are distributed around a value of approximately 1.4×10^5 (±50%). Having due regard for the fact that the calculations are based upon extreme conditions and Bushnell's criterion probably relies heavily upon experimental data taken from wind tunnels it may be concluded that the present criterion is entirely consistent with the one suggested by Bushnell whilst possessing a much wider range of validity. In addition it is also possible to compare the present result to a piece of pioneering work produced by Topham in 1964 (ref.47). He was the first to recognise the importance of the attachment line conditions in determining the transition from the laminar to the turbulent boundary layer state for swept circular cylinders in supersonic flow and he

attempted to produce a transition criterion in terms of constant values of $R_{\delta 2L}$ at the attachment line. By using the results of reference 20 he concluded that transition took place as $R_{\delta 2L}$ was increased from 130 ($\phi_* \simeq 310$) to 450 ($\phi_* \simeq 1070$). Although the result for the beginning of transition is close to the present value the prediction of complete turbulence is a considerable over estimate, being almost three times the current value, and since the criterion was based upon $R_{\delta 2L}$ it was only valid for situations with small heat transfer rate. The main reasons for this large discrepancy are, firstly, there was only one complete set of experimental results available and, secondly, Topham used the theory of Beckwith and Gallagher (ref.20) to determine the conditions at which fully turbulent conditions were obtained.

For the low speed transition it was noted that when the attachment line was tripped to the turbulent state the critical values of ϕ_* did not exhibit any hysteresis. This may well have been due to the fact that the entire attachment line including the source of the turbulence (trip wire or wing/plate junction) was aware of the variations in ϕ_*. However, this may not always be the case in high speed flow. Consider the situation sketched in figure 31 where a swept cylinder is mounted on a wedge of semi-angle Θ with a free stream Mach number which is much greater than 1. In region 2 the effective 'free stream' flow properties for the cylinder depend upon the conditions in region 1 and the wedge semi-angle. The effect of the oblique wedge shock is such that

$$M_2 < M_1$$

$$R_{D2} > R_{D1}$$

whilst $\Lambda_2 = \Lambda_1 + \Theta$

Therefore it is quite feasible that the values of ϕ_* in region 2 may be greater than 384 and, consequently, the attachment line will be turbulent due to contamination by the wedge boundary layer whilst in region 1 ϕ_* is less than 384. As the fully turbulent attachment line boundary layer passes through the expansion fan generated as a result of the intersection of the wedge shock and cylinder bow shock there will be a rapid drop in pressure together with the reduction of $\phi*$. Clearly the turbulence cannot disappear immediately and so it would be expected to persist for some distance along the span (possibly indefinitely). References 23 and 24 contain heat transfer measurements for this particular situation and these data show that fully developed heat transfer rates are possible locally at values of ϕ_* as low as 250. There are no examples of complete turbulence for $\phi*$ less than 250. In this case it would appear that the persistence of turbulence at subcritical values of $\phi*$ is related to the re-laminarisation problem since the source of the turbulence (wedge/cylinder junction) and the attachment line boundary layer in region 2 remain unaware of the low value of $\phi*$ in region 1 . Therefore care must be taken when applying the criterion given in equation (5.6.1) to situations where body shocks intersect wing bow shocks.

At present it is not possible to produce a reliable criterion for transition induced by small free stream disturbances in high speed compressible flow. However, Bushnell (ref.46) states that for delta wing leading edge models, for which end contamination from an adjoining surface would not be present, the available data indicate that the attachment line boundary layer may remain laminar up to $R_{D\infty}$ of 8×10^5 (there being no data beyond this value). It may be inferred from figure 30 that a Reynolds number of 8×10^5 corresponds to a ϕ value of about 600 (since $\phi \propto (R_{D\infty})^{\frac{1}{2}}$). This result may be compared with the low speed experimental work where laminar flow was possible up to a ϕ of 600 (see figure 19). Therefore it is tentatively suggested that a conservative estimate for the upper limit of laminar flow may be given by

$$\phi \simeq 600 \qquad 5.6.3$$

5.7 Physical Implications of the Gross Disturbance Criterion

In the previous section it was shown that in the presence of a very large disturbing influence fully developed turbulent flow at the attachment line was only possible for values of ϕ_* in excess of 384. Having developed a criterion for turbulence it is useful to assess the physical implications in the limits of Mach number variation using the asymptotic relationships which have already been developed.

Refering to section 2 equations (2.3.7) and (2.4.2.) or (2.3.4) and (2.4.1) reveal that

$$\frac{h_{turb}}{h_{lam}} = \frac{\tau_{turb}}{\tau_{lam}} = 0.0519\left(\frac{\mu_*}{\mu_e} \cdot \frac{T_e}{T_*}\right)^{0.5} \phi_*^{0.6} \qquad 5.7.1$$

Taking the incompressible limit first, it was found in section 3 that

$$\frac{T_*}{T_e} \rightarrow 0.80 + 0.20 \frac{T_w}{T_\infty}$$

if in addition it is assumed that the viscosity/temperature relationship may be adequately represented by

$$\frac{\mu_*}{\mu_e} = \left(\frac{T_*}{T_e}\right)^{0.76}$$

then it follows that

$$\frac{h_{turb}}{h_{lam}} = \frac{\tau_{turb}}{\tau_{lam}} \simeq \frac{0.0519 \ \phi_*^{0.6}}{(0.80+0.20\frac{T_w}{T_\infty})^{0.12}} \qquad 5.7.2$$

The ratio of the heat transfer rates (skin friction) increases continuously with increasing ϕ_* and has its least value when $\phi_* = 384$ i.e.

$$\left(\frac{h_{turb}}{h_{lam}}\right)_{min} \simeq \frac{1.843}{(0.80+0.20\frac{T_w}{T_\infty})}0.12 \qquad 5.7.3$$

It can be seen that for all physically realistic values of T_w/T_∞ the turbulent heat transfer rate (skin friction) is always greater than the laminar for identical body geometry and free stream conditions.

Using the hypersonic relations presented in equation (3.1.5) and (3.2.5) together with Sutherlands law for the viscosity/temperature relationship it is readily shown that in the limit of infinite free stream Mach number -

$$\frac{\mu_*}{\mu_e} \cdot \frac{T_e}{T_*} \rightarrow \frac{1}{(0.80 + 0.36\ \tan^2\Lambda)}0.5$$

and consequently equation (5.7.1) becomes

$$\frac{h_{turb}}{h_{lam}} = \frac{0.0519\ \ \phi_*^{0.6}}{(0.80 + 0.36\ \tan^2\Lambda)}0.25 \qquad 5.7.4$$

Once again the ratio of the laminar and turbulent results increases with increasing ϕ_* whilst the least value is given by -

$$\left(\frac{h_{turb}}{h_{lam}}\right)_{min} = \frac{1.843}{(0.80 + 0.36\ \tan^2\Lambda)}0.25 \qquad 5.7.5$$

This ratio remains greater than unity until a sweep angle of 80^o is reached. Although the prospect of a turbulent heat transfer rate which is less than the laminar one for identical conditions is rather intriguing it should be noted that at a sweep angle of 80^o the free stream Mach number must exceed 40 before the hypersonic relations of equations (3.1.5) and (3.2.5) are good approximations to the exact results. For a free stream Mach number of 10 equation (5.7.5) is only valid for sweep angles less than 45^o and 70^o for a Mach number of 20. When the minimum value for the ratio of heat transfer rates is calculated from equation (5.7.1) for a sweep angle of 80^o it is found that the ratio is approximately 1.34 for a Mach number of 10 and 1.13 for a Mach number of 20. Therefore it may be concluded that for the range of conditions within which the formulae of section 2 are valid the present transition criterion produces physically realistic and consistent results.

5.8 Implications for Flight Conditions

Since the criteria for the prediction of transition have been developed for an infinite swept cylinder it is possible to apply them to slender bodies at incidence and swept wings with equal validity. However, for the purposes of illustration the implications of 'full scale' conditions will be assessed for the swept wing only.

As a first step ϕ_* is written in terms of free stream conditions

$$\phi_* = \left(R_{D_\infty} \cdot \frac{\sin\Lambda.\tan\Lambda.Co}{U_1 \quad D} \cdot \left(\frac{\mu_\infty}{\mu_*}\right) \cdot \left(\frac{Te}{T_*} \cdot \frac{T_\infty}{Te} \cdot \frac{p_e}{p_\infty}\right) \right)^{\frac{1}{2}} \qquad 5.8.1$$

where $$\frac{\mu_\infty}{\mu_*} = f\left(\frac{T_*}{Te} \cdot \frac{Te}{T_\infty}\right)$$

For zero heat transfer it is apparent that with the exception of $U_1.\frac{D}{Co}$ the parameters occuring in equation (5.8.1) are simple functions of Mach number, sweep angle and atmospheric conditions alone. For subsonic flow $(U_1.D/Co)$ is, in general, a function of the whole aerofoil geometry, the incidence (lift coefficient) and the Mach number normal to the leading edge. The estimation of $(U_1.D/Co)$ from experimental results is difficult since the measurements are usually insufficiently detailed in the vicinity of the attachment line. Moreover, an accurate theoretical calculation presents formidable difficulties unless an analytic velocity distribution, e.g. the conformal mapping of the flow around a circle, is available. The simplest case of an aerodynamically useful shape is that of the ellipse for which it is easily shown that at zero incidence

$$\frac{U_1 D}{Co} = 2(1 + b/a) \qquad 5.8.2$$

where a is the semi-major and b the semi-minor axis. Equation (5.8.2) suggests that for slender shapes the velocity gradient, U_1 is primarily a function of leading edge radius. The elliptic results may also be extended to include the effects of lift by setting the section at incidence and applying the Kutta condition to the aft end of the major axis. Hence for small angles of incidence -

$$\frac{U_1}{U_{1\ \alpha=0}} = \frac{1}{(1 + ((\frac{a}{b})^2 - 1)\ 4\alpha^2)} \qquad 5.8.3$$

with α measured in radians. This implies that the effect of incidence increases with increasing slenderness ratio and, therefore α may be an important parameter when dealing with thin aerofoils in 'off design' situations. The results for the ellipse may also be modified to include the effects of compressibility. This is achieved by the assumption that the complete solution may be expressed as a power series in $M_\infty\cos\Lambda$ (Rayleigh-Janzen series) and that the first two terms provide a valid approximation. The first term is taken to be the incompressible value

and the second is a correction term. Appendix D contains a detailed account of the evaluation of the correction term and so only the result is presented here

$$U_1 = U_{1_{m=0}} \left(1+M_\infty^2\cos^2\Lambda\left(\frac{1-\sigma^2}{4\sigma^2}\right)\left(1-\frac{1}{(1-\sigma^2)}\left(\frac{1+6\sigma^2+\sigma^4}{2\sigma^2}\ \ell n\frac{1+\sigma^2}{1-\sigma^2} - 2\left(\frac{1+\sigma^2}{\sigma}\right)\ell n\frac{1+\sigma}{1-\sigma} + 4\right)\right)\right) \qquad 5.8.4$$

where $\sigma^2 = \dfrac{1 - b/a}{1 + b/a}$

Although the validity of this expression is limited to the zero lift case alone, small angles of incidence are unlikely to introduce significant error. For simple calculations it is found that equations (5.8.2) to (5.8.4) can provide good approximations to (U_1 D/Co) for typical aerofoil sections if b/a is determined by the relation

$$\left(\frac{b}{a}\right)_{effective} = \left(40\left[\frac{\rho}{Co} - 10\left(\frac{y}{Co}\right)^2_{x/Co=0.05}\right]\right)^{\frac{1}{2}} \qquad 5.8.5$$

Figure 32 presents the variation of (U_1 D/Co) with t/C_0, α and $M_\infty\cos\Lambda$ for an aerofoil with an R.A.E. 101 section according to the elliptic approximations.

In situations where the flow normal to the leading edge is supersonic the evaluation of (U_1 D/Co) is simplified by the reduced influence of the section geometry. An increase in Mach number causes the sonic lines to approach the attachment line thereby eleminating all contribution from the downstream geometry. If the Mach number is sufficiently high the local conditions at the attachment line will depend upon the local radius of curvature alone. Under these circumstances it is found that the surface pressure distribution may be represented by the Modified Newtonian formula -

$$\frac{Cp}{Cp_{stag}} \simeq \cos^2\left(\frac{x}{r}\right) \qquad 5.8.6$$

From this it may be shown (see Appendix A)

$$\left(\frac{r}{U_\infty}\cdot\frac{dUe}{dx}\right)_{x=0} = \frac{1}{M_\infty\cos\Lambda}\left(\frac{2}{\gamma}\cdot\frac{Te}{T_\infty}\left(1 - \frac{p_\infty}{p_e}\right)\right)^{\frac{1}{2}} \qquad 5.8.7$$

hence

$$\frac{U_1 D}{Co} = 2.\left(\frac{r}{U_\infty}\cdot\frac{dUe}{dx}\right)_{x=0}\cdot\frac{\rho}{r} \qquad 5.8.8$$

The variation of the attachment line velocity gradient as predicted by equation (5.8.7) is shown in figure 33.

Equations (5.8.1) to (5.8.8) have been used to calculate the transition boundaries for the attachment line layer formed on a swept wing with an R.A.E.101 section normal to the leading edge and a thickness chord ratio of 12% operating at 35,000' in the Standard Atmosphere. This particular situation has been chosen since it is typical of the cruise conditions for a modern civil aircraft and the range of leading edge radii used encompasses most types in service at present. Figure 34 presents the boundaries for gross contamination i.e. transition to turbulence as Φ_* increases from 245 to 300, whilst figure 35 shows the smallest two-dimensional roughness height consistent with these boundaries i.e. $d/\psi = 2$. It is apparent from the data listed in table 1 and presented graphically in figure 36 that the majority of present generation aircraft will have turbulent flow at the leading edge in the cruise condition since wing sweep angles are generally larger than the critical values. Furthermore the results of figure 35 indicate that any attempt to produce laminar flow without reducing wing sweep would involve first preventing root contamination by the fuselage boundary layer and secondly maintaining a very smooth leading edge. Figure 37 illustrates the potential boundaries for a leading edge whose equivalent two-dimensional roughness height is kept below the levels indicated in figure 38. The transition shown in figure 37 takes place as ϕ increases from 600 to 700 and the roughness heights are calculated on the basis of d/ψ equal to 0.8 when ϕ equals 600. The results for the smaller leading edge radii suggests that a laminar attachment line layer is possible provided the disturbances are kept within the specified minimum. However, for the larger radii, which are typical of those found on current 'wide body' aircraft, the potential behaviour is hardly sufficient to guarantee laminar flow since the permitted sweep angles for a cruise Mach number of 0.8 are still below 40^{o}.

6. TRANSITION VIA THE MECHANISM OF CROSS FLOW INSTABILITY

6.1 General Remarks on the Stability of Three-Dimensional Boundary Layer Flows

In general, three-dimensional flows are characterised by the presence of streamline curvature. For the flow outside the boundary layer the effect of viscosity is usually negligibly small and, consequently, this curvature must be maintained by a pressure gradient normal to the streamline (centrifugal forces balanced by pressure forces). However, inside the boundary layer viscosity causes the velocity, and hence the centrifugal forces, to decrease as the wall is approached whilst the pressure gradients remain essentially unaltered since $\partial p/\partial z$ is very small. The result of this viscous induced imbalance is an increase in curvature for the streamlines inside the boundary layer, which implies a transportation of fluid in a direction inclined to the direction of the streamlines at the edge of the layer. A simple sketch of this process is given in figure 39. The extra motion of the fluid may be described in terms of a cross flow profile which is the velocity profile taken in a direction normal to the external streamline. Cross flow profiles have the general properties of zero velocity at the wall and boundary layer edge and a maximum velocity at some point within the layer. It should be noted, however, that the velocity is not necessarily limited to a single sign as shown in figure 39 and there may in fact be several local velocity maxima.

There have been several direct and indirect investigations into three-dimensional boundary layer transition where surface flow visualisation techniques have been used to detect the transition fronts. Under the appropriate conditions it has been found that transition has occured at much lower Reynolds numbers than would be expected from simple quasi two-dimensional considerations and the visualisation technique has revealed a well ordered, closely spaced streak pattern nearly aligned with the external streamline in the laminar region immediately preceeding the transition front. Examples discovered so far are flow over a swept back wing (see figure 3), flow over an inclined ellipsoid (see Eichelbrener and Michel, ref.48), flow over a spinning axisymmetric body at zero incidence (Knapp and Roache, ref.49), flow over the leeward side of a slender delta wing (Squire, ref.50), flow over a disc rotating at high angular velocities (Gregory et al. ref.5 also Fales ref.51) and, finally, flow over a stationary surface when the fluid above it is in rotation (Lilly ref.52). The visualisation techniques which have shown the streak pattern are surface oil flow, china-clay evaporation, dye injection into water and smoke. In the past it has been supposed that these streaklines have been produced by the presence of stationary vortices inside the laminar boundary layer - directly analogous to the Taylor-Göertler vortices found in the two-dimensional boundary layer on a concave surface and that the 'premature' transition has been induced by the bursting of these vortices. However, it will be shown that this need not necessarily be the case and, indeed, the word 'premature' may be totally inappropriate to this form of transition

Figure 40 presents a coordinate system suitable for any of the cases mentioned above, however, in the present context the emphasis will be placed upon the problem of transition on the swept back wing. In the figure t denotes the direction tangential to the external streamline and n the normal, with the t direction inclined at an angle θ to the surface coordinate x. For the infinite swept wing case x is the distance measured along the surface from the attachment line in a direction perpendicular to the leading edge and the angle θ is given by the familiar equation

$$\tan\theta = \frac{dy}{dx} = \frac{V_\infty}{U_e} \qquad 6.1.1$$

In addition an arbitrary set of orthogonal axes t_ε and n_ε are shown where t_ε is inclined at an angle ε to the t direction. Having defined a co-ordinate system figure 41 presents a typical variation for the velocity profile in the n_ε direction as ε increases from 0^o to 90^o. It should be noted that the cross flow profile ($\varepsilon = 0$) shown is of the single sign (all velocities negative), single maximum type which is typical of those found on a swept wing in the region between the attachment line and the peak suction isobar or at any point well away from the perimeter of a rotating disc. However for the sake of graphical clarity, the profiles are not drawn to scale.

Stuart (ref.5) has demonstrated that for very small disturbance levels in a localised region of a three-dimensional incompressible boundary layer, the velocity component in the direction of propogation of the disturbance may be regarded as a two-dimensional flow for stability purposes and the usual linear stability theory applied. The problem is, therefore, reduced to the solution of the Orr-Sommerfeld equation -

$$\left(\frac{u}{U_\infty} - \frac{\omega}{\alpha}\right)\left(\frac{d^2\sigma}{d(z/L)^2} - \alpha^2\sigma\right) - \frac{d^2(u/U_\infty)}{d(z/L)^2}\cdot\sigma = -\frac{i}{\alpha R}\left(\frac{d^4\sigma}{d(z/L)^4} - 2\alpha^2\frac{d^2\sigma}{d(z/L)^2} + \alpha^4\sigma\right) \qquad 6.1.2$$

(see equation (5.5.6) of section (5.5)). Solutions of equation (6.1.2) for a given profile ($u(z)$ and $u''(z)$) are usually presented graphically and the typical form is sketched in figure 42. It can be seen that for Reynolds numbers larger than R_{crit} disturbances with wave numbers which lie within the neutral loop will be amplified whilst those outside will be damped and consequently R_{crit} represents the lower limit for which any small disturbance may be amplified.

Although the value of R_{crit} may only be obtained by a full solution of equation (6.1.2) it has been found that a good deal of useful information may be provided by the solution of the much simpler Rayleigh equation.

$$\left(\frac{u}{U_\infty} - \frac{\omega}{\alpha}\right)\left(\frac{d^2\sigma}{d(z/L)^2} - \alpha^2\sigma\right) - \frac{d^2(u/U_\infty)}{d(z/L)^2}\cdot\sigma = 0 \qquad 6.1.3$$

which represents equation (6.1.2) in the limit of very large Reynolds number ($R \to \infty$). A thorough examination of the implications of this equation when applied to the profiles of figure 41 is presented by

Stuart (reference 5). The results of direct relevence to the present investigation are firstly, profiles which contain a point of inflection (i.e. types m of figure 41) are ALWAYS unstable at very large Reynolds number and, secondly, when the inflection point coincides with a point of zero velocity i.e. $\epsilon = \epsilon_I$ - figure 41, the profile, commonly called the 'critical' profile, may amplify disturbances with zero phase velocity. Clearly, such disturbances could result in the formation of vortices which are stationary relative to the solid surface and which might be detected by flow visualisation techniques if their strength became sufficiently large. Moreover, when these theoretical results are supplemented by the practical observation that two-dimensional laminar velocity profiles whose shapes are similar to the pure cross flow type ($\epsilon = 0$) e.g. wake, jet, free convection layer (reference 53), wall jet (reference 54) and impulsively stopped flat plate (reference 51) or rotating cylinder (reference 55) undergo transition via a mechanism which involves the formation of discrete vortex lines normal to the direction of flow, but which are in motion relative to the solid surface. This phenomenon is found to occur at Reynolds numbers, based upon viscous layer thickness, in the range 100 to 1000 whilst more conventional two-dimensional profiles ($\epsilon = 90^o$) require Reynolds numbers in the range 10,000 to 100,000 for transition. It may be concluded that in situations where the flow is highly three-dimensional the initial small disturbance instability will be governed by the properties of the type m profiles (figure 41). However, the determination of the absolute minimum value of R_{crit} still requires a full solution of equation (6.1.2) for a range of values of ϵ.

For the infinite swept cylinder the determination of the velocity profiles at a general point, P, involves the solution of the simplified boundary layer equations -

$$u\frac{\partial u}{\partial x} + w\frac{\partial u}{\partial z} = Ue\frac{dUe}{dx} + \nu\frac{\partial^2 u}{\partial z^2}$$

$$u\frac{\partial v}{\partial x} + w\frac{\partial v}{\partial z} = \nu\frac{\partial^2 v}{\partial z^2} \qquad 6.1.4$$

$$\frac{\partial u}{\partial x} + \frac{\partial w}{\partial z} = 0$$

for an external (inviscid) flow of the form

$$Ue = Ue\,(x/C_o)$$

$$Ve = \text{constant} = V_\infty \qquad 6.1.5$$

If the full viscous stability calculations are to be performed (equation (6.1.2)) then it becomes necessary to calculate both the velocity and curvature profiles accurately. This means that any boundary layer calculation method must be numerically exact. It can be seen that, although the problem has been simplified considerably, the amount of computation necessary to determine the position of first instability is

extremely large and even if it is completed there is still the problem of predicting the position of transition. Consequently for practical purposes it is necessary to consider limiting cases only and base prediction criteria on experimental data.

Although the primary objective is the prediction of transition on a swept wing many of the concepts introduced will be applicable to three-dimensional flows in general. Therefore wherever possible the results for the swept wing will be compared directly with those for the case of the rotating disc which is a fully three-dimensional flow whose properties may be evaluated from a solution of the full Navier-Stokes equations and for which there is a large body of theoretical stability data and experimental transition data.

6.2 The Flow Close to the Infinite Swept Attachment Line

If the external velocity distribution in the x direction is expanded about the attachment line (x = 0) in the form of a power series -

$$\frac{U_e}{U_\infty} = U_1 \left(\frac{x}{C_0}\right) + U_3 \left(\frac{x}{C_0}\right)^3 + U_5 \left(\frac{x}{C_0}\right)^5 + \ldots\ldots \qquad 6.2.1$$

then for sufficiently small values of x there is always a region in which

$$\frac{U_e}{U_\infty} = U_1 \left(\frac{x}{C_0}\right) \qquad 6.2.2$$

is a good approximation to the actual velocity distribution. Further more if the length scale η is introduced where -

$$\eta = z\left(\frac{U_1 U_\infty}{\nu C_0}\right)^{\frac{1}{2}}$$

and the u and w components of the velocity are expressed in the form of a stream function such that

$$\psi = \left(\frac{\nu C_0}{U_1 U_\infty}\right)^{\frac{1}{2}} . U_e . f(\eta)$$

i.e. $u = \frac{\partial \psi}{\partial z} = U_e f'(\eta)$ and $w = -\frac{\partial \psi}{\partial x} = -\left(\frac{\nu U_1 U_\infty}{C_0}\right)^{\frac{1}{2}} f(\eta)$

then the boundary layer equations (6.1.4) have the following form -

Chordwise momentum $\quad f''' + ff'' - (f')^2 + 1 = 0 \qquad 6.2.3$

Spanwise momentum $\quad g'' + fg' = 0 \qquad 6.2.4$

where

$$\frac{v}{Ve} = g(\eta)$$

with boundary conditions -

$$\eta = 0 \quad f = 0 \quad f' = 0 \quad g = 0$$

$$\eta = \infty \quad f' = 1 \quad g = 1$$

It should be noted that the solution of equation (6.2.4) may be obtained by direct integration and applying the appropriate boundary conditions this may be written as -

$$g(\eta) = \frac{\int_0^{\eta} (\exp(-\int_0^{\eta} f \, d\eta))d\eta}{\int_0^{\infty} (\exp(-\int_0^{\eta} f \, d\eta))d\eta} \qquad 6.2.5$$

Therefore the problem is reduced to that of finding a solution for $f(\eta)$ from equation (6.2.3). However, since the chordwise momentum equation is independent of the spanwise momentum equation, equation (6.2.3) is unaffected by sweep angle and, consequently, it also represents the flow close to a two-dimensional stagnation point. The two-dimensional problem has been solved by several authors but for the present work the solution due to Bickley (see reference 9, page 232) has been used and the solution for $g(\eta)$ has been produced by numerical integration of the tabulated values of $f(\eta)$. The function $f^1(\eta)$ and $g(\eta)$ are presented as Table 2.

Having obtained the spanwise and chordwise boundary layer flows the profiles shown in figure 40 may be generated by a simple coordinate transformation -

$$\begin{aligned} s_{\varepsilon} &= v \sin(\theta-\varepsilon) + u \cos(\theta-\varepsilon) \\ c_{\varepsilon} &= v \cos(\theta-\varepsilon) - u \sin(\theta-\varepsilon) \end{aligned} \qquad 6.2.6$$

or alternatively

$$\begin{aligned} s_{\varepsilon}(\eta) &= V_{\infty}\sin(\theta-\varepsilon) \cdot \left(g(\eta) + \frac{f'(\eta)}{\tan\theta \cdot \tan(\theta-\varepsilon)}\right) \\ c_{\varepsilon}(\eta) &= V_{\infty}\cos(\theta-\varepsilon) \cdot \left(g(\eta) - \frac{f'(\eta)\tan(\theta-\varepsilon)}{\tan\theta}\right) \end{aligned} \qquad 6.2.7$$

For the present investigation there are two profiles which are of particular interest.

Case 1 $\epsilon = 0$

When ϵ equals zero the distributions of s_ϵ and c_ϵ are the pure streamwise and cross flow profiles in the t and n directions and equations (6.2.7) become

$$\frac{s(\eta)}{Qe} = \frac{V_\infty^2}{Qe^2}\left(g(\eta) + \left(\frac{Ue}{U_\infty}\right)^2 \cdot \frac{f'(\eta)}{\tan^2\Lambda}\right) \qquad 6.2.8$$

and $$\frac{c(\eta)}{Qe} = \frac{UeV_\infty}{Qe^2}\left(g(\eta) - f'(\eta)\right)$$

Therefore the shape of the streamwise velocity distribution is, in general, a function of U_1, (x/Co) and sweep angle, Λ, whereas the shape of the cross flow profile is independent of all the variables. This is a particularly useful result since the cross flow profile is one of the 'm' family (figure 41) which are believed to dominate the transition behaviour. Moreover if the velocity c is normalised with the profile maximum value, c_{max} where -

$$c_{max} = -0.240\,\frac{UeV_\infty}{Qe}$$

and the values of η are normalised with the value of η at which c is equal to 1% of c_{max} i.e.

$$\eta_{1\%c_{max}} = 3.490$$

then the profile is completely specified by a non-dimensional velocity distribution which is independent of all the variables and a Reynolds number – the cross flow Reynolds number χ where

$$\chi = \left/\frac{c_{max}\ \delta(1\%c_{max})}{\nu}\right/ \qquad 6.2.9$$

i.e. $$\chi = 0.240\frac{UeV_\infty}{Qe} \cdot 3.490\left(\frac{\nu x}{Ue}\right)^{\frac{1}{2}} \cdot \frac{1}{\nu} = 0.838\,\frac{V_\infty}{Qe}\left(\frac{Uex}{\nu}\right)^{\frac{1}{2}}$$

or $$\chi = 0.838\left(\frac{Uex}{\nu}\right)^{\frac{1}{2}}\left(1 + \left(\frac{U_1(x/C_o)}{\tan\Lambda}\right)^2\right)^{-\frac{1}{2}} \qquad 6.2.10$$

It follows that stability calculations for the cross flow profile are particularly simple since equation (6.1.2) can be solved once and for all using a suitably wide range of $\chi(R)$ and the results applied directly to any combination of U_1, x/Co and Λ provided that the equations (6.1.4) and (6.1.5) are valid.

The normalised cross flow profile is shown in figure 43 together with the radial profile for flow over a rotating disc (Cochran ref.56), the free convection profile for a verticle flat plate in air (Ostrach ref.57) and the plane wall jet (Glauert ref.58)all

suitably normalised with the maximum velocity and 0.01 c_{max} thickness. The corresponding cross flow Reynolds numbers are -

$$\text{Rotating disc} \qquad \chi = 1.267 \left(\frac{a^2\Omega}{\nu}\right)^{\frac{1}{2}}$$

$$\text{Free Convection Layer} \qquad \chi = 4.449 \left(Gr_x\right)^{\frac{1}{4}} \quad (Pr = 0.733)$$

$$\text{Plane Wall Jet} \qquad \chi = 2.490 \left(\frac{U.x}{\nu}\right)^{\frac{1}{4}} \qquad 6.2.11$$

Case 2 $\varepsilon = \varepsilon_I$

When ε equals ε_I the velocity profile is refered to as the critical profile and has a point of inflection which coincides with a point of zero velocity. Therefore ε_I must be such that the equations

$$c_I(\eta_I) = 0 = V_\infty \cos(\theta-\varepsilon_I) \cdot \left(g(\eta_I) - \frac{f'(\eta_I)\tan(\theta-\varepsilon_I)}{\tan\theta}\right)$$

and $$c_I''(\eta_I) = 0 = V_\infty \cos(\theta-\varepsilon_I) \cdot \left(g''(\eta_I) - \frac{f'''(\eta_I)\tan(\theta-\varepsilon_I)}{\tan\theta}\right)$$

are satisfied simultaneously i.e.

$$\frac{g(\eta_I)}{f'(\eta_I)} = \frac{g''(\eta_I)}{f'''(\eta_I)} = A$$

and $$\tan\varepsilon_I = \frac{(1-A)\tan\theta}{A\tan^2\theta + 1}$$

using the solution given in Table 2 it may be shown that

$$\eta_I = 1.382$$

$$A = 0.799 \qquad 6.2.12$$

and, therefore

$$\tan\varepsilon_I = \frac{0.201\tan\theta}{0.799\tan^2\theta + 1}$$

In general the shape of the critical profile is a function of all the independent variables and the stability characteristics will be different for different geometries (U_1), positions and sweep angles. However it should be noted that ε_I equation (6.2.12) has a maximum value of 6.42^o when θ takes a value of 48.21^o and the velocity profile corresponding to this maximum deviation is given by -

$$\frac{c_I}{Qe} = 1.119 . \frac{UeV_\infty}{Qe^2} \cdot (g(\eta) - 0{,}799\ f'(\eta)) \qquad 6.2.13$$

Figure 44 shows this velocity profile together with the corresponding profile for the rotating disc where a similar analysis shows that ε_I equals 13.30^o. It is not possible to include corresponding profiles for the free convection layer or the wall jet since these are purely two-dimensional flows.

6.3 Previous Theoretical and Low Speed Experimental Work

The de-stabilising effect of sweep back was first noted by Gray (ref.1) during tests on the experimental Armstrong Whitworth 52 aircraft at R.A.E.Farnborough in December 1951. However, since the work was carried out in flight the results were only qualitative in nature. Once recognised, the problem received rapid attention and by May 1952 two quantitative (though crude) experiments had been performed, one, at R.A.E.Farnborough by Anscombe and Illingworth (ref.6) and another at N.P.L.Teddington by Gregory and Walker (ref.5).

Anscombe and Illingworth used a wing of rectangular planform with a chord of 4' a thickness/chord ratio of 0.15 and which was mounted through the floor of the R.A.E. No.2 wind tunnel. The investigations were limited to zero incidence with the sweep angle ranging from 0^o to 50^o and the chordwise position of transition being determined by the china clay evaporation technique. In addition to the rapid forward movement of the indicated transition position with increasing sweep angle at constant free stream Reynolds number ($Q_\infty C_O/\nu_\infty$) they found that even before transition began to advance from the zero sweep location ($x/C_O \simeq 0.6$) a series of streaks became visible in the china clay under the laminar part of the boundary layer. These streaks extended from a line very close to the leading edge to the transition front which had a ragged 'saw-tooth' form unlike the smooth line produced in two-dimensional flows. The streaks were closely spaced (0.10" - 0.13" apart), parallel and with an inclination to the undisturbed flow direction close to that of the inviscid surface streamlines. The results of this investigation are summarised in figure 45. In the tests conducted concurrently at the N.P.L. Gregory and Walker used a rectangular planform wing with a Griffith suction aerofoil section which had a chord of 30", a maximum thickness chord ratio of 0.30 and which was mounted in the 13' x 9' low speed wind tunnel. The sweep angle was varied from 0^o to 60^o at zero incidence and the transition front was made visible with the china clay evaporation technique. Their results were entirely consistent with those of Anscombe and Illingworth and are summarised in figure 46. Shortly after the publication of these experimental results Gray (ref.2) succeeded in detecting the streak pattern in the boundary layer flow near the leading edge of a Sabre (F86) aircraft, thereby confirming that the phenomenon was important at flight scale.

At the same time the problem was being tackled theoretically by Owen and Randall at the R.A.E. Their preliminary report (ref.3) appeared in June 1952 and in it they identified the cross flow

profile (see section 6.1) as the probable instigator of the instability. Moreover, they suggested that a suitable criterion for the onset of instability and transition might be of the form -

$$\chi = \text{constant} \qquad \text{(see equation 6.2.9)}$$

where χ was based upon the maximum cross flow velocity and some undefined boundary layer thickness. Using the experimental and flight test data available at the time they were able to suggest that the critical values might be

$$\chi \simeq 125 \quad - \quad \text{for the appearance of vortices}$$

and 6.3.1

$$\chi \simeq 175 \quad - \quad \text{for transition very close to L.E.}$$

Although this represented a significant advance it should also be said that similar conclusions had been reached independently by H.B.Squire who had summarised the basic nature of the instability, identified the relevence of χ and estimated its order of magnitude in a single paragraph of a letter sent to the R.A.E. in March 1952. A more rigorous investigation of the problem was compiled by Owen and Randall (ref.4) in February 1953. These results confirmed the somewhat tentative conclusions of their original work and they also identified the critical profile (see section 6.1) as the source of the disturbances which were stationary with respect to the solid wall. In addition they considered the closely related problem of the rotating disc. This work was followed by Stuart's classic report (ref.5) which considered the general problem of stability in three-dimensional incompressible flows.

In the United States the Northrop aircraft company began exploratory investigations into the possible use of suction to maintain full chord laminar flow on a wing in flight in 1954. Research into boundary layer transition and its prevention was led by Pfenninger and the Northrop team carried out extensive research, both theoretical and experimental, into the many problems associated with laminar flow control (see Pfenninger ref.59). However, for the purpose of the present study the most significant publications were, firstly, the numerical solutions of the Orr-Sommerfeld equation for the flow close to the swept attachment line and the flow over a rotating disc which were produced by Brown (ref.60) in 1959 and, secondly, the experimental measurements of transition on a 33° swept wing with a thickness chord ratio of 0.25 which were made by Carlson (ref.61) in 1964. In addition, Boltz, Keynon and Allen (ref.62) carried out extensive investigations into the dependence of transition position upon Reynolds number, sweep angle and incidence for a rectangular wing with a 4' chord and NACA 64_2 A015 section using the Ames 12' Pressure Tunnel . Transition was detected by surface microphone and flow visualisation was provided by a sublimation technique using biphenyl crystals dissolved in petroleum ether. The sweep angle was varied between 0° and 50°, the incidences considered were in the range +3° to -3° and Reynolds numbers in excess of 3×10^7 were achieved. By using Polhausen's two-dimensional method for the flow normal to the leading edge and assuming that the streamwise

profile was the same as that found on a flat plate they were able to calculate values of χ and thereby correlate the transition results. They found that for their wing χ at transition lay in the range 200 to 240 when the distance from the attachment line to the transition front was between 20 and 60% of the chord, C_o.

In addition to the swept wing work there have been several detailed investigations into associated problems. Eichelbrener and Michel (ref.48) made transition measurements on an ellipsoid with a slenderness ratio of 6:1 at incidences in the range $+10^o$ to -10^o and Reynolds numbers $(\frac{Q_\infty C_o}{\nu_\infty})$ from 2×10^6 to 6×10^6 using the china clay evaporation technique. They found that at zero incidence the transition front position was consistent with the two-dimensional criterion. However, as the incidence was increased the orientation of the transition front was modified by three-dimensional effects. At ten degrees incidence it was found that the transition front lay along a line of constant χ where χ took a value of approximately 300. Unfortunately, the value of χ at transition was extremely sensitive to the order of polynomial chosen to represent the boundary layer profiles and so the value of 300 can only be regarded as an order of magnitude. The problem of transition on a rotating disc has been studied by several authors. Theodorson and Regier (ref.63) measured the turning moment coefficients required by highly polished discs of 12" and 24" diameter and found that there was a departure from the laminar variation when χ (equation (8.10)) was greater than 712. Gregory and Walker (see ref.5) performed flow visualisation experiments on rotating discs (12" and 24" diameter) which were coated with china clay and methyl salicylate was used to show the transition. In addition to the transition which took place at values of χ in the range 658 to 693 they observed streaks in the laminar region for χ between 538 and 583 where the normals to these streaks were inclined at about 14^o to the radial direction. There were between 28 and 31 streaks distributed around the disc and in order to be visualised by the china clay technique they must have been stationary relative to the surface. By contrast Fales (ref.51) performed a similar test for a rotating disc with a 24" diameter submerged in water. Using dye, introduced at the hub, for flow visualisation he found that a 'vortex' like pattern was formed when χ was approximately 572. In this case there were 22 'dark lines' distributed around the disc and the normals to these lines were inclined at about 10^o to the radial direction. However, these 'dark lines' were not stationary relative to the disc instead they propogated outwards at a finite speed in direction normal to their axes. This important result suggests that the use of a sublimation technique may well be 'fixing' vortices which would otherwise be in motion relative to the surface

6.4 The Shortcomings of the Early Work

One of the most serious difficulties encountered in the interpretation of the early work on cross flow instability lies in the fact that the mechanism of leading edge contamination was not identified as a separate instigator of boundary layer transition. Consequently some of the early results for transition 'close to the leading edge' were being caused by leading edge contamination. From figures 45 and 46 it can be seen that results for 'transition at L.E.' are almost perfectly correlated by the leading edge contamination criterion of ϕ equal to 270. In this case an intermediate value of ϕ would be expected since the transition front indicated by a sublimation technique should lie somewhere within the limits determined by a hot-wire or pitot survey. Moreover, it is interesting to note that Owen's (ref.3) original criterion for transition, equation (6.3.1), does not provide a satisfactory correlation for the experimental data upon which it was based - see figure 45 where the appropriate values of speed and sweep have been deduced from Owen's original calculations. In addition the use of a sublimation technique for detecting transition is unsatisfactory for two reasons. Firstly, it does not give an indication of the extent of the transition region, thereby making it difficult to compare results with more quantitative techniques, and secondly, the surface coating introduces roughness which undoubtedly causes premature transition. The results of Boltz, Kenyon and Allen (ref.62) indicate that the values of χ at transition may be reduced by up to 25%

Finally, with the exception of the Northrop team, the various authors have been inconsistent in their choice of a reference boundary layer thickness and χ, itself, has been determined by some grossly oversimplified calculation techniques. This makes it difficult to compare the criteria from different sources and also invalidates their use in the accurate boundary layer calculation methods which are currently available.

6.5 Full Solutions of the Orr-Sommerfeld Equation

In a remarkable piece of early electronic computing work Brown (ref.60) took advantage of the two-dimensional approximation provided by Stuart (ref.5) and solved the complete Orr-Sommerfeld equation (equation (6.1.2)) for small amplitude temporal disturbances introduced into several three-dimensional boundary layer flows. The cases considered were, the flow near the attachment line of a swept wing, the flow over a rotating disc and two examples of boundary layer flows typical of those found towards the trailing edge of a swept wing when moderate boundary layer suction is applied. In each instance calculations were performed for the cross flow profile ($\varepsilon = 0$, figure 41) and the critical profile ($\varepsilon = \varepsilon_I$, figure 41). To avoid ambiguity in the case of the swept wing attachment line flow the critical profile considered was the one for which ε_I was a maximum i.e. the profile shown in figure 44. The resulting neutral curves are presented in figure 47 and the complete stability diagrams for the attachment line and rotating disc flows are given in figures 48 to 51.

The results show that with the exception of the attachment line flow the cross flow profiles have lower critical values of χ than the corresponding critical profiles with the difference increasing with increasing χ. However, since the difference for the attachment profiles is only 15% for the maximum deviation condition it may be concluded that the properties of the pure cross flow profile may be used as a suitable criterion for the onset of instability in three-dimensional flows. This represents a very significant simplification since the cross flow profile is generally directly available from boundary layer calculation methods. whereas the critical profile requires the specification of the angle ε_I which involves a great deal of extra computational effort. In addition the results show that for the critical profiles (figures 49 and 51) there are disturbances which are amplified and which are stationary relative to the surface since the phase velocity, (ω_r/α_r) is zero. However, it should be noted that there is also a broad spectrum of travelling disturbances which experience comparable amplification rates and may, therefore, be equally likely to cause transition to turbulence.

Since Brown's computations were performed almost twenty years ago it is not unreasonable to question the accuracy of the results. A simple check on the reliability which may be placed on the minimum critical values of χ can be obtained by comparing Brown's results with more recent independent calculations by other authors. For the free convection profile (air, Pr = 0.733) Brown's result for χ_{crit} was 159 (see ref.64 page 922) whilst a method developed by Kurtz and Crandall (ref.65) gave a value of 161 - a difference of 1%. The rotating disc problem has been studied by Cebeci and Keller (ref.66) who have found χ_{crit} to be 240 as compared to Brown's value of 234 - a 2.5% difference. Therefore Brown's results are supported by the limited amount of independent data.

In addition to the cases already discussed another relevent profile is that of the plane wall jet. The stability of this profile has been studied by Chun and Schwartz (ref.67) and they have found that the minimum value of χ for instability is 122. The special feature of the wall jet profile is the appearance of two points of inflection, one beyond c_{max} and the other at the wall. In reference 64 Brown proposes that the minimum critical values of χ for cross flow profiles may be adequately correlated as a single function of the profile curvature at the wall (an idea originally conceived by Gregory (ref.68)) and suggests the following linear relationship

$$\chi_G)_{crit} \simeq 58.8 + 0.7077 \left(\frac{\partial^2(c/c_{max})}{\partial(z/z_{0.1c_{max}})^2}\right)_{z=0} \qquad 6.5.1$$

where $\chi_G = /\frac{c_{max} \cdot z_{0.1\,c_{max}}}{\nu}/$

Using this formula the value of $\chi_G)_{crit}$ for the plane wall jet should be 58.5 whereas complete calculation shows it to be 85. Therefore, in this particular case equation (6.5.1) is subject to an error of 45%. Clearly, the correlating variable suggested by Gregory is unreliable. However, since the instability of this family of profiles is determined by the presence of an inflection point in the outer part of the flow it is reasonable to postulate that the minimum value of χ for instability is a function of the position of the inflection point within the layer

i.e. $(z_I/z_{0.01_{Cmax}})$ in our notation. Figure 52 shows the available data plotted against this parameter and it can be seen that all the results, including the plane wall jet, are well represented by a single line. It is suggested that the minimum critical values of χ may be estimated from the simple correlating function

$$\chi_{crit} \simeq \frac{20.3}{(z_I/z_{0.01_{Cmax}})^{1.875}} \qquad 6.5.2$$

for $0.15 < (\frac{z_I}{z_{0.01_{cmax}}}) < 0.45$

which agrees with the available data to better than ±10%.

6.6 The Present Investigation

The objectives of the present investigation were, firstly, to set up an experiment in which the values of χ produced were much higher than those achieved in previous experiments, secondly, create an environment which was free from the effects of leading edge contamination and, thirdly, make transition measurements in a region sufficiently close to the attachment line to enable a general criterion to be produced via the direct application of the similar solution for the cross flow profile (equation (6.2.8)) and Brown's stability results.

A simple study of the equations governing the development of χ - see Appendix E - shows that the value of χ_{max} increases with increasing leading edge radius and achieves an absolute maximum when the sweep angle is of order 60°. Therefore the model used in the experimental investigation of leading edge contamination was found to be equally suitable for the study of cross flow instability. Moreover, since the leading edge contamination characteristics of this model had already been determined the problem of ensuring a disturbance free attachment line was simplified considerably. As in the previous work the model was mounted vertically in the Cranfield 8' x 6' low speed wind tunnel - see figure 12.

In order that a hot-wire probe could be used to determine the state of the boundary layer a second supporting cradle was constructed. This was very similar to the original (see figure 13) except that it could be attached to any part of the curved wing surface with the hot wire set at 0.010 inches from the wall. Once again the hot-wire output signal was monitored on an oscilloscope. An alternative method of detecting transition was available in the form of two flattened pitot tubes with aperture heights of 0.005" and 0.010". These were made from steel hyperdermic tubing and could be attached to any point on the surface facing any desired direction. The pressures (both pitot and surface static) were measured on an inclined manometer bank. In addition surface oil flow visualisation was

obtained by the use of a suspension of titanium dioxide in paraffin (for mixing details see Maltby and Keating ref.69) and the results were recorded photographically.

The high curvature of the leading edge region of the model made it difficult to obtain quantitative results directly from the photographs of the oil flow patterns and so a simple technique for producing planar flow patterns was developed. When a flow pattern was to be used for direct measurements the wind tunnel speed was maintained until the pattern had dried out completely (usually 10-15 minutes was sufficient). A piece of sellotape 2" wide was then carefully applied to the surface with the aid of a smooth roller and subsequently peeled off taking the titanium dioxide deposit with it. Finally, the tape was rolled onto a piece of flat black paper, the resulting plane flow pattern photographed and the negative printed full size. This process produced a permanent record which had minimal distortion and could be used for estimating the orientation and pitch of streak lines.

Since the free stream speeds necessary for transition via cross flow instability were such that the laminar boundary layer forming on the model was typically less than 0.020 ins. thick, accurate determination of the boundary layer profiles was beyond our experimental capabilities. Therefore, it was decided that the relevant parameters would be provided by an accurate boundary layer calculation method. The technique adopted was the one due to Beasley (ref.70) which involves the solution of equations (6.1.4) by using finite difference substitutions and integrating across the layer by a matrix method. Calculations begin at the attachment line and proceed in a marching fashion towards the trailing edge, the profiles at each point being obtained by iteration using those obtained at the previous point as a first guess. In its present form the solution is restricted to the case of an infinite swept cylinder in an incompressible flow, however, this was quite adequate for the present investigation. A copy of the program was supplied by the author and it was adapted to the College computing system with a minimum of effort.

6.7 Boundary Layer Computations

The input data for the boundary layer calculation consists of the surface chordwise velocity distribution as a function of the surface coordinate x, the velocity gradient at the attachment line, U_1 and six control parameters which govern the step lengths in the x and z directions, the number of steps, the number of iteration cycles and the iterative tolerance.

In order to obtain a smooth variation for (U/U_∞) with (x/C_0) the surface pressure distributions (see figure 15) were measured at intervals of 2.5^0 for sweep angles in the range 52.5^0 to 70^0. The results were then corrected for the effects of tunnel blockage and transformed into distributions of (U/U_∞) by using Bernoulli's equation. Finally, the data were smoothed by fitting a polynomial of the form -

$$\frac{U}{U_\infty} = a_1\left(\frac{x}{C_0}\right) + a_2\left(\frac{x}{C_0}\right)^3 + a_3\left(\frac{x}{C_0}\right)^5 + a_4\left(\frac{x}{C_0}\right)^7 \qquad 6.7.1$$

where the coefficients a_η were determined by a criterion of least squares error. An odd polynomial was chosen since it gives the flow the correct behaviour in the vicinity of the attachment line ℄ the circular cylinder potential flow result where -

$$\frac{U}{U_\infty} = 2\sin\left(\frac{2x}{C_0}\right) = 4\left(\frac{x}{C_0}\right) - \frac{8}{3}\left(\frac{x}{C_0}\right)^3 + \frac{8}{15}\left(\frac{x}{C_0}\right)^5 - \frac{16}{315}\left(\frac{x}{C_0}\right)^7 + \text{-----}$$

It was found that over the range of sweep angles considered the velocity distributions could be adequately represented by three polynomials namely -

Sweep Range	a_1	a_2	a_3	a_4
52.5^0 - 57.5^0	+7.7549	-16.901	-51.967	+195.89
57.5^0 - 65.0^0	+8.0148	-21.746	-16.673	+112.80
65.0^0 - 72.0^0	+8.2898	-24.053	- 0.2390	+ 63.793

The variation of (U/U_∞) with (x/C_0) was then calculated for values of (x/C_0) in the range 0 to 0.45 in steps of 0.01 and the resulting table was used as the input data whilst the program control parameters were taken to be -

Maximum number of iterations	= 50
Iterative tolerance	= 0.00001
Steplength in z direction	$= 0.1 \cdot (x.\frac{\nu}{U})^{\frac{1}{2}}$
Number of steps in z direction	= 70
Steplength in x direction	$= 0.0125 \cdot C_0$
Maximum permitted change in (U/U_∞) across any x step	= 0.05

Some typical sets of results are presented in figure 53.

6.8 The Experimental Results

Flow Visualisation

In the present experiment it was found that the streak pattern previously seen with sublimation visualisation techniques was plainly visible with the much simpler surface oil flow method and figure 54 presents a photographic record of some of the patterns obtained. By using the technique already described in section (6.6) it was possible to transfer the flow patterns to a plane surface so that the pitch of the streak, their inclination to the x axis and their point of origin could be accurately determined. Measurements of this kind were carried out for sweep angles of 55^{o}, 63^{o} and 71^{o} with free stream speeds ranging from 80 to 110 ft/sec and the results are given in tables 3 to 5.

Hot-Wire Investigation

With the wing set at 62.8^{o} of sweep a hot-wire probe was mounted on the curved surface just upstream of the mid-span pressure tappings at an (x/C_0) of 0.28 and approximately aligned with the external flow direction. The wind tunnel speed was then gradually increased and the hot-wire output signal was monitored on an oscilloscope which was scanning continuously. It was found that the appearance of the transition process was fundamentally different from that observed at the attachment line during the leading edge contamination experiment (see figure 14). In the latter case transition from laminar to turbulent flow was accomplished by the appearance of bursts or spots of turbulence separated by regions of undisturbed laminar flow. For the cross flow transition, however, there were no bursts of turbulence as such, instead the signal became modulated with disturbances whose frequencies were confined initially to the 0 to 10 KHz range. The amplitudes of these disturbances increased rapidly with increasing speed. In the advanced stages of transition spikes began to appear in the signal which gradually acquired the appearance characteristic of a uniformly turbulent flow. By way of a check it was found that when bursts of turbulence were generated artificially by a trip wire placed across the attachment line their presence was readily discernable on the oscilloscope despite the large distortions on the signal.

Figure 55 presents photographs of typical oscilloscope traces. In each case the location of the hot-wire probe and the voltage and time scales were the same being 0.28, 5msec/cm (horizontal) and 100mV/cm (vertical) respectively. The signal in photograph (a) represents transition resulting from contamination of the attachment line by an 0.016" diameter trip wire (ϕ = 445, χ = 258) with the characteristic turbulent bursts clearly shown. Photograph (b) represents a typical trace for flow breakdown produced by cross flow instability (ϕ = 546, χ = 317) with the heavily disturbed signal and the voltage spikes. In each case the tunnel conditions were such that the surface skin friction had just begun to rise above the laminar level - this being determined by surface pitot probe. Finally it was noted that for the case of leading edge contamination the surface pitot probe indicated an increase in local skin friction as soon as the turbulent bursts were detected by the hot-wire. However for cross flow transition the signal distortions were visible long before skin friction departure occured with a basic

sinusoidal modulation of about 1.3 KHz being observed when χ was approximately 270 and spikes appearing for values of χ greater than 285.

Surface Pitot Tube Measurements

Since the hot-wire signal could not be used to detect the 'skin friction transition' zone the familiar surface pitot tube method was adopted. The validity of the method was explored by detecting the transition at an (x/C_0) of 0.27 with the model swept at 63^0 and turbulence introduced by a trip wire across the attachment line. Figure 56 shows the variation of pitot dynamic head (pitot pressure minus local static pressure) with tunnel free stream dynamic head for trip wire on and trip wire off. The transition from laminar to turbulent flow is clearly visible and is in excellent agreement with the attachment line hot-wire results. It was found that similar variations were obtained when transition was produced by cross flow instability with the 'beginning' and 'end' points being easily determined. Figures 57 and 58 present the results of transition measurement made at the mid-span section for sweep angles in the range 52.5^0 to 70^0.

6.9 Discussion

In previous investigations it has been found that the conditions necessary for the production of stationary disturbances have been well correlated in terms of a constant value of the cross flow Reynolds number χ -equation (6.2.9), evaluated at the point of origin of the streaks. Consequently the values of χ corresponding to the results given in table 3 have been calculated and are presented in figure 59. It is apparent that χ is a suitable parameter for correlation, with the present data suggesting a constant value of 220. This may be compared directly with Carlson's result of 240 (ref.61) where the disturbances were detected by stethoscope and pitot survey and also with the results of Boltz, Kenyon and Allen (ref.62) where pitot survey revealed that χ for the onset of disturbances lay in the range 180 to 220. Therefore it is suggested that for a smooth surface the conditions necessary for the production of detectable stationary disturbances may be predicted by use of the equation

$$\chi = 220 \qquad 6.9.1$$

However, when a surface sublimation technique is used the streaks are found to occur at lower values of χ. Boltz et.al.(ref 62) found that when transition was indicated by biphenyl crystals dissolved in ether the streaks appeared at values of χ in the range 140 to 160, whilst Anscombe and Illingworth (ref.6) using methyl salicylate in a china clay matrix found the critical value to be between 140 and 150 where χ has been re-calculated to conform to the present definition. In the present experiment it is believed that the surface oil flow did not affect the value of χ because the ratio of boundary layer thickness to particle size is at least ten times greater than those occurring in references 61 and 62.

The theoretical considerations outlined in section (6.1) indicated that the orientation of the streaks should have been such that they were always normal to the direction of the critical profile ($\varepsilon=\varepsilon_I$) i.e. using the notation of figure 40

$$\varepsilon_s = \theta - \left(\frac{dy}{dx}\right)_{streak} = \varepsilon_I \qquad 6.9.2$$

Figure 60 shows the variation of ε_s and ε_I with (x/C_o) where the values of $(dy/dx)_{streak}$ have been taken from table 5, ε_I has been determined from the calculated boundary layer profiles and θ from the measured pressure distribution. With the exception of those chordwise stations which are close to the laminar separation point ($x/C_o \simeq 0.42$) the experimental results are in excellent agreement with the theoretical prediction given by equation (6.9.2). In addition it is possible to compare the measured pitch of the streaks (table 4) with the predictions of Brown's stability calculations for the critical profile (figure 47). For values of χ in excess of 220 it is found that the stationary disturbance which is characterised by a zero phase velocity, $(\omega r/\alpha_r)$ has a constant wave number α_r given by

$$\alpha_r = 0.4\left(\frac{U_1 U_\infty}{\nu_\infty C_o}\right)^{\frac{1}{2}}$$

Hence the corresponding wave length λ is given by -

$$\lambda = \frac{2\pi}{0.4}\left(\frac{\nu_\infty C_o}{U_1 U_\infty}\right)^{\frac{1}{2}} = 15.7\left(\frac{\nu_\infty C_o}{U_1 U_\infty}\right)^{\frac{1}{2}} \qquad 6.9.3$$

and this allows the following comparison to be made

Sweep (degrees)	Speed (ft/sec)	(x/C_o)	θ degrees	λ measured (ins)	λ predicted (ins)
55^o	$\simeq$ 100	0.26-0.40	40-38	0.15±0.03	0.14
63^o	$\simeq$ 95	"	49-47	0.18±0.03	0.16
71^o	$\simeq$ 90	"	59-57	0.22±0.03	0.19

It should be noted, however, that the predictions of equation (6.9.3) are only approximations to the situation studied in the experiment since the profile used for the stability calculations corresponds to a condition of maximum deviation between the critical and cross flow direction and therefore the results are only exact when θ equals 48.21^o. Nevertheless despite this limitation the predictions of equation (6.9.3) are in reasonable agreement with the observed wavelengths.

Since the appearance of the streaklines has been successfully correlated in terms of a constant value of χ the local values of χ were calculated for conditions corresponding to the beginning of transition (figure 57). The results are shown in figure 61 where χ is plotted against the laminar attachment line momentum thickness Reynolds number, $R_{\delta 2A}$. It is immediately apparent that transition conditions are not, in general, correlated by a single value of χ . However, for values of $R_{\delta 2A}$ less than 220 the appropriate values of χ are a function of (x/C_o) only. Moreover, there is an asymptotic tendancy towards a constant value of χ as (x/C_o) decreases and for values less than 0.25 χ_T takes a value of approximately 325 i.e.

$$\chi_T = 325 \quad \text{when} \quad \left(\frac{x}{C_o}\right) < 0.25 \qquad 6.9.4.$$

when $R_{\delta 2A}$ is greater than 220 there is clearly some interaction between the instability of the cross flow and the instability of the spanwise flow which begins at an $R_{\delta 2A}$ of 230 and dominates the transition behaviour for values of $R_{\delta 2A}$ in excess of 270. The present results show that this interaction is small and causes a maximum reduction of 15% in the value of χ at transition. Finally a comparison of figures 57 and 58 reveals that the complete transition process requires a 20% increase in the free stream Reynolds number.

The limiting value for χ_T presented in equation (6.9.4) may be compared with the results obtained by Carlson (ref.61) who found that transition occurred close to the leading edge of a wing swept at 33^o when χ was approximately 310. In view of this close agreement it is desirable to compare this result with some reliable theoretical model of the transition process. At the present time the best two-dimensional approach is to determine the amplification characteristics of the boundary layer by linear stability theory and then estimate the transition position by the amplitude ratio method (see section (5.5)). The extension of this method to general three-dimensional flow has been considered by Mack (reference 71) and although his analysis is not entirely rigorous (see Stewartson - reference 72) it is the only general three-dimensional transition model available at the present time.

By using linear stability theory in conjunction with the kinematic wave theory Mack has shown that for a three-dimensional disturbance travelling through a three-dimensional parallel boundary layer the spatial and temporal amplification rates are related approximately by a generalised form of the Gaster transformation -

$$-\underset{\sim}{\alpha i} \simeq \left(\underline{\omega i}/\underline{Cg}\right)$$

where Cg is the group velocity. One of the significant features of this result is that the equation applies to any arbitrary orientation of the spatial amplification rate vector, $\underset{\sim}{\psi}$ when the group velocity is replaced by its component in the $\underset{\sim}{\psi}$ direction - see figure 62 for the notation

i.e. $$\underset{\sim}{\alpha_i})_{\underset{\sim}{\psi}} = \underset{\sim}{\alpha_i} / \cos(\underset{\sim}{\psi} - \underset{\sim}{\psi_g})$$

Therefore $/\underset{\sim}{\alpha_i}/$ is the minimum value of $/\underset{\sim}{\alpha_i}/_{\underset{\sim}{\psi}}$. Moreover, if $\underset{\sim}{\psi}$ is taken as the direction of propagation of the wave crests then $\underset{\sim}{\psi} = \psi$ and the spatial amplification rate $\alpha i)_{\psi}$ may be evaluated using two-dimensional stability theory provided that the velocity profile is taken in the ψ direction i.e.

$$\underset{\sim}{\alpha_i} = \underset{\sim}{\alpha_i}_{\psi_{2\text{-}D}} \cos(\psi - \underset{\sim}{\psi_g})$$

Finally the maximum amplitude ratio necessary for the prediction of the transition point is given by integrating the three-dimensional spatial amplification rate along a group line for constant disturbance frequency -

$$\left[\log_e(A_2/A_1) = -\int_{\ell_{11}}^{\ell_{12}} \underset{\sim}{\alpha_i} \cdot \frac{d\,\ell_1}{\cos\underset{\sim}{\psi_g}}\right]_{\underset{\sim}{\omega_r} = \text{constant}}$$

$$= -\int_{\ell_{11}}^{\ell_{12}} \underset{\sim}{\alpha_i})_{\psi_{2\text{-}D}} \cdot \left(\frac{\cos(\psi - \underset{\sim}{\psi_g})}{\cos\underset{\sim}{\psi_g}}\right) d\ell_1$$

Consequently if the two-dimensional characteristics are evaluated for the velocity profile taken in the ℓ direction then $\psi = 0$ and

$$\left[\log_e(A_2/A_1) = -\int_{\ell_{11}}^{\ell_{12}} \underset{\sim}{\alpha_i})_{\psi=0_{2\text{-}D}} \cdot d\ell_1\right]_{\underset{\sim}{\omega_r} = \text{constant}} \qquad 6.9.5$$

If the orientation of the wavefronts of the unstable disturbances is known i.e. the relationship between x and ℓ_1 is known, then the integral may be evaluated in complete generality using only two-dimensional amplification characteristics.

In the present context flow visualisation has shown that at least one of the highly amplified disturbances has wavefronts which propagate in the direction of the critical velocity profile - see figure 60. Therefore since the critical and crossflow directions never differ by more than 6.42° (see section (6.2)) it follows that the use of the crossflow stability characteristics in equation (6.9.5) should produce a fairly good approximation to the general three-dimensional result. For the crossflow profile ℓ_1 is always normal to the external streamline and hence, it may be readily shown that -

$$d\ell_1 = \frac{dx}{\sin\theta} = \frac{Qe}{V_\infty}\, dx$$

Therefore since

$$-\alpha_i \simeq \frac{\alpha_r}{Cg} \cdot \left(\frac{\omega i}{\alpha_r}\right) \quad \text{when} \quad C_g = \left(\frac{\partial \omega r}{\partial \alpha_r}\right)_R$$

by the Gaster Transformation - see reference 32, equation (6.9.5) maybe re-written in terms of the non-dimensional parameters used in figure 50 -

$$\left[N \simeq \frac{1}{3.490} \cdot \int_{x_I}^{x} \frac{\alpha_r}{Cg} \cdot \left(\frac{\omega i}{\alpha_r}\right) \cdot \left(\frac{Ue}{\nu_\infty x}\right)^{\frac{1}{2}} \cdot \left(\frac{Qe}{V_\infty}\right) \cdot dx\right]_{\underline{\omega r} = \text{constant}} \qquad 6.9.6$$

It is apparent that this equation is a general function of the free stream conditions, sweep angle and body geometry. However, if local values of (x/C_o) are small then

$$\frac{V_\infty}{Qe} = \sin\theta \simeq 1.0$$

and equation (6.2.10) becomes

$$\chi \simeq 0.838\left(\frac{Uex}{\nu_\infty}\right)^{\frac{1}{2}} = 0.838\left(\frac{U_1 U_\infty}{\nu_\infty C_o}\right)^{\frac{1}{2}} x \qquad 6.9.7$$

hence $$\frac{d\chi}{dx} \simeq 0.838 \left(\frac{Ue}{\nu_\infty x}\right)^{\frac{1}{2}}$$

Finally equation (6.9.6) becomes

$$\left[N \simeq \frac{1}{2.925} \int_{x_I}^{x} \frac{\alpha_r}{Cg} \cdot \left(\frac{\omega i}{\alpha_r}\right) d\chi\right]_{\underline{\omega r} = \text{constant}} \qquad 6.9.8.$$

which is a function of χ alone. Figure 63 shows the resulting variation of N with χ for several values of the non-dimensional frequency parameter $\bar{\omega}$ where

$$\bar{\omega} = 12.18\left(\frac{\omega_r . Co}{U_1 . U_\infty}\right) \quad \text{or} \quad f = \frac{1}{12.18}\left(\frac{\bar{\omega} . U_1 . U_\infty}{2 . \pi . Co}\right) \qquad 6.9.9$$

with the complete calculations being presented in Appendix F. The results show that the value of N at transition is approximately 16 whilst the streaks appear when N is about 6. For transition in two-dimensional flows comparisons between theory and experiment have shown that the value of N at transition may vary between 4 and 20 but that a value of 10 appears to be a useful average for prediction pruposes (see Jaffe et.al. reference 33). The value of 16 observed in the present case is within the limits found in two-dimensional flows although

a higher than average value may have been expected because the surface curvature, which has not been included in the theory, is believed to have a stabilising effect since the centrifugal forces tend to damp out large scale disturbances. However, despite the approximations a quasi two-dimensional prediction based upon N equal to 10 gives a transition Reynolds number, χ_T a value of 265 which is only 18% lower than the value found by experiment.

In addition the analysis reveals that the frequency which has undergone maximum amplification when transition occurs is given by -

$$f \simeq \frac{22}{2.\pi} \left(\frac{U_1 U_\infty}{C_o}\right) \qquad 6.9.10$$

and that all the amplified frequencies lie in the range

$$\frac{7}{2.\pi} \left(\frac{U_1 U_\infty}{C_o}\right) < f < \frac{56}{2.\pi} \left(\frac{U_1 U_\infty}{C_o}\right)$$

for the experiment this corresponds to actual frequencies between 350Hz and 3000 Hz with maximum amplification occurring at 1000 Hz. These predictions are in good agreement with the observed disturbance frequencies which were in the range 0 - 10 KHz - see section (6.8)

In view of the satisfactory agreement between experiment and theory it is proposed that a transition criterion based upon a constant value of χ is justifiable for those chordwise stations which are sufficiently close to the attachment line for the cross flow profile to be accurately predicted by equation (6.2.10). For typical aerofoil geometries this restriction means that (x/C_o) must be less than (ρ/C_o) - a result which is borne out by the present experiment and the data from Carlson (ref.61). Therefore the suggested form of the criterion is

$$\chi_T = 325$$

$$\text{for} \quad \frac{x}{C_o} < \frac{\rho}{C_o} \qquad 6.9.11$$

Moreover, since the criterion applies in the region where the cross flow profile is governed by a similar solution it is a simple matter to adopt different definitions for χ. One particularly useful alternative definition is that due to Beasley (ref.70) where an integral boundary layer thickness is used -

$$\chi_B = \frac{c_{max}\,\Delta}{\nu} \qquad 6.9.12$$

$$\text{where} \quad \Delta = \int_0^\infty \frac{c}{c_{max}}\, dz$$

The thickness Δ is directly related to the conventional cross flow displacement thickness which is usually available in integral boundary layer calculation methods. Using this definition the criterion becomes

$$x_{B_T} = 150 \qquad 6.9.13$$

for $\left(\frac{x}{C_o}\right) < \left(\frac{\rho}{C_o}\right)$

As an example of the application of the criterion and an illustration of the effect of sweep angle upon transition figure 64 shows the combination of free stream Reynolds number ($Q_\infty D/\nu$) and sweep angle necessary for a transition front to be located at a distance D/2 from the attachment line on a circular cylinder. Also shown are the criteria for leading edge contamination, the linear stability theory prediction (e^{10} transition model) for the cylinder at zero sweep and an experimental result due to Achenbach (ref.71). It is apparent that in the presence of large upstream disturbances e.g. wing/body junction the leading edge contamination mechanism will dominate transition between the attachment line and this chordwise position for all sweep angles greater than 2^o. However, if the attachment line is clean the cross flow instability mechanism will produce transition at (D/2) for sweep angles less than 65^o. This simple result may be extended to thin aerofoil shapes by the use of equation (5.2.1) and (6.2.10) from which it is easily shown that

$$\chi \simeq 0.84.\phi.\cos\Lambda \qquad 6.9.14$$

when $\frac{x}{C_o} = \frac{\rho}{C_o}$

Therefore if

$$\chi = 325 \qquad 6.9.15$$

then $\phi = \frac{388}{\cos\Lambda}$

Once again if gross upstream disturbances are present leading edge contamination will dominate whereas for a clean attachment line cross flow instability is the governing transition mechanism for sweep angles below 50^o.

For transition at chordwise positions greater than (ρ/C_o) the situation is much more complicated. In this case linear stability theory does not give any assistance beyond a general indication that transition conditions are a complex function of all the independent variables, see equation (6.9.6). In order to obtain a useful correlation the experimental results presented in references 5,6,61 and 62 have been re-analysed using Beasley's calculation method. By restricting the

investigation to the situation where transition occurs at the x location at which χ is itself a maximum it is found that for small angles of incidence (<3°) the values of χ_T may be correlated approximately as a function of sweep only. The results are presented in figure 65 and the suggested variation of

$$\chi_T = 212 + 1.25\,\Lambda \qquad 6.9.16$$

for $\frac{x}{C_o} = \frac{x}{C_o})_{\chi \text{maximum}}$

correlates the data with a scatter of ±12%. If Beasley's alternative definition for the Reynolds number is used then the function becomes

$$\chi_{B_T} = 100 + 0.56\,\Lambda \qquad 6.9.17$$

for $\frac{x}{C_o} = \frac{x}{C_o})_{\chi \text{ maximum}}$

It should be emphasised that equations (6.9.16) and (6.9.17) are based upon purely empirical data of dubious quality and should be modified as necessary if new data became available. Indeed the scatter on the data is such that the value of χ at transition may not be a function of sweep as suggested, however, these expressions will at least reproduce past experience reasonably accurately.

Finally in the general context of transition in three-dimensional flows it is of interest to apply the linear stability based transition prediction technique to the case of the rotating disc. Figure 66 shows the results of the amplitude ratio calculation using the cross flow profile amplification characteristics given in figure 50 (the details of the calculation are contained in Appendix F). In this case the observed value of χ at transition corresponds to an N of about 10.1 whilst the streaks appear when N is approximately 6. The use of N equal to 10 for a transition prediction gives χ_T a value of 700 which is only 1.7% less than the value of 712 found by experiment. In addition the stability results for the critical profile (figure 51) show that for χ greater than 600 the stationary disturbance ($\omega_r/\alpha_r = 0.0$) has a non-dimensional wavelength of about 1.4 i.e. in dimensional terms -

$$\lambda = \frac{2\pi}{0.2}\left(\frac{\nu}{\Omega}\right)^{\frac{1}{2}} \qquad 6.9.18$$

or if NS is the number of streaks at a radius a, then

$$NS = 0.2\,\text{Sin}\,(\varepsilon_I)\,\frac{\chi}{1.267} \qquad 6.9.19$$

From section (6.2) $\varepsilon_I = 13.3^o$

and therefore $NS = 0.0363\,\chi$

The china clay evaporation patterns are always clearest near the beginning of transition (see Gregory ref.5) and consequently taking χ to be 660 gives the number of streaks as 24 which is in close agreement with the 28 to 31 found in the experiment.

For both swept wing and rotating disc flows the linear stability theory has produced satisfactory estimates for the pitch and inclination of the stationary streak pattern. In addition a transition prediction based upon a two-dimensional amplitude ratio method (N = 10) has produced predictions for x_T which are in good agreement with those values observed in the experiments, thereby, showing that the transitions are not 'premature' as previously suggested. The theory has also shown that there is a wide range of disturbance frequencies which undergo large amplification but which are not fixed relative to the surface and therefore not detected by a surface flow technique. Consequently it is doubtful whether the 'vortices' do in fact cause transition by themselves but further work would be required to resolve this problem.

6.10 The Influence of Mach Number and Wall Temperature.

The effects of supersonic free streams have been examined experimentally by several authors e.g. Scott-Wilson and Capps (ref.74), Dunning and Ulman (ref.75) and Jillie and Hopkins (ref.76). All observed the familiar streak pattern and characteristic 'sawtooth' transition fronts using surface sublimation techniques for visualisation. However, all the models tested were representative of geometrically complex situations such as wing/body combinations, delta wings and half wings, and there is little or no information concerning pressure distributions or boundary layer development near the swept leading edges. This has meant that it has been impossible to extract useful quantitative data and these references can only be used to provide qualitative evidence of cross flow instability. An attempt to quantify the transition behaviour was made by Chapman (ref.77) in 1961. He applied the ideas of Owen and Randall(ref.3 and 4) to the results of the experiments performed by Beckwith and Gallagher (ref.20) but since these results have been shown to be governed by leading edge contamination (see section 5.6) Chapman's conclusions are of little value.

Finally, Brown (ref.64 pp.1033-1048) extended his stability calculations to include the effects of compressibility and heat transfer. Although only a few results are available it is clear that for Mach numbers less than 2.0 the values of x_i are almost independent of Mach number whilst cooling the wall raises the stability limit.

7. THE POSSIBILITY OF RE-LAMINARISATION

The reversion of a turbulent boundary layer to a laminar one by the imposition of a large favourable pressure gradient is a well established phenomenon. In the case of the swept leading edge there is the possibility of re-laminarisation in the region close to the attachment line ($x/C_0 < \ell/C_0$) where the flow undergoes large acceleration. Several criteria have been proposed for re-laminarisation in two-dimensional flow - see for example Okamoto and Misu (ref.76) but they all produce similar results. For convenience the criterion proposed by Moretti and Kays (see ref.76) will be used in the present context. They suggest that the appropriate acceleration parameter is K where

$$K = \left(\frac{\nu}{Ue^2}\right) \cdot \frac{dUe}{dx} \qquad 7.1$$

Significant re-laminarisation effects are observed when K exceeds 3×10^{-6} and effectively laminar flow is produced when K is greater than 6×10^{-6}.

Although there is no direct evidence available at present it will be assumed that for three-dimensional flows the Moretti-Kays criterion should be applied along an external streamline. Therefore

$$K_{3\text{-}D} = \left(\frac{\nu}{Qe^2}\right) \cdot \frac{dQe}{d\ell} \qquad 7.2$$

where ℓ is measured along the streamline. After some algebraic manipulation this may be re-written as -

$$K_{3\text{-}D} = \frac{(Ue/U_\infty)^2}{R.\cos\Lambda\,((Ue/U_\infty)^2 + \tan^2\Lambda)^2} \frac{d(Ue/U_\infty)}{d(x/C_0)} \qquad 7.3$$

For elliptic nose sections at zero angle of incidence it is found that when (t/C_0) lies in the range 0.075 to 0.15 the local surface velocity gradient may be approximately represented by the function

$$\frac{d(Ue/U_\infty)}{d(x/C_0)} \simeq \frac{d(Ue/U_\infty)}{d(x/C_0)}_{x=0} \cdot (1 - 1.5(Ue/U_\infty)^2) \qquad 7.4$$

and therefore the acceleration parameter becomes -

$$K_{3\text{-}D} \simeq \frac{(Ue/U_\infty)^2\ U_1(1-1.5(Ue/U_\infty)^2)}{R.\cos\Lambda((Ue/U_\infty)^2 + \tan^2\Lambda)^2} \qquad 7.5$$

Simple differentiation reveals that this function exhibits a maximum

$$\text{i.e.} \quad K_{3\text{-}D_{max}} = \frac{0.25}{(1 + 1.5\ \tan^2\Lambda)} \left(\frac{U_1}{R.\sin\Lambda.\tan\Lambda}\right) \qquad 7.6$$

$$= \frac{0.25}{(1 + 1.5\ \tan^2\Lambda)} \cdot \frac{1}{\phi^2}$$

$$\text{when} \quad \frac{Ue}{U_\infty} = \frac{\tan\Lambda}{(1 + 3\ \tan^2\Lambda)^{\frac{1}{2}}}$$

Equations (7.6) reveal two important features. Firstly, the peak value of $K_{3\text{-}D}$ occurs very close to the attachment line, x/C_o being typically 0.5% and secondly $K_{3\text{-}D_{max}}$ is inversely proportional to the square of the leading edge similarity parameter ϕ.

The proximity of $K_{3\text{-}D_{max}}$ to the attachment line means that only turbulence produced by leading edge contamination is likely to be subject to re-laminarisation. However, since fully developed turbulence can only be produced at the attachment line when ϕ is greater than 384 equation (7.6) reveals that under these conditions $K_{3\text{-}D}$ is always less than 1.2×10^{-6} for sweep angles typical of current aircraft i.e. 30^o - 40^o. Although this argument is based upon results for zero incidence, general calculations for the lifting ellipse suggest that the critical values of $K_{3\text{-}D}$ will not be exceeded if the streamwise angle of attack is less than 3^o and, consequently, re-laminarisation is unlikely to occur at cruise conditions on a conventional wing having sections with noses of approximately elliptic form. This conclusion is supported by all the wind tunnel and flight data available at the present time.

CONCLUSIONS

It has been shown that it is possible to produce a simple calculation technique for the skin friction and heat transfer rate at a swept attachment line by using the reference temperature and Reynolds analogy concepts. Formulae have been produced for both laminar and turbulent flow conditions and the predictions are valid for free stream Mach numbers ranging from 0 to 8 with and without heat transfer. The results have been used to investigate the effects of varying sweep angle whilst keeping free stream conditions constant. By considering the limits of incompressible flow ($M_\infty \to 0$) and hypersonic flow ($M_\infty \to \infty$) it has been shown that for the laminar state the skin friction is a maximum when the angle of sweep is 55^o ($M_\infty \to 0$) and 45^o ($M_\infty \to \infty$) whilst heat transfer rate decreases monotonically with increasing sweep under all conditions. For the turbulent boundary layer both skin friction and heat transfer rate exhibit maxima, the appropriate sweep angles being 70.5^o($M_\infty \to 0$) and 48.0^o ($M_\infty \to \infty$) for skin friction and 60.0 ($M_\infty \to 0$) and 35.6^o($M_\infty \to \infty$) for heat transfer. In all cases simple expressions have been produced which enable the maxima of skin friction and heat transfer to be estimated.

A comprehensive experimental investigation of the transition characteristics of the incompressible attachment line boundary layer has shown that for disturbances introduced by two-dimensional trip wires the state of the boundary layer is a function of the three parameters ϕ, s/ψ and d/ψ. The range of conditions covered has been such that it has been possible to infer behaviour at both very large and very small values of $d/\psi$and s/ψ. It has been found that in the limit of very large s/ψ the value of ϕ necessary for the detection of first bursts of turbulence has upper and lower bounds. The lower bound of ϕ equal to 245 for very large disturbances and the upper bound of 600 for very small disturbances, the latter being in good agreement with an estimate based upon two-dimensional linear stability theory. For the prediction of transition at intermediate values of s/ψ and d/ψ the criteria currently employed in boundary layer calculation methods are inadequate. Simple, more accurate criteria have been proposed. In situations where direct comparison has been possible the response of the attachment line flow has been entirely consistent with the established transition behaviour in pipes and on flat plates.

The validity of the lower bound on ϕ (245) has been extended to situation of high free stream Mach number with heat transfer at the wall. This has been achieved by the re-interpretation of several experimental investigations into the local heat transfer rate to swept circular cylinders. In addition it has been shown that the intermittency distributions in the transition region are statistically similar and are well represented by the functions which have been derived for flat plate transition. Calculations based upon the present criteria indicate that most of the civil aircraft which are currently in service have fully turbulent attachment lines in the cruise condition.

When boundary layer transition is caused by cross flow instability hot-wire measurements have shown that the change from laminar to turbulent conditions is not by the production of bursts of turbulence separated by quiescent laminar flow but by spikes of turbulence superimposed upon a laminar signal which is heavily modulated with periodic disturbances in the 0 - 10 KHz range. Surface oil flow visualisation has revealed the characteristic streak pattern in the laminar layer ahead of the transition front and a quantitative analysis of the pattern shows that the orientation of the streaks is closely linked with the critical profile direction as suggested by Stuart's quasi two-dimensional theory. The variation of the position of the transition front with sweep angle and Reynolds number has been investigated using the familiar surface pitot tube technique and the results show that a transition prediction criterion based upon a constant value of the cross flow Reynolds number χ is inadequate.

By using linear stability theory as a guide it has been possible to produce a criterion for transition close to the attachment line which is believed to be universally valid in incompressible flow. In addition a simple approximate criterion has been proposed for transition occurring at the chordwise position at which χ is itself a maximum. Predictions based upon two-dimensional linear stability theory and the e^{10} transition model have shown reasonable agreement with the experimentally observed streak pitch and transition Reynolds numbers for both the swept wing and rotating disc flows. This is an encouraging result which suggests that transition prediction in strongly three-dimensional flows may be possible without an excessive amount of calculation. In addition the theoretical transition model has shown that there is a broad spectrum of disturbance frequencies which undergo amplification and, consequently, the stationary disturbance observed in flow visualisation patterns may not govern transition.

Finally the possibility of the re-laminarisation of a turbulent boundary layer in the strong favourable pressure gradient near the attachment line has been considered. It has been shown that the governing parameter, K, has a maximum value very close to the attachment line and therefore only turbulence resulting from leading edge contamination is likely to be affected. However, for typical aerofoil leading edge shapes at small angles of incidence the maximum values of K at full scale cruise conditions are never large enough to cause significant re-laminarisation effects.

REFERENCES *

1.	GRAY, W.E.	The effect of wing sweep on laminar flow. R.A.E. TM 255, 1952 (ARC 14,929)
2.	GRAY, W.E.	The nature of the boundary layer flow at the nose of a swept wing R.A.E. TM 256, 1952 (ARC 15,021)
3.	OWEN, P.R. RANDALL, D.G.	Boundary layer transition on a sweptback wing. R.A.E. TM 277, 1952 (ARC 15,022)
4.	OWEN, P.R. RANDALL, D.G.	Boundary layer transition on a sweptback wing: a further investigation. R.A.E. TM 330, 1953
5.	GREGORY, N. STUART, J.T. WALKER, W.S.	On the stability of three dimensional boundary layers with application to the flow due to a rotating disc. Philosophical Transactions of the Royal Society of London, Series A, Vol.248, pp.155-199
6.	ANSCOMBE, A. ILLINGWORTH, L.N.	Wind tunnel observations of boundary layer transition on a wing at various angles of sweep back. ARC R and M 2968.
7.	HIRSCHEL, E.H.	Recommendations for research work on transitions in boundary layers (Eurovisc Working Party on Transition in Boundary Layers). DFVLR TM WT 1/75, 1975
8.	CUMPSTY, N.A. HEAD, M.R.	The calculation of three-dimensional turbulent boundary layers. Part II Attachment-line flow on an infinite swept wing. The Aeronautical Quarterly, Vol.XVIII, May, 1967, pp.150-164
9.	ROSENHEAD, L.	Laminar Boundary Layers Oxford University Press, 1963.
10.	GREGORY, N. LOVE, E.M.	Laminar flow on a swept leading edge - final progress report. NPL Aero.Memo.26, 1965.

* N.B. Reports quoted are not necessarily available.

11. GASTER, M. — On the flow along swept leading edges. The Aeronautical Quarterly, Vol.XVIII, May, 1967, pp.165-184

12. PFENNINGER, W. — Flow phenomena at the leading edge of swept wings. Recent developments in Boundary Layer Research - Part IV. AGARDograph 97, May 1965.

13. CUMPSTY, N.A. HEAD, M.R. — The calculation of the three-dimensional turbulent boundary layer. Part III Comparison of attachment line calculations with experiment. The Aeronautical Quarterly, Vol.XX, May 1969, pp.99-113.

14. ECKERT, E.R.G. — Engineering relations for friction and heat transfer to surfaces in high velocity flows. Journal of The Aeronautical Sciences, Vol.22, August 1955, pp.585-587.

15. RUBESIN, M.W. JOHNSON, H.A. — A critical review of skin friction and heat transfer solutions of the laminar boundary layer on a flat plate. Transactions of the ASME, Vol.71, 1949 pp.385-388

16. SOMMER, S.C. SHORT, B.J. — Free flight measurements of turbulent boundary-layer skin friction in the presence of severe aerodynamic heating at Mach numbers from 2.8 to 7.0. NACA Report 3391, 1955.

17. CLARK, F.L. CREEL, T.R. — Reference temperature method for predicting turbulent compressible skin friction coefficient. AIAA Journal, Vol.II,2, Feb.1973 pp.239-240.

18. ZOBY, E.V. GRAVES, R.A. — Comparison of turbulent prediction methods with ground and flight test data. AIAA Journal, Vol.15,7,July 1977,pp.901-902

19. BECKWITH, I.E. — Similar solutions for the compressible boundary layer on a yawed cylinder with transpiration cooling. NASA Technical Report R-42, 1959.

20. BECKWITH, I.E.
GALLAGHER, J.J.
Local heat transfer and recovery temperatures on a yawed cylinder at a Mach number of 4.15 and high Reynolds numbers.
NASA Technical Report R-104, 1961.

21. HUNT, J.L.
BUSHNELL, D.M.
BECKWITH, I.E.
The compressible turbulent boundary layer on a blunt swept slab with and without leading edge blowing
NASA TN D-6203, March 1971.

22. ACHENBACH, E.
Total and local heat transfer from a smooth circular cylinder in cross-flow at high Reynolds number.
International Journal of Heat and Mass Transfer, Vol.18, 1975, pp.1387-1396.

23. BRUN, E.A.
DIEP, G-B
LE FUR, B.
Transport de chaleur et de masse sur des cylindres circulaires en fleche dans un ecoulement supersonique.
Recent Developments in Boundary Layer Research - Part 2.
AGARDograph 97, May 1965.

24. BUSHNELL, D.M.
Interference heating on a swept cylinder in region of intersection with a wedge at Mach number 8.
NASA TN D-3094, December 1965.

25. BRADLEY, R.G.
Approximate solutions for compressible turbulent boundary layers in three dimensional flow.
AIAA Journal, Vol.6,5 May 1968, pp.859-864.

26. HEAD, M.R.
VASANTA RAM, V.
Simplified presentation of Preston tube calibration.
The Aeronautical Quarterly, Vol.XXII, August 1971, pp.295-300.

27. BECKWITH, I.E.
Experimental investigation of heat transfer and pressures on a swept cylinder in the vicinity of its intersection with a wedge and flat plate at Mach number 4.15 and high Reynolds number.
NASA TN D-2020, July, 1964.

28. JONES, R.A.
Heat transfer and pressure investigation of a fin-plate interference model at a Mach number of 6.
NASA TN D-2028, July, 1964.

29. KEYES, F.G. — A summary of viscosity and heat-conduction data for He, A, H_2, O_2, N_2, CO, CO_2, H_2O, and air. Transactions of the ASME, Vol.73, July, 1951, pp.589-596.

30. GOLDSTEIN, S. — Modern Developments in Fluid Dynamics Vol.II. Ist ed. Dover, 1965.

31. PFENNINGER, W. BACON, J.W. — Amplified laminar boundary layer oscillations and transition at the front attachment line of a 45^0 swept flat-nosed wing with and without boundary layer suction. Viscous Drag Reduction, C.S.Wells(editor), Plenum Press, 1969, pp.85-105.

32. OBREMSKI, H.J. et al. — A portfolio of stability characteristics of incompressible boundary layers. AGARDograph 134, March 1969.

33. JAFFE, N.A. OKAMURA, T.T. SMITH, A.M.O. — Determination of spatial amplification factors and their application to predicting transition. AIAA Journal, Vol.8,2, Feb.1970.pp.301-308.

34. CARLSON, J.C. — Investigation of the laminar flow characteristics of a 33^0 swept suction wing at high Reynolds numbers in the NASA Ames 12-foot pressure wind tunnel. Northrop Report, NOR-66-58,January 1966.

35. GIBBINGS, J.C. — On boundary layer transition wires. ARC CP 462, December 1958.

36. LESSEN, M. KO, S-H — Viscous instability of an incompressible fluid half jet flow. The Physics of Fluids, Vol.9,6,June 1966 pp.1179-1183.

37. KLEBANOFF, P.S. TIDSTROM, K.D. — Mechanism by which a two-dimensional roughness element induces boundary layer transition. The Physics of Fluids, Vol.15,7,July 1972, pp.1173-1188.

38. FASEL,H. BESTEK, H. SCHEFENACKER, R. — Numerical simulation studies of transition phenomena in incompressible two-dimensional flows. AGARD Conference Proceedings No.224, Laminar-Turbulent Transition, Copenhagen, May 1977, paper number 14.

39. TANI, I.
Einige bemerkungen über den laminar-turbulenten umschlag in grenzschichtstrominger.
ZAMM, Vol.53,Part 4 (sonderheft), 1973, pp.T25-T32.

40. HAMA, F.R.
LONG, J.D.
HEGARTY, J.C.
On transition from laminar to turbulent flow.
Journal of Applied Physics, Vol.28,4, April 1957, pp.388-394.

41. PRESTON, J.H.
The minimum Reynolds number for a turbulent boundary layer and the selection of a transition device.
Journal of Fluid Mechanics, Vol.3,4. Jan.1958, pp.373-384.

42. NARASIMHA, R.
On the distribution of intermittency in the transition region of a boundary layer.
Journal of the Aeronautical Sciences, Vol.24,Sept.1957, pp.711-712

43. EMMONS, H.W.
The laminar-turbulent transition in a boundary layer - Part I.
Journal of the Aeronautical Sciences, Vol.18, July 1951, pp.490-498.

44. WYGNANSKI, I.
SOKOLOV, M.
FRIEDMAN, D.
On a turbulent 'spot' in a laminar boundary layer.
Journal of Fluid Mechanics, Vol.78,4, 1976, pp.785-819.

45. FIRMIN, M.C.P.
COOK, P.H.
Unpublished work - R.A.E.Farnborough

46. BUSHNELL, D.M.
Effects of shock impingement and other factors on leading-edge heat transfer
NASA TN D-4543, April 1968.

47. TOPHAM, D.R.
A correlation of leading edge transition and heat transfer on swept cylinders in supersonic flow.
Journal of the Royal Aeronautical Society, Vol.69,1, Jan.1965. pp.49-52

48. EICHELBRENNER, E.A.
MICHEL, R.
Observations sur la transition laminair-turbulent en trois dimensions.
La Recherche Aeronautique, No.65, July-August 1958, pp.3-10.

49.	KNAPP, C.F. ROACHE, P.J.	A combined visual and hot-wire anemometer investigation of boundary layer transition. AIAA Journal, Vol.6,1. Jan.1968, pp.29-36.
50.	SQUIRE, L.C.	An experimental investigation at supersonic speeds of the characteristics of two gothic wings, one plane and one cambered. ARC R and M 3211, 1959.
51.	FALES, E.N.	A new laboratory technique for investigation of the origin of fluid turbulence. Journal of the Franklin Institute, Vol.259,6,June 1955, pp.491-515
52.	LILLY, D.K.	On the instability of the Ekman boundary flow. Journal of Atmospheric Science, Vol.23. Sept.1966, pp.481-494
53.	ECKERT, E.R.G. SOEHNGHEN, E.	Interferometric studies on the stability and transition to turbulence of a free convection boundary layer. Proceedings of the General Discussion on Heat Transfer, 11-13th September 1951, London, Institute of Mechanical Engineers, pp.321-323.
54.	TSUJI, Y. MORIKAWA, Y. NAGATANI, T. SAKOU, M.	The stability of a two-dimensional wall jet. The Aeronautical Quarterly, Vol.XXVIII, Nov.1977, pp.235-246.
55.	COLES, D.	Transition in circular Couette flow. Journal of Fluid Mechanics, Vol.21,3, March 1965, pp.385-425.
56.	COCHRAN, W.G.	The flow due to a rotating disc. Proceedings of the Cambridge Philosophical Society, Vol.30, 1934, pp.365-375.
57.	OSTRACH, S.	An analysis of laminar free-convection layer flow and heat transfer about a flat plate parallel to the direction of the generating body force. NACA Report No.1111, 1951.

58.	GLAUERT, M.B.	The wall jet. Journal of Fluid Mechanics, Vol.1, 1956 pp.625-632.
59.	PFENNINGER, W.	Laminar Flow Control. AGARD Report 654, Special Course on Concepts for Drag Reduction, March 1977.
60.	BROWN, W.B.	Numerical calculation of the stability of cross-flow profiles in laminar boundary layers on a rotating disc and on a swept backwing and an exact calculation of the stability of the Blasius velocity profile. Northrop Report NAI-59-5(BLC-117), January 1959.
61.	CARLSON, J.C.	Results of a low speed wind tunnel test to investigate the influence of leading edge radius and angle of attack on the spread of turbulence along the leading edge of a sweptback wing. Northrop Report NOR-64-30,March 1964.
62.	BOLTZ, F.W. KENYON, G.C. ALLEN C.Q.	Effects of sweep angle on the boundary-layer stability characteristics of an untapered wing at low speeds. NASA TN D-338, July 1960.
63.	THEODORSEN, T. REGIER, A.	Experiments on drag of revolving discs, cylinders and streamline rods at high speeds. NACA Report No.793, 1944.
64.	LACHMANN, G.V. (Editor)	Boundary Layer and Flow Control No.2 Pergamon Press Limited, 1961.
65.	KURTZ, E.F. CRANDALL, S.H.	Computer-aided analysis of hydrodynamic stability. Journal of Mathematical Physics, Vol.41, 1962, pp.264-279.
66.	CEBECI, T. KELLER, H.B.	Stability calculations for a rotating disc. AGARD Conference Proceedings No.224, Laminar-Turbulent Transition, Copenhagen, May 1977, paper number 7.

67. CHUN, D.H.
SCHWARTZ, W.H.
Stability of the plane incompressible viscous wall jet subjected to small disturbances.
Physics of Fluids, Vol.10,1967,pp.911-915.

68. GREGORY, N.
The present position of research on laminar flow over swept wings.
Unpublished MOD Report, 1957.

69. MALTBY, R.L.
KEATING, R.F.A.
The surface oil flow technique for use in low speed wind tunnels.
AGARDograph 70, April 1962

70. BEASLEY, J.A.
Calculation of the laminar boundary layer and the prediction of transition on a sheared wing.
ARC R and M 3787, October 1973.

71. MACK, L.M.
Transition prediction and linear stability theory.
AGARD Conference Proceedings No.224, Laminar-Turbulent Transition, Copenhagen, May 1977, paper number 1.

72. STEWARTSON, K.
Some aspects of non-linear stability theory.
Fluid Dynamic Transactions, Polish Academy of Science, Vol.7, 1975, pp.101-128.

73. ACHENBACH, E.
Distribution of local pressure and skin friction around a circular cylinder in cross-flow up to Re = 5 x 10^6.
Journal of Fluid Mechanics, Vol.34, 4, 1968, pp.625-639.

74. SCOTT-WILSON,J.B.
CAPPS, D.S.
Wind tunnel observations of boundary layer transition on two sweptback wings at a Mach number of 1.61.
R.A.E.Tech.Note Aero.2347, December 1954.

75. DUNNING, R.W.
ULMANN, E.F.
Effects of sweep and angle of attack on boundary layer transition on wings at Mach number 4.04.
NACA TN 3473, March 1955.

76. JILLIE, D.W.
HOPKINS, E.J.
Effects of Mach Number, leading edge bluntness and sweep on boundary layer transition on a flat plate.
NASA TN D-1071, 1961.

77. CHAPMAN, G.T. Some effects of leading edge sweep on boundary layer transition at supersonic speeds.
NASA TN D-1075, 1961.

78. OKAMOTO, T.
MISU, I. Reverse transition of a turbulent boundary layer on plane wall of two-dimensional contraction.
Transactions of the Japan Society of Aeronautical and Space Sciences, Vol.20, 47, 1977, pp.1-12.

APPENDIX A

Conditions at the Attachment Line in Supersonic Flow

Notation

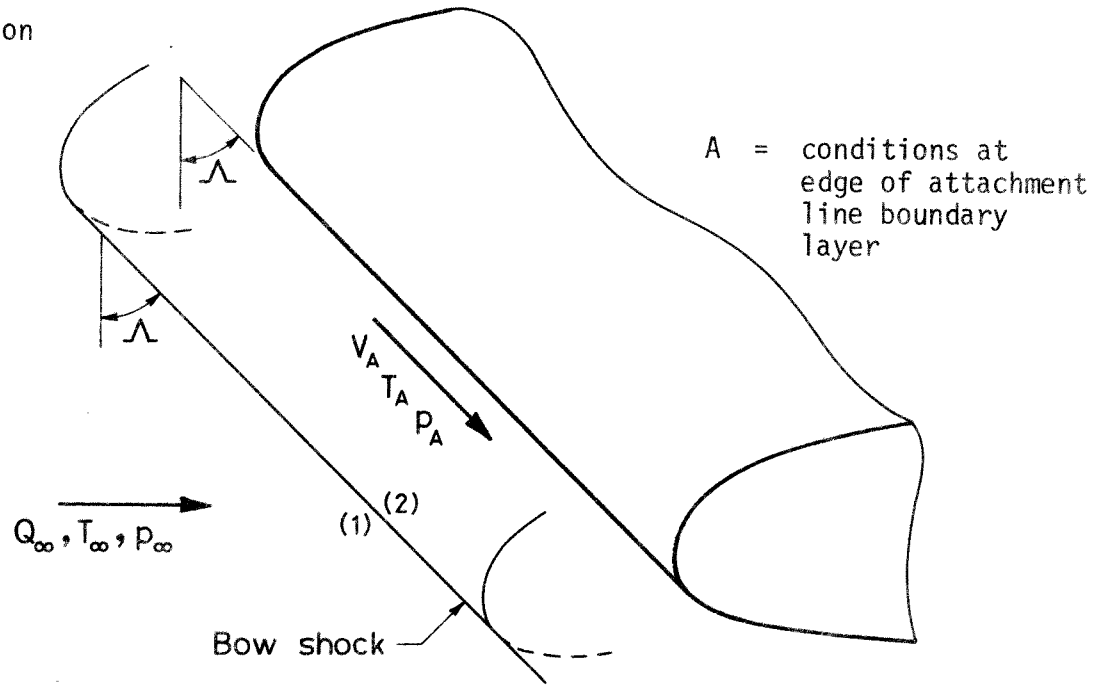

For an infinite swept cylinder the following assumptions are made

a) the bow shock is parallel to the attachment line

b) the flow is adiabatic i.e. T_0 is constant throughout the flow field

c) the flow is isentropic up to station (1) and between station (2) and the edge of the attachment line boundary layer

d) the gas is 'Perfect' i.e. it has constant values of $\mathcal{R}$, Cp and γ

Using (a) to (d) it follows immediately that

$$\frac{To}{T_\infty} = 1 + (\frac{\gamma-1}{2})M_\infty^2 \qquad (1)$$

and

$$\frac{T_A}{T_\infty} = 1 + (\frac{\gamma-1}{2})M_\infty^2 \cos^2\Lambda \qquad (2)$$

since $M_A = \frac{V_A}{(\gamma \mathcal{R} T_A)^{\frac{1}{2}}} = M_\infty \sin\Lambda \, (\frac{T_\infty}{T_A})^{\frac{1}{2}}$ and $\frac{T_0}{T_A} = 1 + (\frac{\gamma-1}{2})M_A^2$

for zero heat transfer (adiabatic wall case)

$$\frac{T_W}{T_A} = 1 + r\left(\frac{\gamma-1}{2}\right) M_A^2$$

or

$$\frac{T_W}{T_O} = \frac{1 + \left(\frac{\gamma-1}{2}\right)M_\infty^2 \left(\cos^2\Lambda + r \sin^2\Lambda\right)}{1 + \left(\frac{\gamma-1}{2}\right)M_\infty^2} \qquad (3)$$

In general, the flow about an infinite swept cylinder is three-dimensional. However, the streamwise plane containing the attachment line is a plane of symmetry and hence there are no velocity components normal to this plane. Moreover, for supersonic flow normal to the leading edge of the cylinder the bow shock intersects this plane of symmetry at 90^0 and, consequently, conditions at the swept attachment line are determined by the two-dimensional oblique shock relations.

Hence for $M_\infty \cos\Lambda \leq 1$

$$\frac{pA}{p_\infty} = \frac{pA}{p_O}\cdot\frac{p_O}{p_\infty} = \left(1 + \left(\frac{\gamma-1}{2}\right)M_A^2\right)^{-\left(\frac{\gamma}{\gamma-1}\right)} \cdot \left(1 + \left(\frac{\gamma-1}{2}\right)M_\infty^2\right)^{\left(\frac{\gamma}{\gamma-1}\right)}$$

and since

$$1 + \left(\frac{\gamma-1}{2}\right)M_A^2 = \frac{1 + \left(\frac{\gamma-1}{2}\right)M_\infty^2}{1 + \left(\frac{\gamma-1}{2}\right)M_\infty^2\cos^2\Lambda} \qquad \text{from (1) and (2)}$$

$$\frac{pA}{p_\infty} = \left(1 + \left(\frac{\gamma-1}{2}\right)M_\infty^2 \cos^2\Lambda\right)^{\left(\frac{\gamma}{\gamma-1}\right)} \qquad (4)$$

When $M_\infty \cos\Lambda > 1$

$$\frac{pA}{p_\infty} = \frac{pA}{p_{O_2}}\cdot\frac{p_{O_2}}{p_1}$$

where

$$\frac{pA}{p_{O_2}} = \left(1 + \left(\frac{\gamma-1}{2}\right)M_A^2\right)^{-\left(\frac{\gamma}{\gamma-1}\right)} = \left(\frac{1 + \left(\frac{\gamma-1}{2}\right)M_\infty^2\cos^2\Lambda}{1 + \left(\frac{\gamma-1}{2}\right)M_\infty^2}\right)^{\left(\frac{\gamma}{\gamma-1}\right)}$$

and from the oblique shock relations (see reference 1)

$$\frac{p_{o_2}}{p_1} = \left(\frac{\gamma+1}{2\gamma M_\infty^2\cos^2\Lambda - (\gamma-1)}\right)^{\left(\frac{1}{\gamma-1}\right)} \cdot \left(\frac{(\gamma+1)M_\infty^2\cos^2\Lambda\left[(\gamma-1)M_\infty^2+2\right]}{2\left[(\gamma-1)M_\infty^2\cos^2\Lambda+2\right]}\right)^{\left(\frac{\gamma}{\gamma-1}\right)}$$

therefore

$$\frac{pA}{p_\infty} = \left(\frac{(\gamma+1)M_\infty^2\cos^2\Lambda}{2}\right)^{\left(\frac{\gamma}{\gamma-1}\right)} \cdot \left(\frac{\gamma+1}{2\gamma M_\infty^2\cos^2\Lambda - (\gamma-1)}\right)^{\left(\frac{1}{\gamma-1}\right)} \qquad (5)$$

Chordwise Velocity Gradient ($U_1\ D/C_0$)

If $M_\infty\cos\Lambda$ is greater than 2.5 then the pressure distribution in the visinity of the attachment line is found to be in good agreement with the predictions of Modified Newtonian theory (see for example Topham - reference 2) i.e.

$$\frac{Cp}{Cp_{max}} \simeq \cos^2\left(\frac{2x}{D}\right)$$

then since

$$Cp = (p - p_\infty)/\tfrac{1}{2}\rho_\infty U_\infty^2 \quad \text{by definition and } pA = p_{max}$$

$$\frac{p}{pA} = \left(1 - \frac{p_\infty}{pA}\right) \cdot \cos^2\left(\frac{2x}{D}\right) + \frac{p_\infty}{pA}$$

At the attachment line the Mach number normal to the leading edge M_n is zero, therefore, in the vicinity of the attachment line M_n will be small. Moreover, since the chordwise and spanwise components of the inviscid flow are independent it follows that Bernoulli's equation

$$p_A \simeq p_e + \tfrac{1}{2}\rho_A U_e^2$$

is valid locally for the chordwise flow very close to the attachment line i.e.

$$U_e \simeq \left(2\frac{p_A}{\rho_A}\left(1 - \frac{p_e}{p_A}\right)\right)^{\frac{1}{2}}$$

Substituting for p/p_A and using the perfect gas equation of state it follows that

$$\frac{U_e}{U_\infty} \simeq \frac{\sin(2x/D)}{M_\infty \cos\Lambda} \left(\frac{2}{\gamma} \cdot \frac{T_A}{T_\infty} \cdot \left(1 - \frac{p_\infty}{p_A}\right)\right)^{\frac{1}{2}}$$

and hence by simple differentiation

$$\frac{D}{U_\infty} \left(\frac{dU_e}{dx}\right)_{x=0} = U_1 \frac{D}{C_0} = \frac{2}{M_\infty \cos\Lambda} \cdot \left(\frac{2}{\gamma} \frac{T_A}{T_\infty} \left(1 - \frac{p_\infty}{p_A}\right)\right)^{\frac{1}{2}}$$

In the limit as $M_\infty \cos\Lambda$ tends to infinity

$$\frac{T_A}{T_\infty} \rightarrow \left(\frac{\gamma-1}{2}\right) M_\infty^2 \cos^2\Lambda$$

and

$$\frac{p_A}{p_\infty} \rightarrow \left(\frac{\gamma-1}{2}\right)^{\left(\frac{\gamma+1}{\gamma-1}\right)} \left(\frac{1}{\gamma}\right)^{\left(\frac{1}{\gamma-1}\right)} M_\infty^2 \cos^2\Lambda$$

therefore

$$\frac{T_A}{T_\infty} \left(1 - \frac{p_\infty}{p_A}\right) \rightarrow \left(\frac{\gamma-1}{2}\right) M_\infty^2 \cos^2\Lambda$$

i.e.

$$\frac{D}{U_\infty} \left(\frac{dU_e}{dx}\right)_{x=0} \rightarrow 2\left(\frac{\gamma-1}{\gamma}\right)^{\frac{1}{2}}$$

Reference

1. AMES RESEARCH STAFF — Equations, tables and charts for compressible flow. NACA Report 1135, 1953

2. TOPHAM, D.R. — An empirical formula for stagnation point velocity, gradient for spheres and circular cylinders in hypersonic flow. Journal of the Royal Aeronautical Society, Vol.69, June 1965, pp.407-408.

APPENDIX B

The Application of Linear Stability Theory the Problem of the Prediction of Transition in the Attachment Line Boundary Layer

In section (5.5) of the main text it was shown that the behaviour of small amplitude harmonic waves which travel along the attachment and whose rate of amplification or damping is determined by their position in space is given by the solution of a fourth order ordinary differential equation -

$$\left(\frac{v}{V_\infty} - \frac{\omega r}{\alpha}\right)\left(\frac{d^2\sigma}{d(z/\delta_1)^2} - \alpha^2\sigma\right) - \frac{d^2(v/V_\infty)}{d(z/\delta_1)^2}\,.\sigma = -\frac{i}{\alpha R_{\delta_1}}\left(\frac{d^4\sigma}{d(z/\delta_1)^4} - 2\alpha^2\frac{d^2\sigma}{d(z/\delta_1)^2} + \alpha^4\sigma\right) \tag{1}$$

subject to the boundary conditions -

$$\sigma = 0 \qquad \frac{d\sigma}{d(z/\delta_1)} = 0 \qquad \text{when} \quad z/\delta_1 = 0$$

and $$\sigma = 0 \qquad \frac{d\sigma}{d(z/\delta_1)} = 0 \qquad \text{when} \quad z/\delta_1 \to \infty$$

These homogeneous boundary conditions lead to a boundary value problem of the eigenvalue type and since the equation can only be solved analytically for certain special velocity profiles it is common practise to produce solutions numerically. In the present work the solution has been obtained by using the method developed by Wazzan, Okamura and Smith (reference 1). Briefly, the procedure begins by recognising that equation (1) has a general solution which is composed of a linear combination of four independent solutions i.e. -

$$\sigma = A\sigma_1 + B\sigma_2 + C\sigma_3 + D\sigma_4 \tag{2}$$

where A, B, C and D are constants of integration. However, in the free stream equation (1) has constant coefficients and so the independent solutions take the form

$$\begin{aligned}
\sigma_1 &= \exp\,(-\alpha\, z/\delta_1) \\
\sigma_2 &= \exp\,(+\alpha\, z/\delta_1) \\
\sigma_3 &= \exp\,(-(\alpha^2 + i\alpha R(1-\tfrac{\omega r}{\alpha}))^{\frac{1}{2}}\, z/\delta_1) \\
\sigma_4 &= \exp\,(+(\alpha^2 + i\alpha R(1 - \tfrac{\omega r}{\alpha}))^{\frac{1}{2}}\, z/\delta_1)
\end{aligned} \tag{3}$$

Clearly the boundary conditions for z/δ_1 tending to infinity can only be satisfied by σ_1 and σ_3 and so the complete solution is reduced to

$$\sigma = A\sigma_1 + C\sigma_3 \tag{4}$$

The numerical solution begins with a specification of the values of R and ω_r and estimates for α_r and α_i. Equations (3) are then used to provide starting values for σ_1 and σ_3 at the edge of the boundary layer (in this case $z = \delta_{0.999}$) and the equation is then integrated numerically to the wall to produce $\sigma_1(0)$ and $\sigma_3(0)$. In general a linear combination of $\sigma_1(0)$ and $\sigma_3(0)$ may be found which satisfies one of the two boundary conditions at the wall and the numerical procedure continues by progressively correcting the initial guesses for α_r and α_i until a value of $\sigma(0)$ is found which satisfies all the boundary conditions - the Eigen solution. Although the solution is quite straightforward in principle, there are serious problems associated with the build up of round off errors in the numerical integration and full details of the sophisticated computational techniques necessary to cope with these difficulties are contained in reference 1. The results of the present calculations are presented in figure.1.

The actual prediction of the conditions necessary for transition requires a model for the mechanism which induces a breakdown of the laminar flow and in the present case the 'amplitude ratio' method is used - see Jaffe Okamura and Smith (ref.2). This method suggests that first burst of turbulence appear when any single frequency disturbance reaches a situation in which its' amplitude is e^n times greater than the amplitude it possessed when it first became unstable i.e.

$$\left[\log_e \left(\frac{A_T}{A_i}\right) = -\int_{s_i}^{s_T} \underline{\alpha_i}\, ds = n\right]_{\underline{\omega r}=\text{constant}} \tag{5}$$

The value of n is fixed by a correlation of experimental data and Jaffe et al, suggest that a value of 10 is suitable for prediction purposes. Since the semi-infinite attachment line boundary layer has constant thickness the amplification proceeds at a constant rate $\underline{\alpha_i}$ for a fixed value of the Reynolds number $R\delta_1$. The maximum amplification rate for a given value of $R\delta_1$ occurs at a fixed disturbance frequency ω_r and those disturbances which enter the layer first will be the most highly amplified. Therefore disturbances which enter the boundary layer at the upstream tip (s = 0) will be the ones most likely to produce transition and consequently equation (5) is simplified to

$$\left(-\underline{\alpha_i}\, s_T\right)_{\substack{\max \\ \underline{\omega r}=\text{constant} \\ R_{\delta 1}=\text{constant}}} = \log_e \left(\frac{A_T}{A_i}\right) = n \tag{6}$$

since $\underline{\alpha_i}$ is independent of s and $s_i = 0$

$$\therefore \quad \log_e \left(\frac{A_T}{A_i}\right) = -(\underline{\alpha_i} \times \delta_1)_{min} \cdot \frac{s_T}{\delta_1} = -\alpha_i \cdot \frac{s_T}{\delta_1}$$

or

$$\frac{s_T}{\delta_1} = \frac{n}{(-\alpha_i)_{max}} \qquad (7)$$

ω_r=constant
$R\delta_1$=constant

The variation of $(-\alpha_i)_{max}$ with $R\delta_1$ is obtained from figure 1 and is plotted separately as figure 2. Finally the variation of R_{δ_1} at transition with $(s_T/n.\delta_1)$ as given by equation (7) is presented in figure 3.

REFERENCES

1. WAZZAN, A.R.
OKAMURA, T.T.
SMITH, A.M.O.
Spatial and temporal stability charts for the Falkner-Skan boundary layer profiles.
McDonnell Douglas Report No.DAC-67086, 1968.

2. JAFFE, N.A.
OKAMURA, T.T.
SMITH, A.M.O.
Determination of spatial amplification factors and their application to predicting transition.
AIAA Journal, Vol.8,No.2.February 1970, pp.301-308.

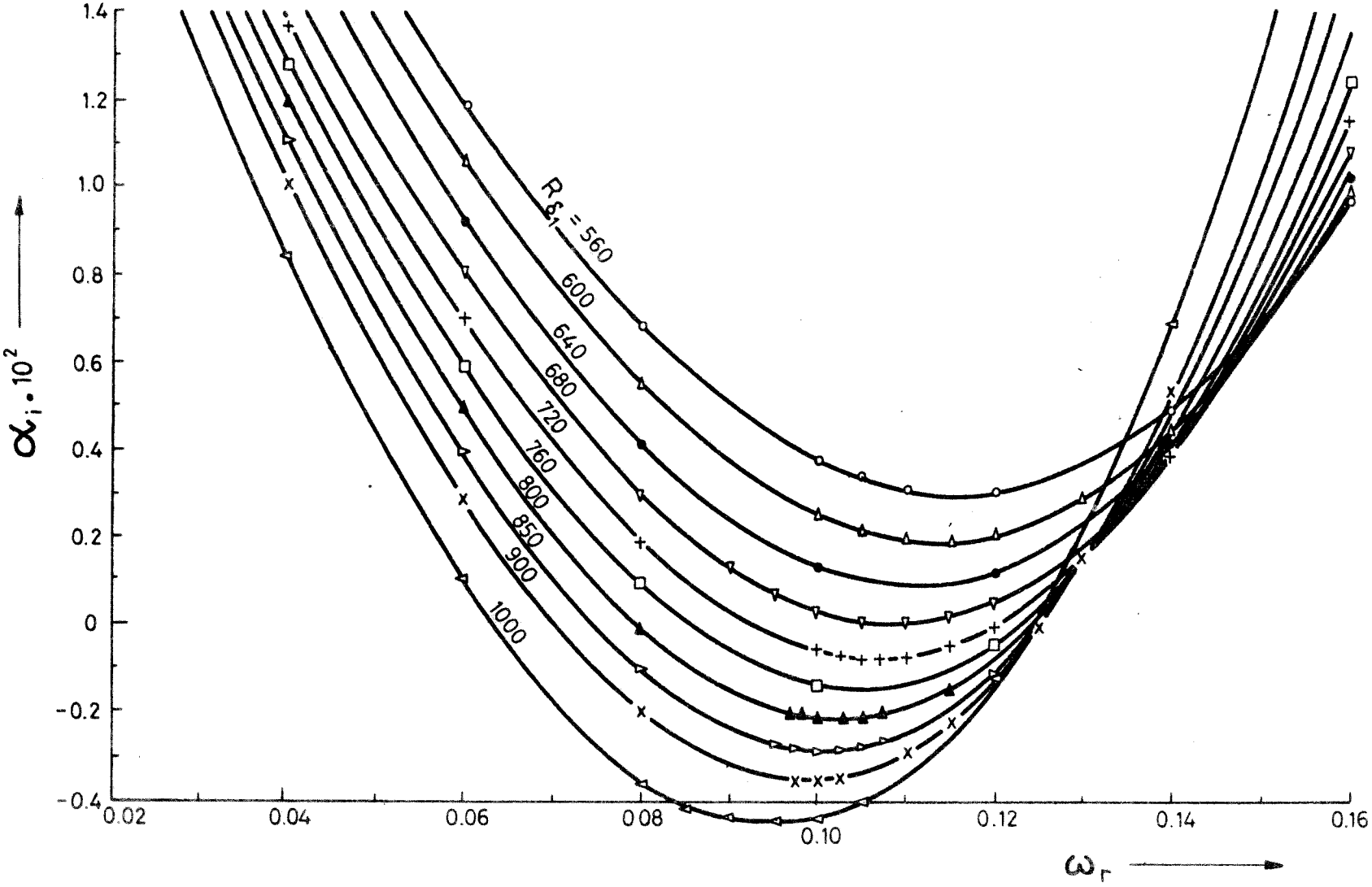

Fig. 1.b. The variation of spatial amplification rate with frequency and Reynolds number for the attachment line boundary layer.

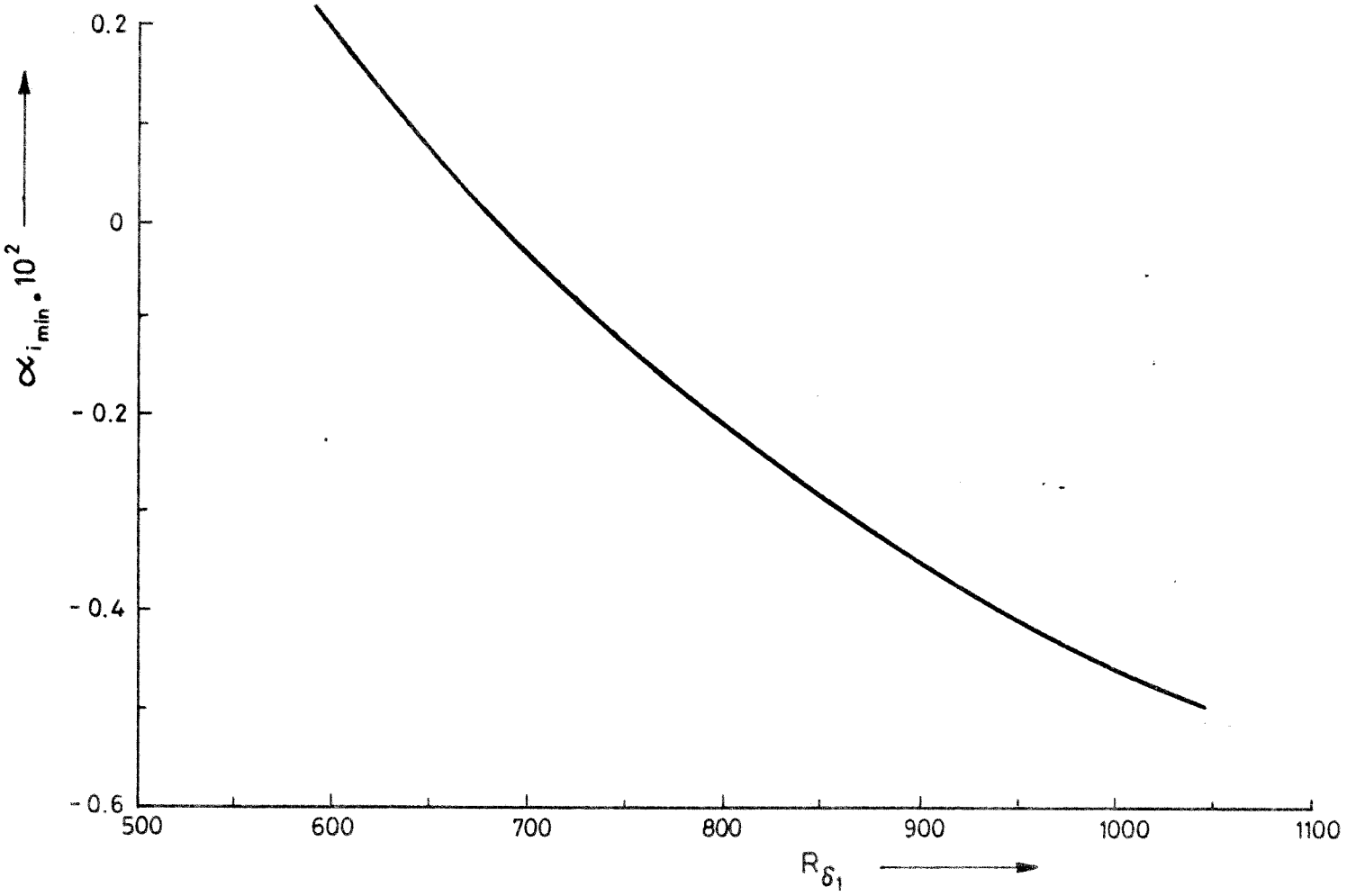

Fig. 2.b. The variation of $\alpha_{i_{min}}$ with Reynolds number for the attachment line boundary layer.

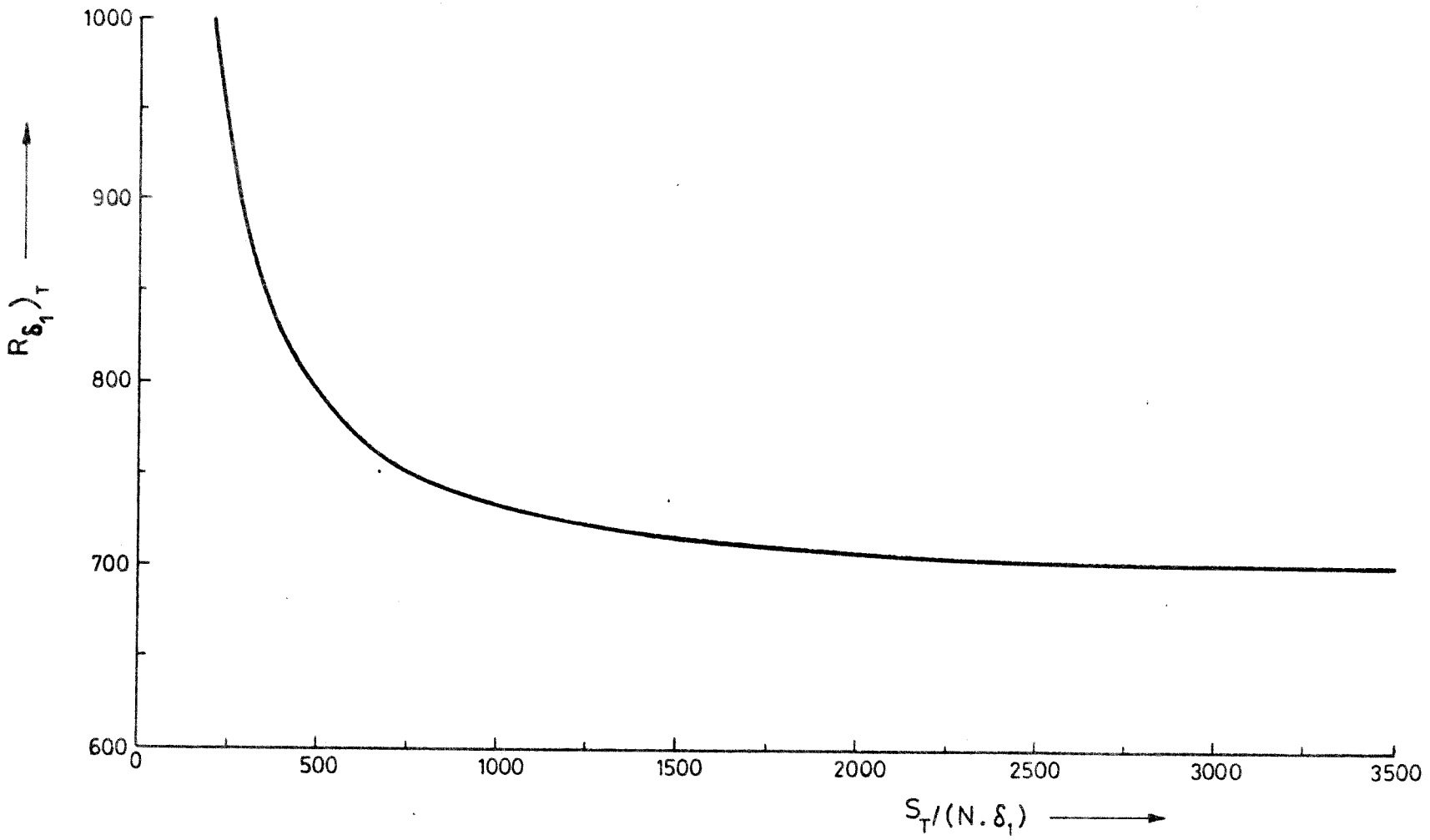

Fig. 3.b. The variation of displacement thickness Reynolds number at transition with transition front position $S_T/(N.\delta_1)$ for the attachment line boundary layer.

APPENDIX C

A Simple Criterion for the Largest 2-D Roughness Height which will not affect the position of 'natural' Transition on a Flat Plate

The estimation of the diameter of the largest two-dimensional trip wire which may be introduced into a laminar boundary layer and yet not affect the natural transition position x_{NT} is a problem of some practical importance. Although several simple criteria have been suggested for the flat plate case the most recent and probably the most reliable is that due to Gibbings and Hall (ref.1) where for a flow with a free stream speed U_∞ and a 2-D trip wire diameter d positioned a distance x_d from the plate leading edge -

$$\frac{826}{\left(\frac{U_\infty d}{\nu}\right)} = 1 + \frac{1}{3}\left(\frac{R_{x_{NT}}}{R_{x_d}} - 1\right) \qquad (1)$$

which may be rewritten as -

$$\frac{826}{Rd} = \frac{2 + \left({}^{x_{NT}}/_{x_d}\right)}{3} \qquad (2)$$

Whilst acknowledging that this may well be the best possible form for a criterion, equation (2) does have the disadvantage that it does not readily convey an impression of the size of the trip wire in relation to the thickness of the undisturbed boundary layer.

Several experiments have been conducted into the tripping characteristics of the flat plate boundary layer (see for example references 2, 3 and 4) and in all cases it has been found that the data may be well correlated by an expression of the form

$$\left(\frac{U_\infty \delta_1}{\nu}\right)_{x_T} = K\left(\frac{\delta_1}{d}\right)_{x_d} \qquad (3)$$

or

$$\frac{U_\infty d}{\nu} = K\left(\frac{x_d}{x_T}\right)^{\frac{1}{2}} \qquad (4)$$

where K lies somewhere in the range 780 to 840. Taking the average value of 826 suggested by Tani (reference 5) and considering the particular case of largest value of d which will leave x_{NT} unaltered equation (4) becomes

$$\frac{826}{Rd} = \left(\frac{x_{NT}}{x_d}\right)^{\frac{1}{2}} \tag{5}$$

a form which may be compared directly with equation (2). For x_{NT}/x_d lying in the range 1.0 to 5.5 the two expressions differ by less than 6% and since there appears to be no experimental data available for the justification of either equation for values of x_T/x_d in excess of 3 equation (5) and consequently equation (3) may be considered to be good approximations to equation (1) for most practical purposes. However in the present context equation (3) is the most useful since it may be rewritten in the form

$$\left(\frac{d}{\delta_1}\right)_{x_d} = \frac{826}{1.721\ (Rx_{NT})^{\frac{1}{2}}} = \frac{480}{(Rx_{NT})^{\frac{1}{2}}} \tag{6}$$

or alternatively

$$\left(\frac{d}{\delta_2}\right)_{x_d} = \frac{1244}{(Rx_{NT})^{\frac{1}{2}}}$$

Therefore in a given situation where Rx_{NT} is either known from experiment or predicted from a theory the criterion for the maximum permissible roughness height becomes simply

$$\frac{d}{\delta_2} = \text{constant} \tag{7}$$

This result has immediate physical significance and it can be applied in a boundary layer calculation without difficulty. By way of an example if Rx_{NT} is taken to be 2.6×10^6 then

$$\frac{d}{\delta_2} = 0.77 \text{ or } \frac{d}{\delta_1} = 0.30 \text{ or } \frac{d}{\delta_{.99}} = 0.10 \tag{8}$$

are alternative forms for the criterion. Figure 1 presents a comparison between the predictions of equations (1) and (8).

References

1. GIBBINGS,J.C. HALL, D.J. — Criterion for tolerable roughness in a laminar boundary-layer. Journal of Aircraft, Vol.6,No.2. 1969 pp.171-173

2. TANI, I. SATO, H. — Boundary-layer transition by roughness element. Journal of the Physical Society of Japan, Vol.11, No.12, 1956, pp.1284-1291

3. POTTER, J.L. — Subsonic boundary-layer transition caused by single roughness elements. Journal of the Aeronautical Sciences, Vol.24, No.2, February 1957,pp.158-159

4. GIBBINGS, J.C. — On boundary-layer transition wires. ARC, C.P.No.462, 1959

5. TANI, I. — Boundary-layer transition. Annual Review of Fluid Mechanics, Vol.1 (1969), Annual Reviews Inc.,Palo Alto, California, U.S.A. pp.186-188.

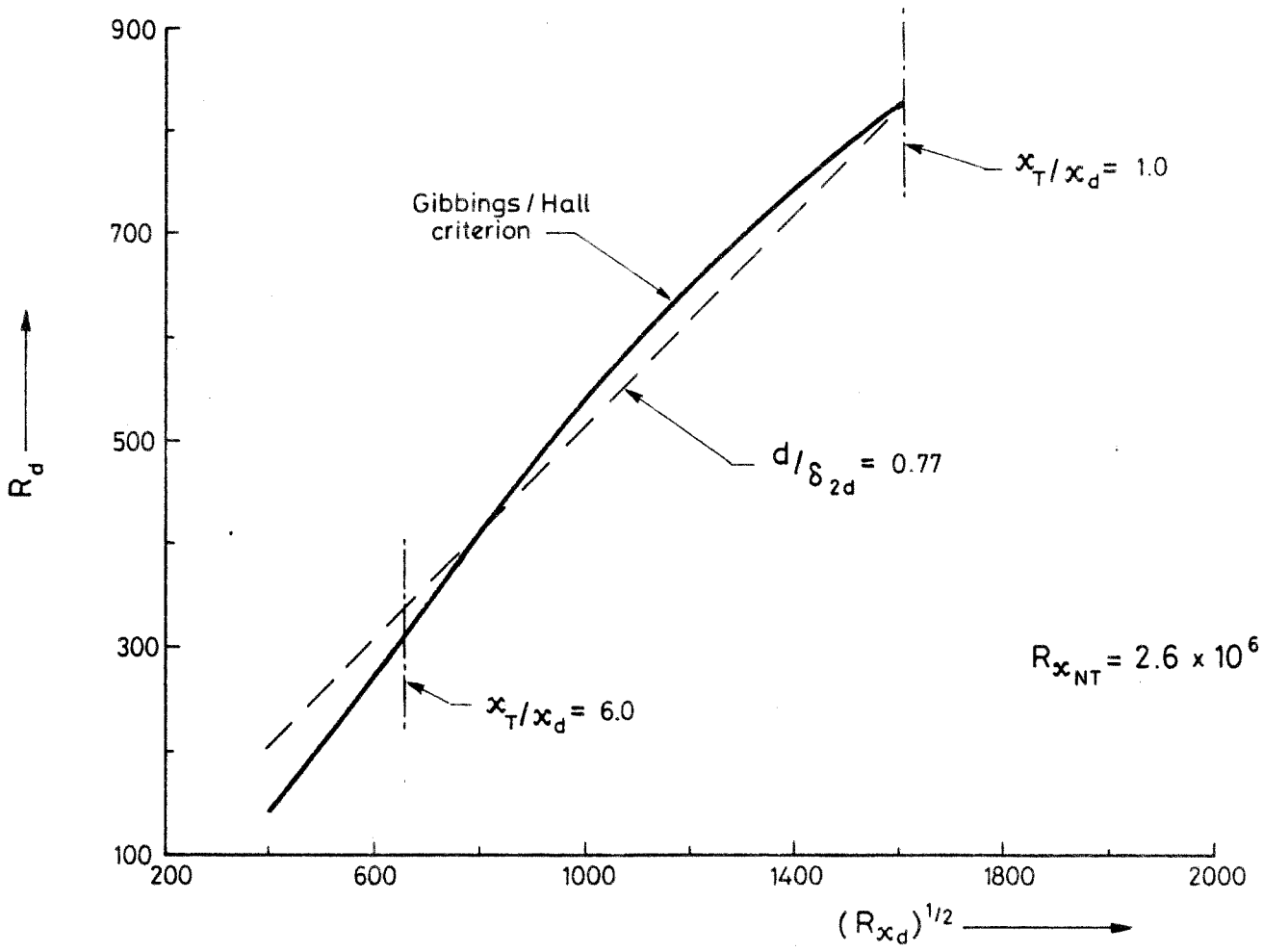

Fig. 1.c. Minimum critical roughness Reynolds number as a function of roughness position Reynolds number.

APPENDIX D

A First Order Subsonic Compressibility Correction to the Inviscid Velocity Gradient at the Attachment Line of an Ellipse

For points on the surface of an ellipse which are at or near the stagnation line compressibility corrections derived via small perturbation assumptions e.g. Prandtl-Glauert, are no longer valid. To overcome this problem it is assumed that the exact solution may be expressed as a power series of the form

$$\Phi = q_\infty \cdot (\Phi_0 + M_\infty^2 \Phi_1 + M_\infty^4 \Phi_2 + \ldots\ldots) \qquad (1)$$

where Φ_0 Φ_1 Φ_2 etc. are taken to be independent of Mach number and q_∞ Lighthill (ref.1) presents formal proof of the validity of this approach and shows that the first two terms in the series are given by -

$$\begin{aligned} \nabla^2\Phi_0 &= 0 \\ \nabla^2\Phi_1 &= \nabla\Phi_0 \cdot \nabla \left(\tfrac{1}{2}(\nabla\Phi_0)^2\right) \end{aligned} \qquad (2)$$

and consequently evaluation of Φ_0 and Φ_1 is possible in principle for a two-dimensional shape if the conformal mapping onto a circle is known. In reference (2) Kaplan presents a calculation method for the evaluation of Φ_1 for non-lifting ellipses of arbitrary thickness/chord ratio emersed in a purely subcritical inviscid flow. The method is extremely laborious and only the results are summarised here -

$$\frac{U}{U_\infty}_{\text{circle}} = 2 \sin\delta + \frac{\Delta U}{U_\infty} \qquad (3)$$

for a unit circle in the z plane

where $\frac{\Delta U}{U_\infty} = \frac{\mu}{2}\cdot\frac{1-\sigma^2}{\sigma^2}\left(\sin\delta - \frac{(1-\sigma^2)}{(1-2\sigma^2\cos2\delta+\sigma^4)^2}\left\{\frac{(1-\sigma^2)^2}{2\sigma^2}\left[(1+3\sigma^2+\sigma^4)\sin\delta\right.\right.\right.$

$\left. + \sigma^3 \sin3\delta\right] \ell n \frac{1+\sigma^2}{1-\sigma^2} - \frac{(1+\sigma^2)(1-\sigma^2)^2}{2\sigma}\cdot\sin2\delta\,\ell n\frac{1+2\sigma\cos\delta+\sigma^2}{1-2\sigma\cos\delta+\sigma^2}$

$\left.\left. + \frac{1-\sigma^2}{\sigma}\left[(1+\sigma^4)\cos2\delta - 2\sigma^2\right]\tan^{-1}\frac{2\sigma\sin\delta}{1-\sigma^2} + 2\left[(1+\sigma^2+\sigma^4)\sin\delta - \sigma^2\sin3\delta\right]\right\}\right)$

$\mu = M_\infty^2$ $\qquad \sigma^2 = \frac{1-t/Co}{1+t/Co}$ $\qquad$ and δ = angle subtended on the director circle

The corresponding velocity distribution for the ellipse is then obtained by suitable mapping i.e.

$$\left(\frac{U}{U_\infty}\right)_{ellipse} = \frac{1}{(1 - 2\sigma^2\cos 2\delta + \sigma^4)^{\frac{1}{2}}} \left(\frac{U}{U_\infty}\right)_{circle} \qquad (4)$$

To obtain velocity gradients it is necessary to differentiate equation (4) i.e.

$$\frac{d(U/U_\infty)_e}{d\delta} = \frac{1}{(1-2\sigma^2\cos 2\delta+\sigma^4)^{\frac{1}{2}}} \cdot \frac{d(U/U_\infty)_c}{d\delta} - \frac{2\sigma^2 \sin 2\delta}{(1-2\sigma^2\cos 2\delta+\sigma^4)^{3/2}} \left(\frac{U}{U_\infty}\right)_c \qquad (5)$$

where $$\frac{d(U/U_\infty)_c}{d\delta} = 2\cos\delta + \frac{d(\Delta U/U_\infty)}{d\delta}$$

and $$\frac{d(\Delta U/U_\infty)}{d\delta} = \frac{\mu}{2} \cdot \frac{1-\sigma^2}{\sigma^2}\Bigg(\cos\delta - \frac{1-\sigma^2}{(1-2\sigma^2\cos 2\delta+\sigma^4)^2}\Bigg\{\frac{(1-\sigma^2)^2}{2\sigma^2}\Big[(1+3\sigma^2+\sigma^4)\cos\delta$$

$$+ \quad 3\sigma^2\cos 3\delta\Big] \ell n\frac{1+\sigma^2}{1-\sigma^2} - \frac{(1+\sigma^2)(1-\sigma^2)^2}{2\sigma}\Bigg\langle\frac{\sin 2\delta(-4\sigma(1+\sigma^2)\sin\delta)}{(1+\sigma^2)^2 - 4\sigma^2\cos^2\delta}$$

$$+ \quad 2\cos 2\delta \cdot \ell n\frac{1+2\sigma\cos\delta+\sigma^2}{1-2\sigma\cos\delta+\sigma^2}\Bigg\rangle + \frac{1-\sigma^2}{\sigma}\Bigg\langle\Big[(1+\sigma^4)(-2\sin 2\delta)\Big]\tan^{-1}$$

$$\frac{2\sigma\sin\delta}{1-\sigma^2} + \Big[(1+\sigma^4)\cos 2\delta - 2\sigma^2\Big]\frac{(1-\sigma^2)2\sigma\cos\delta}{(1-\sigma^2)^2+4\sigma^2\sin^2\delta}\Bigg\rangle$$

$$+ \quad 2\Big[(1+\sigma^2+\sigma^4)\cos\delta - 3\sigma^2\cos 3\delta\Big]\Bigg\}$$

$$+ \quad \frac{8\sigma^2\sin 2\delta(1-\sigma^2)}{(1-2\sigma^2\cos 2\delta+\sigma^4)^3}\Bigg\{\frac{(1-\sigma^2)^2}{2\sigma^2}\Big[(1+3\sigma^2+\sigma^4)\sin\delta + \sigma^2\sin 3\delta\Big]\ell n\frac{1+\sigma^2}{1-\sigma^2}$$

$$- \quad \frac{(1+\sigma^2)(1-\sigma^2)^2}{2\sigma}\sin 2\delta \cdot \ell n\frac{1+2\sigma\cos\delta+\sigma^2}{1-2\sigma\cos\delta+\sigma^2} + \frac{1-\sigma^2}{\sigma}\Big[(1+\sigma^4)\cos 2\delta - 2\sigma^2\Big]$$

$$\times \quad \tan^{-1}\frac{2\sigma\sin\delta}{1-\sigma^2} + 2\Big[(1+\sigma^2+\sigma^4)\sin\delta - \sigma^2\sin 3\delta\Big]\Bigg\}\Bigg)$$

Taking the special case of the stagnation point i.e. $\delta = 0$

$$\left(\frac{d(U/U_\infty)_e}{d\delta}\right)_{\delta=0} = \frac{1}{(1-2\sigma^2+\sigma^4)^{\frac{1}{2}}}\Bigg\langle 2 + \frac{\mu}{2} \cdot \frac{1-\sigma^2}{\sigma^2}\Bigg(1 - \frac{1-\sigma^2}{(1-2\sigma^2+\sigma^4)^2}\Bigg\{\frac{(1-\sigma^2)^2}{2\sigma^2}\Big[(1+3\sigma^2+\sigma^4)+3\sigma^2\Big]\times$$

$$\ell n\frac{1+\sigma^2}{1-\sigma^2} - \frac{(1+\sigma^2)(1-\sigma^2)^2}{2\sigma}2\ell n\frac{1+2\sigma+\sigma^2}{1-2\sigma+\sigma^2} + \frac{1-\sigma^2}{\sigma}\Big[1-2\sigma^2+\sigma^4\Big]\times$$

$$\frac{(1-\sigma^2)2\sigma}{(1-\sigma^2)^2} + 2\Big[1-2\sigma^2+\sigma^4\Big]\Bigg\}\Bigg)\Bigg\rangle$$

or

$$\frac{d(U/U_\infty)_e}{d\delta}\Big)_{\delta=0} = \frac{2}{(1-\sigma^2)} + \frac{\mu}{2\sigma^2}\left(1-\frac{1}{(1-\sigma^2)}\left\{\frac{1+6\sigma^2+\sigma^4}{2\sigma^2}\,\ell n\frac{1+\sigma^2}{1-\sigma^2} - \frac{2(1+\sigma^2)}{\sigma}\ell n\frac{1+\sigma}{1-\sigma} + 4\right\}\right) \tag{6}$$

Furthermore if x is the surface coordinate measured from the stagnation point then

$$\frac{d(x/\rho)}{d\delta} = \frac{(1+\sigma^2)}{(1-\sigma^2)} \cdot \left\{1+\frac{2\sigma^2\sin^2\delta}{(1-\sigma^2)^2}\right\}^{\frac{1}{2}} \quad \text{when } \rho = \text{leading edge radius}$$

$$\therefore \quad \frac{d(x/\rho)}{d\delta}\Big)_{\delta=0} = \frac{1+\sigma^2}{(1-\sigma^2)}$$

hence

$$\frac{\rho}{U_\infty}\cdot\frac{dU}{dx}\Big)_{x=0} = \frac{2}{(1+\sigma^2)} + \frac{\mu(1-\sigma^2)}{2\sigma^2(1+\sigma^2)}\left(1-\frac{1}{(1-\sigma^2)}\left\{\frac{1+6\sigma^2+\sigma^4}{2\sigma^2}\ell n\frac{1+\sigma^2}{1-\sigma^2} - \frac{2(1+\sigma^2)}{\sigma}\ell n\frac{1+\sigma}{1-\sigma} + 4\right\}\right)$$

Moreover if $\frac{2\rho}{U_\infty}\cdot\frac{dU}{dx}\Big)_{x=0} = \frac{U_1 D}{C_o}$ then

$$\frac{U_1}{U_{1_{m=0}}} = 1+\frac{\mu(1-\sigma^2)}{4\sigma^2}\left(1-\frac{1}{(1-\sigma^2)}\left\{\frac{1+6\sigma^2+\sigma^4}{2\sigma^2}\ell n\frac{1+\sigma^2}{1-\sigma^2} - \frac{2(1+\sigma^2)}{\sigma}\ell n\frac{1+\sigma}{1-\sigma} + 4\right\}\right) \tag{7}$$

Comparison with Experiment

The predicted variation with Mach number may be compared directly with the experimental work of Firmin and Cook (reference 3). They present measurements of U_1 for a swept wing with an R.A.E. 100 section and a thickness chord ratio of 0.25. Since the foregoing theory was developed for elliptic sections it is necessary to obtain an equivalent value of σ^2. Using equation (5.8.5) from the main text -

$$\frac{b}{a}\Big)_{\substack{\text{equivalent}\\ \text{ellipse}}} = \left(40\left[\frac{\rho}{C_o} - 10\left(\frac{y}{C_o}\right)^2_{x/C_o=0.05}\right]\right)^{\frac{1}{2}}$$

For an R.A.E.100 with a t/C_o of 0.25 ρ/C_o equals 0.06863 and $y/C_o)_{x/C_o=0.05}$ equals 0.07715 - see Parkhurst and Squire (ref.4), and

hence -

$$\left(\frac{b}{a}\right)_{ee} = 0.6035$$

or $$\sigma^2 = 0.2473$$

Consequently from equation (7)

$$U_1 = U_1)_{m=0} \times (1-0.3753(M_\infty \cos\Lambda)^2) \qquad (8)$$

Figure 1 shows the experimental data for various sweep angles Reynolds numbers and free stream Mach numbers together with the theoretical prediction based upon equation (8) where the non-dimensional incompressible velocity gradient has been taken to be 21.2 (based upon the experimental results). It is apparent that there is good agreement between experiment and theory confirming the assumption that for typical aerofoil sections the terms Φ_0 and Φ_1 in equation (1) dominate the full solution. In addition it is of interest to note that despite the fact that the theory leading to equation (8) is valid for subcritical flows only the leading edge region is hardly affected by the small area of supercritical flow which forms in the region of minimum Cp ($x/c \simeq 0.1$) at values of $M_\infty \cos\Lambda$ in excess of about 0.55.

References

1. LIGHTHILL, M.J. — General Theory of High Speed Aerodynamics, Vol.VI,section E,Oxford University Press, 1955, pp.252-256.

2. KAPLAN, C. — Two-dimensional subsonic compressible flow past elliptic cylinders NACA Report No.624, 1938.

3. FIRMIN, M.C.P. COOK, P.H. — Unpublished work - R.A.E.Farnborough

4. PANKHURST, R.C. SQUIRE, H.B. — Calculated pressure distributions for the R.A.E.100-104 aerofoil sections. ARC C.P.80, 1952.

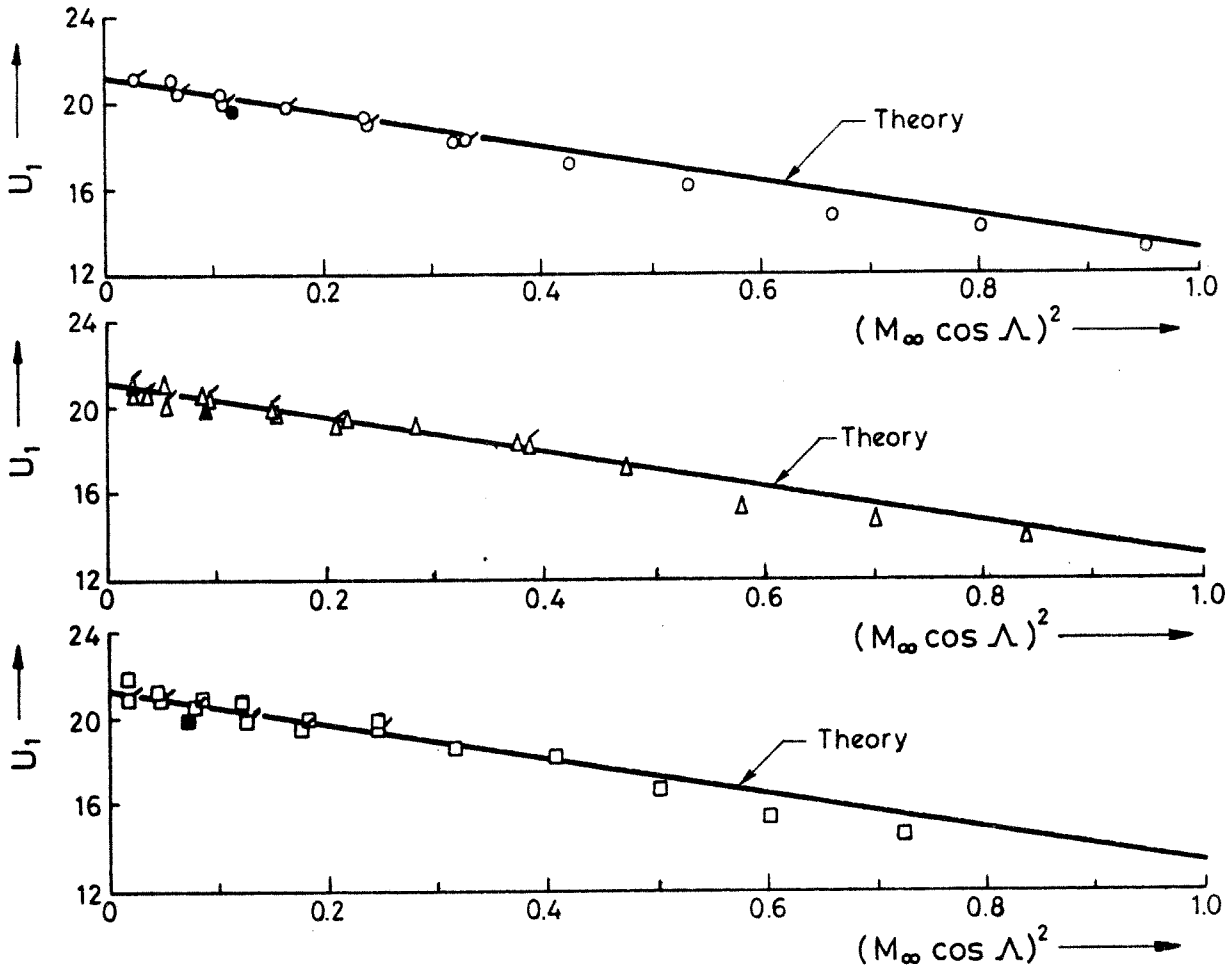

Symbol	Q_∞/υ	Sweep
o	2×10^6 per. ft.	35.33°
ơ	4×10^6 per. ft.	
●	7.5×10^6 per. ft.	

Symbol	Q_∞/υ	Sweep
Δ	2×10^6 per. ft.	40°
Δ	4×10^6 per. ft.	
▲	7.5×10^6 per. ft.	

Symbol	Q_∞/υ	Sweep
□	2×10^6 per. ft.	45°
□	4×10^6 per. ft.	
■	7.5×10^6 per. ft.	

Fig. 1.d. Variation of attachment line velocity gradient for R.A.E 100 section with Mach number, sweep and unit Reynolds number.

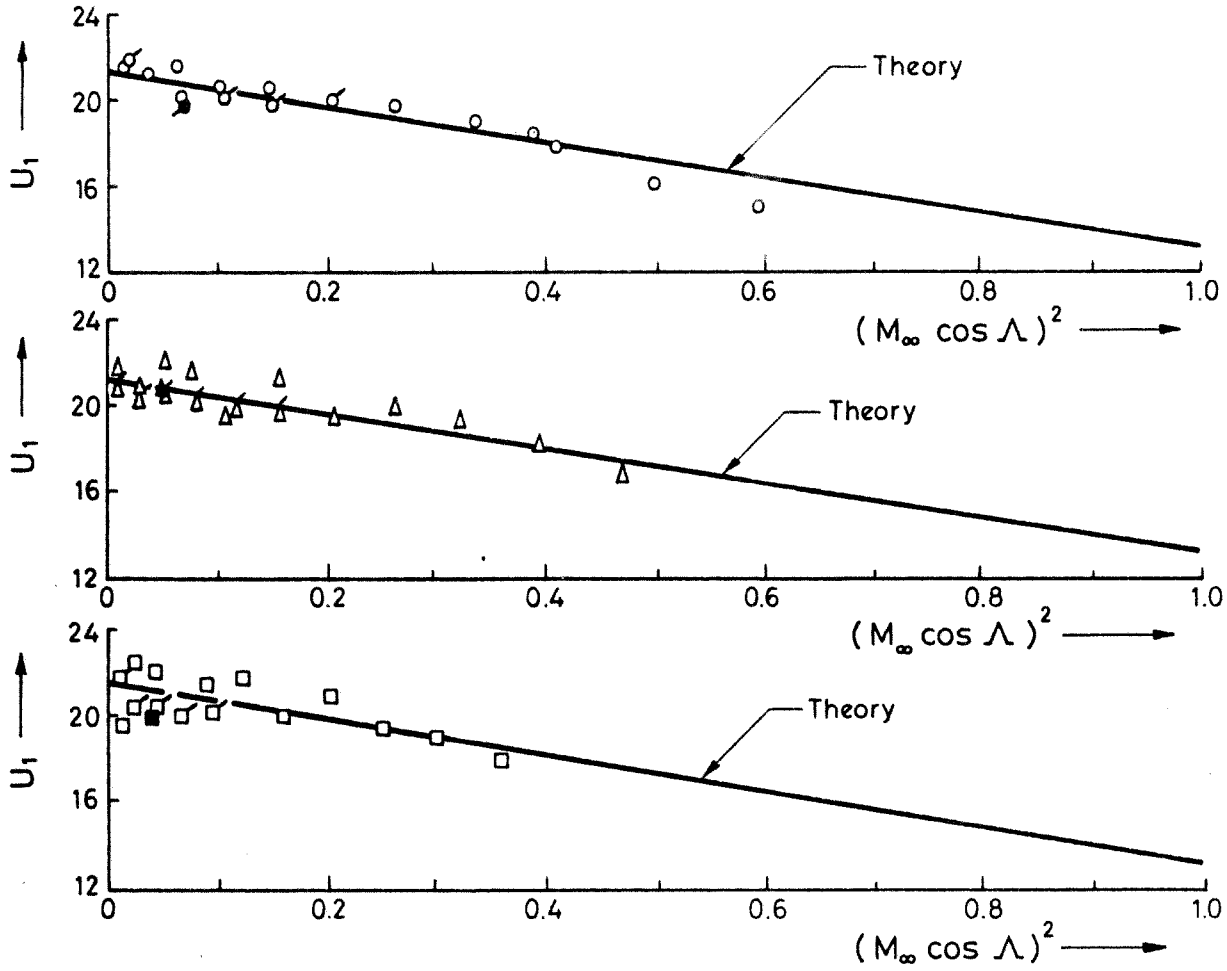

Symbol	Q_∞/υ	Sweep
○	2×10^6 per.ft.	50°
◎	4×10^6 per.ft.	
●	7.5×10^6 per.ft.	

Symbol	Q_∞/υ	Sweep
△	2×10^6 per.ft.	55°
◬	4×10^6 per.ft.	
▲	7.5×10^6 per.ft.	

Symbol	Q_∞/υ	Sweep
□	2×10^6 per.ft.	60°
◱	4×10^6 per.ft.	
■	7.5×10^6 per.ft.	

Fig. 1.d. (continued)

APPENDIX E

A Simple Estimate of the Maximum Value of X for a Swept Cylinder with an Elliptic Section

In section (6.2) of the main text it is shown that in regions close to the attachment line X is given by -

$$X = 0.838 \frac{V_\infty}{Q_e} \left(\frac{Ue\,x}{\nu}\right)^{\frac{1}{2}} \qquad (1)$$

If in addition the section of the cylinder in a plane normal to the leading edge is an ellipse then -

$$\text{a)} \quad \left.\frac{d(Ue/U_\infty)}{d(x/Co)}\right)_{x=0} = \frac{Co}{\rho}\left(1 + \frac{t}{Co}\right) \qquad (2)$$

and

$$\text{b)} \quad \frac{U_{max}}{U_\infty} = 1 + \frac{t}{Co} \qquad (3)$$

By making the assumption that for positions ahead of the peak suction location the velocity distribution taken in the direction normal to the leading edge may be represented approximately by two straight lines i.e.

$$\text{For} \quad 0 < x/Co < x/Co)_{U_{max}} \qquad Ue/U_\infty = \left(\frac{d(Ue/U_\infty)}{d(x/Co)}\right)_{x=0} \cdot \frac{x}{Co}$$

$$\text{and for} \quad x/Co > x/Co)_{U_{max}} \qquad Ue/U_\infty = \frac{U_{max}}{U_\infty}$$

it follows that the maximum velocity is achieved when

$$\left.\frac{x}{Co}\right)_{U_{max}} = \frac{\frac{U_{max}}{U_\infty}}{\left.\frac{d(U/U_\infty)}{d(x/Co)}\right)_{x=0}} = \frac{(1 + t/C_o)}{\frac{Co}{\rho}(1 + t/Co)} = \frac{\rho}{C_o} \qquad (4)$$

The maximum value of X may now be estimated from equation (1) with the use of equations (2), (3) and (4).

$$X_{max} \simeq 0.84 \frac{Q_\infty \sin\Lambda}{Q_\infty \cos\Lambda \left(\left(\frac{Ue}{U_\infty}\right)^2_{max} + \tan^2\Lambda\right)^{\frac{1}{2}}} \left(\frac{(Ue\,x)max}{\nu}\right)^{\frac{1}{2}}$$

$$\simeq 0.84 \left(\frac{\sin^2\Lambda \cdot Q_\infty \cdot \cos\Lambda \cdot \rho(1 + t/Co)}{\cos^2\Lambda((1+t/Co)^2 + \tan^2\Lambda) \cdot \nu}\right)^{\frac{1}{2}}$$

$$X_{max} \simeq 0.84 \left(\frac{Q_\infty \rho}{\nu}\right)^{\frac{1}{2}} \cdot \left(\frac{\tan\Lambda \cdot \sin\Lambda\,(1 + t/Co)}{((1+t/Co)^2 + \tan^2\Lambda)}\right)^{\frac{1}{2}} \qquad (5)$$

It is readily shown that equation (5) also exhibits a maximum with varying sweep. For values of t/Co in the range 0 to 1 this maximum occurs at sweep angles somewhere between 55^{o} and 67^{o} with the corresponding absolute maximum value of χ being a very weak function of t/Co i.e.

$$\chi_{max} \simeq 0.54 \left(\frac{Q_{\infty}\rho}{\nu}\right)^{\frac{1}{2}} \qquad (6)$$

when $\Lambda \simeq 60^{o}$

APPENDIX F

The Evaluation of the Amplitude Ratio Integral from Brown's Temporal Stability Results

In the main text it was shown that in order to calculate the amplitude ratio for a fixed frequency disturbance the following integral must be evaluated

$$\left[\log_e \left(\frac{A}{A_I}\right) = \int_{\ell_{11}}^{\ell_{12}} \frac{\alpha_r}{Cg} \cdot \left(\frac{\omega_i}{\alpha_r}\right) d\ell_1\right] \qquad (1)$$

$\underline{\omega_r}$ = constant

Case 1 - The swept wing cross flow profile.

As a first step it is necessary to identify lines of constant $\underline{\omega_r}$ on the temporal stability charts and since -

$$\underline{\omega r} = \frac{\omega r . c_{max}}{\delta_{0.01} c_{max}} = \frac{\omega r . \chi . \nu}{(\delta_{0.01} c_{max})^2}$$

$$\text{or} \quad \underline{\omega_r} = \left(\frac{\omega r}{\alpha r}\right) . \alpha r . \chi . \frac{\nu}{(\delta_{0.01} c_{max})^2} = \left(\frac{\omega r}{\alpha r}\right) . \frac{\alpha r . \chi . U_1 . U_\infty}{12.18 . Co}$$

$$\text{then} \quad \frac{12.18 . \underline{\omega r} . Co}{U_1 . U_\infty} = \left(\frac{\omega r}{\alpha r}\right) . \alpha r . \chi = \bar{\omega} \qquad (2)$$

Therefore $\bar{\omega}$ is constant for a fixed section geometry when the free stream speed U_∞ and the disturbance frequency $\underline{\omega_r}$ are constant. Figure 1 shows Brown's temporal stability results (main text figure 48) with lines of constant frequency parameter $\bar{\omega}$ added. The curves given in figure 1 may now be used to estimate the value of the group velocity Cg which is defined as

$$Cg = \left(\frac{\partial \omega r}{\partial \alpha r}\right)_\chi$$

and from the definitions of the non-dimensionalising parameters it is readily shown that

$$Cg = \frac{1}{\chi} \left(\frac{\partial \bar{\omega}}{\partial \alpha_r}\right)_\chi \qquad (4)$$

The variation of $(\bar{\omega}/\chi)$ with α_r for constant values of χ is presented in figure 2 from which it is clear that for the range of variables considered the phase velocity may be taken to be constant with a non-dimensional value of 0.460.

For the swept wing cross flow profile ℓ_1 is equal to x and in the main text it has been shown that equation (1) is reduced to

$$\log_e \left(\frac{A}{A_I}\right) = \frac{1}{2.925} \int_{\chi_1}^{\chi} \frac{\alpha r}{Cg} \cdot \left(\frac{\omega i}{\alpha_r}\right) \cdot d\chi$$

and values of the integral are presented in table 1 for a range of disturbance frequencies.

Case 2 - The rotating disc radial profile

By a similar arguement it may be shown that for the rotating disc radial profile

$$\bar{\omega} = \left(\frac{\omega_r}{\alpha_r}\right).\alpha_r.\chi = \frac{49.\ \omega_r}{\Omega}$$

where $\bar{\omega}$ is constant for constant disturbance frequency ω_r when the disc is rotating at a steady angular velocity, Ω and figure 3 shows lines of constant $\bar{\omega}$ superimposed upon the temporal stability chart (main text figure 50). This figure again allows the variation of $(\bar{\omega}/\chi)$ with α_r for constant χ to be determined and the results are presented in figure 4 from which it may be seen that the non-dimensional group velocity is substantially constant with a value of 0.492. Finally by taking the distance ℓ_1 in equation (1) to be the radial distance, a and using the appropriate non-dimensionalising variables the integral is reduced to the following form

$$\log_e \left(\frac{A}{A_I}\right) = \frac{1}{8.869} \int_{\chi_1}^{\chi} \frac{\alpha r}{Cg} \cdot \left(\frac{\omega i}{\alpha_r}\right) \cdot d\chi$$

and values for a range of disturbance frequencies are presented in table 2.

TABLE 1-F Swept Wing Cross Flow Profile Results

$\bar{\omega}$	x	α_r	C_i	$\alpha_r C_i/C_g$	$\log_e(A/A_I)$
97	102	1.85	0	0	0
	126	1.29	0.009	0.025	0.10
	147	1.05	0.010	0.024	0.27
146	111	2.62	0	0	0
	126	2.30	0.017	0.088	0.23
	147	1.85	0.042	0.168	1.14
	168	1.55	0.054	0.183	2.40
	189	1.29	0.063	0.175	3.69
	210	1.12	0.066	0.160	4.89
	230	0.98	0.067	0.142	5.97
195	130	2.97	0	0	0
	147	2.58	0.023	0.129	0.37
	168	2.23	0.045	0.217	1.61
	189	1.92	0.060	0.252	3.30
	210	1.71	0.071	0.265	5.15
	230	1.47	0.079	0.252	7.01
	251	1.31	0.084	0.239	8.77
	272	1.17	0.086	0.219	10.41
	293	1.08	0.088	0.207	11.95
	314	0.98	0.088	0.187	13.36
244	149	3.23	0	0	0
	168	2.84	0.023	0.142	0.46
	189	2.49	0.045	0.246	1.85
	210	2.20	0.061	0.291	3.78
	230	1.99	0.073	0.317	5.96
	251	1.78	0.083	0.322	8.25
	272	1.61	0.089	0.310	10.52
	293	1.43	0.093	0.290	12.68
	314	1.30	0.097	0.273	14.70
	335	1.19	0.099	0.256	16.60
	356	1.10	0.101	0.241	18.38
	377	1.03	0.102	0.222	20.04
	398	0.96	0.102	0.212	21.60
292	168	3.42	0	0	0
	189	3.04	0.023	0.151	0.54
	210	2.72	0.042	0.249	1.98
	230	2.46	0.057	0.303	3.96
	251	2.25	0.069	0.339	6.27
	272	2.04	0.079	0.352	8.74
	293	1.87	0.087	0.355	11.28
	314	1.70	0.093	0.343	13.78
	335	1.55	0.098	0.332	16.20
	356	1.43	0.103	0.320	18.54
	377	1.33	0.107	0.308	20.80
	398	1.22	0.110	0.293	22.95
	419	1.15	0.113	0.284	25.02

TABLE 2-F Rotating Disc Radial Profile Results

$\bar{\omega}$	X	α_r	C_i	$\alpha_r C_i/Cg$	$\log_e(A/A_I)$
294	245	2.03	0	0	0
	253	1.93	0.006	0.024	0.01
	285	1.65	0.008	0.027	0.10
	317	1.44	0.008	0.023	0.19
	348	1.26	0.003	0.008	0.25
	380	1.12	0	0	0.26
392	243	2.80	0	0	0
	253	2.73	0.003	0.017	0.01
	285	2.38	0.017	0.082	0.19
	317	2.07	0.028	0.118	0.54
	348	1.82	0.033	0.122	0.97
	380	1.61	0.036	0.118	1.40
	412	1.47	0.039	0.117	1.82
	443	1.33	0.040	0.108	2.22
490	266	3.36	0	0	0
	285	3.08	0.008	0.050	0.05
	317	2.70	0.022	0.121	0.36
	380	2.17	0.041	0.181	1.44
	443	1.79	0.052	0.189	2.76
	507	1.51	0.059	0.181	4.08
	570	1.33	0.061	0.165	5.32
588	291	3.64	0	0	0
	317	3.36	0.010	0.068	0.10
	380	2.66	0.034	0.184	1.00
	443	2.24	0.052	0.237	2.50
	507	1.86	0.062	0.234	4.19
	570	1.62	0.067	0.221	5.81
	634	1.40	0.073	0.208	7.34
	697	1.26	0.075	0.192	8.77
686	317	3.85	0	0	0
	380	3.22	0.025	0.164	0.59
	443	2.66	0.044	0.238	2.02
	507	2.24	0.061	0.278	3.86
	570	1.96	0.069	0.275	5.84
	634	1.75	0.077	0.274	7.80
	697	1.54	0.082	0.257	9.70
	760	1.40	0.082	0.233	11.45
	824	1.23	0.082	0.205	13.01
784	342	4.03	0	0	0
	380	3.64	0.012	0.089	0.19
	443	3.08	0.036	0.225	1.31
	507	2.63	0.051	0.273	3.09
	570	2.28	0.066	0.306	5.16
	634	2.03	0.075	0.309	7.35
	697	1.82	0.083	0.307	9.56
	760	1.65	0.087	0.292	11.69
	824	1.51	0.091	0.279	13.73

$\bar{\omega}$	χ	α_r	C_i	$\alpha_r Ci/Cg$	$\log_e(A/A_I)$
882	367	4.17	0	0	0
	380	4.03	0.006	0.049	0.04
	443	3.47	0.028	0.197	0.91
	507	2.98	0.044	0.267	2.57
	570	2.63	0.055	0.294	4.58
	634	2.31	0.070	0.329	6.80
	697	2.07	0.078	0.328	9.15
	760	1.89	0.084	0.323	11.47
	824	1.72	0.092	0.322	13.77
	887	1.54	0.098	0.307	16.02

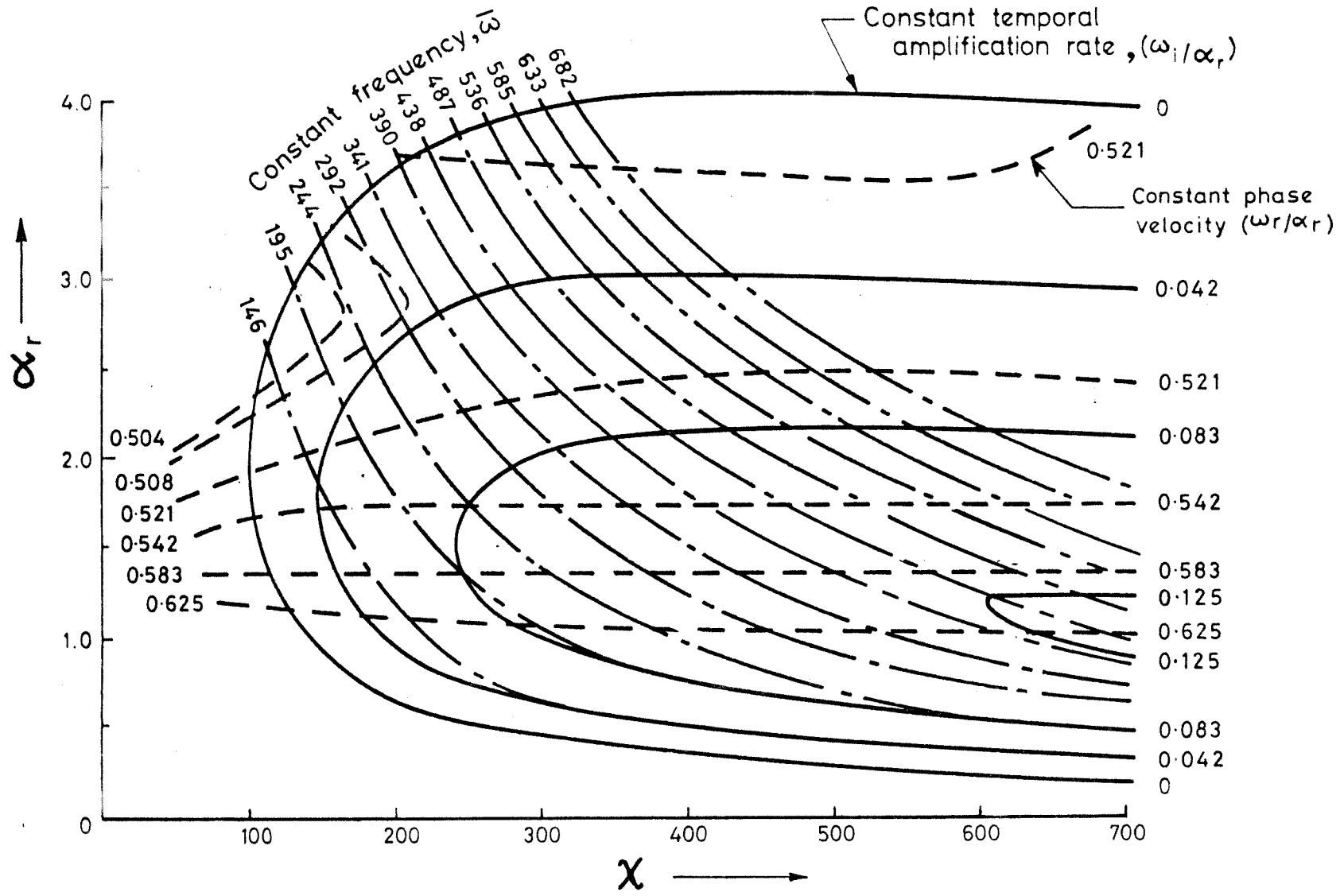

Fig. 1. f. The theoretical stability characteristics for the swept wing cross flow profile.

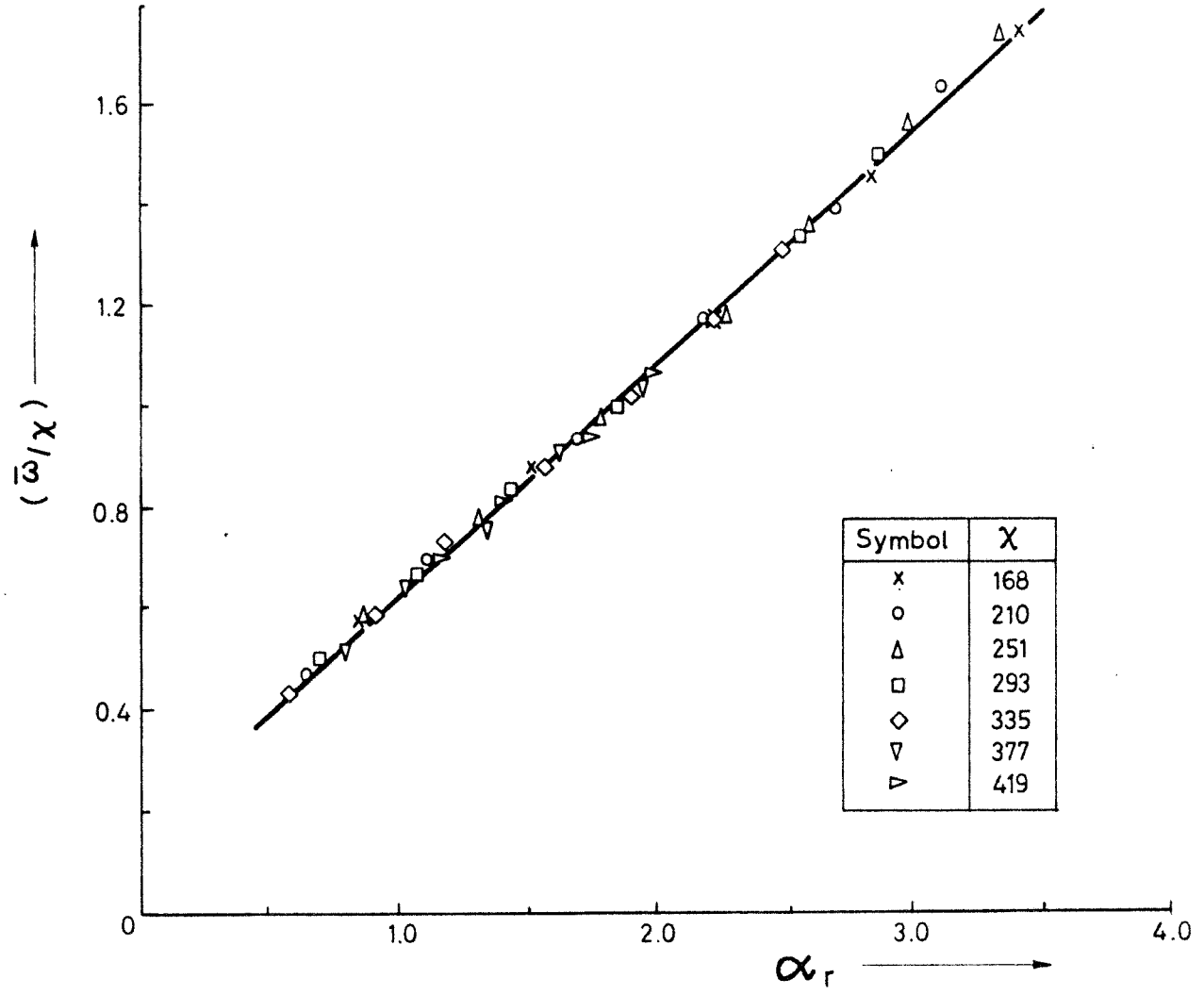

Fig. 2.f. The variation of $(\bar{\omega}/\chi)$ with α_r at constant Reynolds number for for the attachment region cross flow profile.

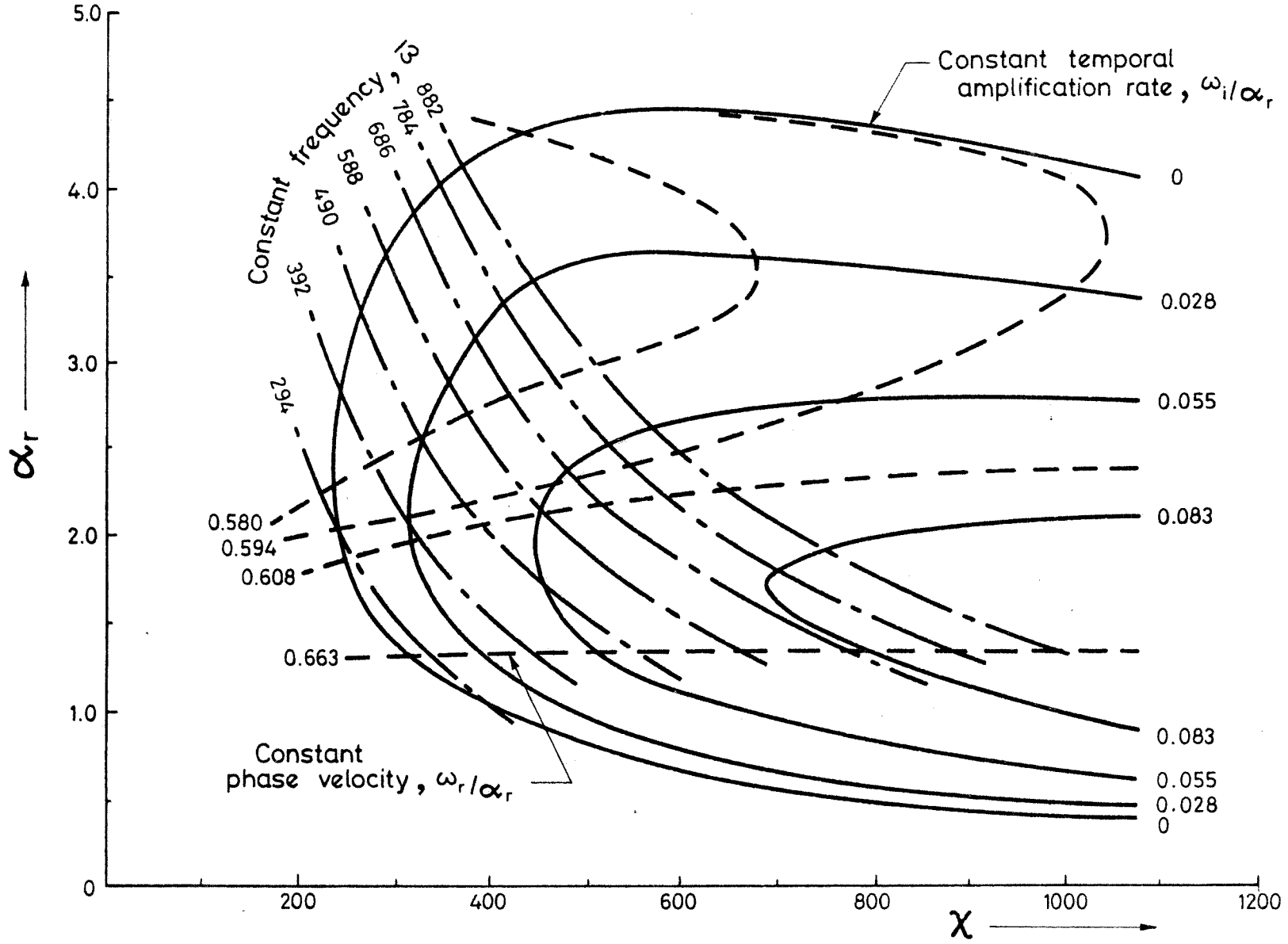

Fig. 3.f. Theoretical stability characteristics for the rotating disc radial profile.

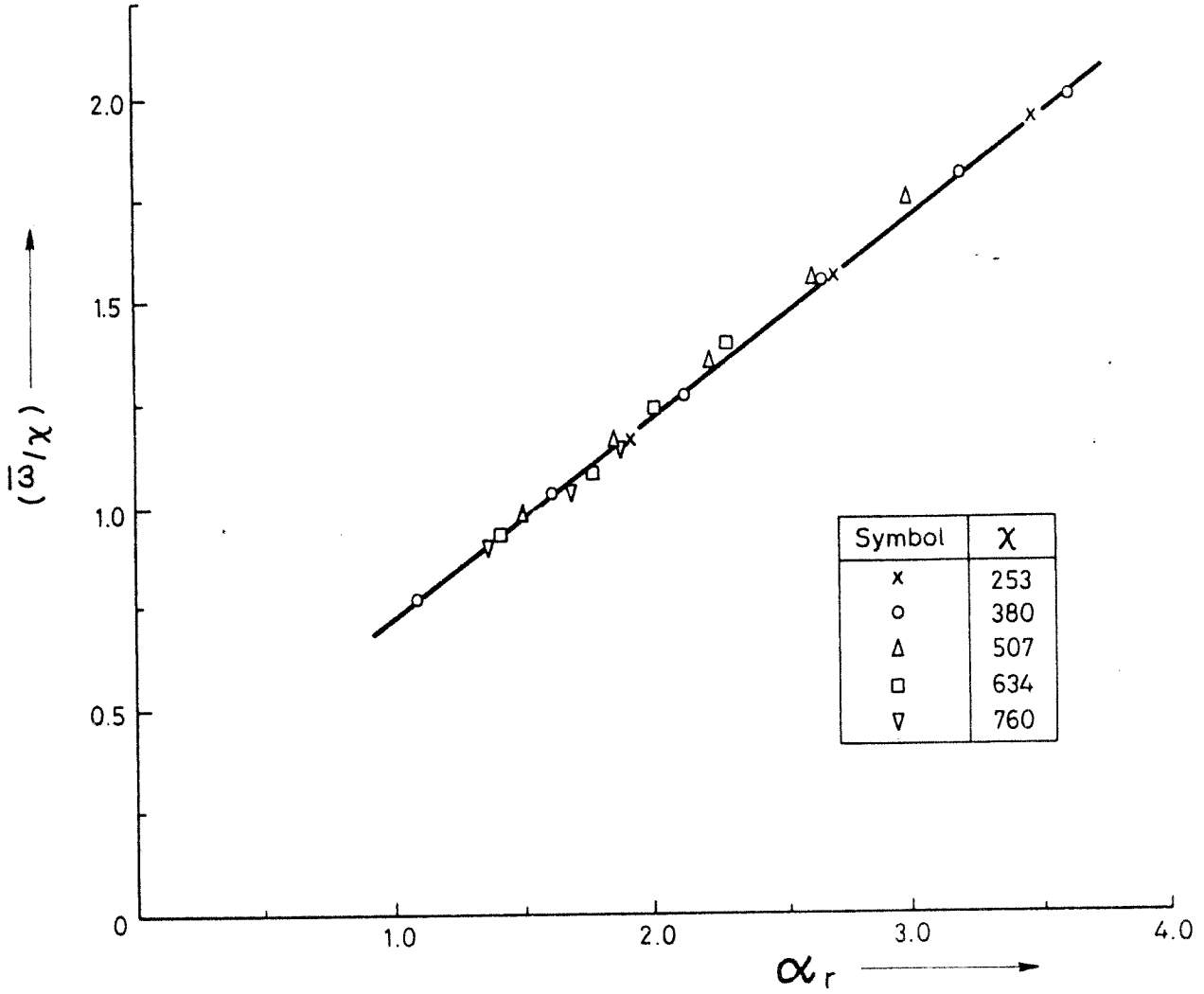

Fig. 4.f. The variation of $(\bar{\omega}/\chi)$ with α_r at constant Reynolds number for the rotating disc radial profile.

APPENDIX G The Results of the Experimental Investigation into the Response of the Attachment Line Boundary Layer to the Presence of 2-D Trip Wires

			FIRST BURSTS		COMPLETE TURBULENCE	
TRIP DIA (Ins)	SWEEP (Degrees)	S (Ins)	Q_∞ (Ft/Sec)	$(\frac{V_\infty d}{\nu})$	Q_∞ (Ft/Sec)	$(\frac{V_\infty d}{\nu})$
0.0093	53.20	1.94	168.9	577	-	-
	53.20	15.38	157.8	548	-	-
	53.25	27.00	157.3	544	-	-
	53.22	40.00	151.0	550	182.2	652
	53.20	40.00	155.0	541	187.0	645
	53.22	52.38	153.1	541	186.2	646
	54.97	1.81	163.0	574	-	-
	55.05	1.94	164.6	582	-	-
	54.97	15.13	152.6	540	188.9	665
	55.00	15.38	154.4	549	-	-
	55.02	27.00	154.3	559	187.1	666
	54.97	27.00	151.6	542	183.1	647
	55.02	40.00	152.4	558	183.4	656
	54.97	40.00	151.6	542	176.9	629
	54.97	52.50	146.3	545	167.6	621
	58.03	1.81	160.3	585	-	-
	58.08	15.13	151.0	557	187.8	685
	58.07	27.00	152.1	557	183.4	668
	57.98	40.00	149.2	556	173.6	643
	58.03	52.50	145.4	555	165.7	628
	60.50	1.81	154.5	575	-	-
	60.45	15.13	146.0	552	178.2	671
	60.42	27.00	146.0	562	171.6	653
	60.42	40.00	143.7	555	169.0	646
	60.40	52.50	142.8	555	161.9	629
	62.85	1.81	144.7	588	188.0	746
	62.88	1.94	137.0	549	-	-
	62.88	15.13	139.9	545	170.7	661
	62.88	27.00	140.4	550	165.4	644
	62.83	40.00	138.3	550	160.2	633
	62.83	52.50	136.8	544	156.9	620
	64.65	1.81	144.2	581	188.6	752
	64.65	15.31	136.8	551	166.8	665
	64.65	27.13	135.6	553	159.6	647
	64.65	39.94	135.8	551	157.9	637
	64.65	52.38	136.8	551	158.5	631
	68.00	1.94	133.1	569	-	-
	68.00	1.94	140.5	559	-	-
	68.00	15.38	132.7	540	164.0	664
	68.00	27.00	133.9	539	157.8	635
	67.97	40.00	135.4	547	153.6	621
	67.98	52.38	135.4	547	154.3	623

			FIRST BURSTS		COMPLETE TURBULENCE	
TRIP DIA (Ins)	SWEEP (Degrees)	S (Ins)	Q_∞ (Ft/Sec)	$(\frac{V_\infty d}{\nu})$	Q_∞ (Ft/Sec)	$(\frac{V_\infty d}{\nu})$
	70.80	1.94	130.2	564	-	-
	70.73	15.38	125.8	528	158.6	658
	70.78	27.00	127.4	522	152.3	624
	70.78	40.00	126.5	521	146.6	603
	70.78	52.38	125.7	517	145.1	597
0.0135	53.17	15.38	107.2	582	120.7	651
	53.22	52.31	106.7	572	120.1	644
	55.02	15.38	108.2	601	119.7	665
	55.05	52.56	107.1	581	119.7	650
	58.00	52.25	103.9	617	112.7	669
	60.40	15.38	99.6	583	119.9	702
	60.48	52.56	98.1	566	118.2	677
	62.88	1.94	96.1	566	128.1	754
	62.88	52.56	95.0	559	116.3	685
	64.65	15.38	94.4	575	119.9	730
	64.68	52.56	94.0	560	115.6	688
	67.87	52.25	85.3	564	100.1	663
	70.67	2.88	89.3	588	113.9	750
	70.75	15.38	90.1	570	112.2	710
	70.67	26.75	87.0	573	99.9	658
	70.67	52.50	84.7	558	97.8	645
	70.65	52.25	83.4	565	94.9	644
	70.77	52.56	89.5	557	107.3	667
0.0160	53.12	2.00	95.6	587	110.7	680
	53.12	15.31	97.7	601	105.9	651
	53.12	27.06	97.7	601	101.9	626
	53.12	40.00	97.7	601	101.9	626
	53.12	52.44	95.1	597	99.3	623
	54.90	2.00	96.5	610	110.5	699
	54.90	15.25	96.5	610	103.7	656
	54.90	27.00	97.4	620	101.6	646
	54.90	40.13	96.4	613	100.5	640
	54.90	52.44	96.2	617	100.4	644
	57.95	1.94	92.8	619	108.1	721
	57.95	15.19	94.0	623	102.4	679
	57.95	27.00	95.3	628	101.6	669
	57.95	40.13	95.3	628	100.5	663
	58.02	52.44	95.1	633	100.5	665
	60.38	1.94	96.9	643	110.0	730
	60.38	15.00	94.7	628	103.1	684
	60.38	27.00	94.7	628	103.1	684
	60.38	40.06	94.5	631	102.0	680
	60.40	52.44	93.1	631	101.5	688
	62.83	1.88	95.6	653	109.8	750
	62.83	15.19	87.7	599	103.0	703

			FIRST BURSTS		COMPLETE TURBULENCE	
TRIP DIA (Ins)	SWEEP (Degrees)	S (Ins)	Q_∞ (Ft/Sec)	$(\frac{V_\infty d}{\nu})$	Q_∞ (Ft/Sec)	$(\frac{V_\infty d}{\nu})$
	62.83	27.00	86.5	591	102.0	696
	62.83	40.06	86.5	591	101.9	696
	62.77	52.44	85.0	589	101.5	704
	64.48	1.88	95.6	662	109.8	761
	64.48	15.06	87.6	610	104.0	720
	64.48	27.00	87.5	610	102.8	716
	64.48	39.94	87.6	610	101.8	709
	64.57	52.44	86.2	607	102.7	719
	67.85	2.00	87.3	629	108.4	781
	67.85	6.19	83.7	603	104.5	753
	67.85	15.13	82.5	594	102.7	736
	67.85	27.00	82.6	592	100.7	721
	67.85	39.94	80.1	574	99.6	714
	67.92	52.44	82.6	593	100.7	723
	70.82	2.00	86.3	632	113.5	826
	70.77	6.19	79.9	587	105.5	775
	70.77	15.13	77.8	575	96.3	708
	70.77	27.00	77.2	570	92.9	687
	70.77	40.00	76.8	571	89.5	662
	70.77	52.38	75.0	558	89.4	664
0.0236	54.90	52.25	48.5	495	58.6	598
	57.62	52.25	48.5	511	56.0	591
	60.28	3.00	41.4	449	60.3	653
	60.33	5.94	40.6	440	59.4	645
	60.33	11.88	41.3	448	58.6	635
	60.33	52.25	45.4	492	55.2	598
	62.77	52.25	46.5	516	55.2	612
	64.53	3.00	43.5	490	60.3	679
	64.57	5.94	43.9	494	60.2	679
	64.58	52.25	47.4	537	55.0	624
	67.88	52.25	47.4	551	55.9	650
	70.80	3.00	49.5	584	64.2	757
	70.80	5.94	49.3	581	61.9	729
	70.75	52.25	51.3	608	57.6	683
	70.67	52.50	48.8	571	58.5	685
0.0280	53.18	1.88	38.9	431	51.6	569
	53.18	15.19	40.5	447	66.4	732
	53.05	27.00	47.4	518	73.0	805
	53.05	40.00	50.2	548	71.6	790
	53.12	52.50	52.5	569	73.0	806
	54.95	1.88	38.9	441	53.5	607
	54.88	15.19	40.2	456	62.5	705
	54.90	27.00	43.8	490	65.7	741
	54.93	40.00	46.3	519	65.7	740
	54.88	52.50	47.7	529	67.2	758
	57.97	1.88	39.7	466	51.6	606
	57.95	15.19	41.5	487	56.3	662
	58.00	27.00	42.1	489	57.5	664

			FIRST BURSTS		COMPLETE TURBULENCE	
TRIP DIA (Ins)	SWEEP (Degrees)	S (Ins)	Q_∞ (Ft/Sec)	$(\frac{V_\infty d}{\nu})$	Q_∞ (Ft/Sec)	$(\frac{V_\infty d}{\nu})$
	57.93	40.00	42.1	488	57.4	666
	58.02	52.50	43.2	496	58.5	672
	60.35	1.88	41.4	499	51.6	621
	60.38	15.19	42.7	514	53.6	642
	60.33	27.00	43.3	515	53.7	639
	60.38	40.00	43.1	512	52.8	628
	60.35	52.50	43.8	519	52.2	618
	62.80	1.88	43.4	535	51.6	636
	62.85	15.19	44.3	547	52.5	648
	62.75	27.00	45.2	550	52.4	637
	62.77	40.00	45.0	547	51.8	630
	62.80	52.50	46.0	554	52.3	630
	64.62	1.88	44.3	555	52.6	658
	64.62	15.19	45.5	569	52.5	658
	64.53	27.00	46.3	572	51.8	640
	64.53	40.00	46.3	572	50.8	627
	64.58	52.50	46.4	568	50.9	623
	67.90	1.88	46.8	601	53.5	687
	67.93	15.19	48.7	626	53.0	681
	67.98	27.00	48.7	618	51.8	657
	67.95	40.00	48.5	615	50.8	644
	70.68	1.88	49.4	643	56.4	734
	70.73	15.19	48.1	629	54.5	713
	70.73	15.19	47.8	618	54.4	698
	70.73	27.00	49.1	634	52.8	682
	70.82	39.94	50.8	654	54.8	701
	70.75	40.00	49.7	643	52.0	671
	70.75	52.50	49.9	645	52.8	682
	70.82	52.50	50.9	651	54.8	701
0.0500	55.05	7.88	18.0	369	52.4	1072
	54.85	12.69	25.1	539	52.4	1129
	54.95	20.13	33.7	690	60.5	1237
	54.88	26.75	36.6	789	54.7	1179
	54.90	39.25	40.4	872	56.9	1229
	54.90	52.00	43.4	937	56.9	1229
	55.03	65.75	45.4	982	58.3	1260
	60.30	12.69	19.8	453	38.9	889
	60.43	20.13	26.3	571	47.3	1027
	60.42	26.75	27.3	627	42.6	978
	60.35	39.25	30.4	697	43.2	990
	60.35	52.00	32.9	754	44.3	1016
	60.38	65.75	34.9	800	46.5	1066
	64.55	12.69	17.7	421	33.6	799
	64.57	20.13	21.6	487	40.3	910
	64.55	26.75	22.6	538	35.2	838
	64.55	39.25	24.3	578	35.5	845
	64.58	52.00	25.8	616	35.7	851
	64.58	65.75	27.7	659	37.1	884

			FIRST BURSTS		COMPLETE TURBULENCE	
TRIP DIA (Ins)	SWEEP (Degrees)	S (Ins)	Q_∞ (Ft/Sec)	$(\frac{V_\infty d}{\nu})$	Q_∞ (Ft/Sec)	$(\frac{V_\infty d}{\nu})$
0.0625	54.85	12.69	24.3	655	51.9	1401
	54.93	26.88	36.1	971	55.3	1489
	54.93	38.94	40.7	1096	57.0	1536
	55.03	65.75	45.6	1238	58.6	1591
	60.27	12.69	17.7	508	39.1	1123
	60.28	26.88	27.4	782	42.4	1210
	60.37	38.94	29.7	854	43.2	1240
	60.35	65.75	34.6	996	46.9	1350
	64.55	12.69	15.3	458	32.9	980
	64.58	26.88	21.7	649	33.8	1005
	64.55	38.94	23.9	712	35.2	1049
	64.58	65.75	27.3	817	37.6	1125
0.0940	53.12	15.13	27.4	1029	66.6	2501
	53.08	27.06	40.6	1518	65.1	2432
	53.08	40.00	45.6	1703	69.2	2585
	53.18	52.50	49.2	1850	73.4	2761
	54.97	15.13	23.9	917	59.7	2294
	54.98	27.06	35.8	1371	60.6	2318
	55.00	40.00	41.4	1584	63.1	2413
	54.92	52.50	45.1	1734	66.9	2572
	58.03	15.13	17.5	695	52.4	2087
	58.00	27.06	29.5	1182	53.3	2134
	58.00	40.00	35.5	1415	53.4	2117
	58.02	52.50	38.0	1514	57.0	2273
	60.43	15.13	15.6	640	46.2	1887
	60.43	27.06	25.1	1030	47.2	1940
	60.37	40.00	30.6	1249	48.4	1975
	60.38	52.50	33.1	1353	50.4	2059
	62.85	15.13	13.5	567	41.5	1745
	62.85	27.06	21.1	887	42.7	1795
	62.83	40.00	25.9	1083	42.8	1788
	62.83	52.50	28.5	1192	45.1	1885
0.1300	55.05	14.94	21.6	1168	63.9	3431
	55.05	20.38	30.3	1627	62.3	3344
	54.90	26.88	36.3	1952	55.3	2970
	54.90	52.38	43.7	2349	58.4	3138
	54.90	62.13	44.3	2396	59.5	3215
	60.37	20.38	19.7	1121	47.4	2698
	60.30	26.88	26.3	1498	43.3	2468
	60.35	52.38	32.9	1879	44.4	2534
	60.33	62.13	33.5	1921	46.5	2669
	64.55	26.88	18.3	1085	34.4	2039
	64.52	52.38	25.5	1512	35.8	2122
	64.53	62.13	26.2	1564	37.1	2212
0.2150	54.97	18.69	23.8	2107	-	-
	54.97	26.81	37.0	3284	-	-
	54.95	27.00	35.6	3107	66.3	5787

			FIRST BURSTS		COMPLETE TURBULENCE	
TRIP DIA (Ins)	SWEEP (Degrees)	S (Ins)	Q_∞ (Ft/Sec)	$(\frac{V_\infty d}{\nu})$	Q_∞ (Ft/Sec)	$(\frac{V_\infty d}{\nu})$
	54.92	39.00	40.9	3801	59.5	5531
	54.97	39.75	41.4	3671	-	-
	54.92	63.12	44.3	4123	59.5	5531
	57.95	26.81	29.8	2734	-	-
	60.43	26.81	24.2	2278	-	-
	60.37	27.00	26.0	2407	49.5	4590
	60.32	39.00	29.4	2903	44.3	4377
	60.43	39.75	30.5	2869	-	-
	60.30	62.13	33.5	3304	46.5	4589
	62.85	39.75	25.4	2448	-	-
	64.67	39.75	22.0	2153	35.5	3635
	64.53	62.13	26.2	2690	37.1	3805

TABLE 1

Aircraft	M_∞ cruise	L.E.ρ Mean*	L.E.Sweep	Probable State of Attachment Line.
H-S 125	0.76	1.2"	24^o	Laminar
H-S Trident	0.76	3.0"	38^o	Turbulent
B.A.C.111	0.73	1.8"	23^o	Laminar?
Boeing 727	0.84	3.0"	36^o	Turbulent
Douglas DC-9	0.80	1.8"	29^o	Turbulent
Douglas DC-10	0.82	4.3"	38^o	Turbulent
A 300B	0.78	2.8"	30^o	Turbulent
L 1011	0.81	4.0"	38^o	Turbulent
Boeing 747	0.89	5.0"	42^o	Turbulent

*It has been assumed that the mean radius measured in a plane normal to the leading edge may be approximated by a simple function of mean streamwise chord and leading edge sweep i.e.

$$\rho \simeq \frac{0.011\ C}{\cos \Lambda}$$

where the constant 0.011 is based on a streamwise t/c of 12%

TABLE 2 - THE FUNCTIONS f' AND g PLUS THEIR SECOND DERIVATIVES

η	f'	f'''	g	g''
0.0	0.0	-1.0000	0.0	0.0
0.1	0.1183	-0.9928	0.0570	-0.0034
0.2	0.2266	-0.9728	0.1140	-0.0133
0.3	0.3252	-0.9421	0.1709	-0.0289
0.4	0.4145	-0.9028	0.2275	-0.0496
0.5	0.4946	-0.8566	0.2836	-0.0745
0.6	0.5663	-0.8054	0.3389	-0.1024
0.7	0.6299	-0.7506	0.3932	-0.1324
0.8	0.6859	-0.6936	0.4462	-0.1631
0.9	0.7351	-0.6356	0.4975	-0.1934
1.0	0.7779	-0.5777	0.5469	-0.2220
1.1	0.8149	-0.5209	0.5941	-0.2479
1.2	0.8467	-0.4659	0.6388	-0.2700
1.3	0.8738	-0.4134	0.6809	-0.2876
1.4	0.8968	-0.3638	0.7200	-0.3001
1.5	0.9162	-0.3177	0.7562	-0.3073
1.6	0.9323	-0.2751	0.7892	-0.3090
1.7	0.9458	-0.2363	0.8192	-0.3056
1.8	0.9568	-0.2013	0.8462	-0.2974
1.9	0.9659	-0.1701	0.8702	-0.2850
2.0	0.9732	-0.1425	0.8913	-0.2691
2.2	0.9839	-0.0975	0.9257	-0.2298
2.4	0.9905	-0.0645	0.9509	-0.1860
2.6	0.9946	-0.0412	0.9686	-0.1428
2.8	0.9970	-0.0254	0.9807	-0.1044
3.0	0.9984	-0.0151	0.9885	-0.0727
3.2	0.9992	-0.0087	0.9934	-0.0483
3.4	0.9996	-0.0048	0.9964	-0.0306
3.6	0.9998	-0.0026	0.9981	-0.0186
3.8	0.9999	-0.0013	0.9990	-0.0108
4.0	1.0000	-0.0006	0.9995	-0.0060
4.2	1.0000	-0.0003	0.9998	-0.0032
4.4	1.0000	-0.0000	0.9999	-0.0016
4.6	1.0000	-0.0000	1.0000	-0.0008
4.8	1.0000	-0.0000	1.0000	-0.0004
5.0	1.0000	-0.0000	1.0000	-0.0002
5.2	1.0000	-0.0000	1.0000	-0.0001
5.4	1.0000	-0.0000	1.0000	-0.0000

$\int_0^\infty (1-f')\,d\eta = 0.6479$

$\int_0^\infty f'(1-f')\,d\eta = 0.2865$

$H = 2.261$

TABLE 3. THE POINT OF ORIGIN OF THE STREAKS AS A FUNCTION OF SWEEP ANGLE AND FREE STREAM SPEED

SWEEP (Degrees)	SPEED (ft/sec)	x/Co -
55	80	0.26 ±0.02
55	90	0.22 ±0.02
55	100	0.19 ±0.02
55	110	0.17 ±0.02
63	62.5	0.33 ±0.02
63	70	0.28 ±0.02
63	80	0.24 ±0.02
63	90	0.22 ±0.02
63	100	0.20 ±0.02
63	110	0.17 ±0.02
71	80	0.26 ±0.02
71	90	0.20 ±0.02
71	100	0.20 ±0.02
71	110	0.18 ±0.02

TABLE 4 STREAK PITCH AS A FUNCTION OF SWEEP ANGLE, FREE STREAM SPEED AND CHORDWISE POSITION

SWEEP (Degrees)	SPEED (ft/sec)	x/Co -	PITCH (ins)
55	≃ 100	0.26 -0.40	0.15 ±0.03
63	≃ 95	0.26 -0.40	0.18 ±0.03
71	≃ 90	0.26 -0.40	0.22 ±0.03

TABLE 5. ORIENTATION OF THE STREAKS WITH RESPECT TO THE x DIRECTION AS A FUNCTION OF SWEEP ANGLE AND POSITION

SWEEP (Degrees)	x/Co -	$(dy/dx)_{streak}$ -
55	0.262	35.0 ±1.0
55	0.306	34.0 ±1.0
55	0.350	34.5 ±1.0
55	0.372	37.5 ±1.0
63	0.262	43.5 ±1.0
63	0.306	42.5 ±1.0
63	0.350	43.0 ±1.0
63	0.372	45.0 ±1.0
71	0.350	53.0 ±1.0
71	0.372	55.5 ±1.0

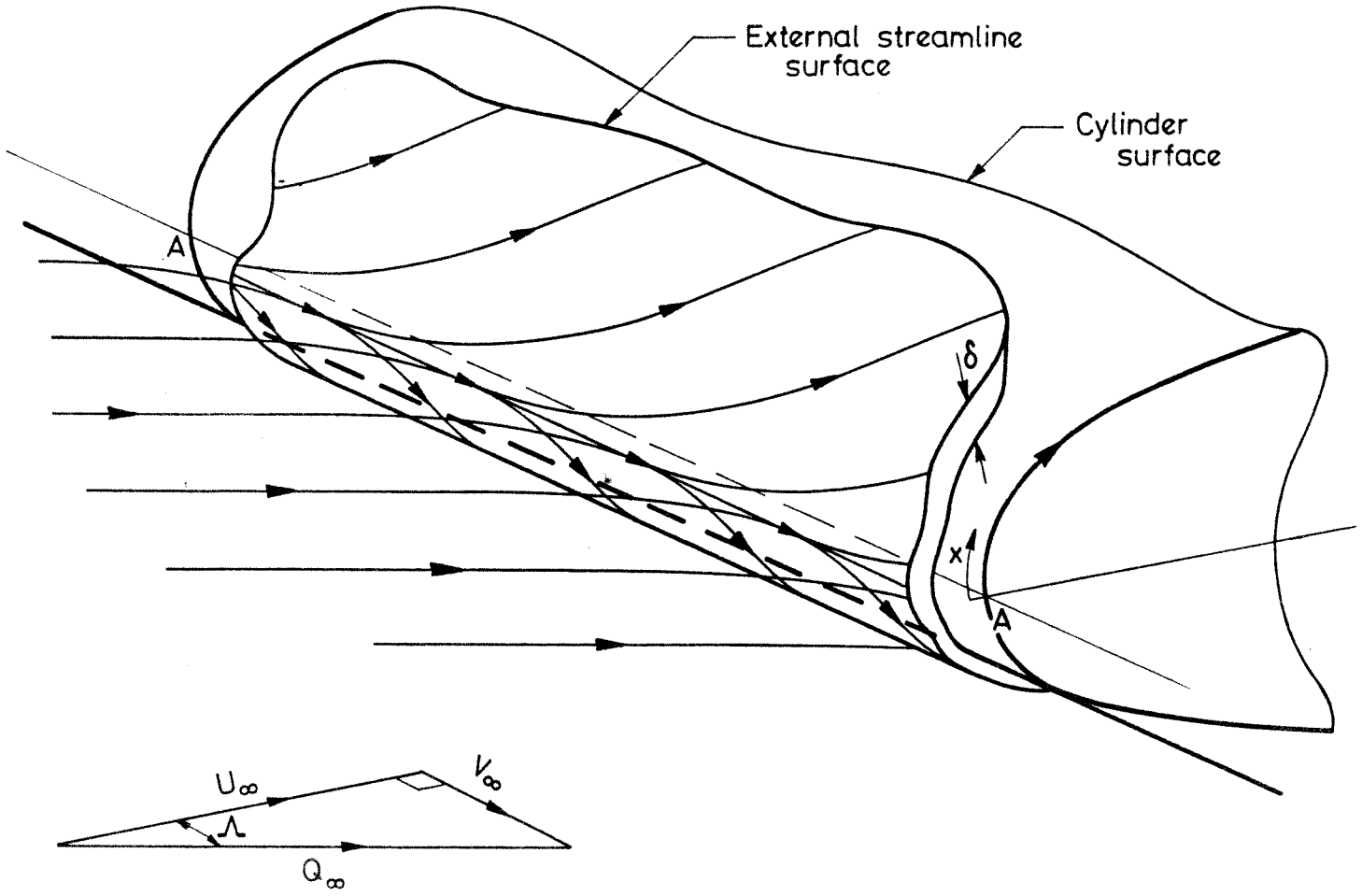

Fig. 1. Flow near the leading edge of a swept cylinder.

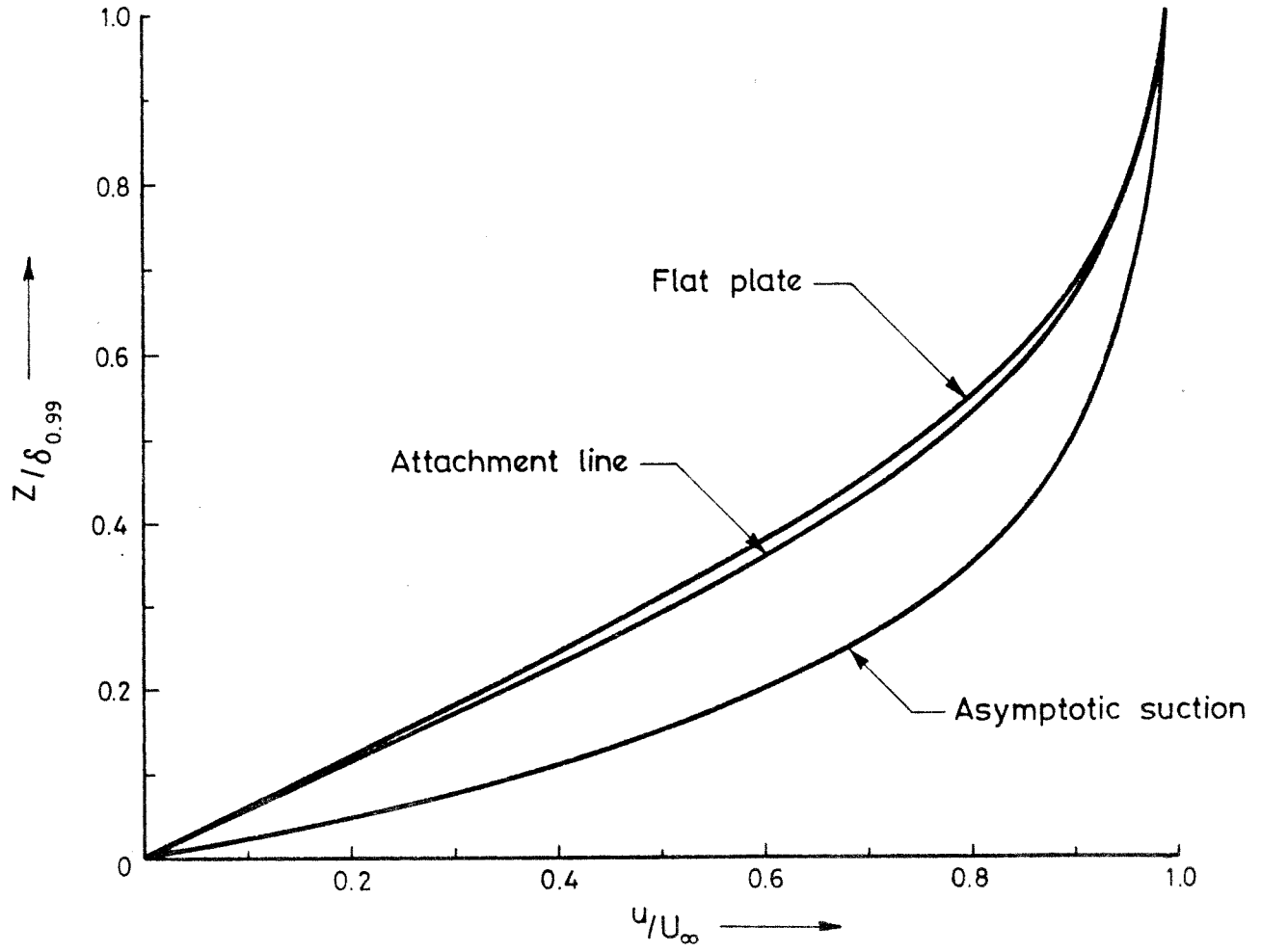

Fig. 2. Incompressible laminar attachment line velocity profile.

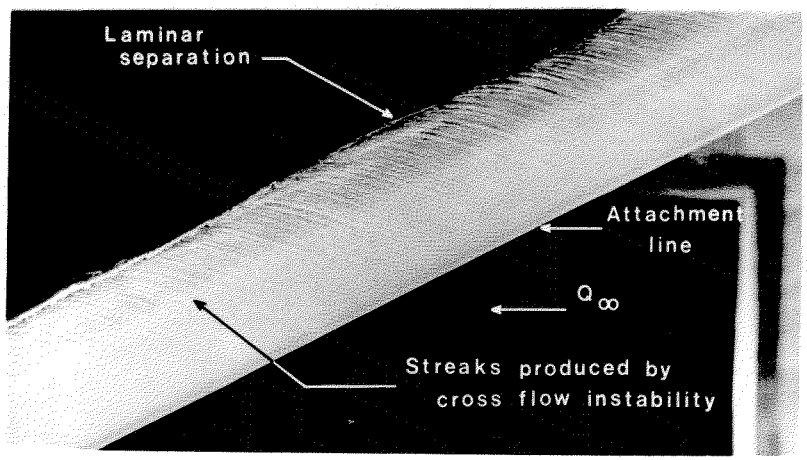

a)

Sweep = 63°

Speed = 90 ft/sec

No trip

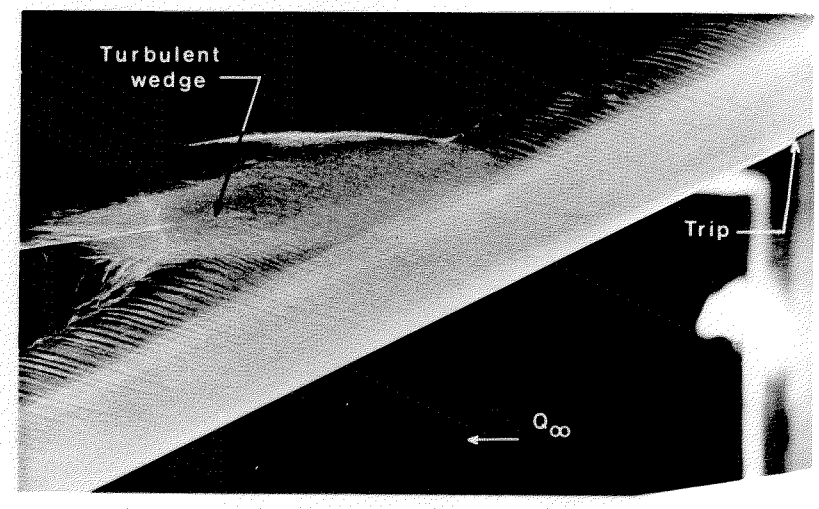

b)

Swept = 63°

Speed = 80 ft/sec

Trip = 0.0135"

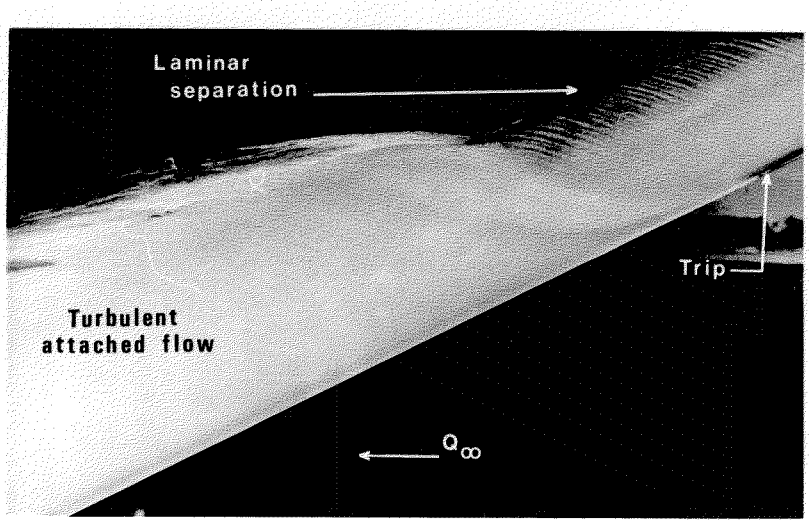

c)

Sweep = 63°

Speed = 90 ft/sec

Trip = 0.0135"

Fig. 3. The response of the swept wing boundary layer to the presence of a trip wire across the attachment line

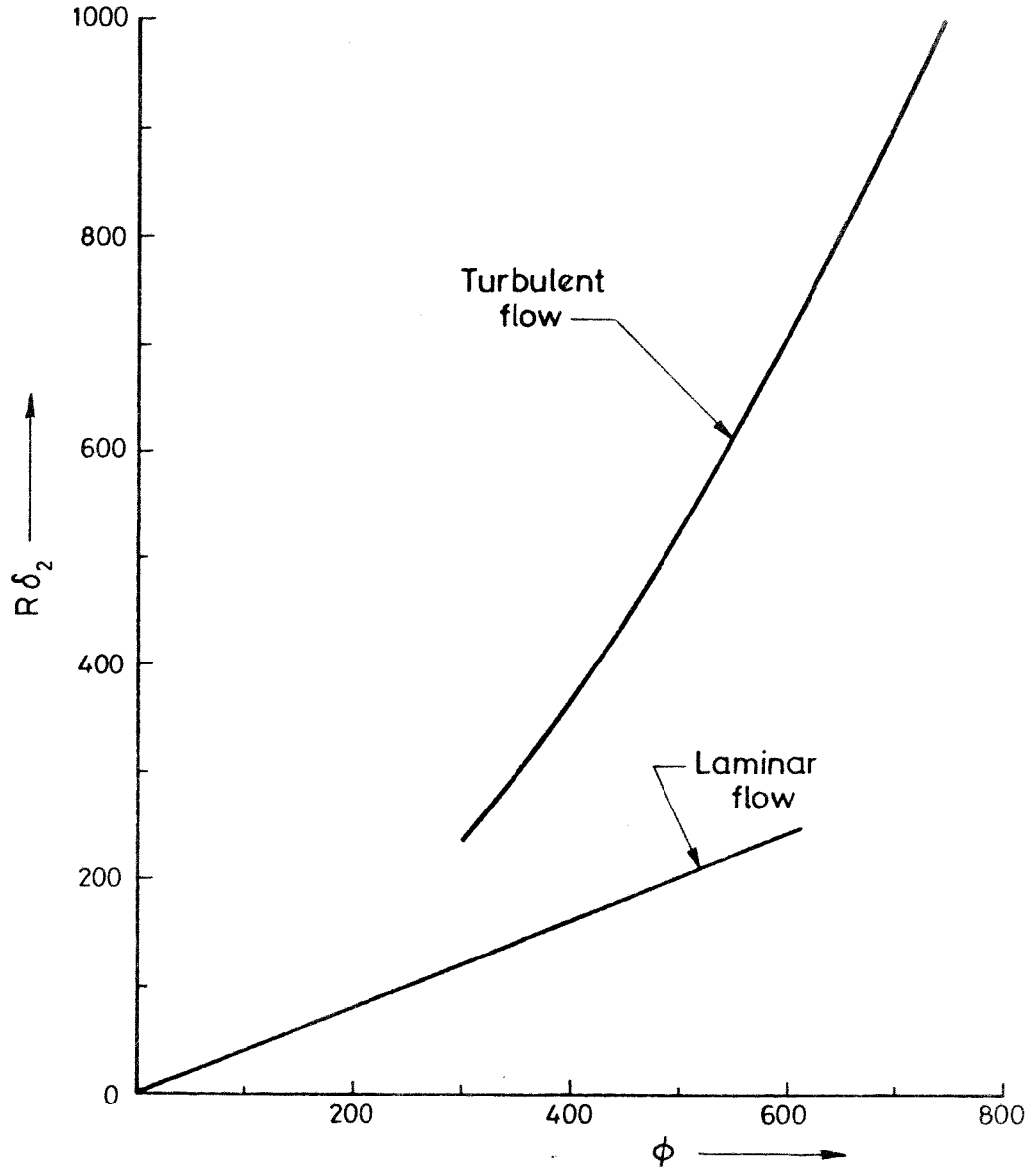

Fig. 4. Variation of the incompressible momentum thickness Reynolds number with the similarity parameter ϕ.

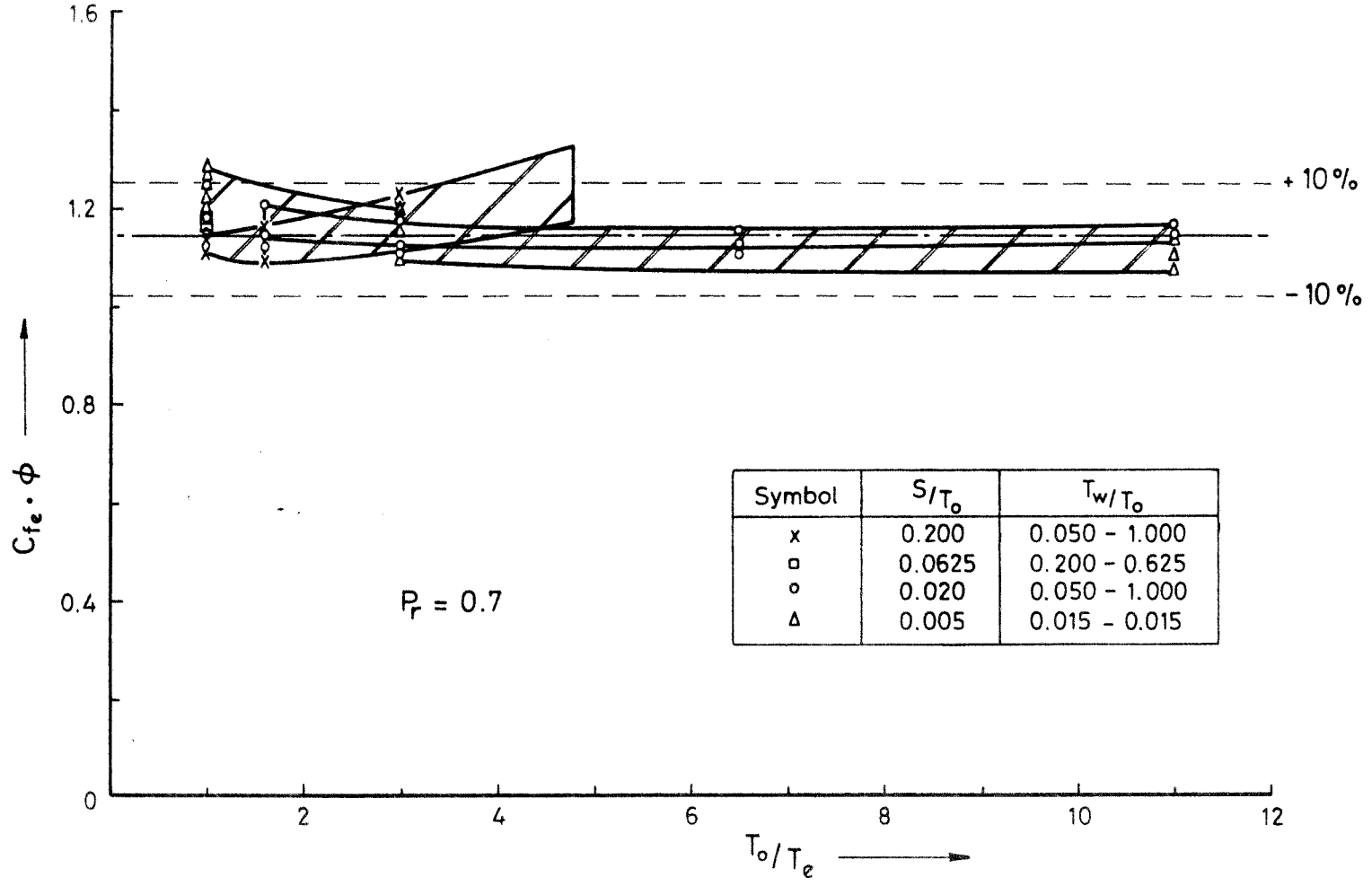

Fig. 5. Comparison between the approximate laminar skin friction relation and exact solutions.

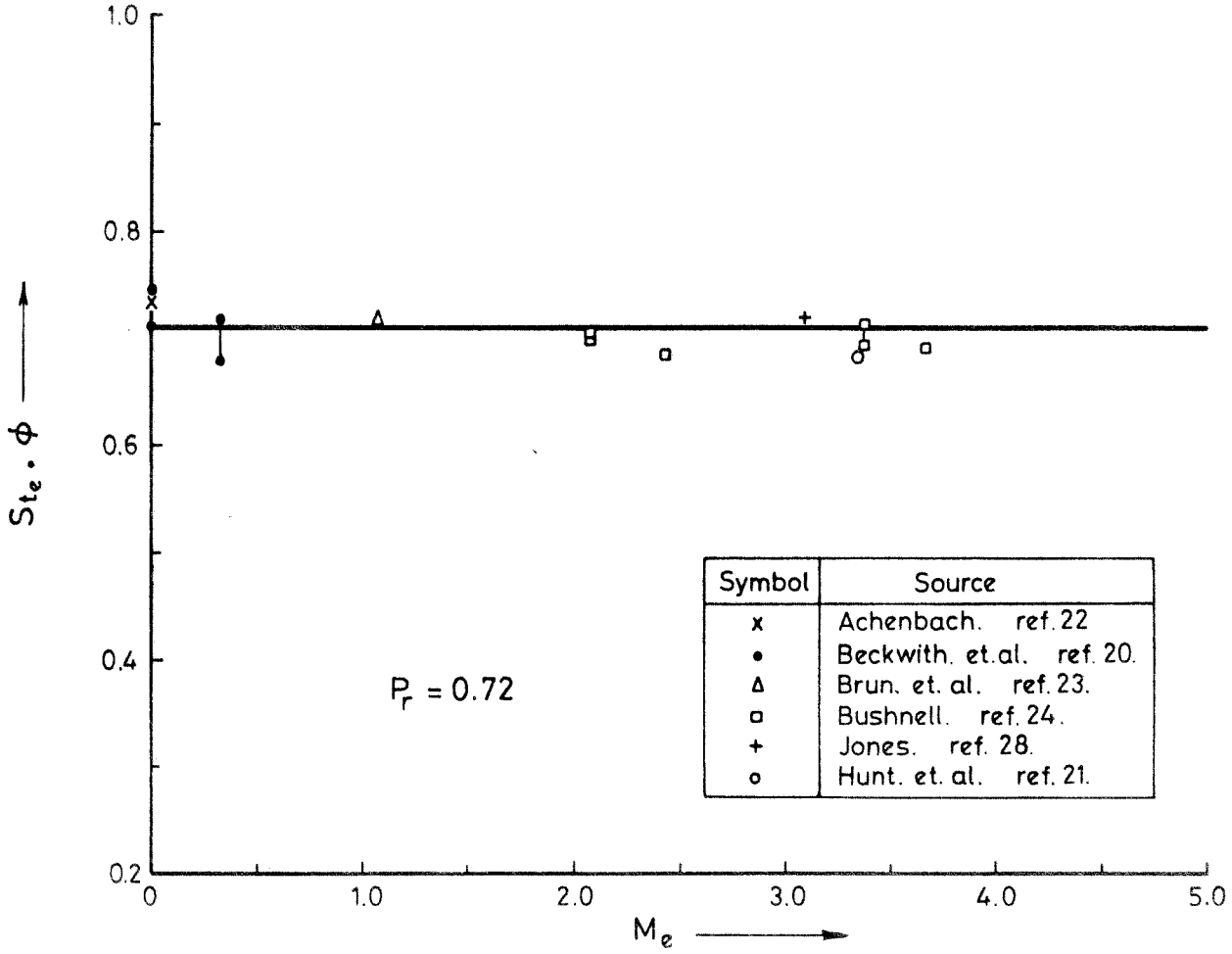

Fig. 6. Comparison between the approximate laminar heat transfer rate and experimental results.

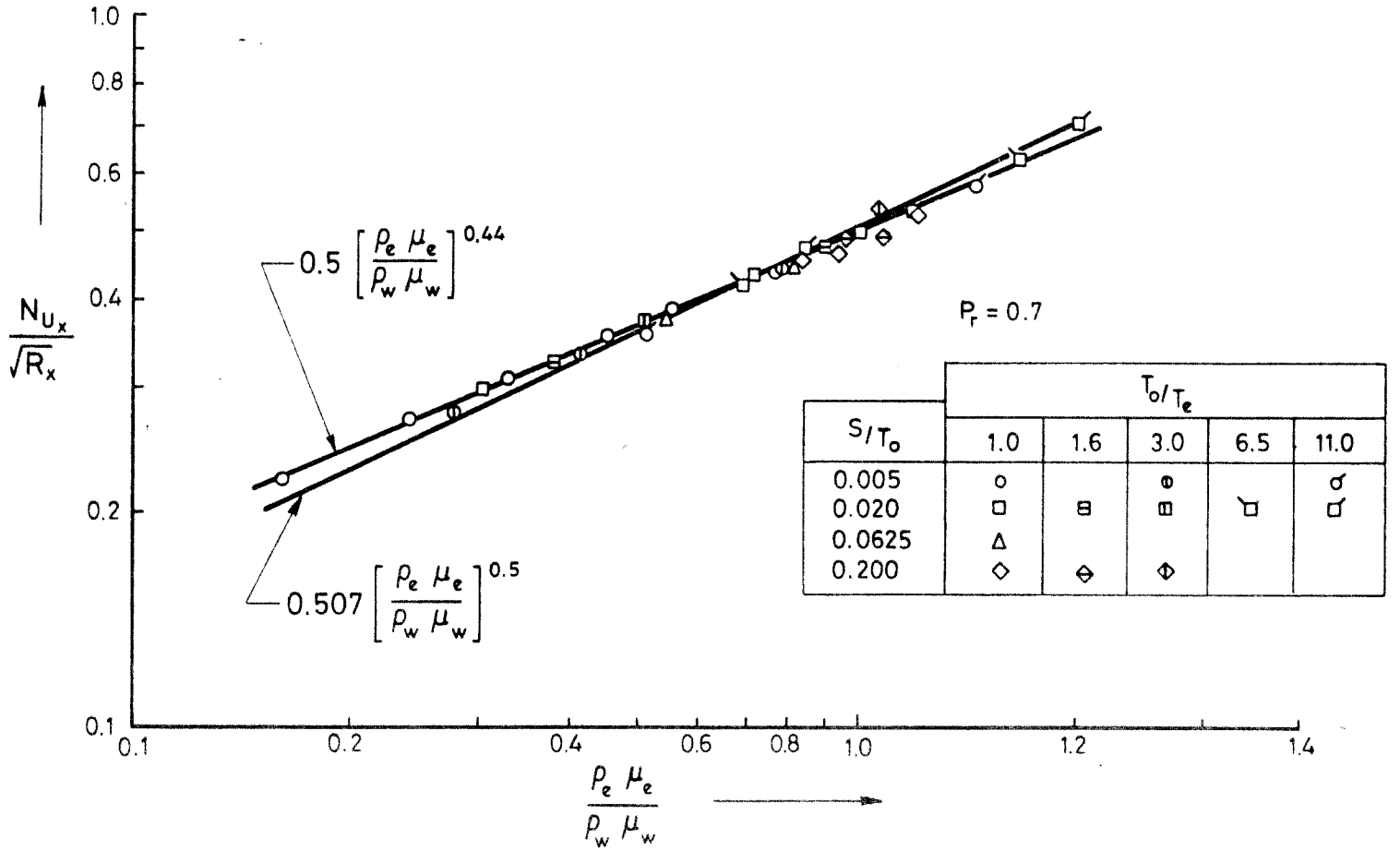

Fig.7. Comparison between the approximate laminar heat transfer rate and exact solutions.

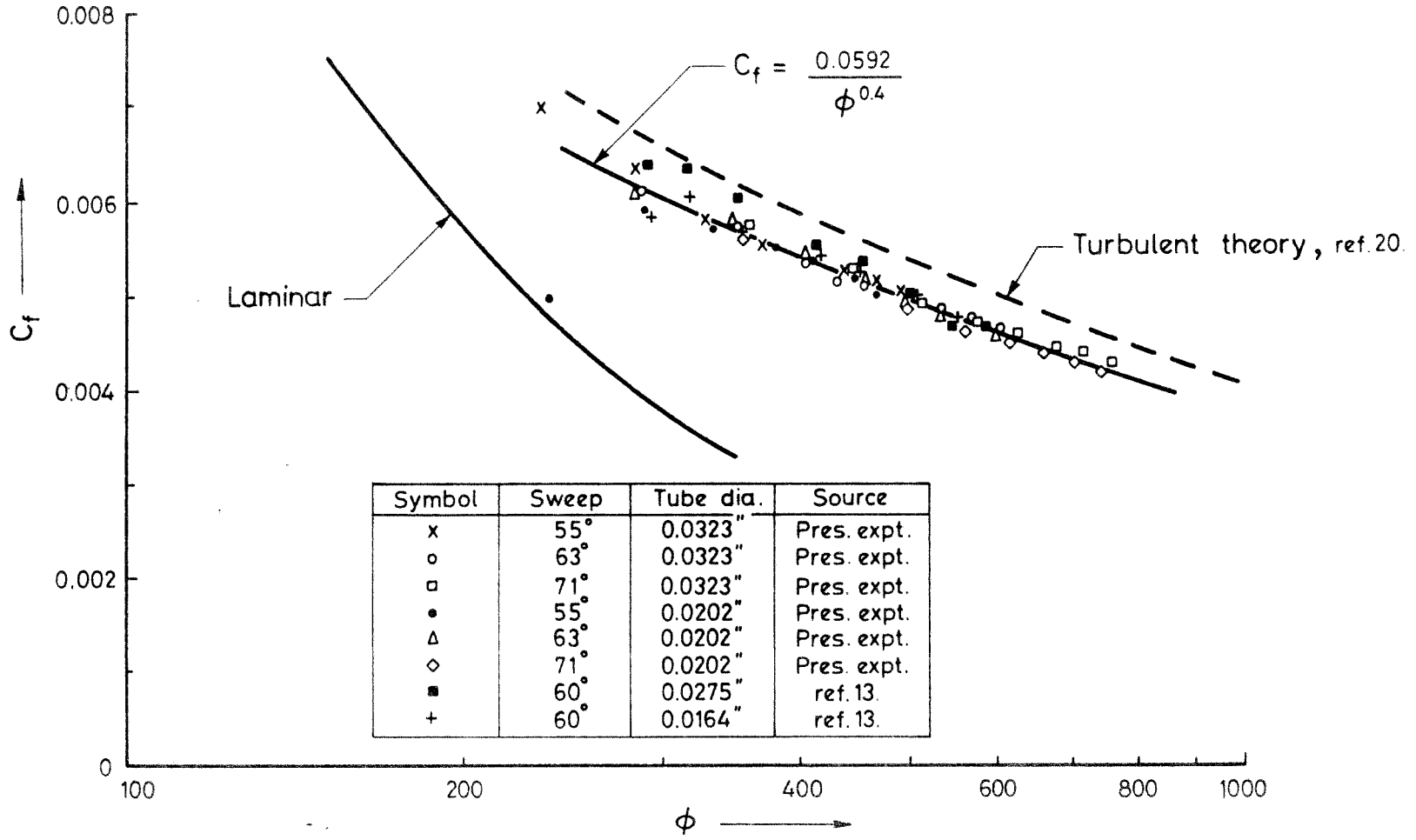

Fig. 8. Variation of the incompressible turbulent skin friction coefficient with ϕ.

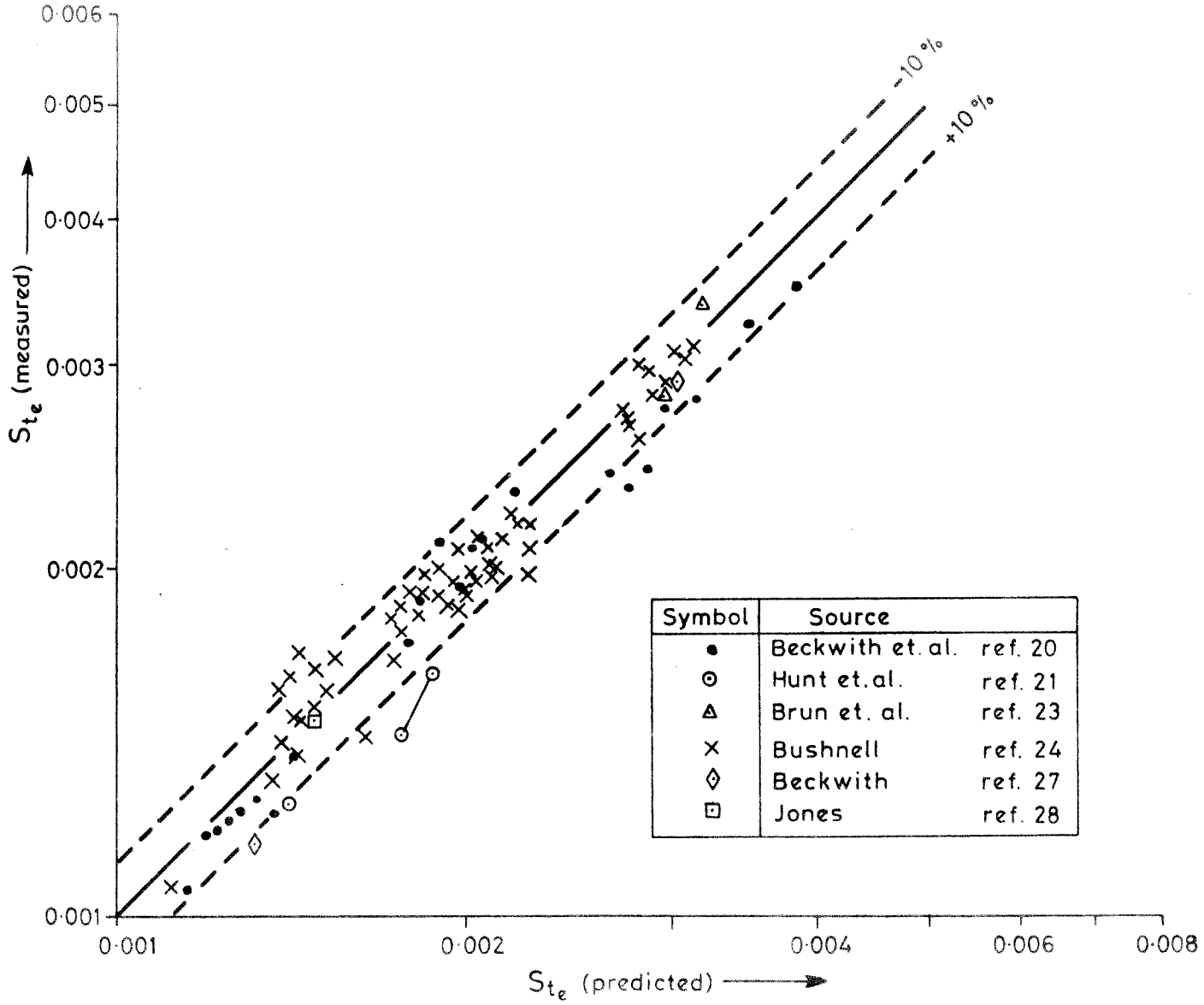

Fig. 9. Comparison between the approximate turbulent heat transfer rate and experimental results.

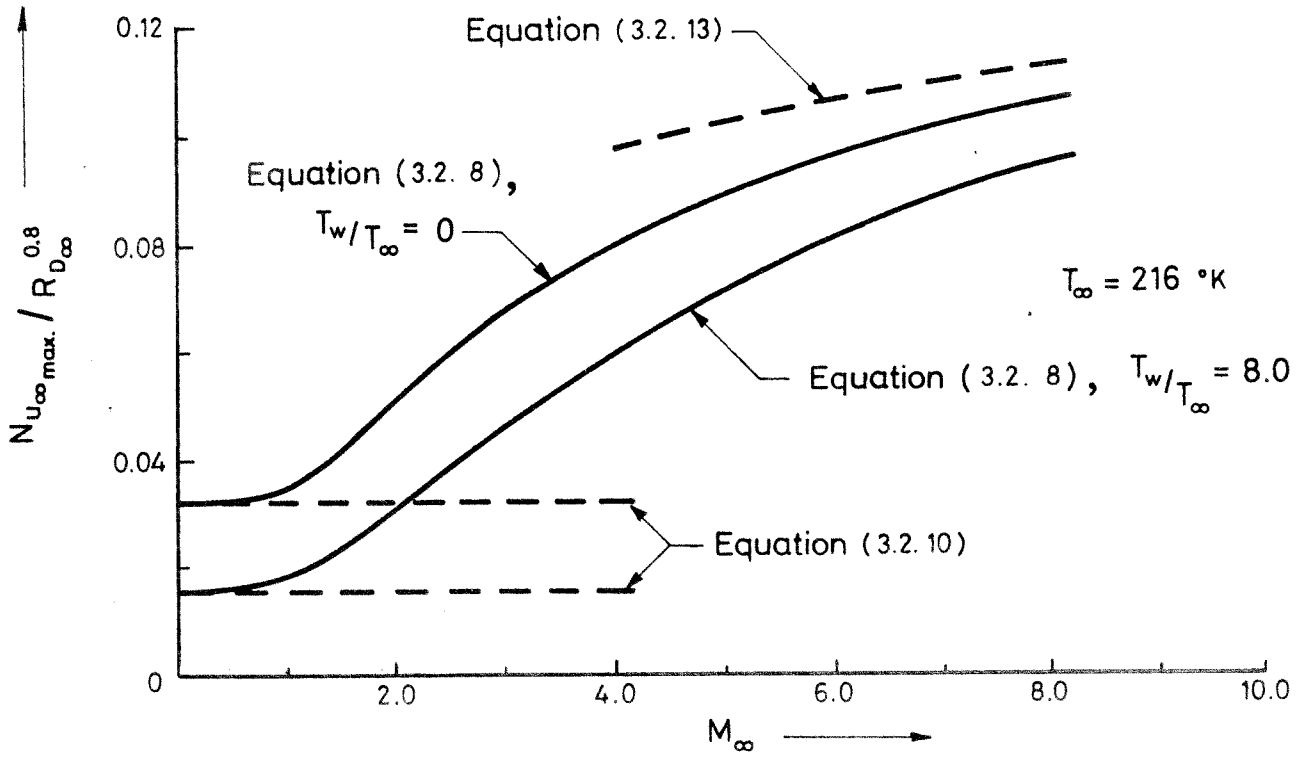

Fig. 10. Variation of max. heat transfer rate with free stream Mach number and wall temperature for a swept circular cylinder when the boundary layer is turbulent.

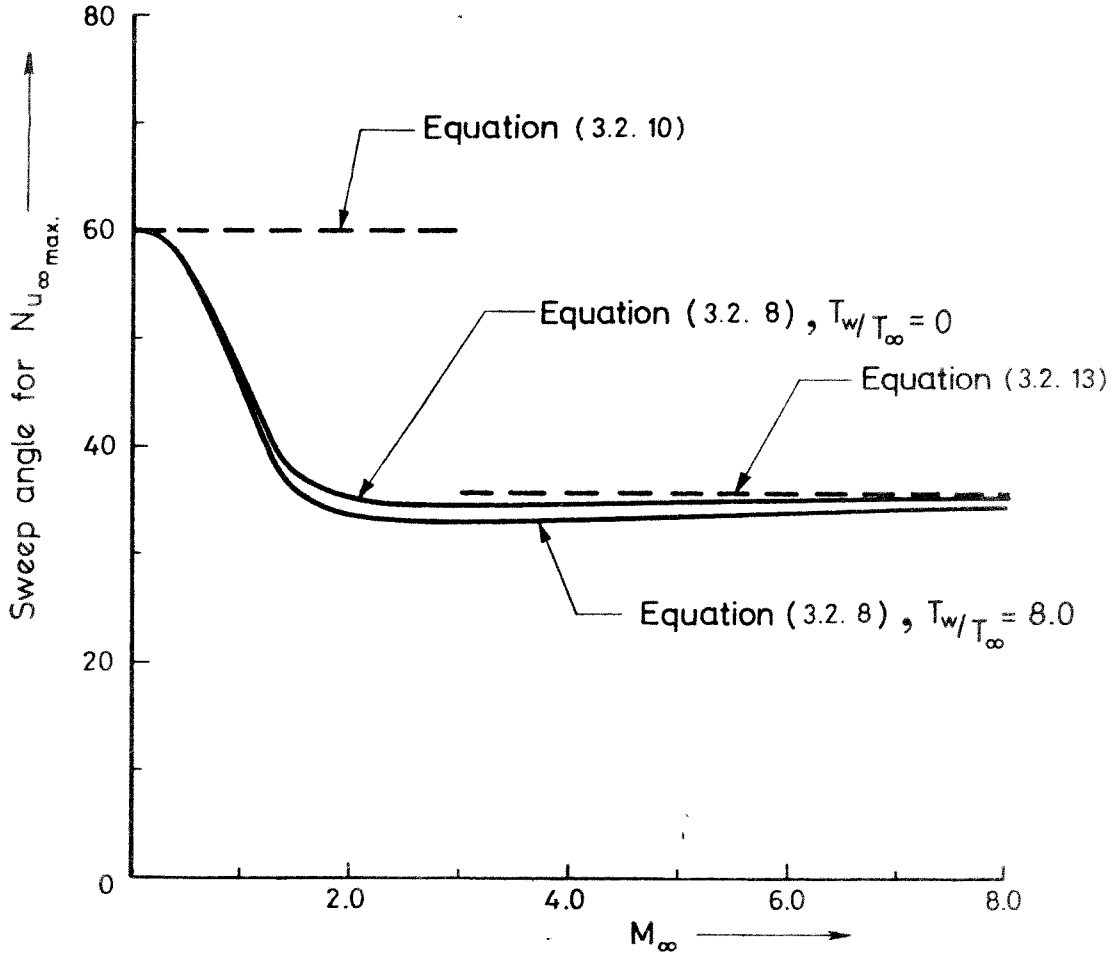

Fig. 11. Variation of sweep angle for max. heat transfer rate with free stream Mach number and wall temperature for a swept circular cylinder when the boundary layer is turbulent.

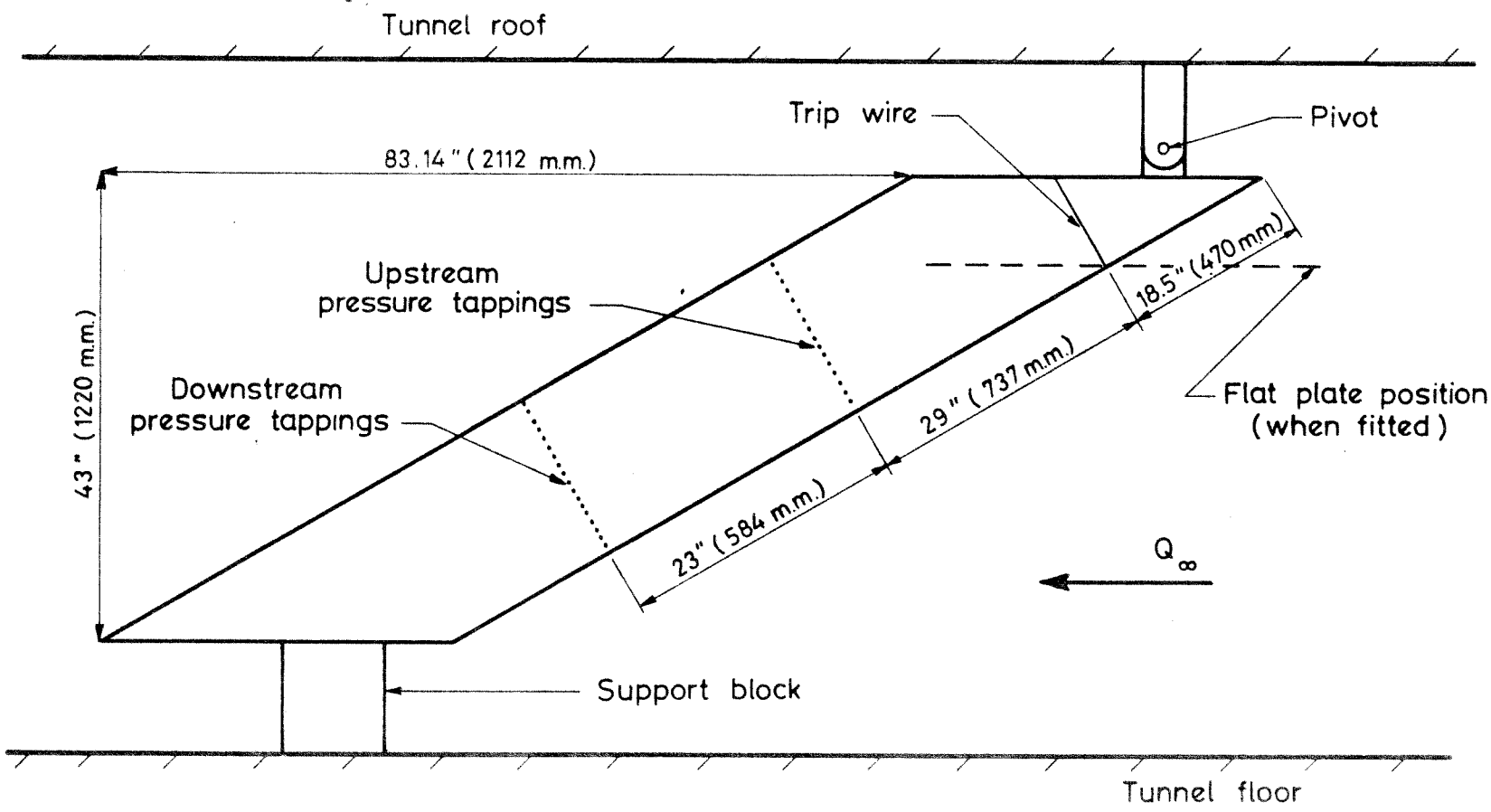

Fig. 12. Experimental arrangement.

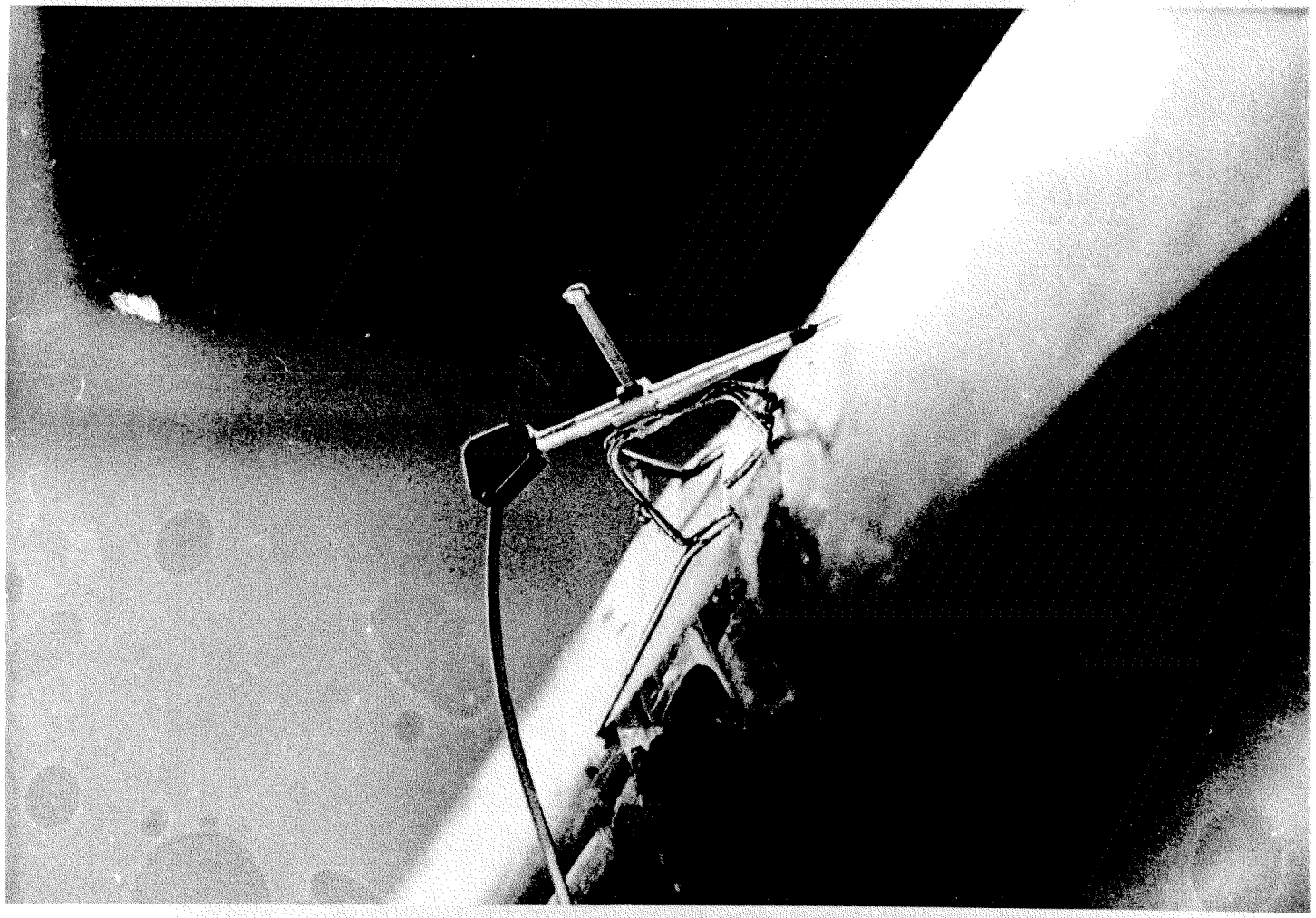

Fig. 13. Hot-wire probe mounted in wire cradle.

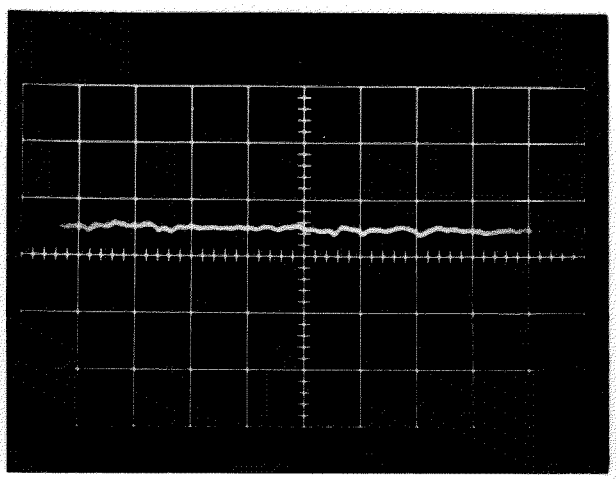

Laminar flow

A burst of turbulence

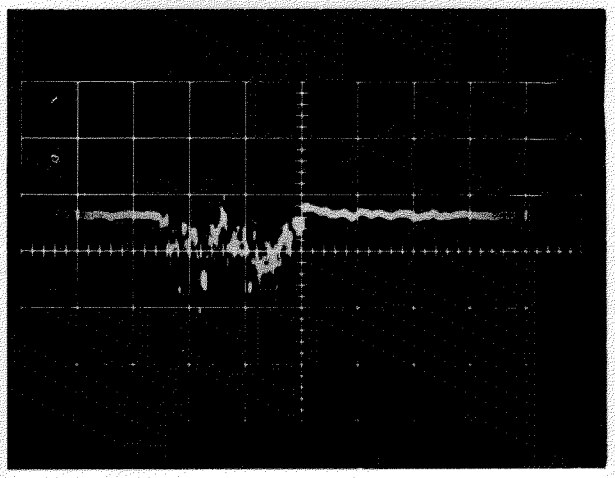

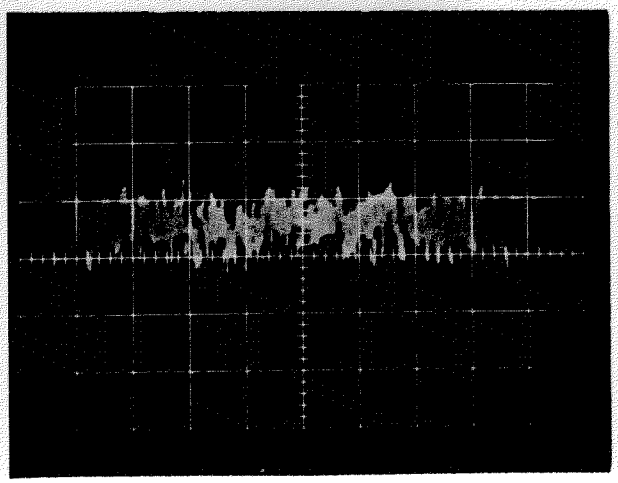

Turbulent flow

Fig. 14. Typical oscilloscope traces of the output from the hot-wire probe.

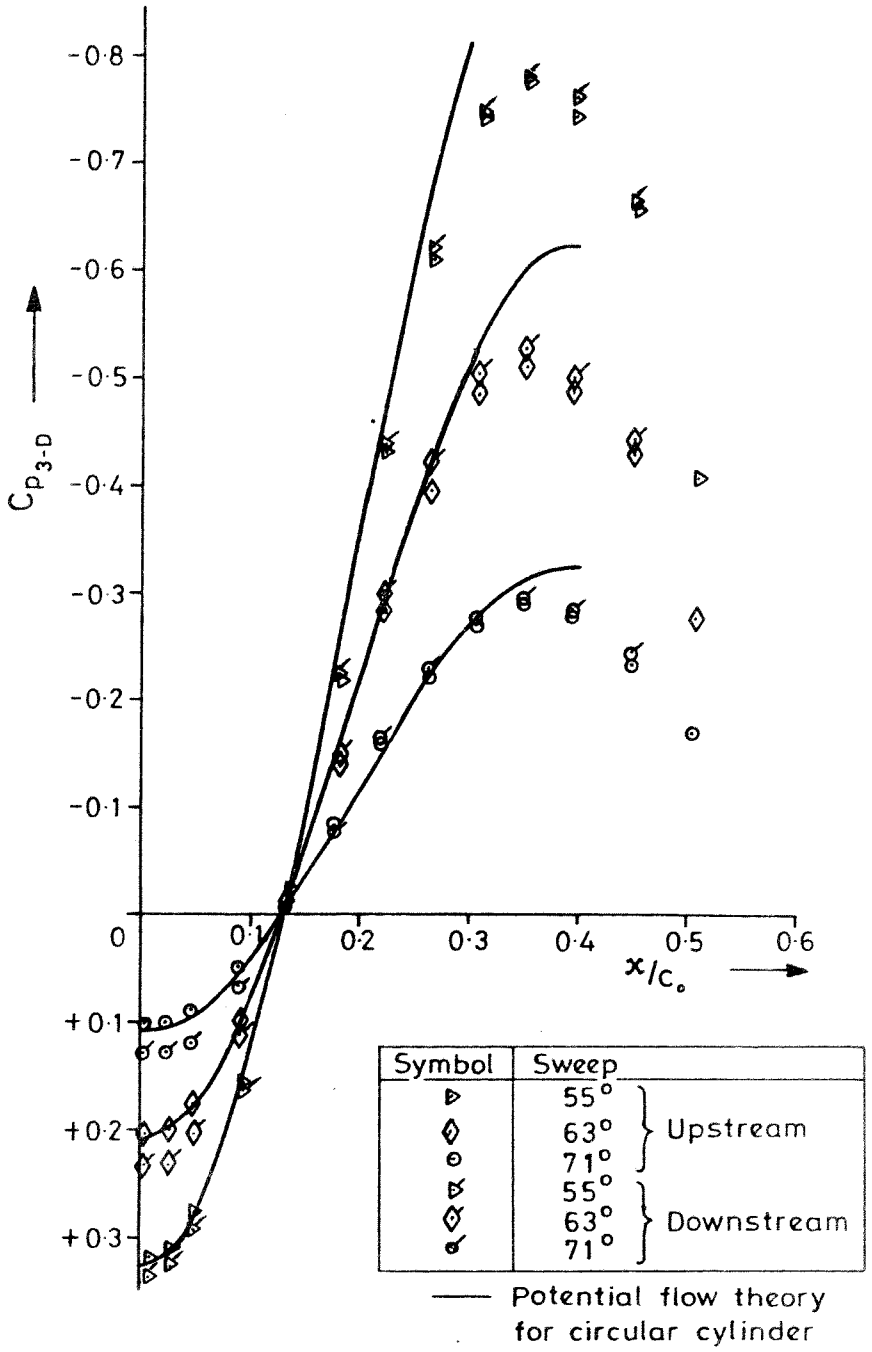

Fig. 15 The model surface pressure distribution

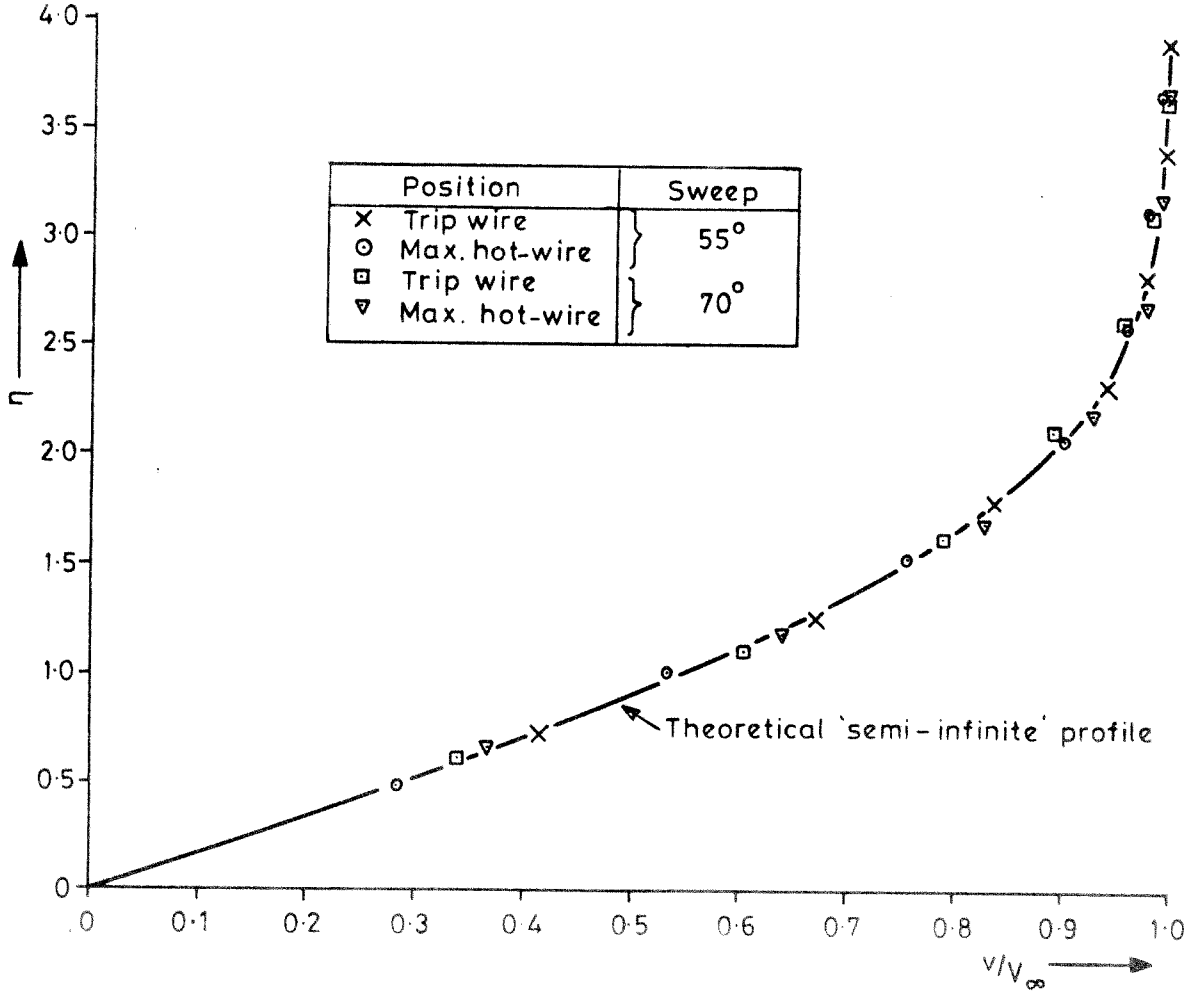

Fig. 16. Measured attachment line velocity profiles

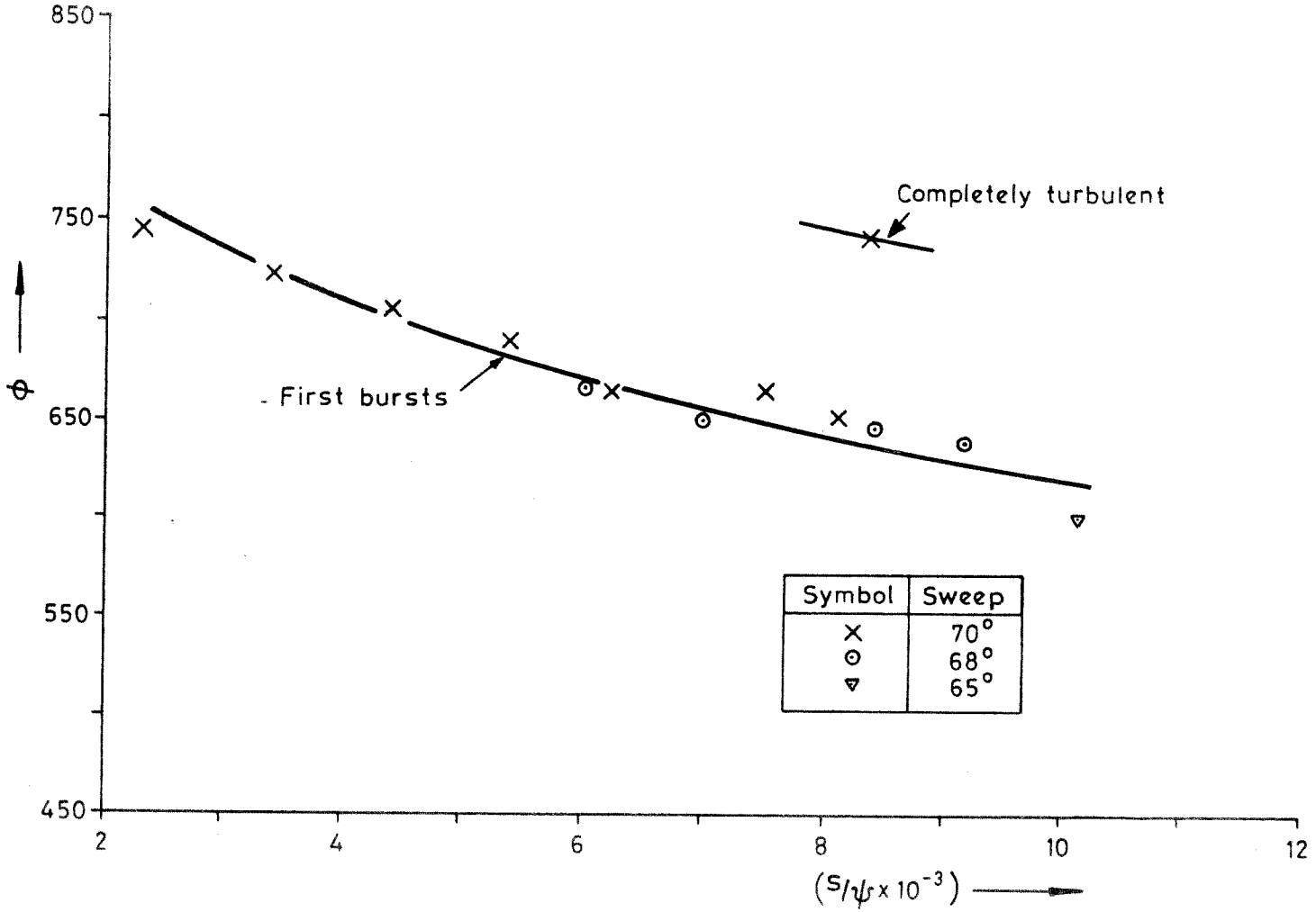

Fig. 17. Transition characteristics in the absence of a trip wire.

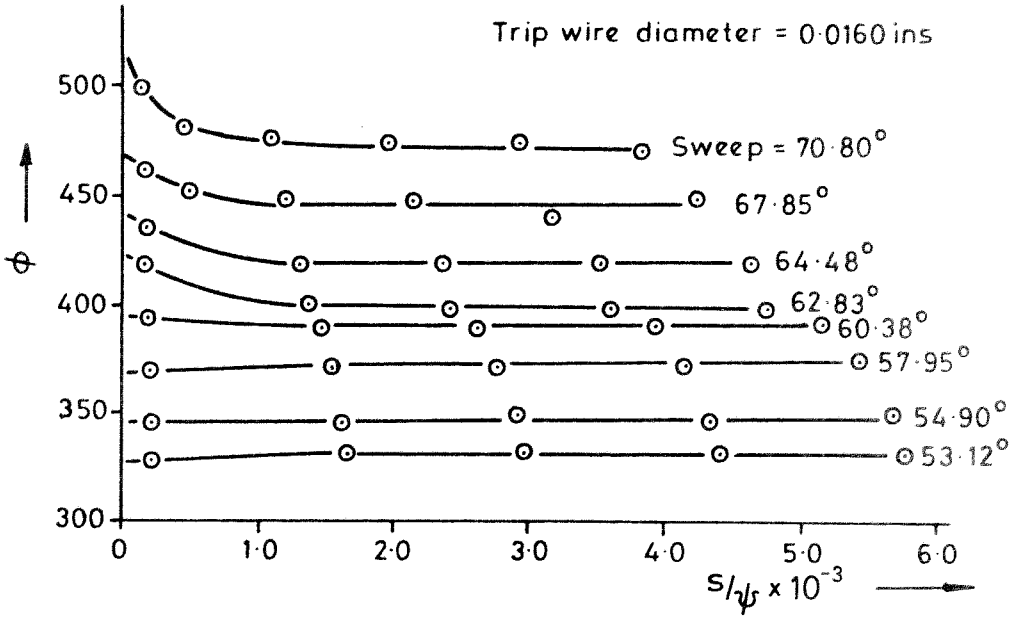

First bursts of turbulence

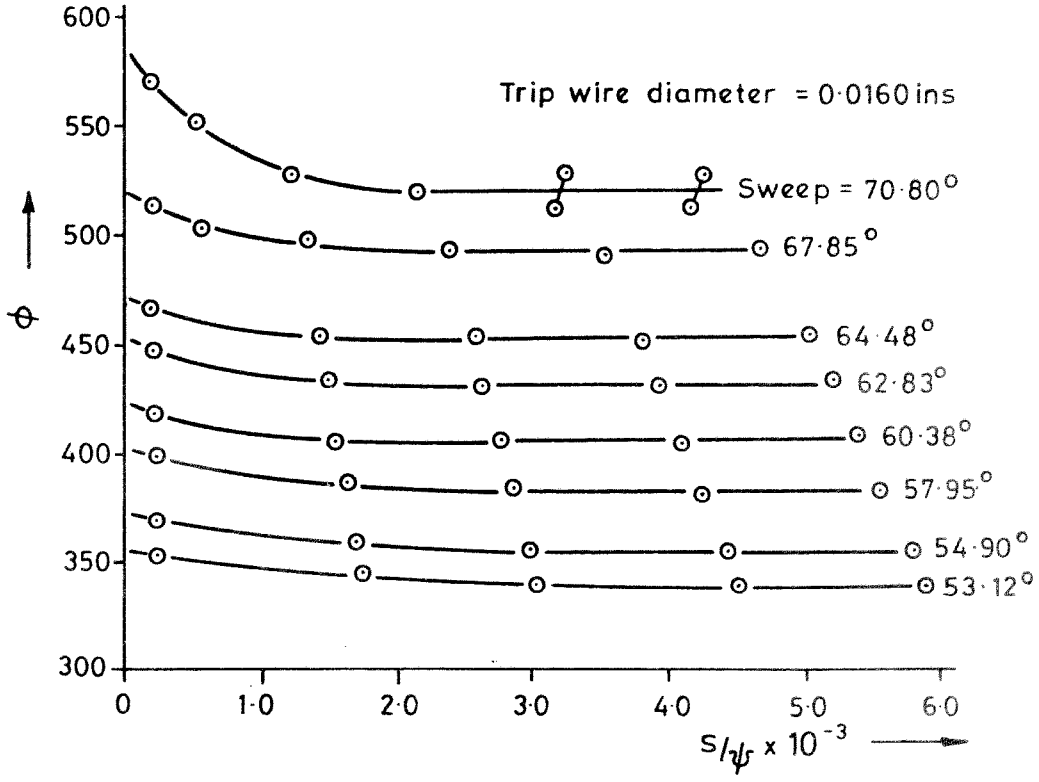

Complete turbulence

Fig. 18. A typical set of experimental results.

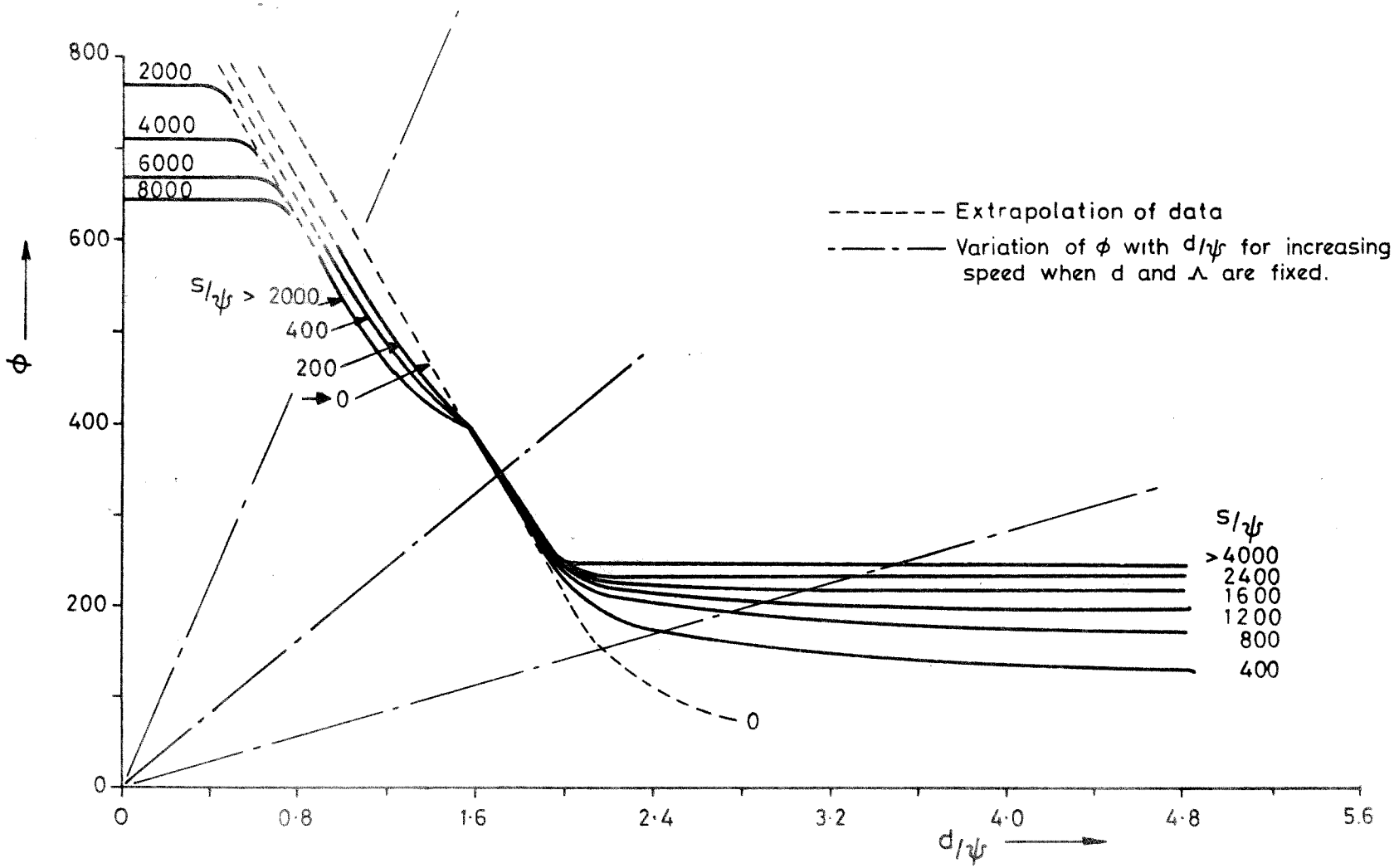

Fig. 19. The variation of ϕ with d/ψ and S/ψ for the appearance of first bursts of turbulence.

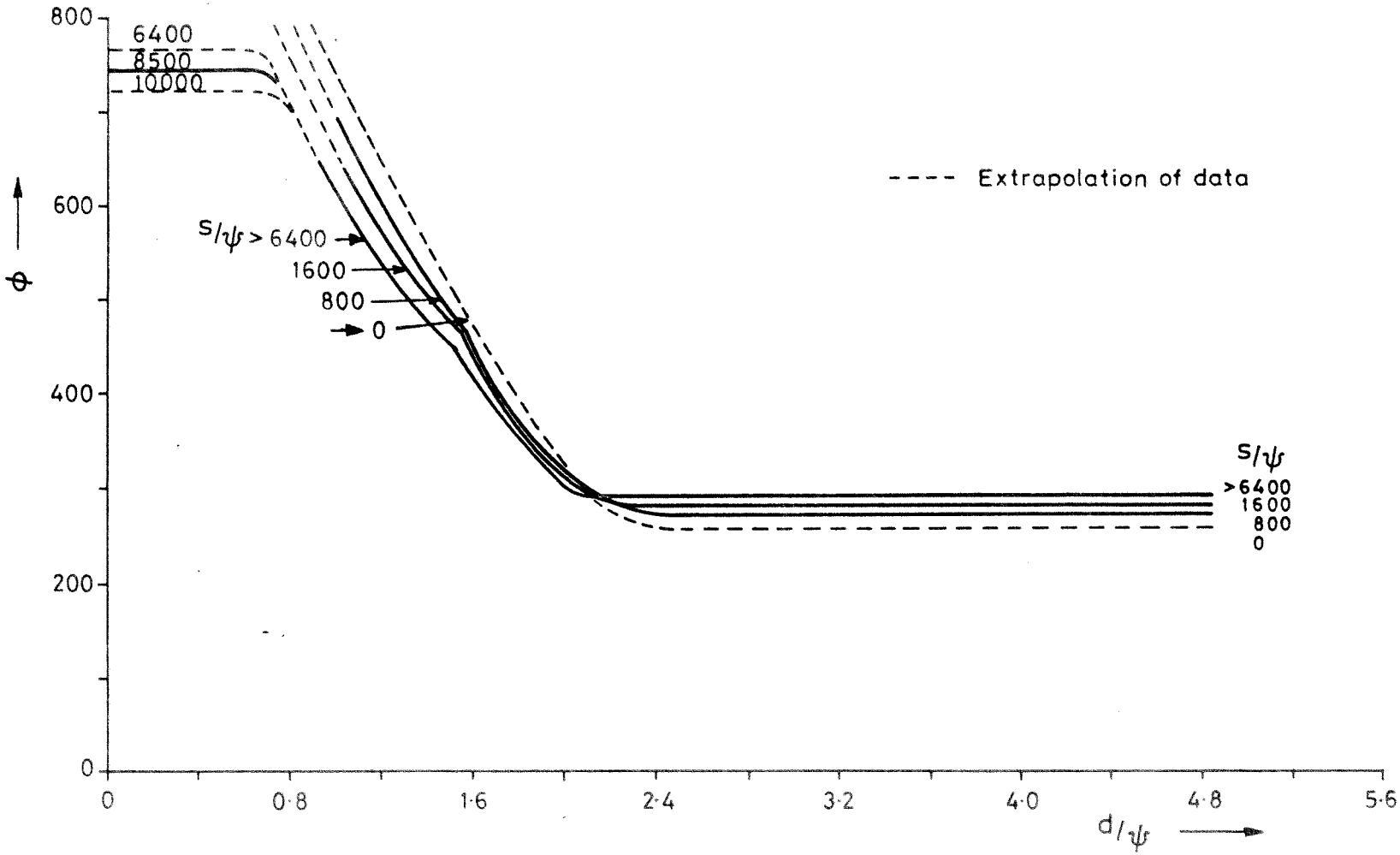

Fig. 20. The variation of ϕ with d/ψ and S/ψ for complete turbulence.

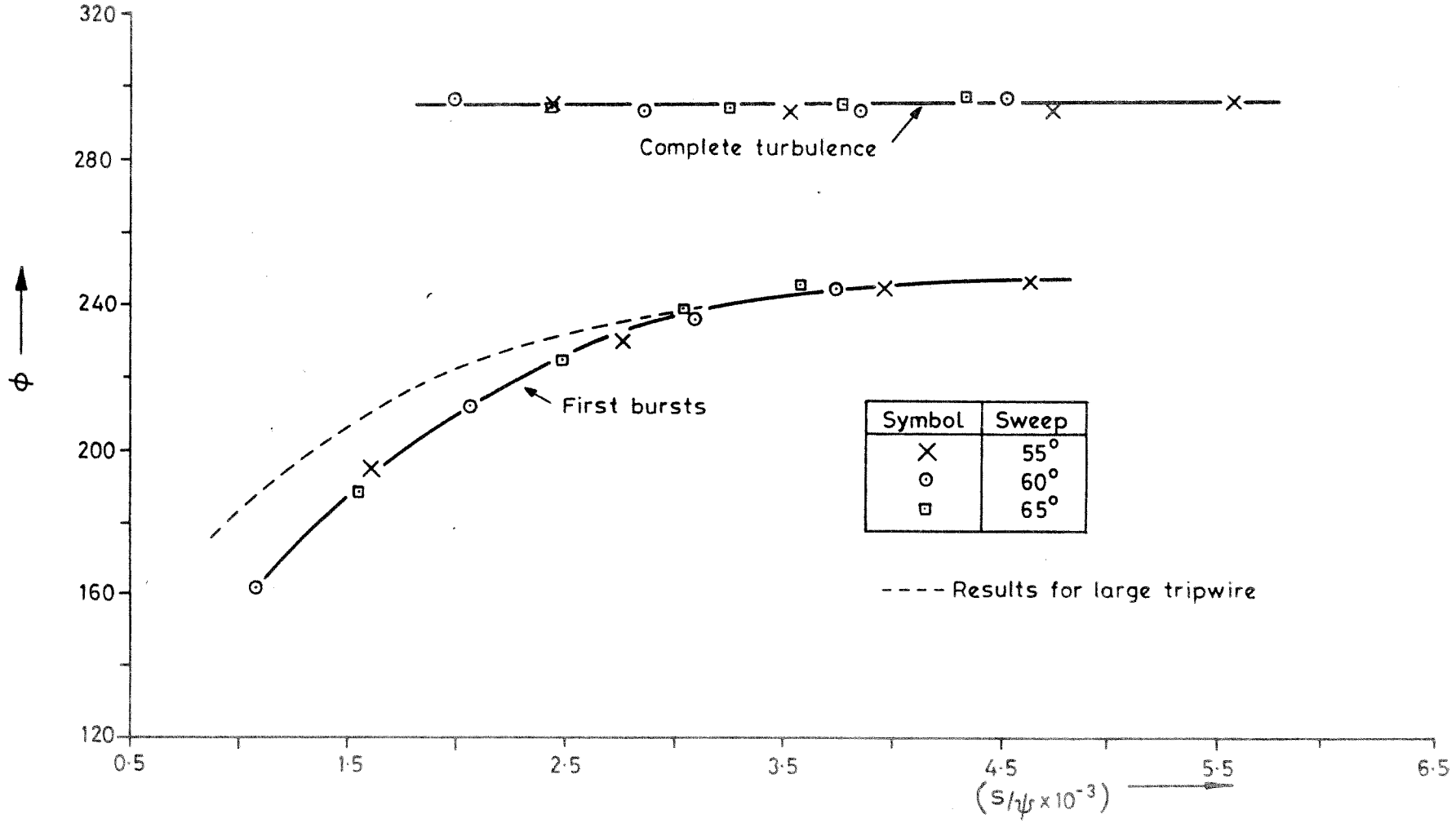

Fig. 21. Transition characteristics for contamination by a flat plate turbulent boundary layer.

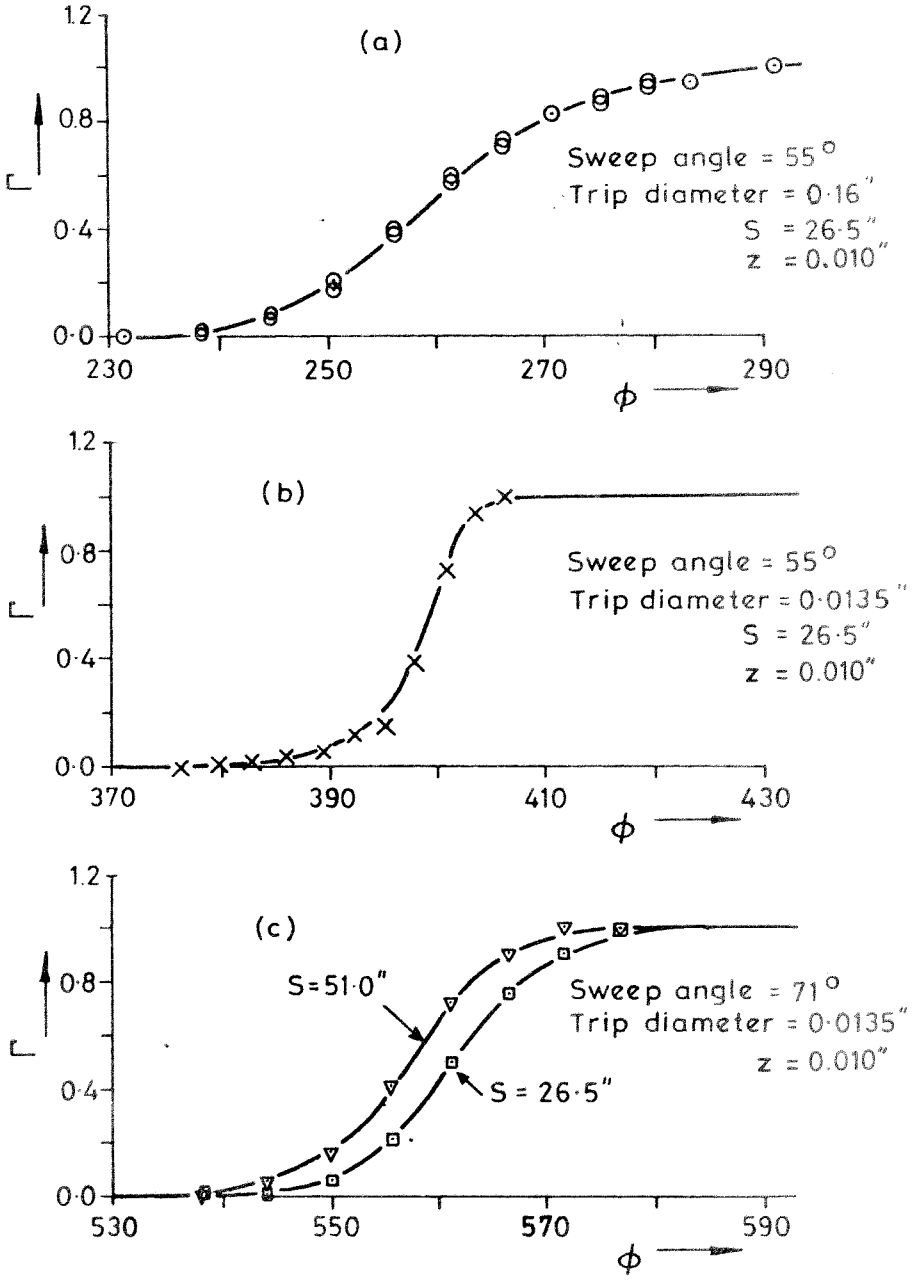

Fig. 22. Variation of intermittency factor with ϕ for several sweep angles, trip wire diameters and spanwise stations.

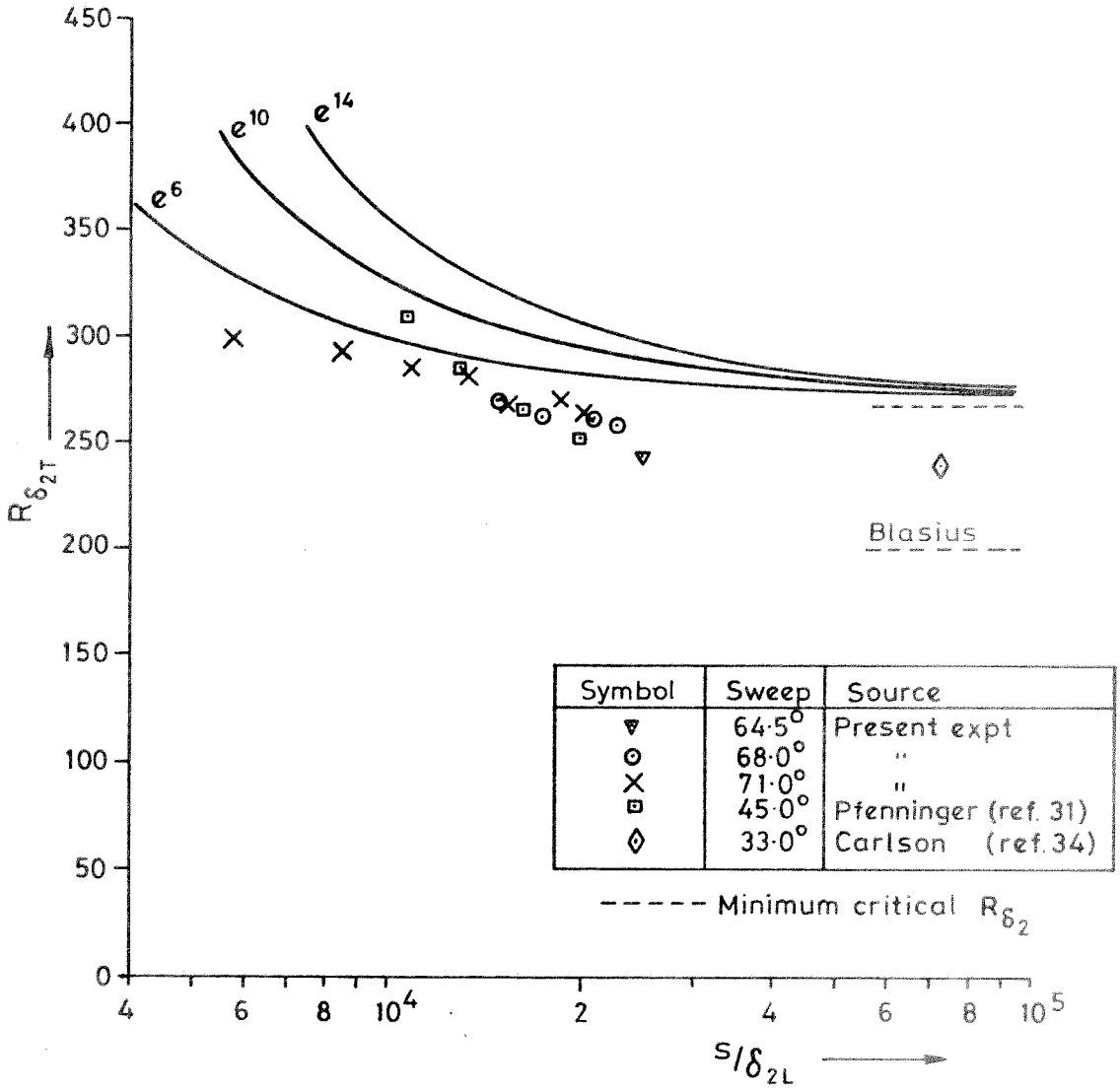

Fig. 23. A comparison between experimental 'free' transition results and a model based upon linear stability theory.

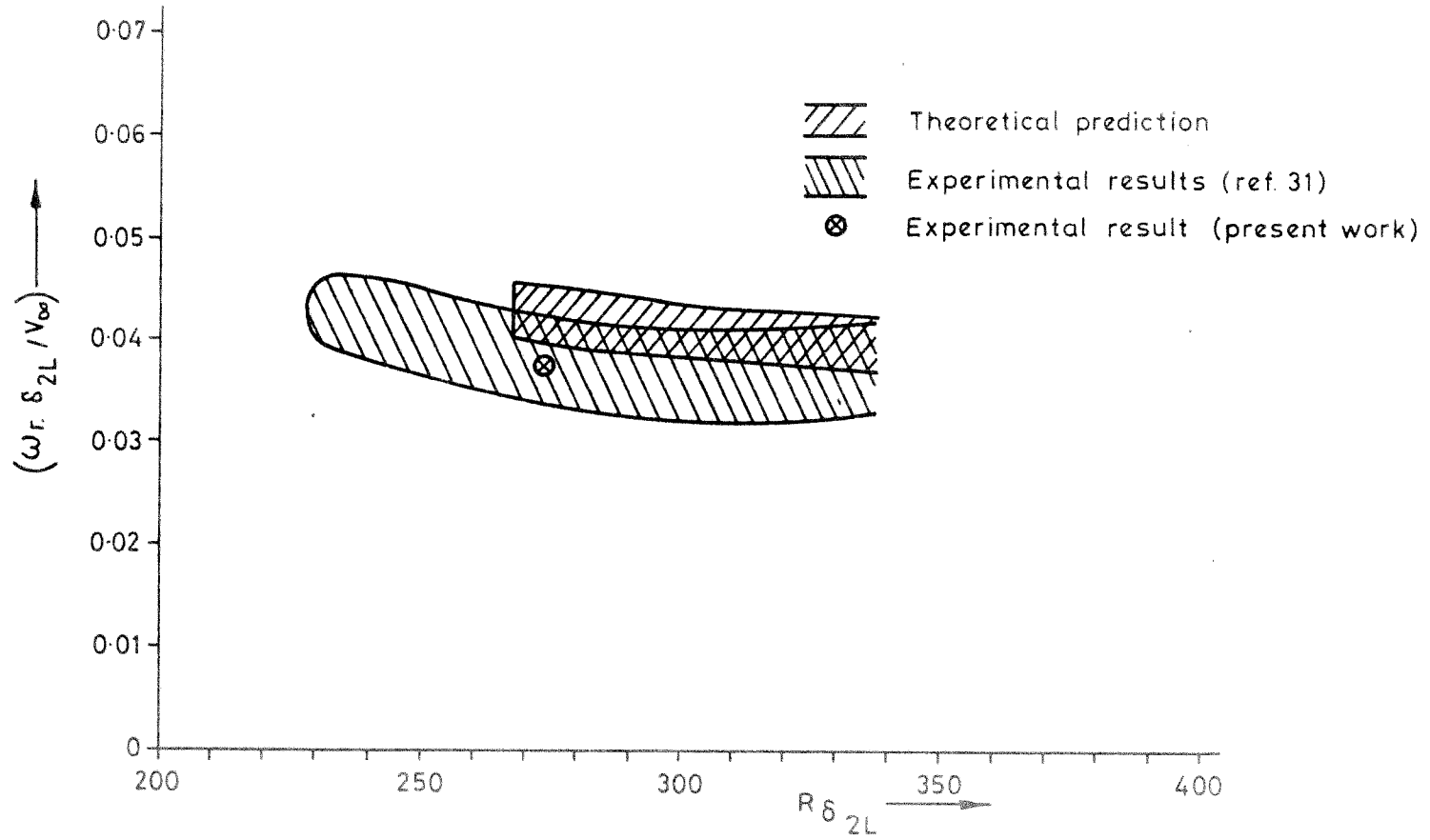

Fig. 24. A comparison between the observed disturbance frequencies and the theoretical predictions for the most unstable disturbance frequencies.

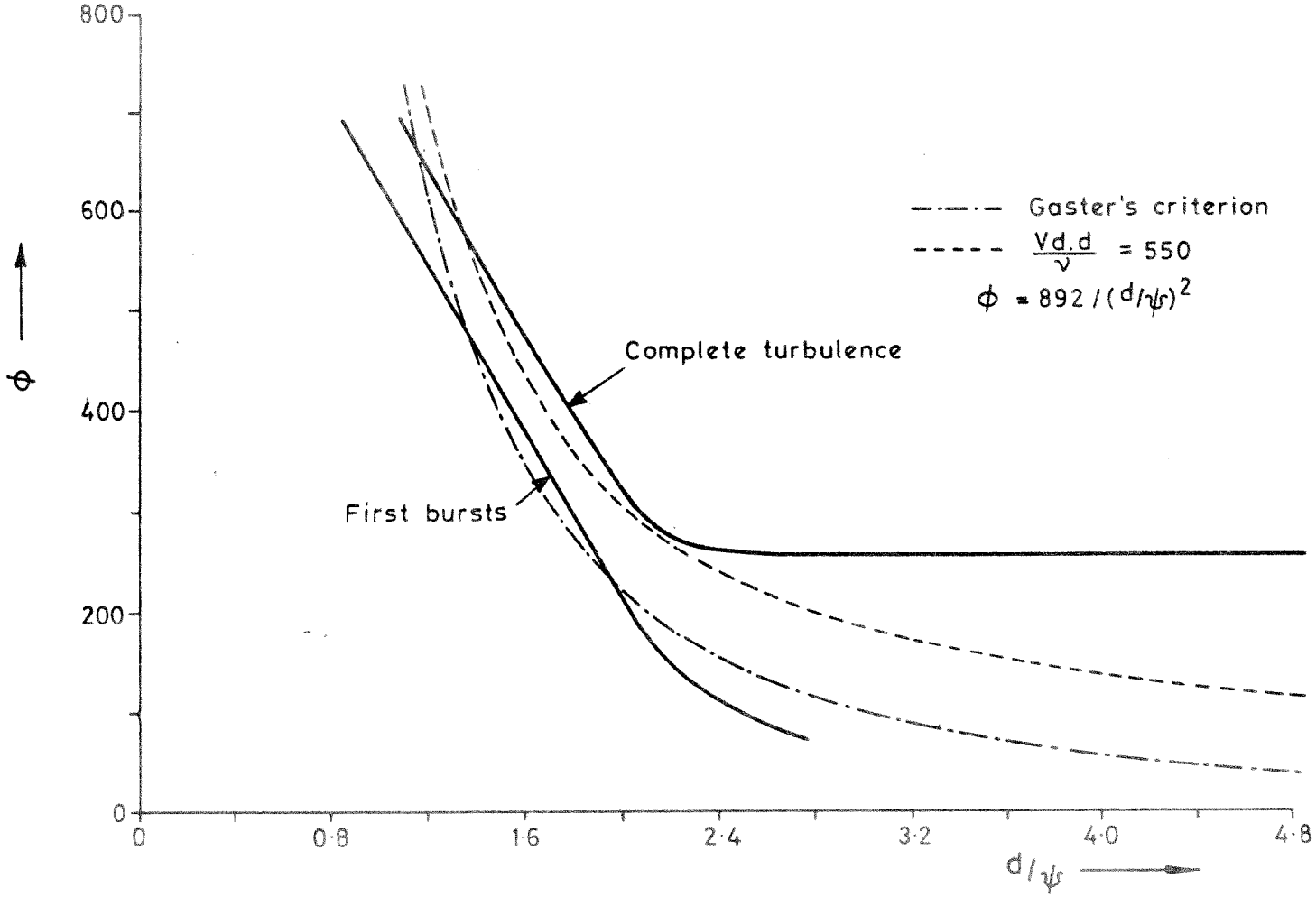

Fig. 25. Variation of ϕ crit. with d/ψ in the limit as s/ψ tends to zero.

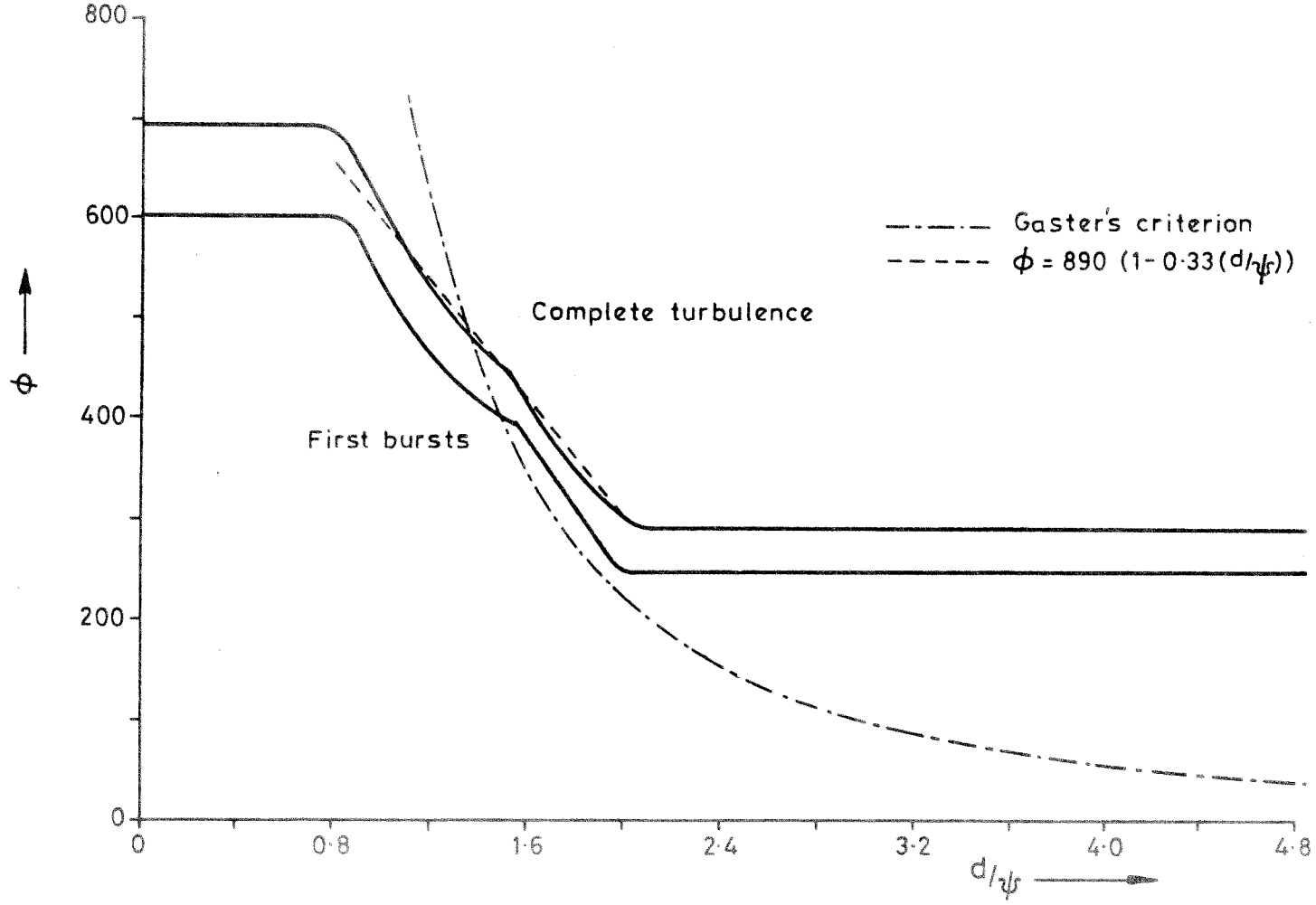

Fig. 26. Variation of ϕ crit. with d/ψ in the limit as s/ψ tends to infinity.

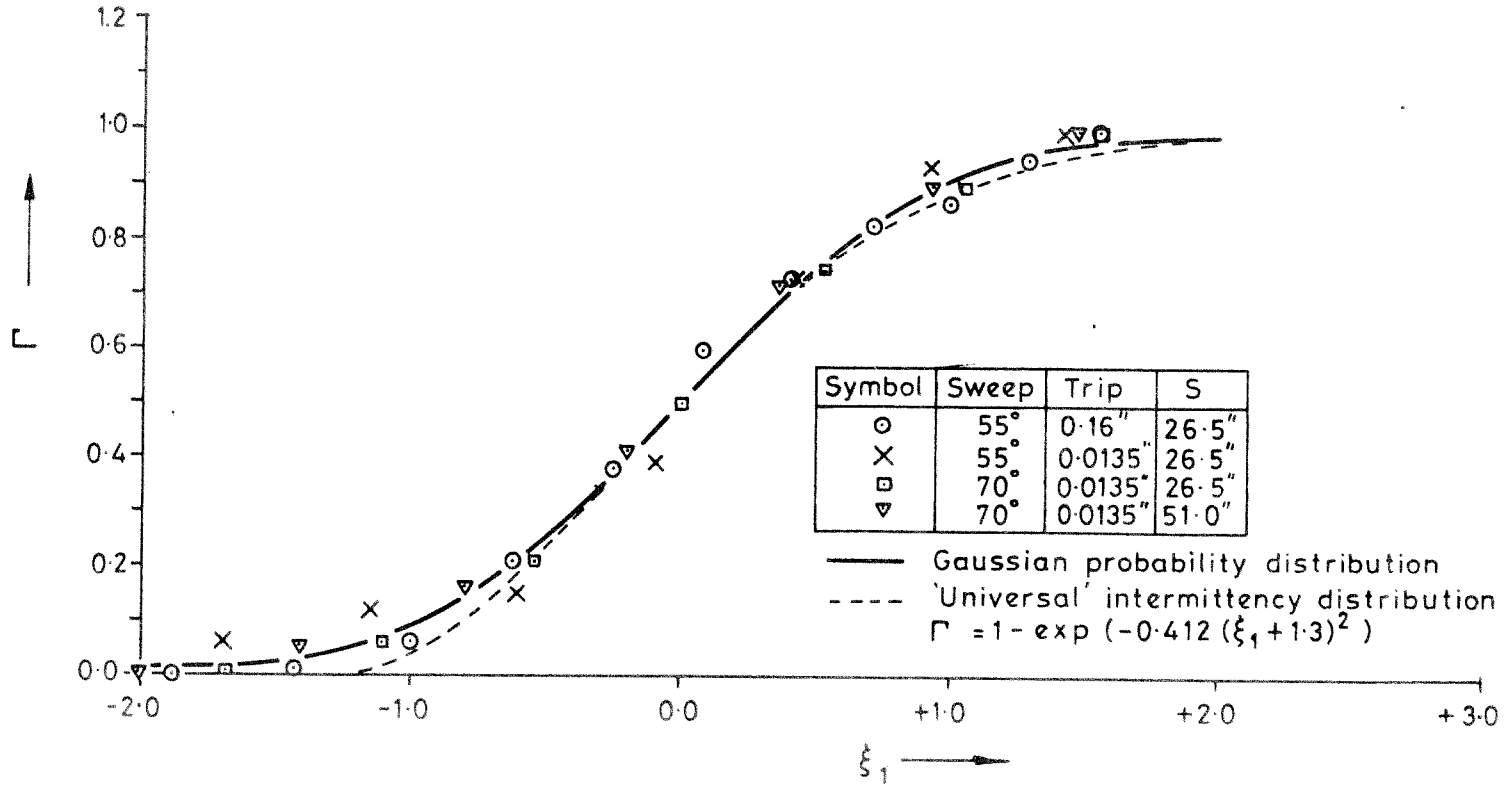

Fig. 27. The normalised low speed intermittency distribution.

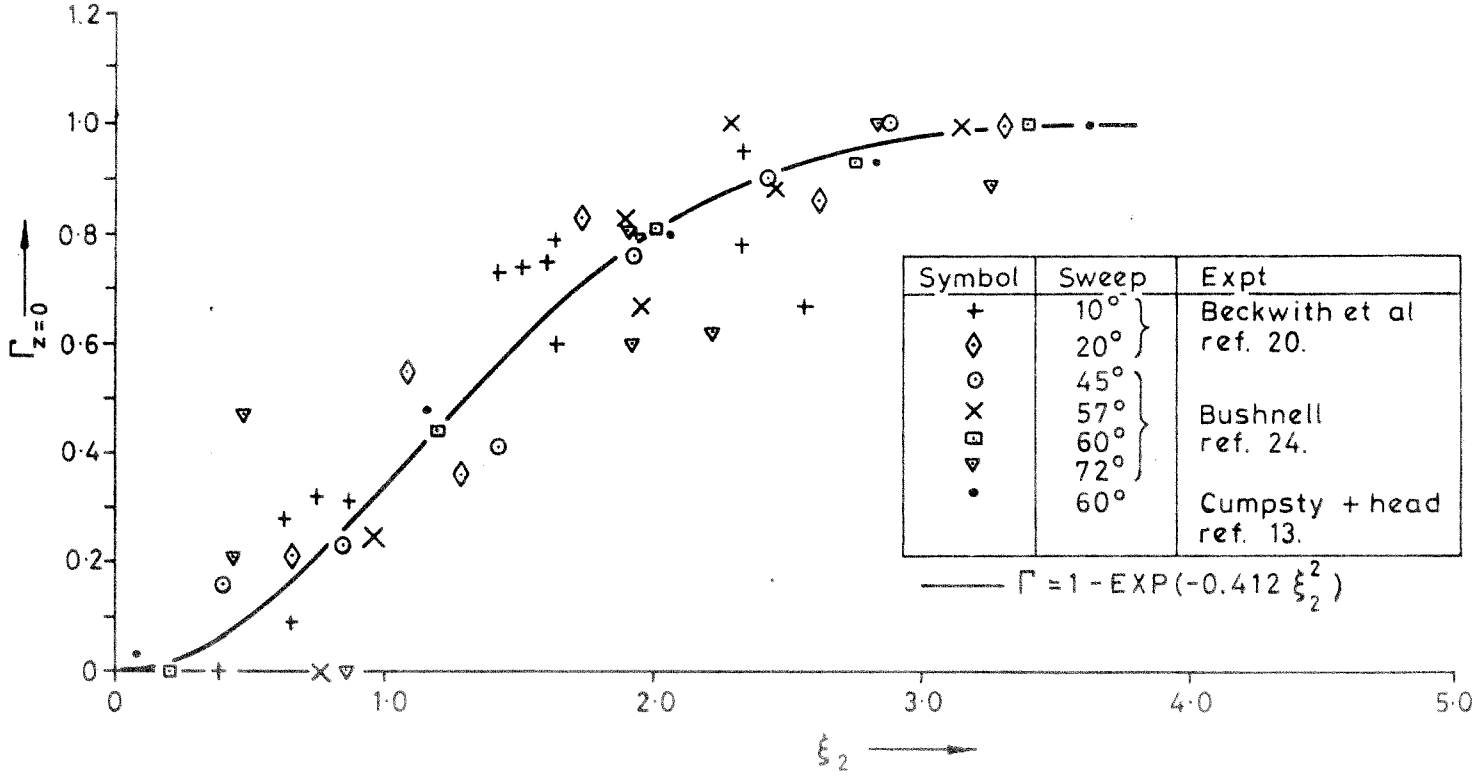

Fig. 28. A comparison between the intermittency results and the 'universal' intermittency distribution.

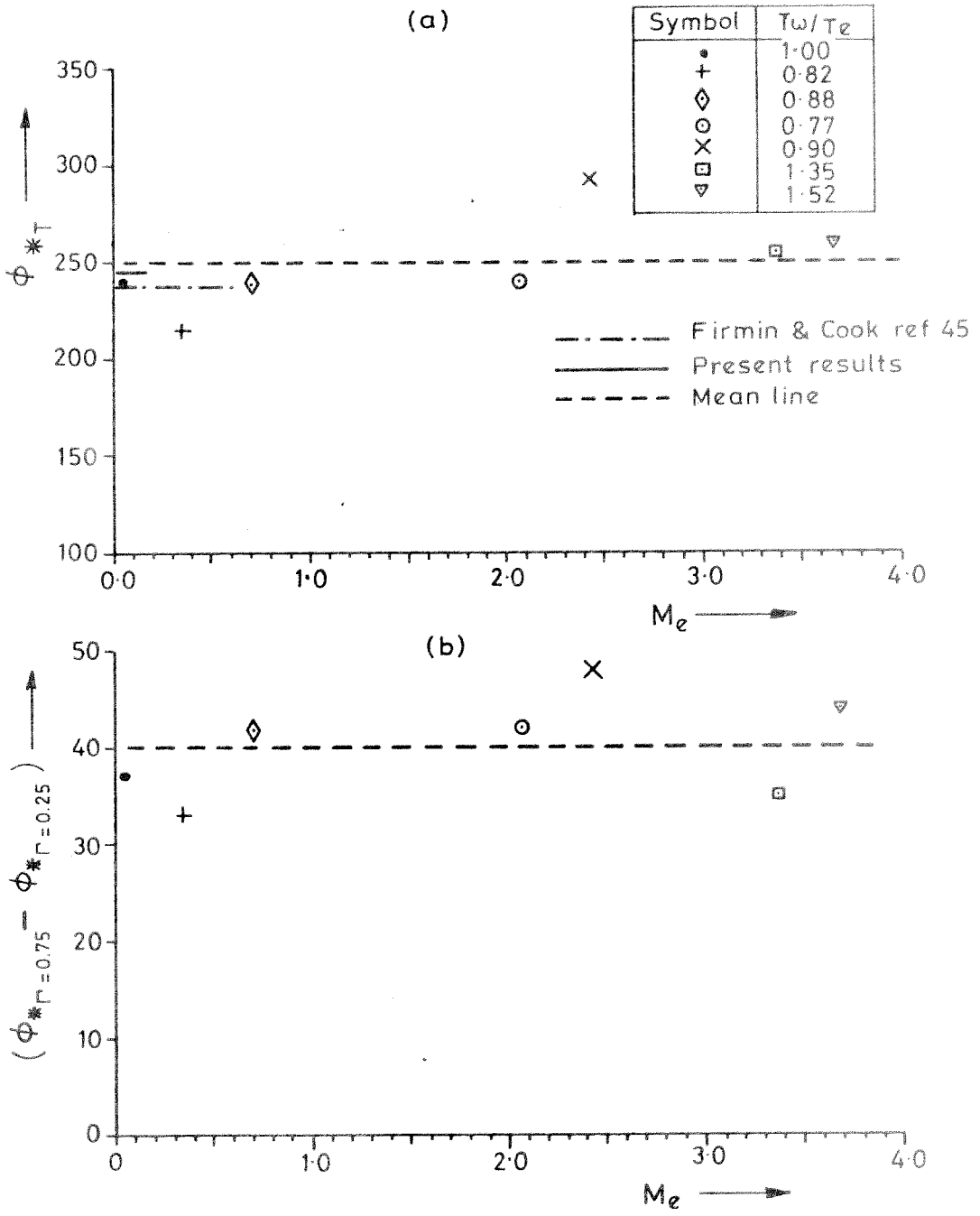

Fig. 29. The variation of the transition parameters with Me and Tw/Te.

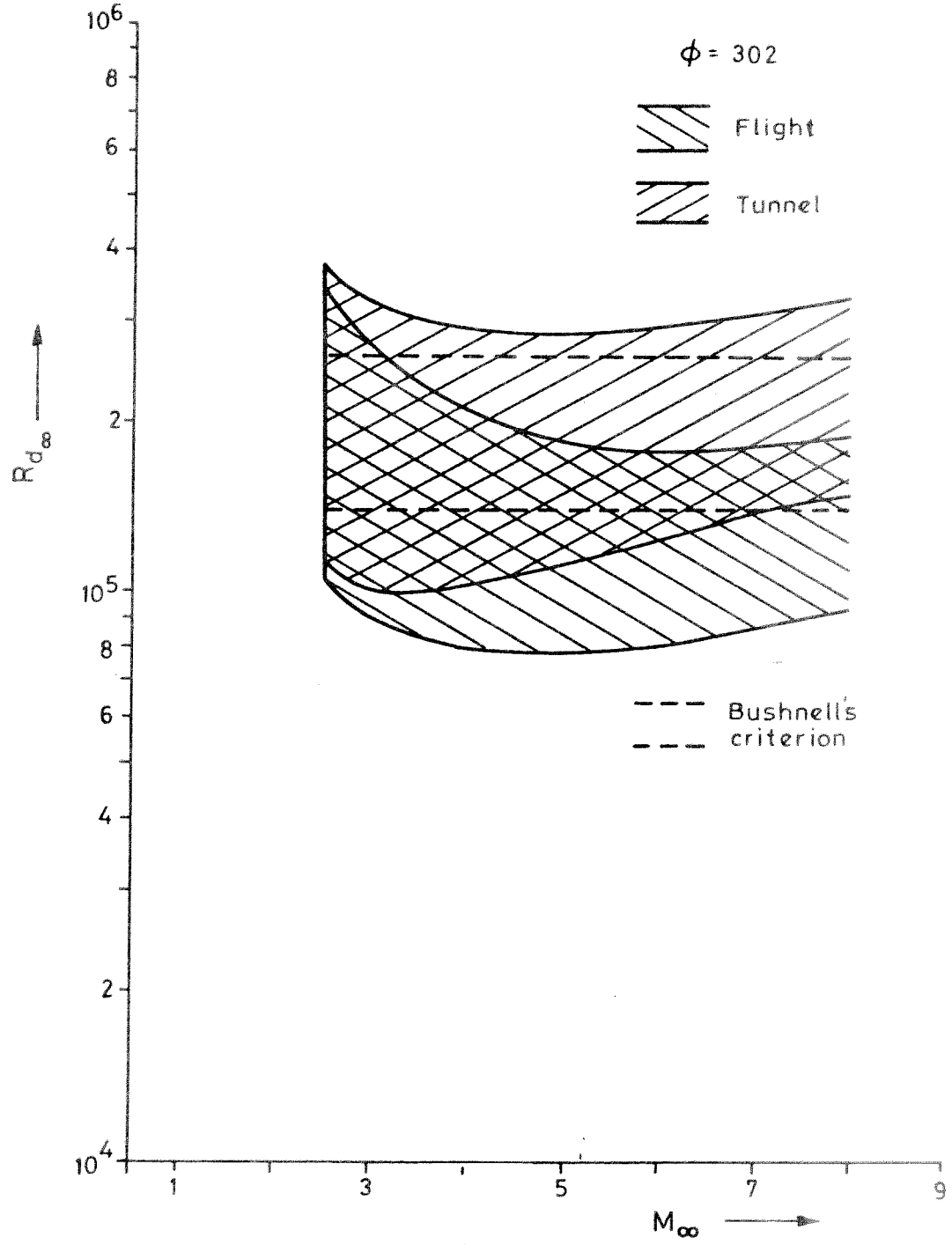

Fig. 30. Envelope of the mid-points of transition for leading edge sweep angles in the range 40° to 75° and a typical range of T_w / T_o

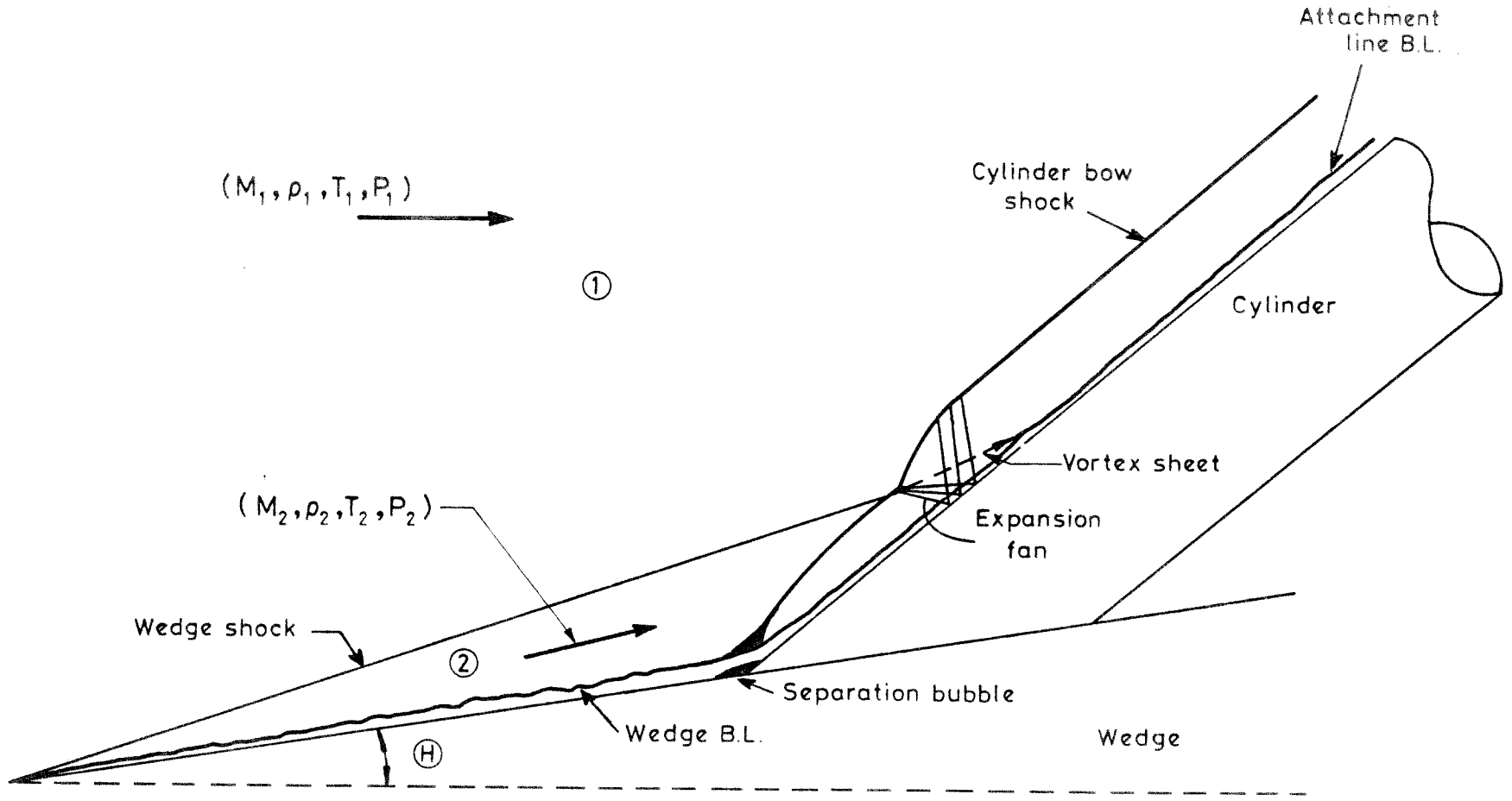

Fig. 31. Typical flow configuration for a wing/body junction at supersonic speeds.

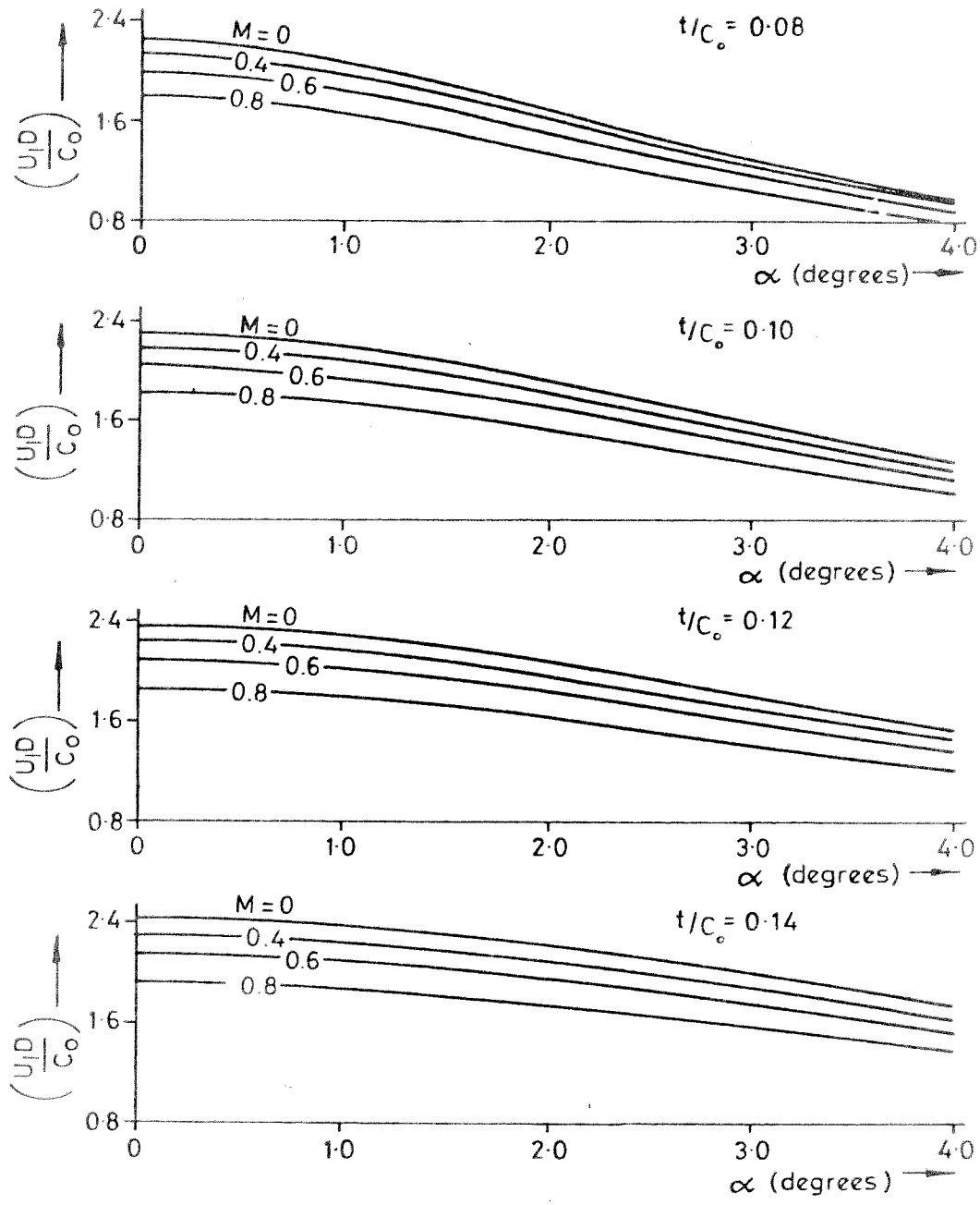

Fig. 32. Variation of (U_1D/C_o) with thickness/chord ratio, Mach number and incidence for an R.A.E. 101 aerofoil section.

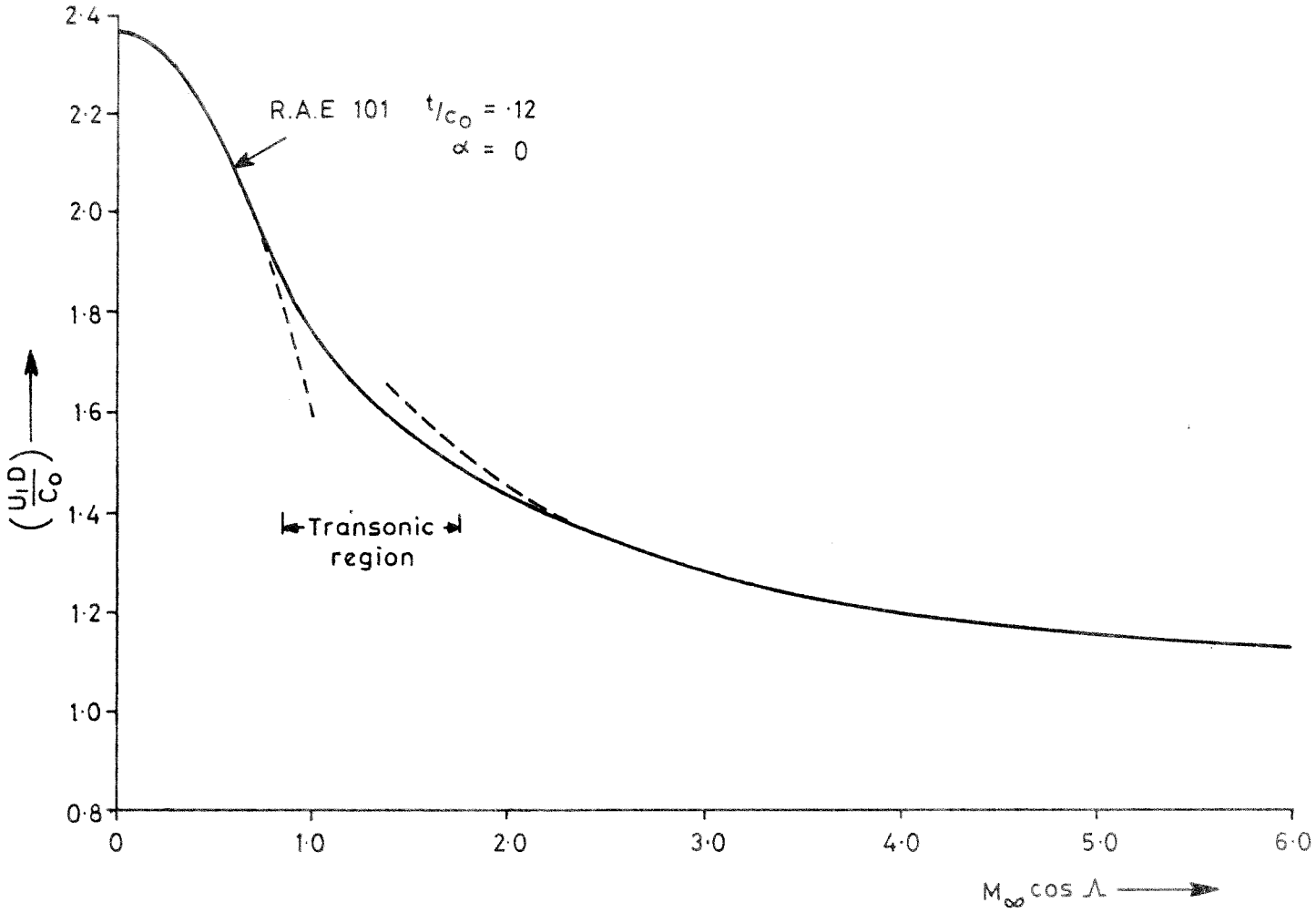

Fig. 33 Variation of $(U_1 D/C_o)$ with normal to leading edge Mach number for an R.A.E. 101 aerofoil with a thickness chord ratio of 0·12 at zero incidence.

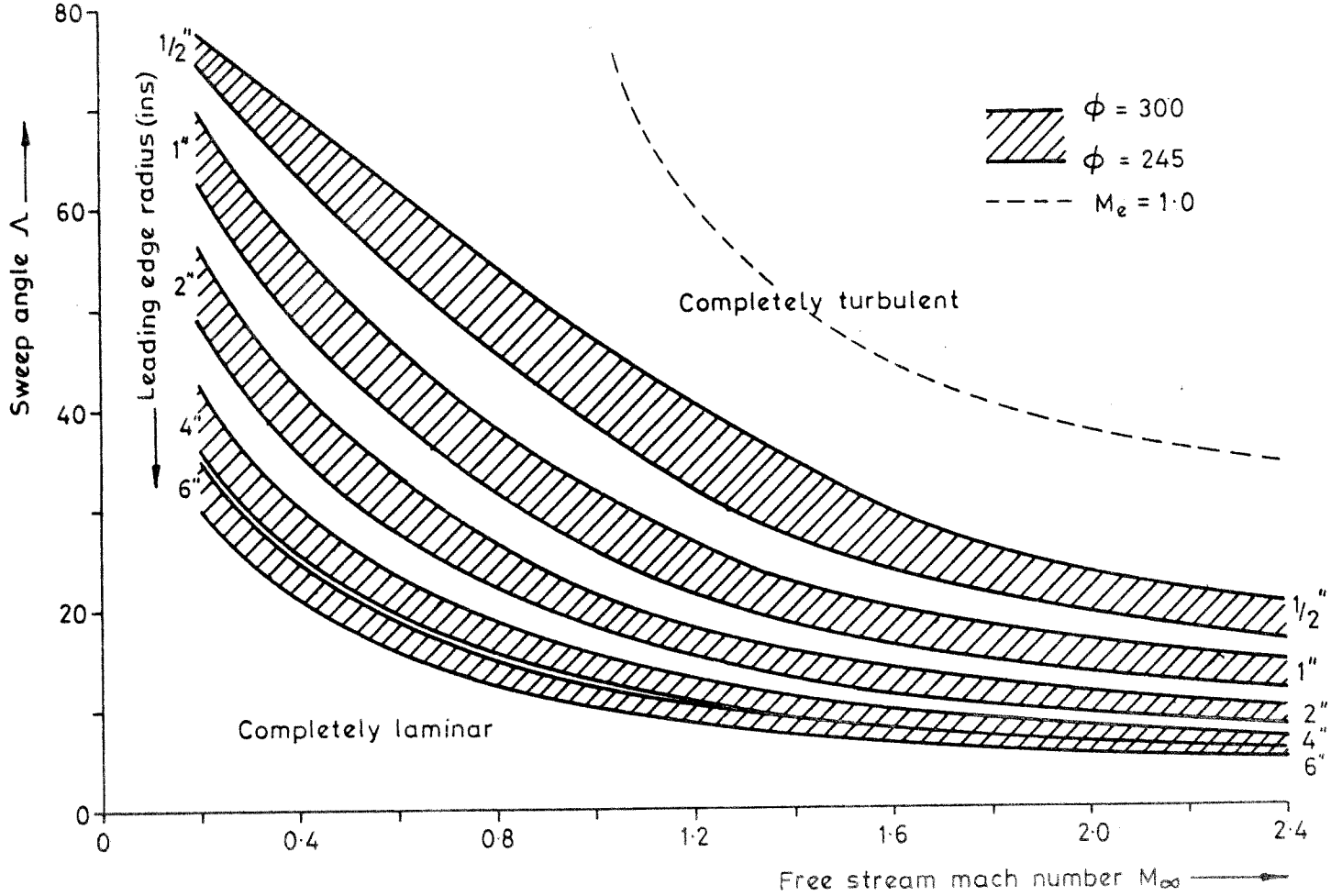

Fig. 34. Transition region boundaries for a 12% t/Co R.A.E. 101 section with gross leading edge contamination and zero heat transfer under 35000′ I.S.A. conditions.

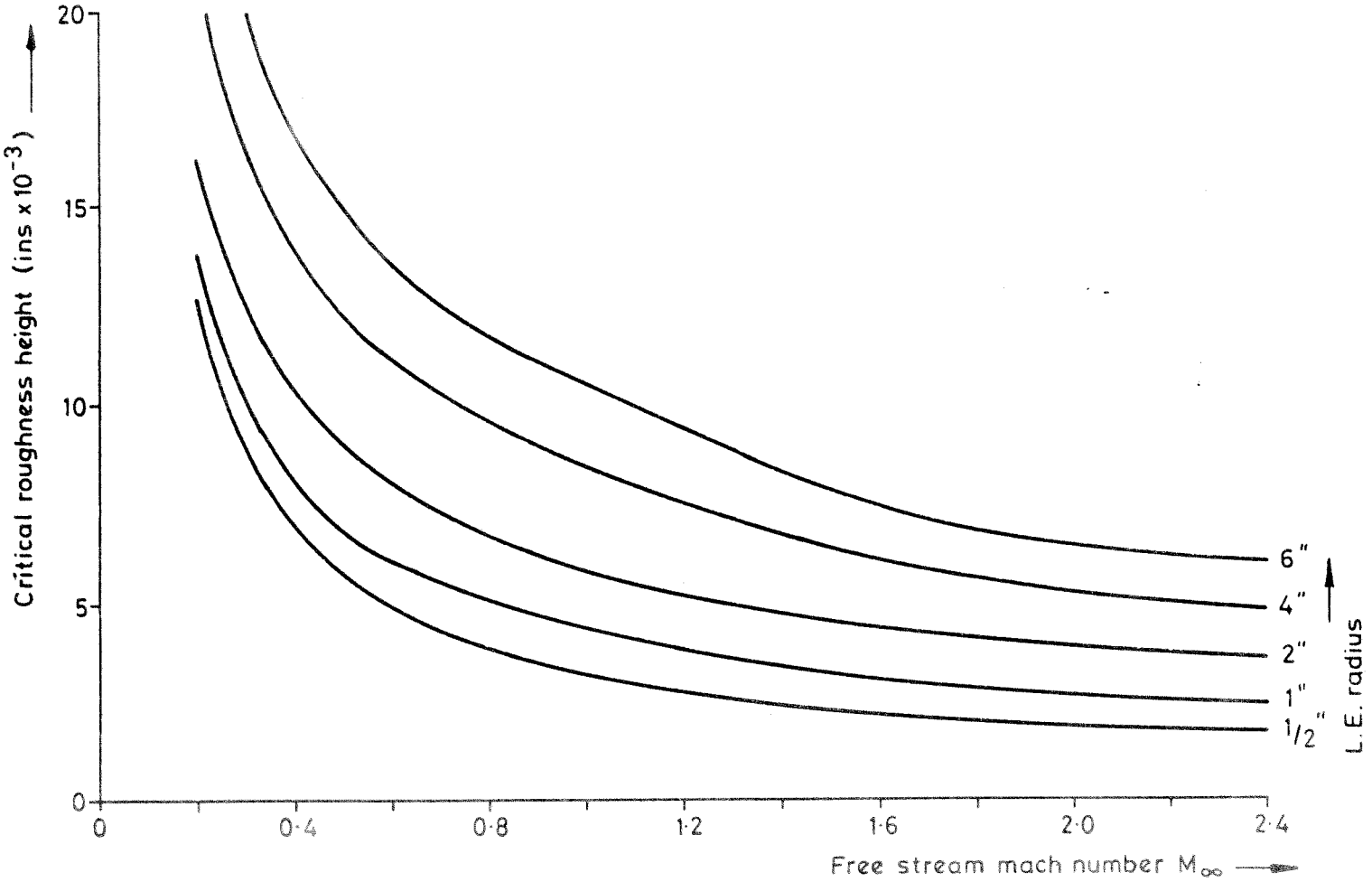

Fig. 35. The minimum trip wire diameter which will induce transition at ϕ = 245 on a 12% $^{t}/_{C_o}$ R.A.E. 101 section with zero heat transfer rate under 35000′ I.S.A. conditions.

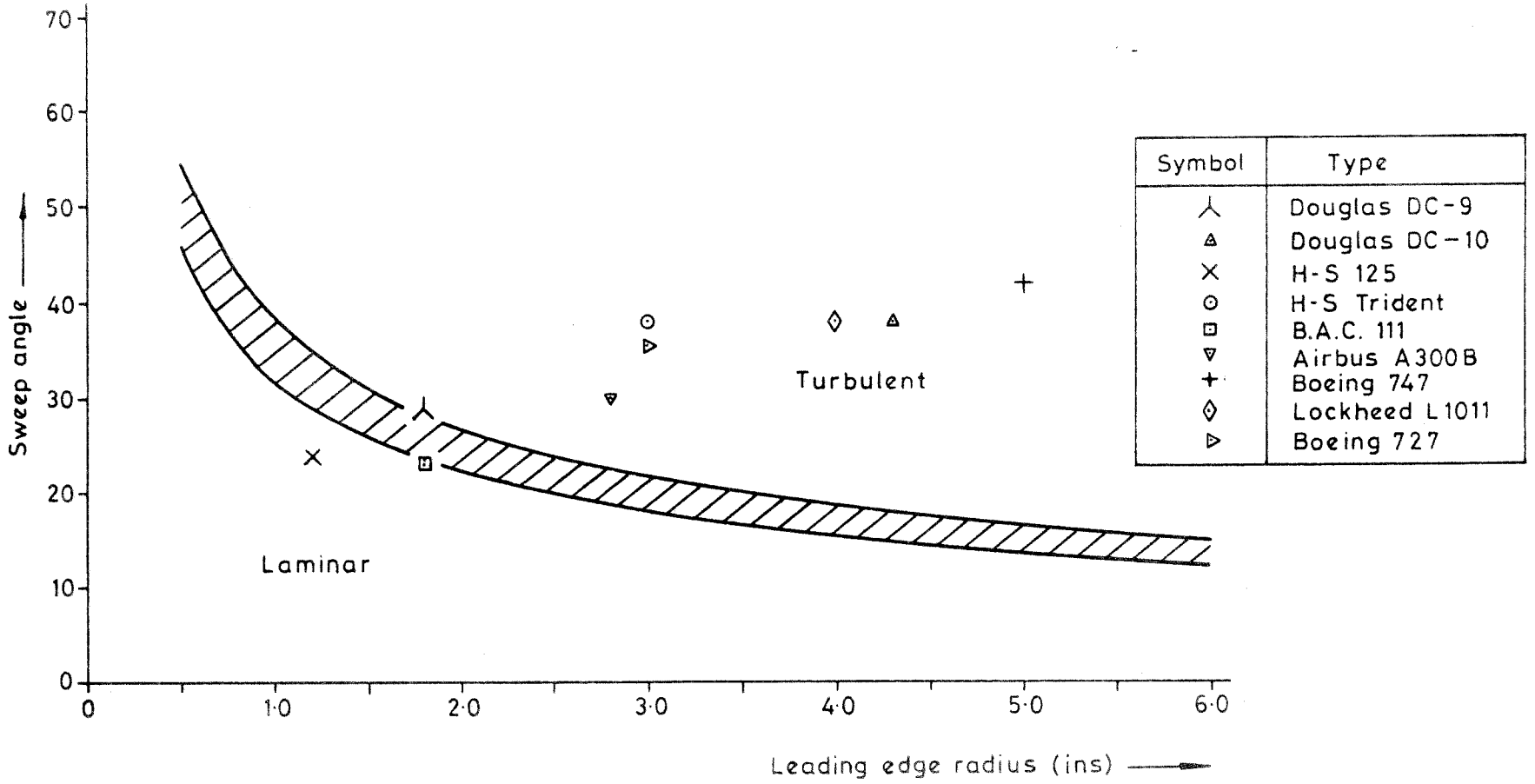

Fig. 36. The variation of sweep angle for attachment line transition with leading edge radius for gross contamination, zero heat transfer, a free stream Mach number of 0.8 and an altitude of 35000′ I.S.A.

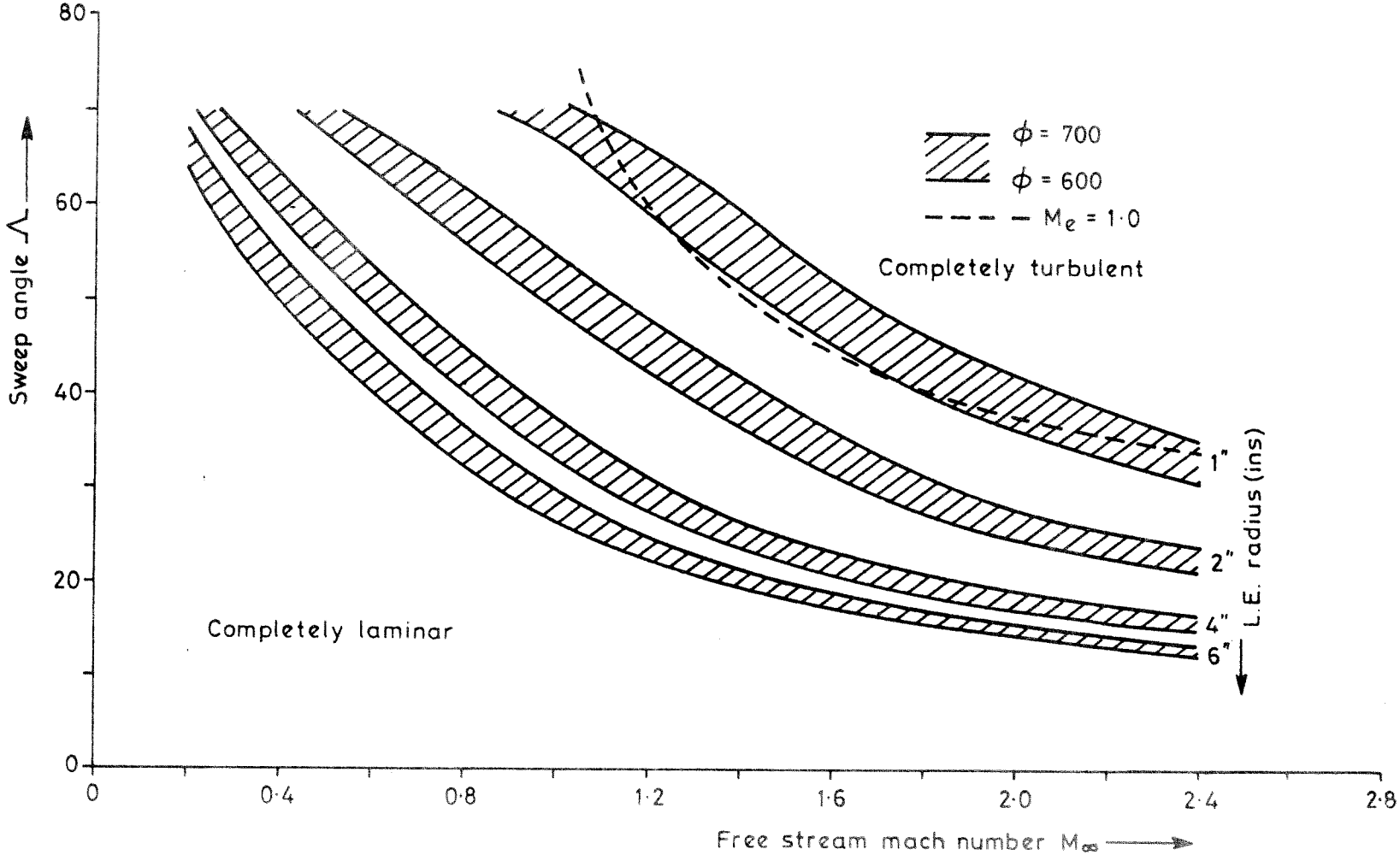

Fig. 37. Transition region boundaries for a 12% $^{t}/_{C_o}$ R.A.E. 101 section with a smooth leading edge and zero heat transfer rate under 35,000′ ISA conditions.

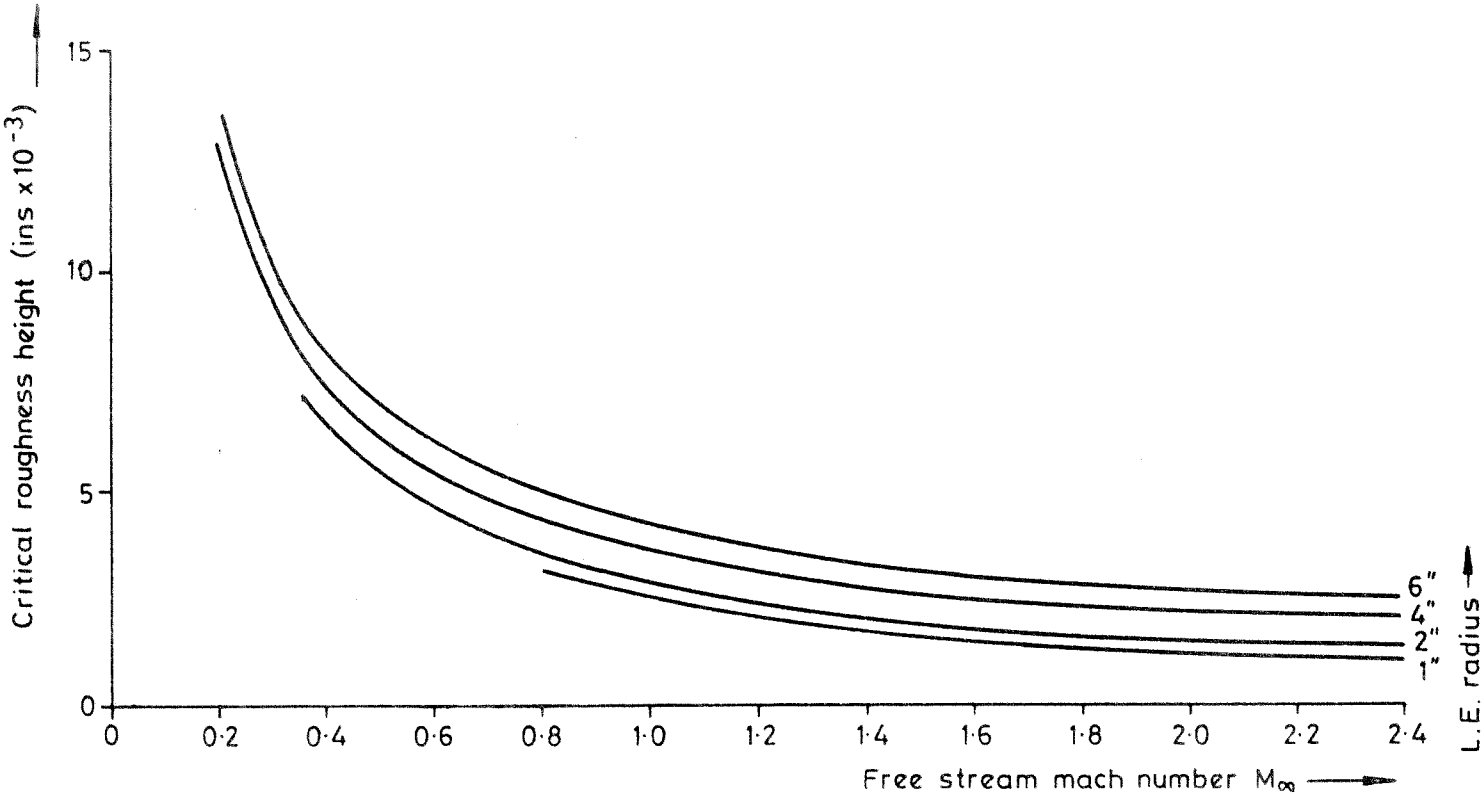

Fig. 38. The maximum trip wire diameter which will not affect 'natural' transition on a 12% t/C_o R.A.E. 101 section with zero heat transfer rate under 35,000′ ISA conditions.

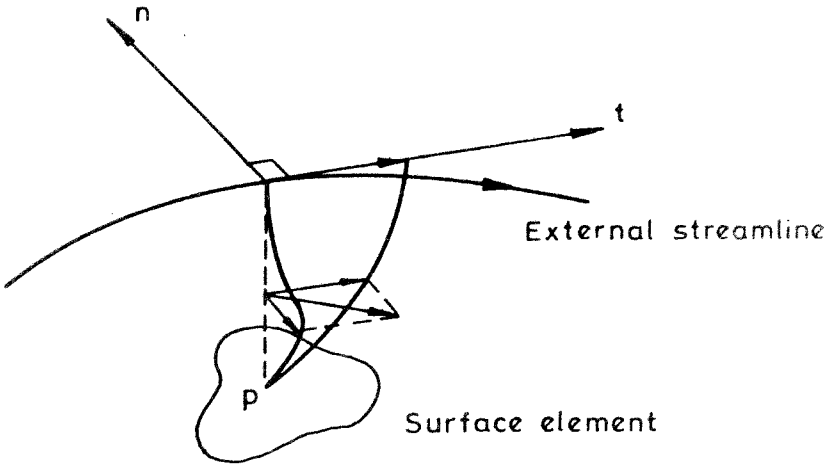

Fig. 39. Typical velocity profile for a 3-D boundary layer flow.

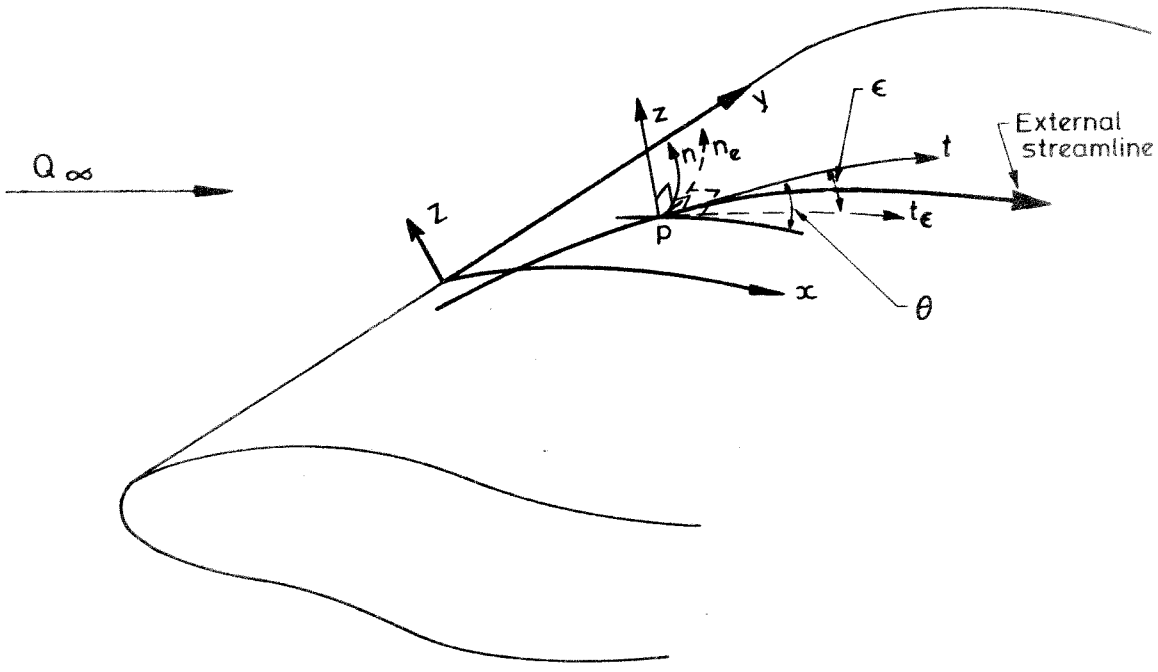

Fig. 40. A coordinate system suitable for 3-D boundary layer flows.

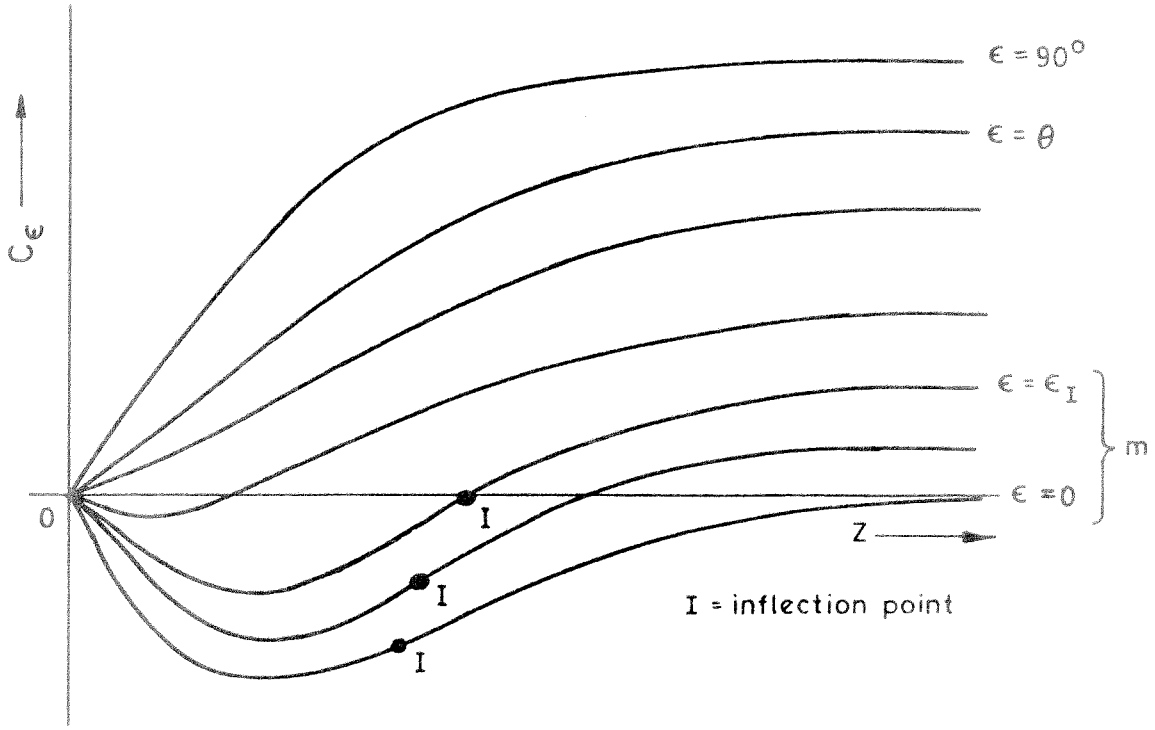

Fig. 41. Variation of velocity profiles with changing coordinate system.

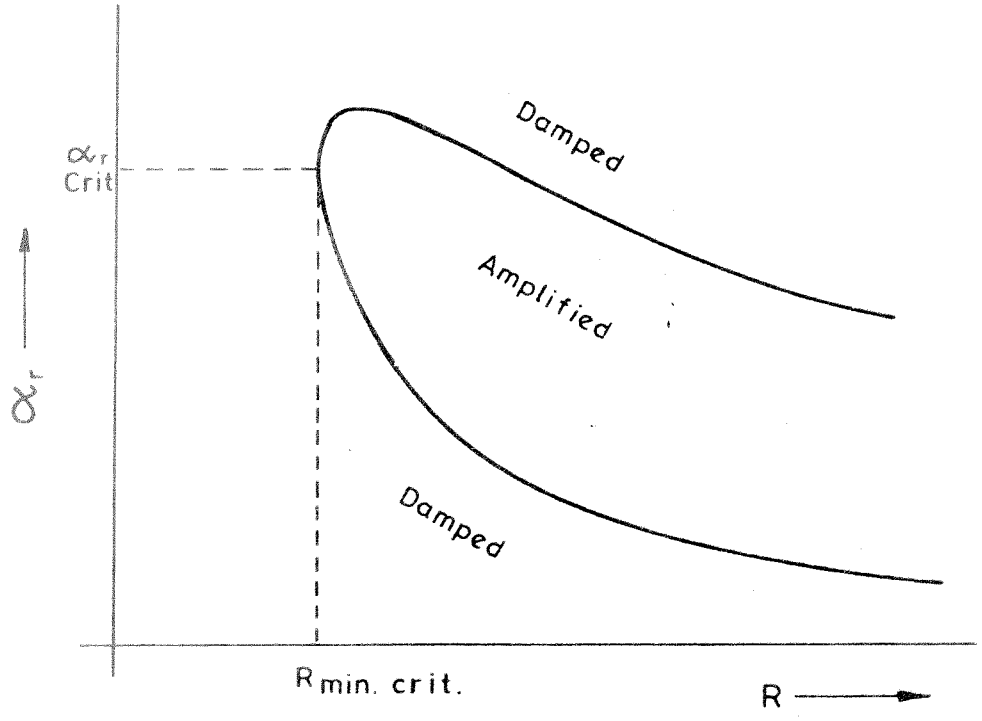

Fig. 42. Typical format for stability results.

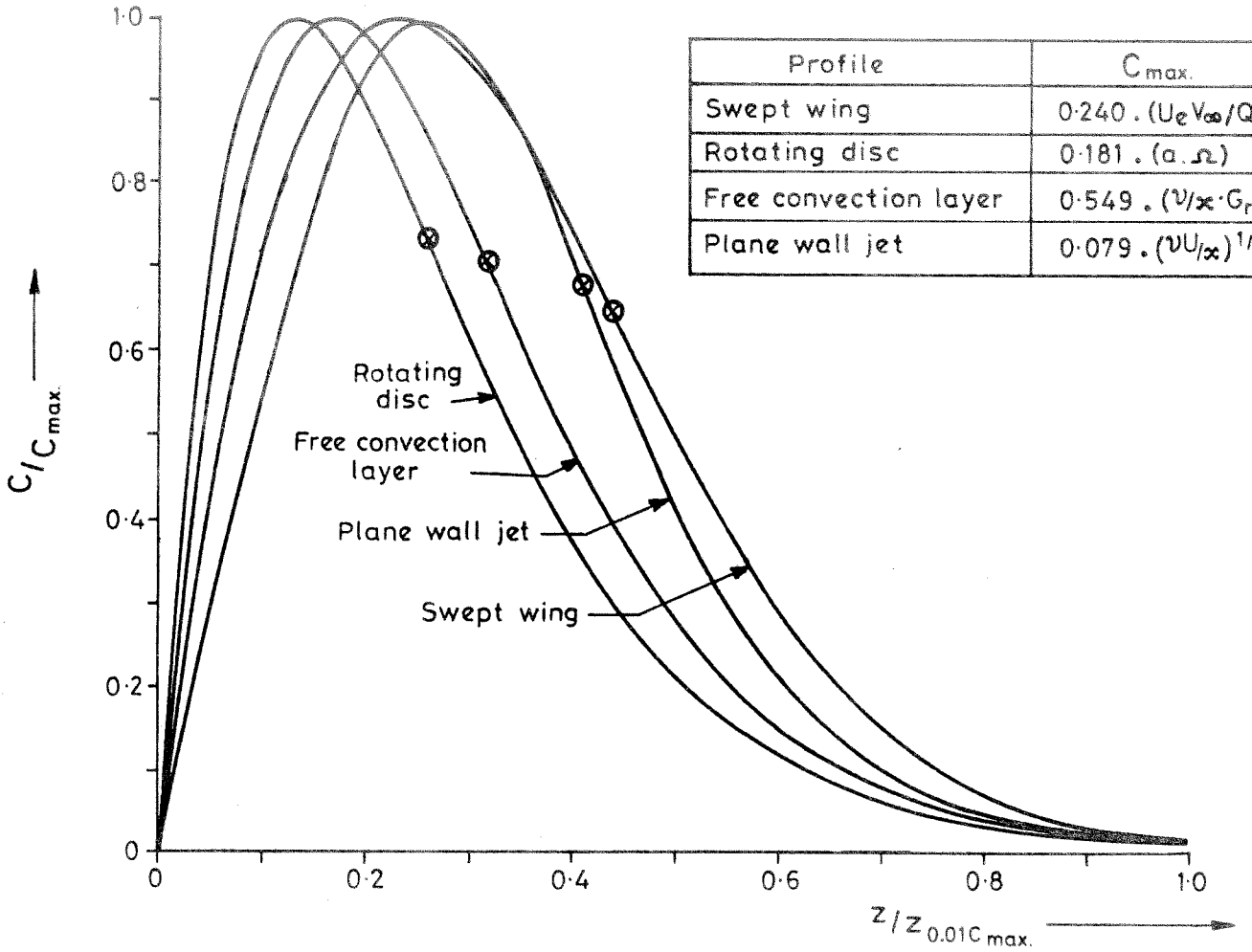

Profile	$C_{max.}$	$z_{0.01C\,max}$
Swept wing	$0{\cdot}240\,.\,(U_e V_\infty/Qe)$	$3{\cdot}490\,.\,(\nu x/U_e)^{1/2}$
Rotating disc	$0{\cdot}181\,.\,(a\,.\,\Omega)$	$7{\cdot}000\,.\,(\nu/\Omega)^{1/2}$
Free convection layer	$0{\cdot}549\,.\,(\nu/x\cdot G_{r_x}^{1/2})$	$5{\cdot}730\,.\,x\,.\,(4/Gr_x)^{1/4}$
Plane wall jet	$0{\cdot}079\,.\,(\nu U/x)^{1/2}$	$31{\cdot}620\,.\,(\nu x^3/U)^{1/4}$

Fig. 43. The cross flow velocity profile for the swept wing and the rotating disc flows plus the 2-D free convection velocity profile and the plane wall jet.

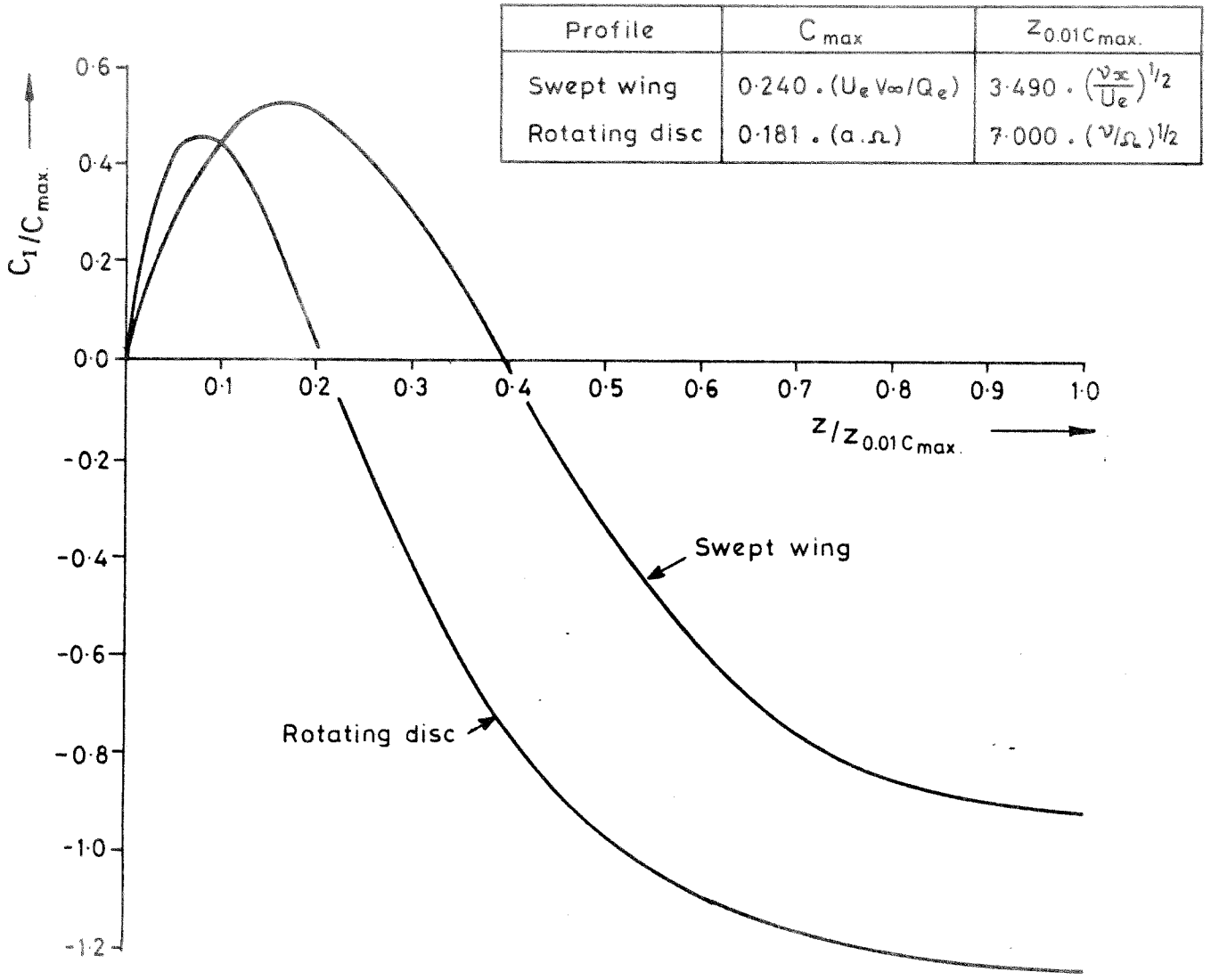

Fig. 44. The critical velocity profiles for the swept wing and rotating disc flows.

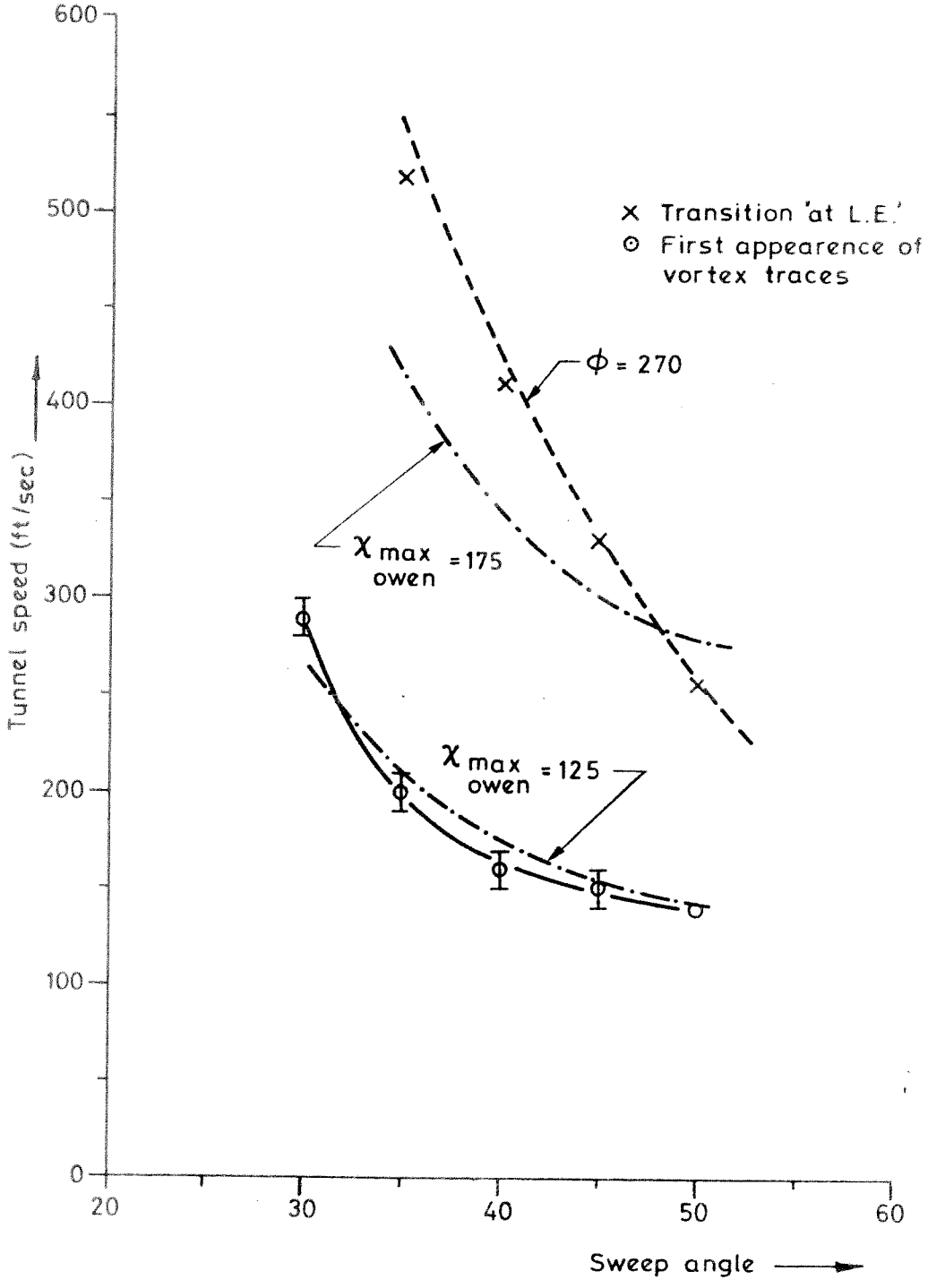

Fig. 45. The Anscombe and Illingworth experimental results.

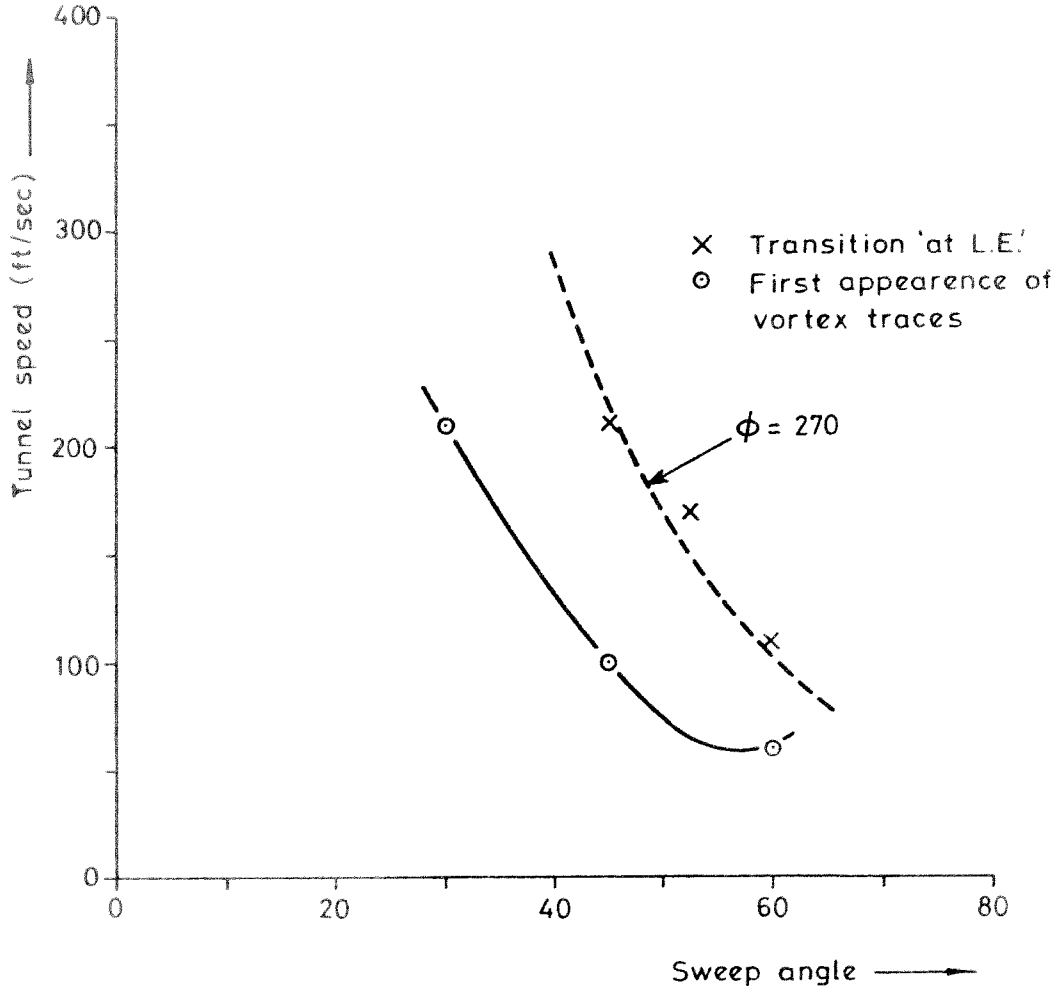

Fig. 46. The Gregory and Walker experimental results.

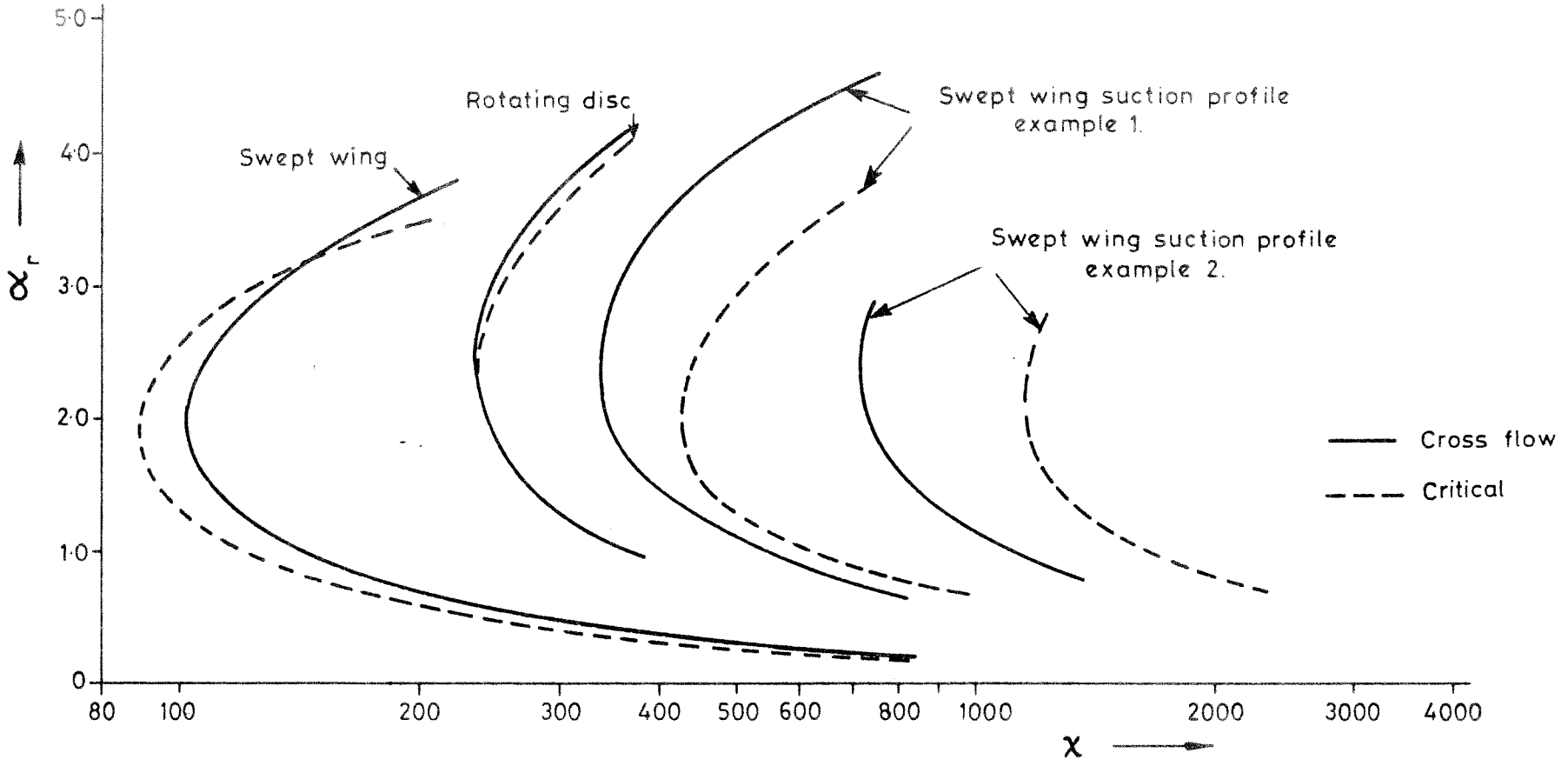

Fig. 47. The neutral curves for several three-dimensional velocity profiles.

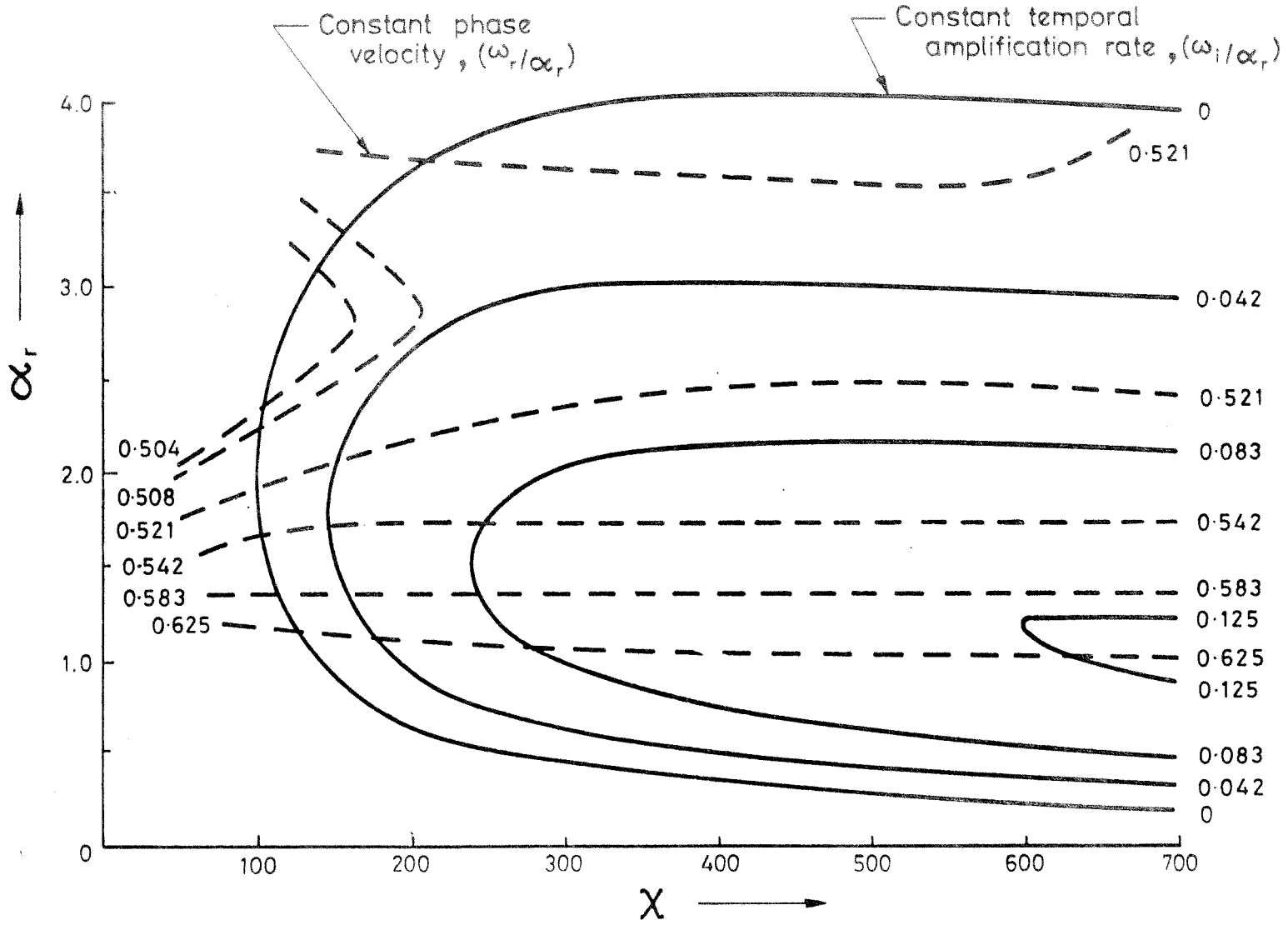

Fig. 48. The theoretical stability characteristics for the swept wing cross flow profile.

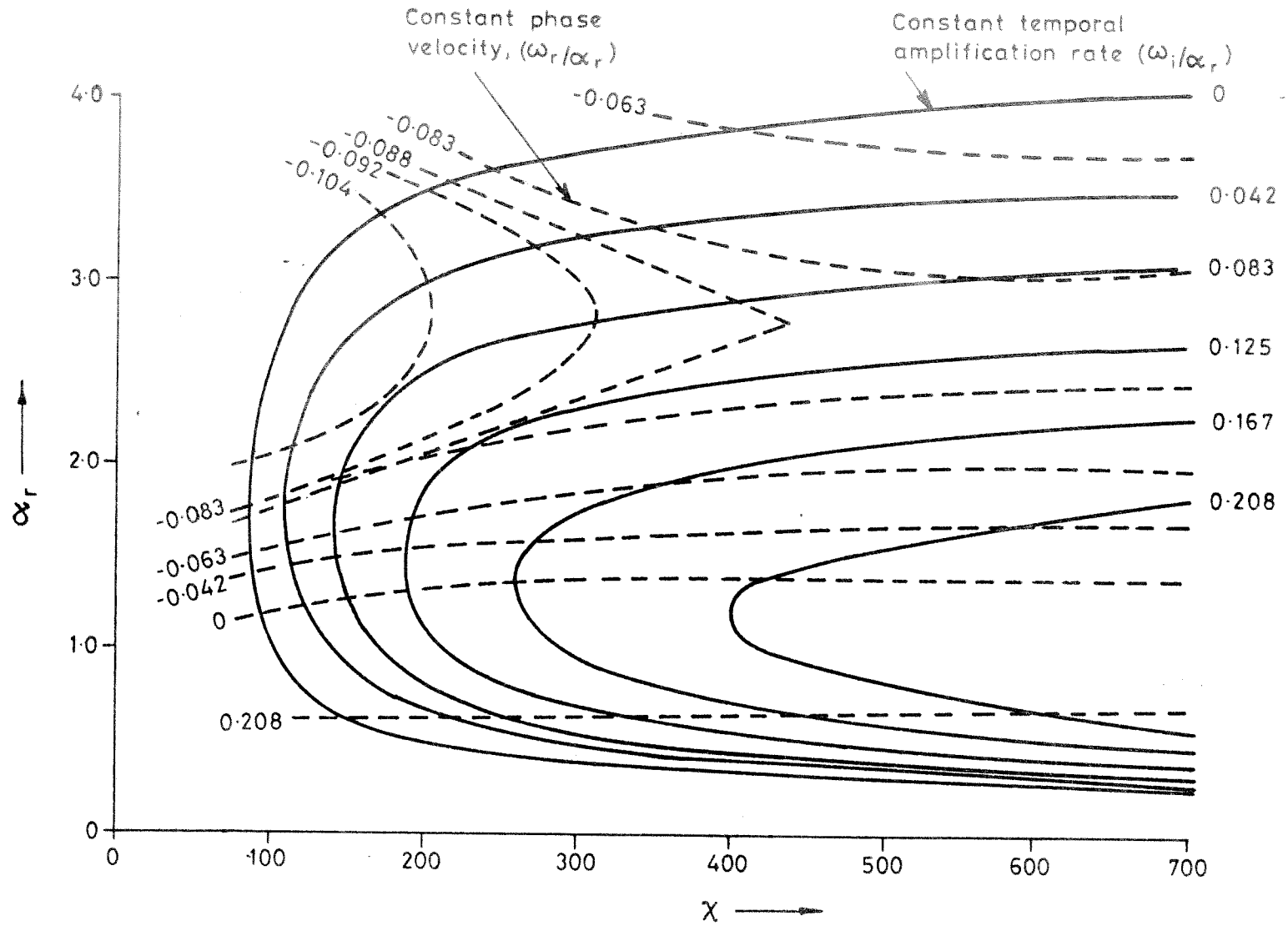

Fig. 49. The theoretical stability characteristics for the swept wing critical profile.

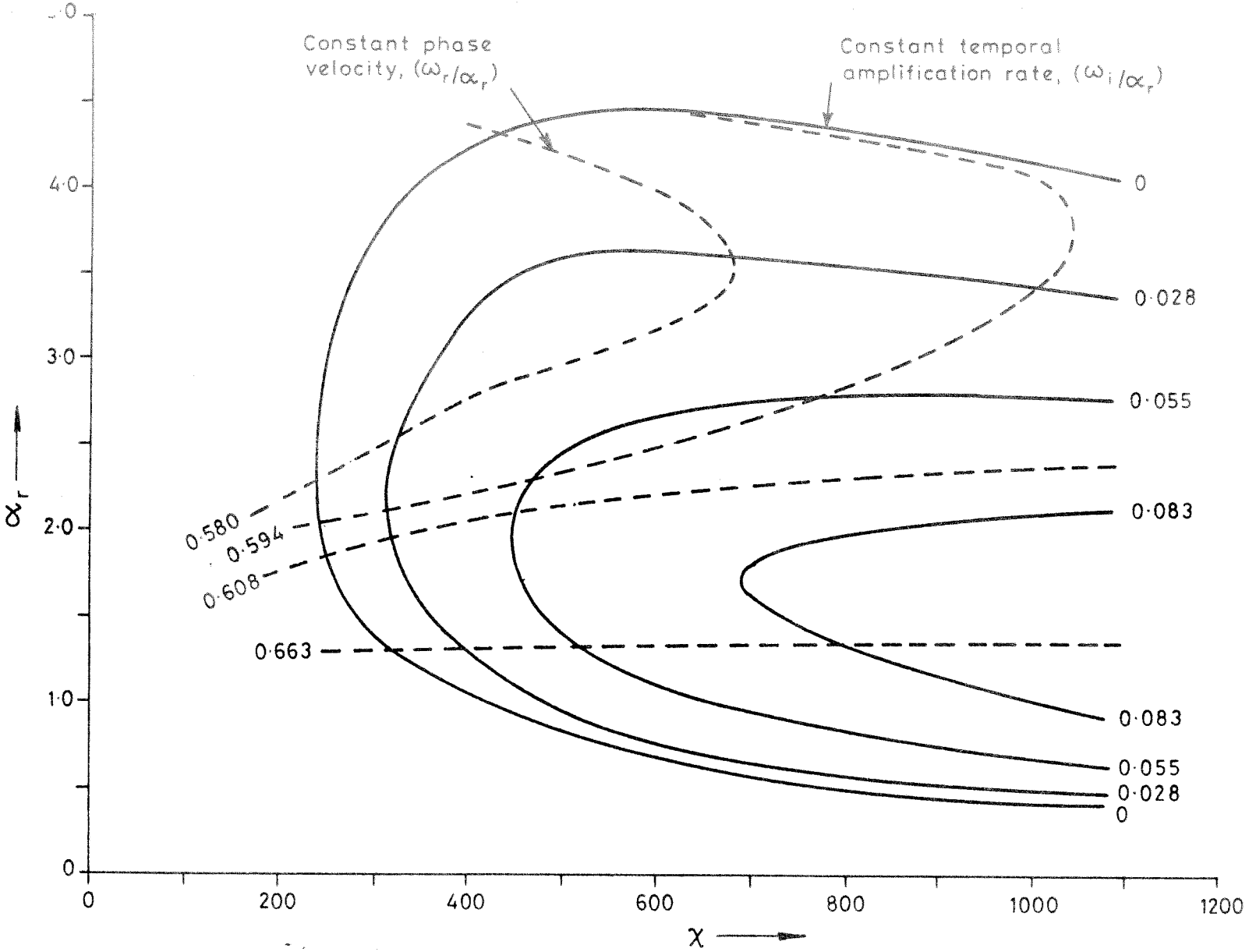

Fig. 50. The theoretical stability characteristics for the rotating disc cross flow profiles.

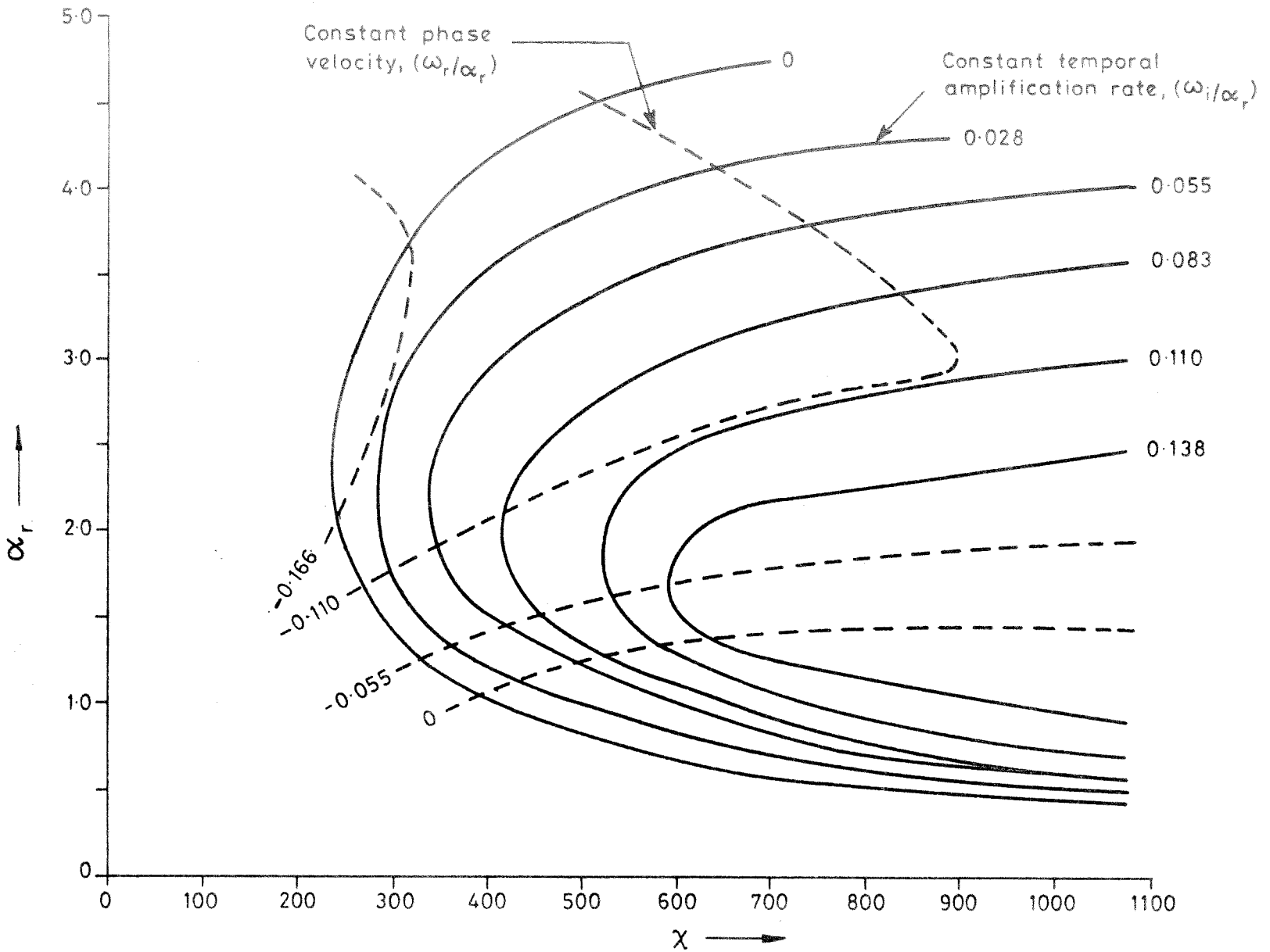

Fig. 51. The theoretical stability characteristics for the rotating disc critical profile.

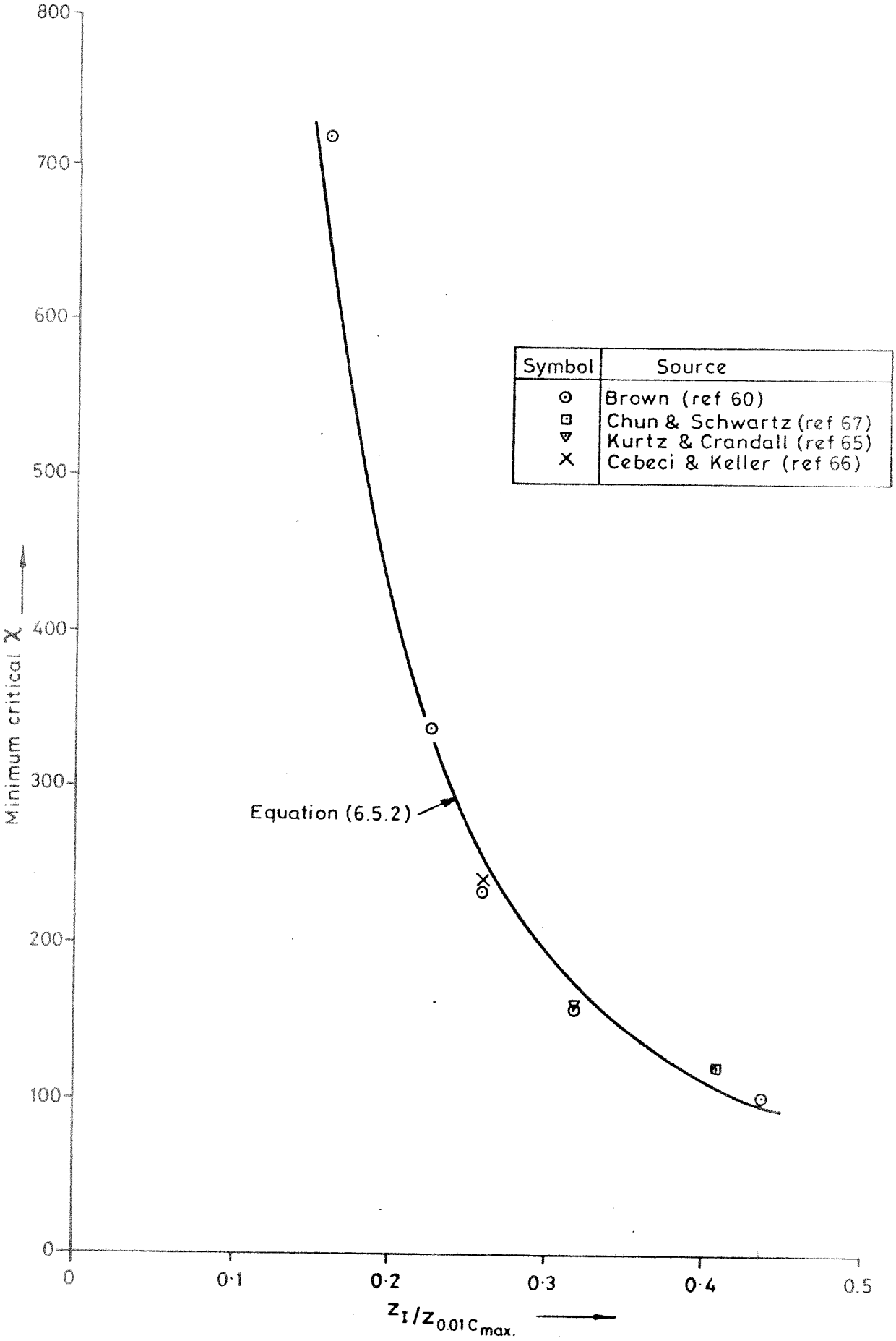

Fig. 52. Variation of χ crit. with the position of the inflection point.

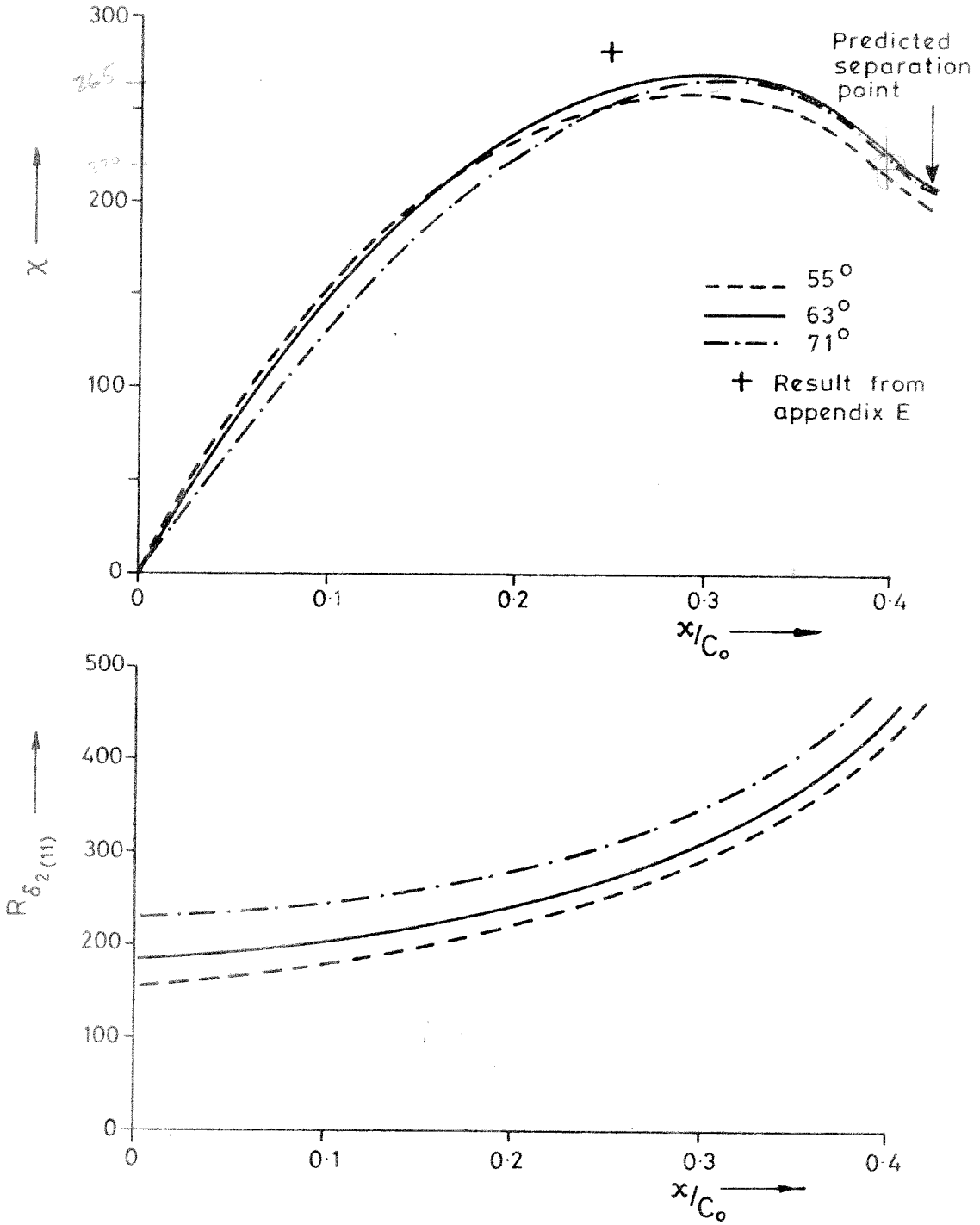

Fig. 53. Typical computational results for a Reynolds number of 10^6

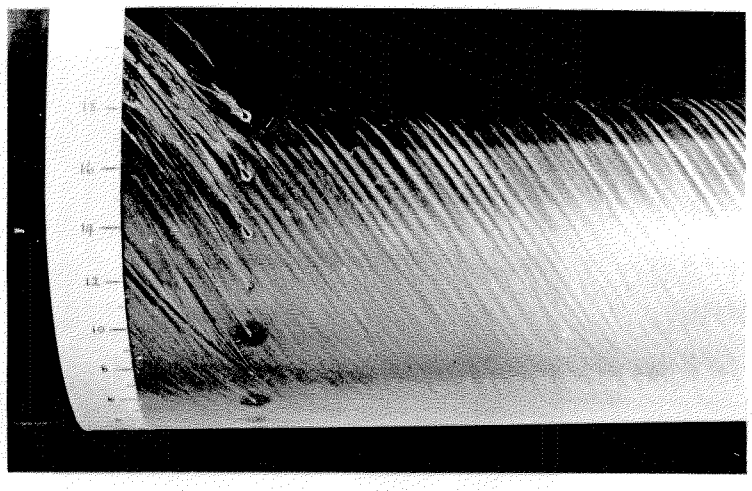

Sweep = 55°
Speed = 90 ft/sec

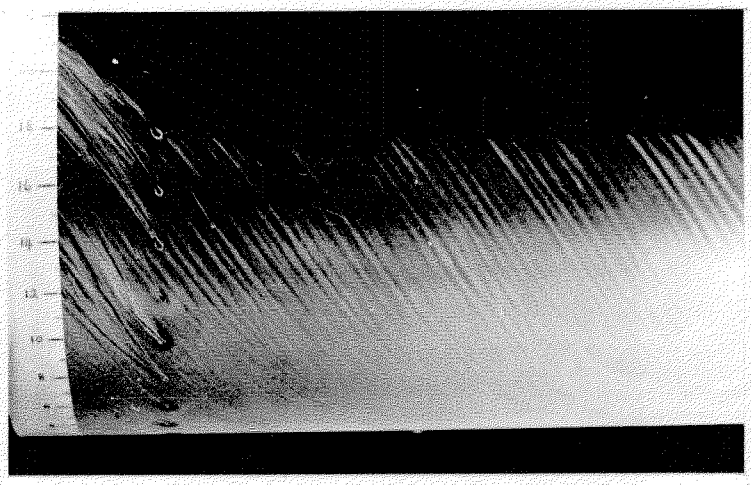

Sweep = 55°
Speed = 100 ft/sec

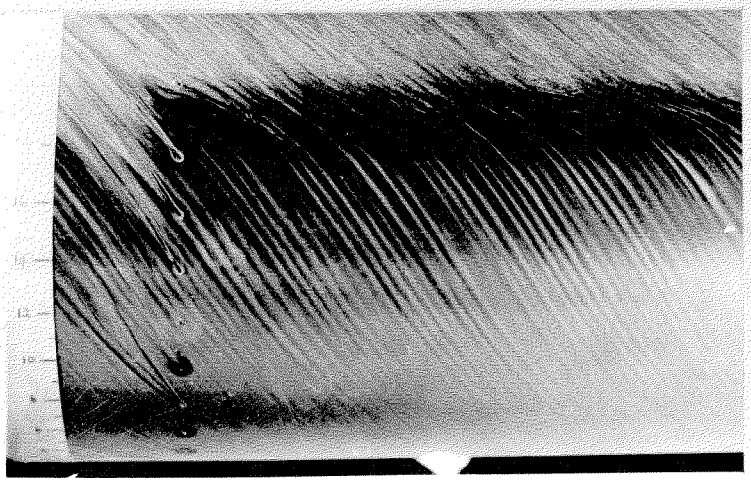

Sweep = 55°
Speed = 110 ft/sec

Fig. 54. Examples of the streak patterns obtained by surface oil flow visualisation.

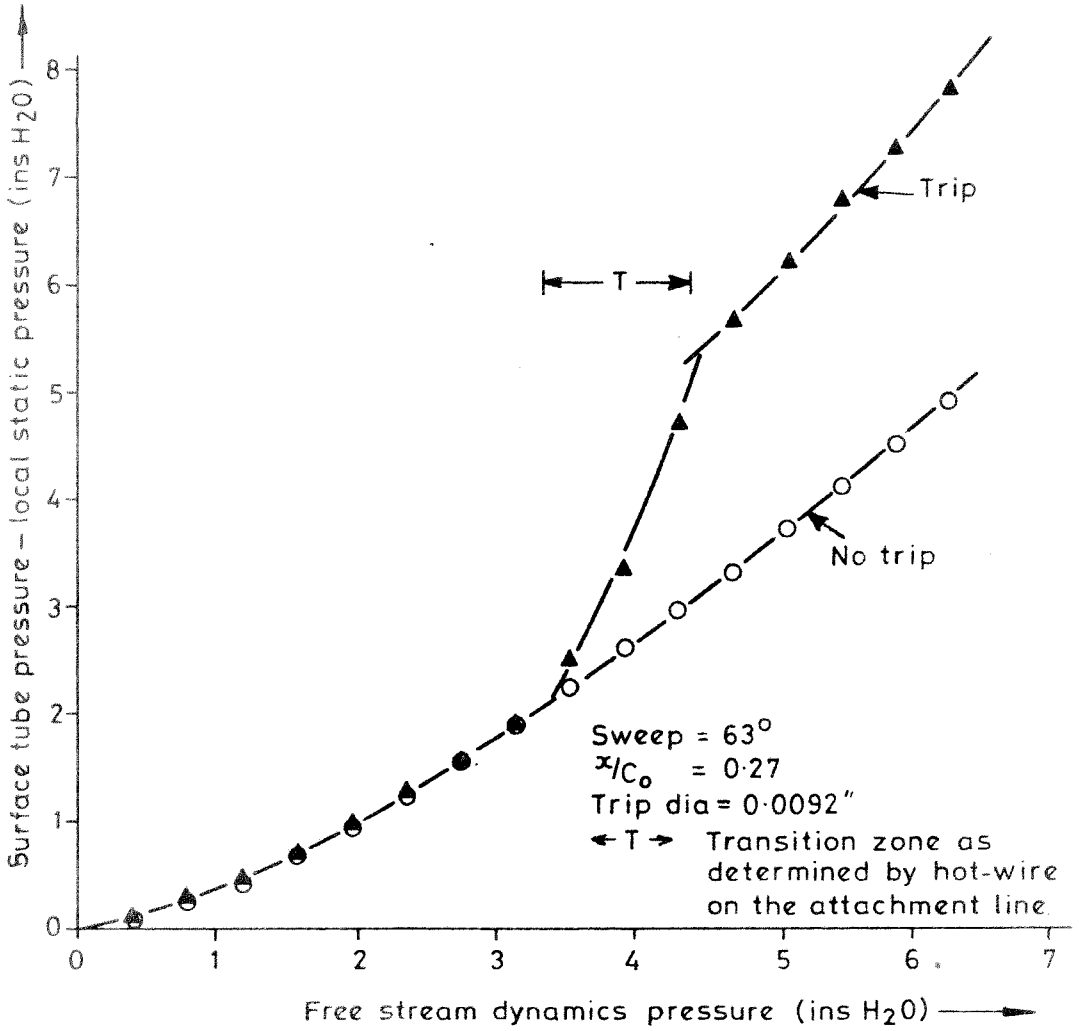

Fig. 56. An example of the variation of surface pitot pressure with free stream dynamic pressure.

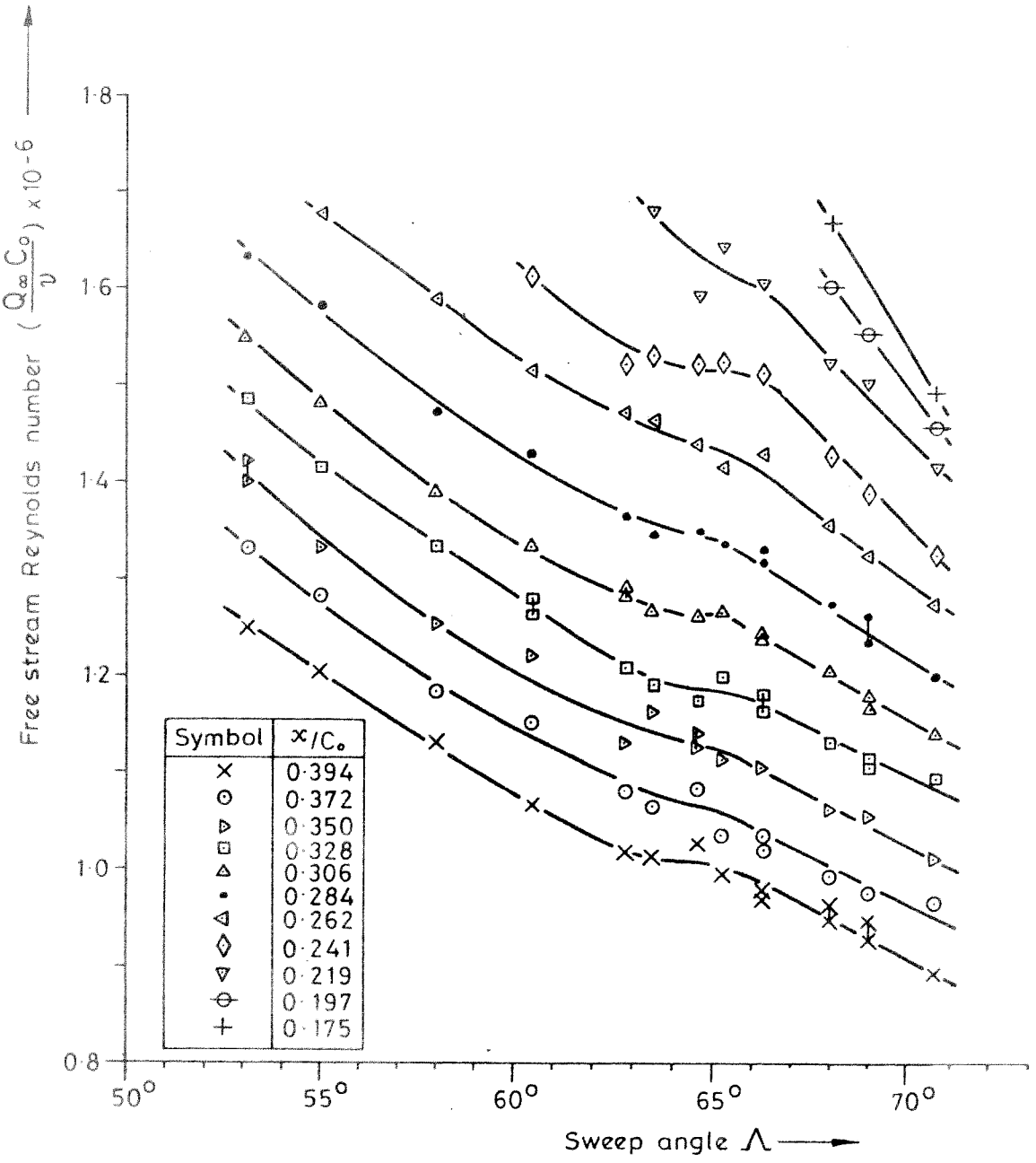

Fig. 57. Variation of free stream Reynolds number with chordwise position and sweep angle for the beginning of transition.

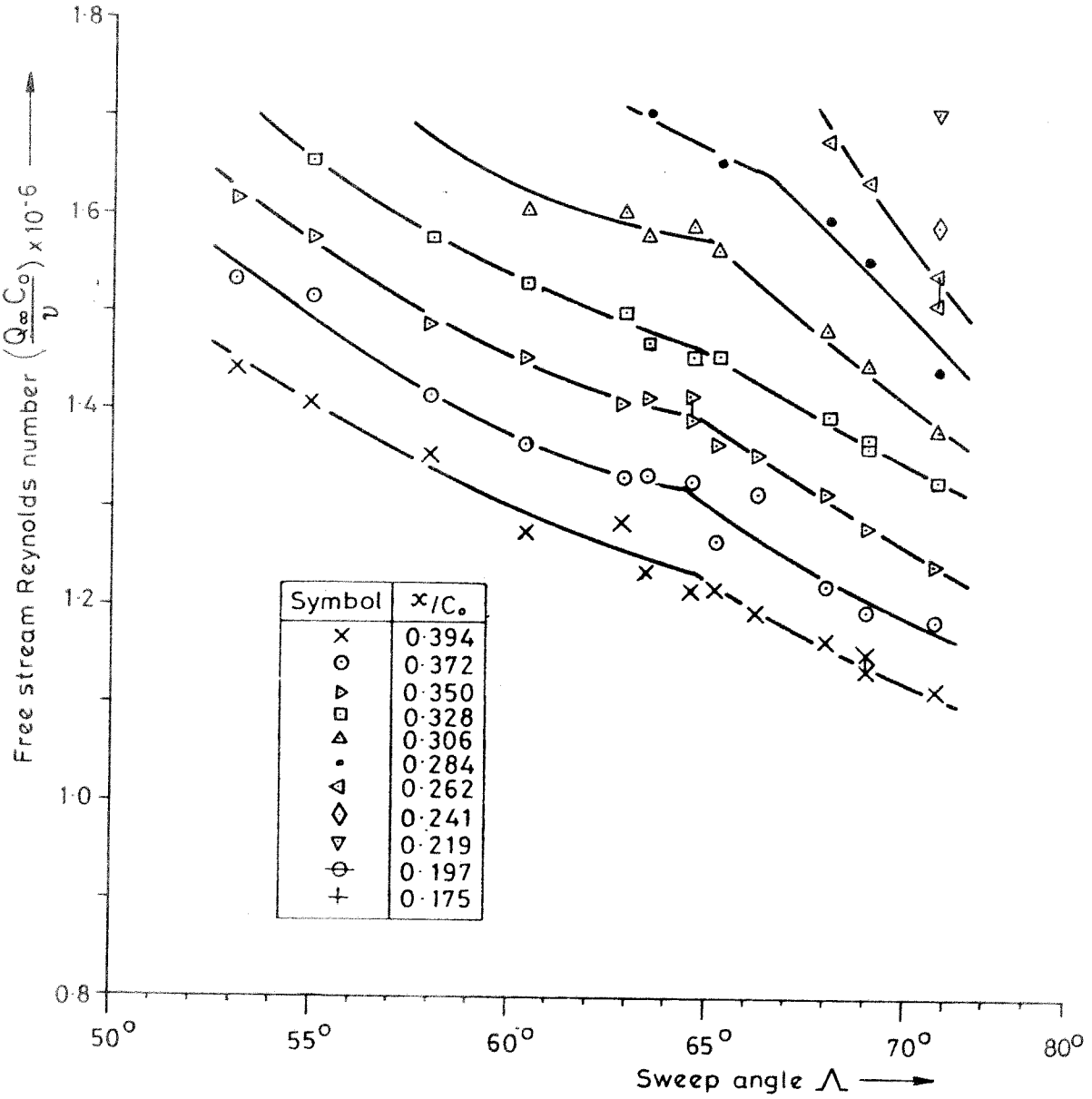

Fig. 58. Variation of free stream Reynolds number with chordwise position and sweep angle for the completion of transition.

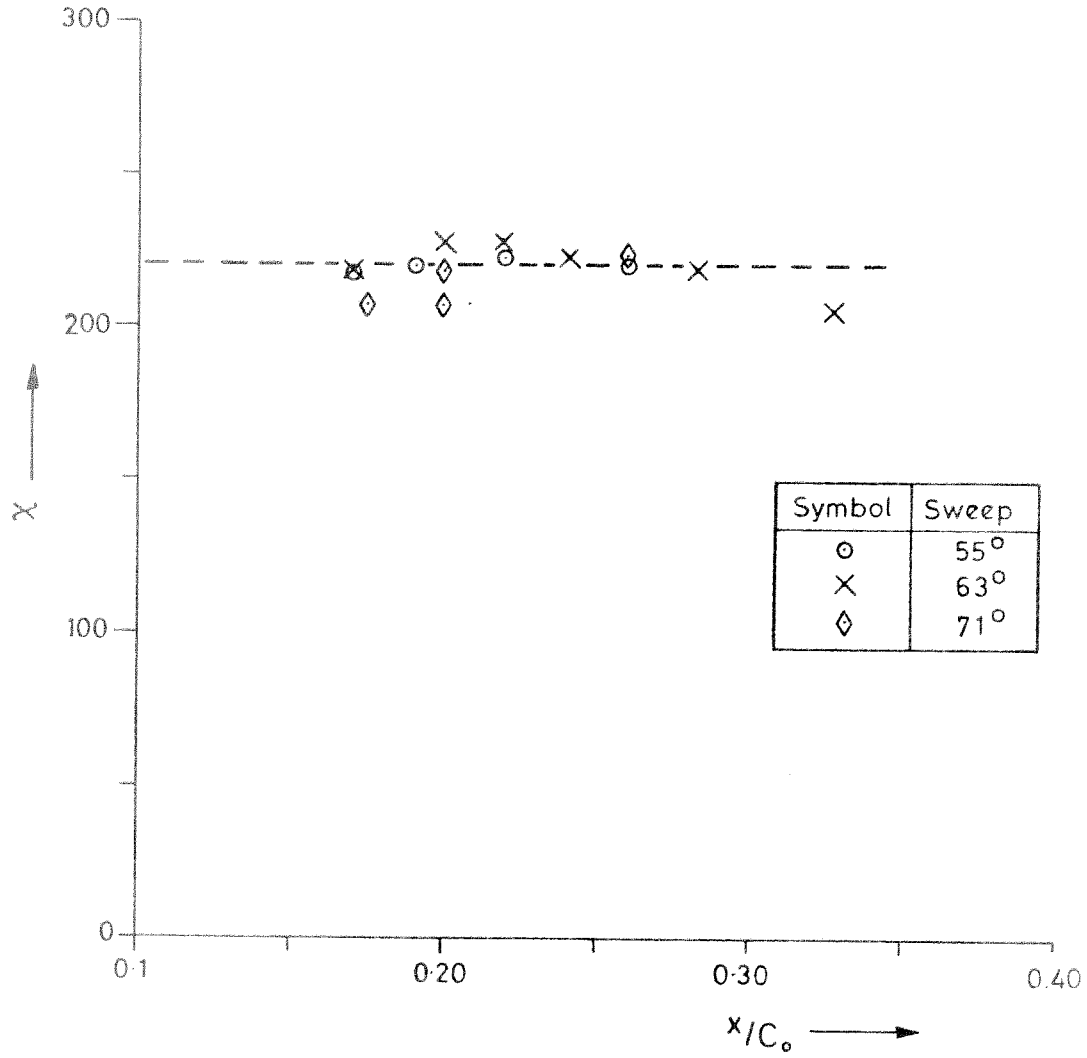

Fig. 59. Variation of χ with chordwise position and sweep angle for the first appearance of streaks.

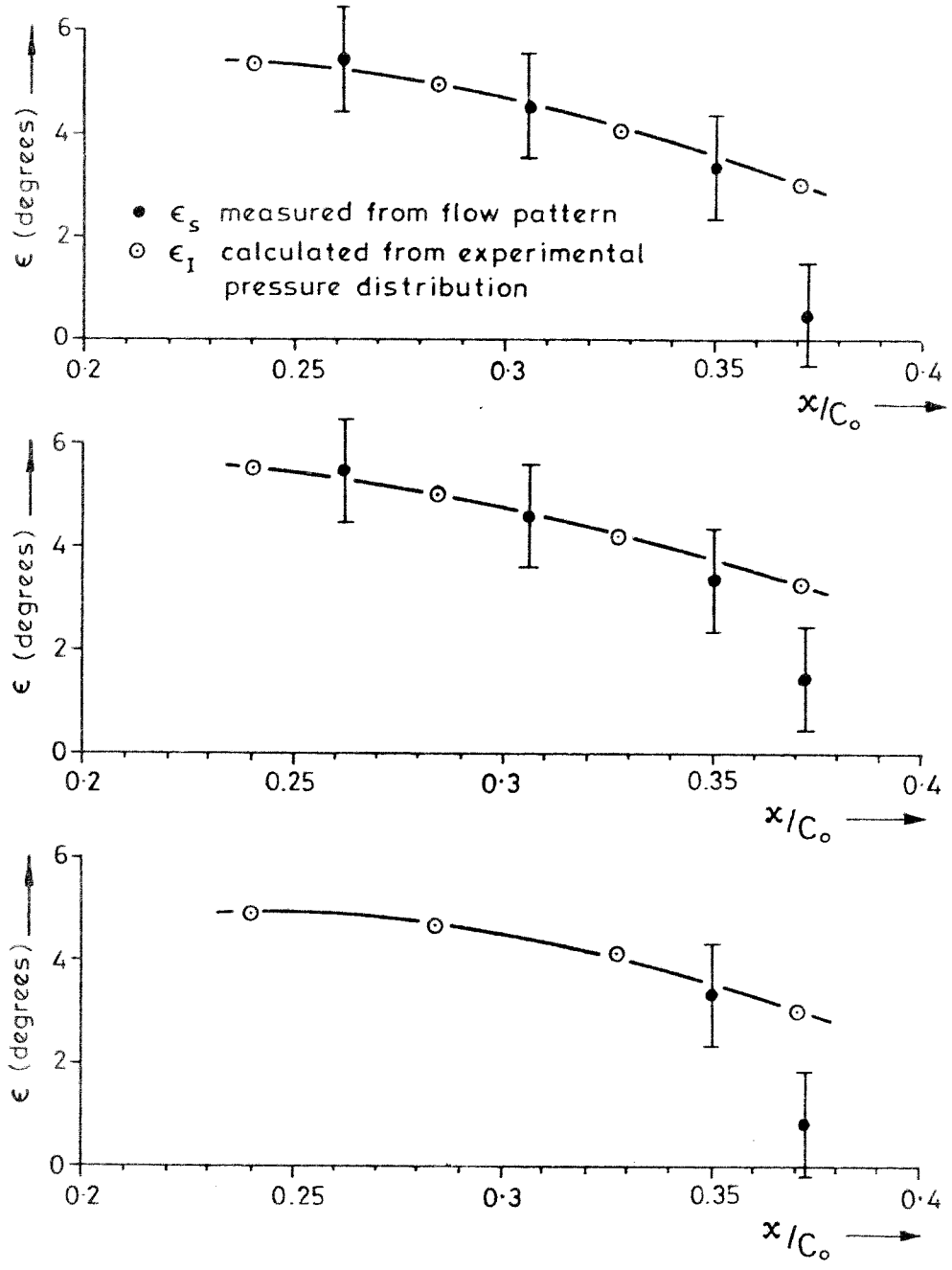

Fig. 60. Comparison between the streak inclination and the critical profile orientation.

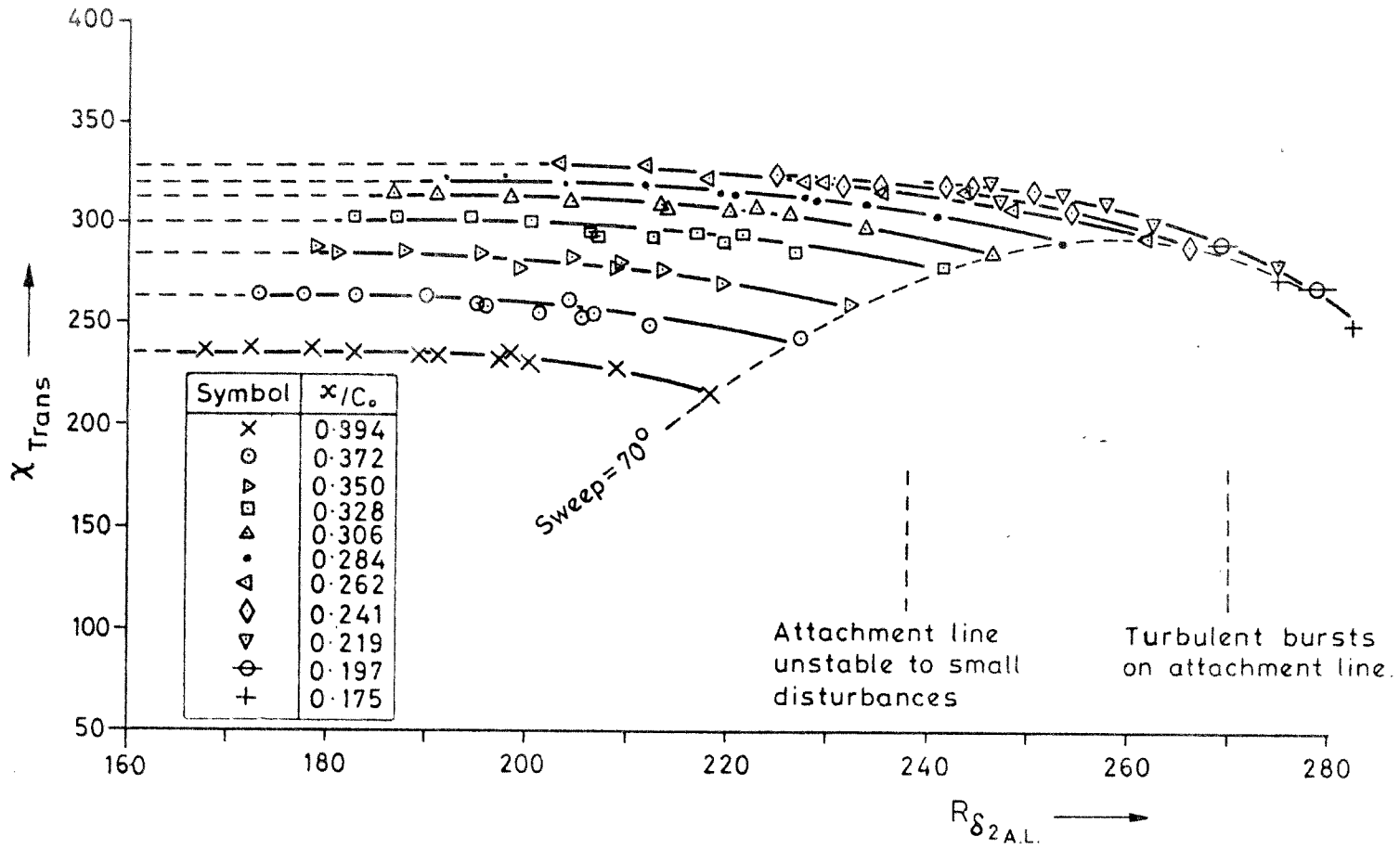

Fig. 61. Variation of χ at transition with attachment line momentum thickness Reynolds number and chordwise position.

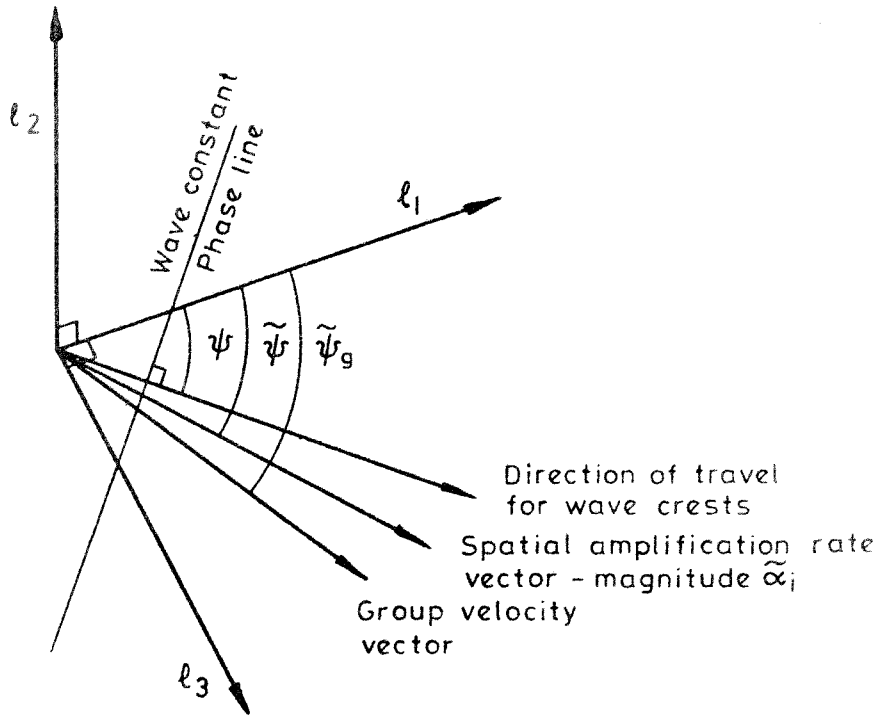

$\psi = \tan^{-1}(\beta r/\alpha r)$

$\tilde{\psi} = \tan^{-1}(\beta i/\alpha_i)$

$\tilde{\alpha}_i = (\alpha_i{}^2 + \beta_i{}^2)^{1/2}$

Fig. 62. Notation for the description of a disturbance travelling through a three-dimensional parallel boundary layer.

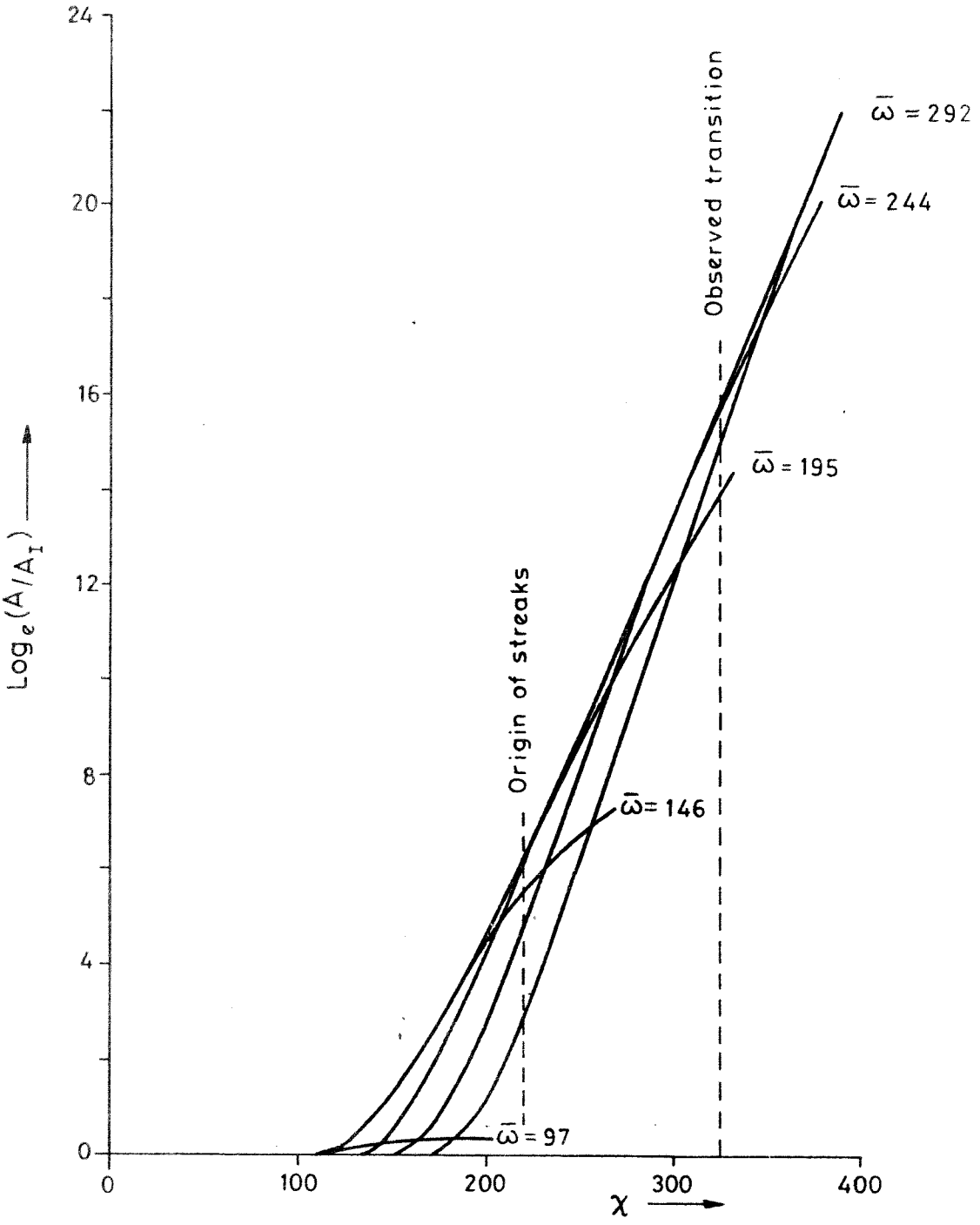

Fig. 63. The variation of theoretical disturbance amplitude ratio with Reynolds number for various frequencies in the swept wing boundary layer.

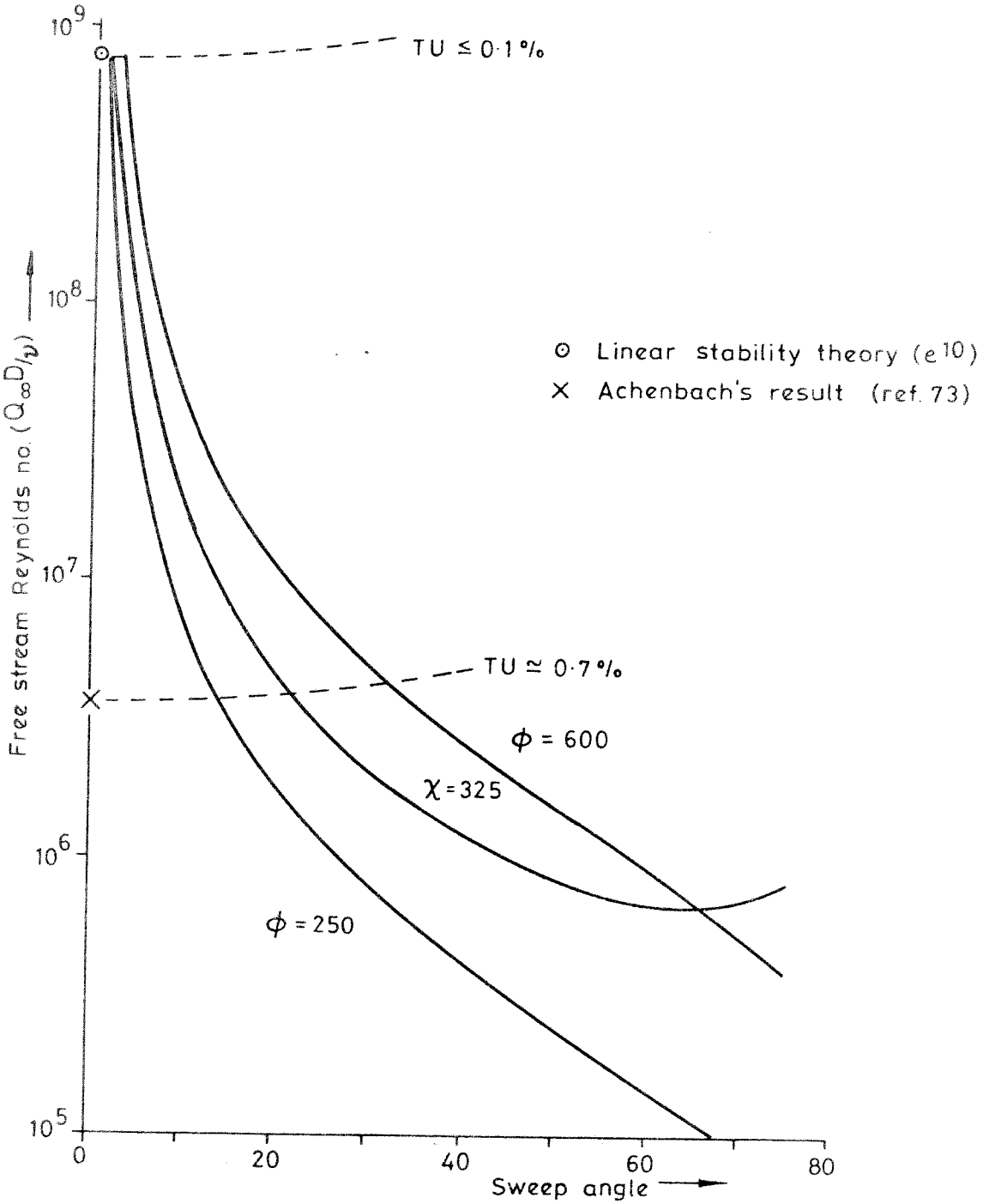

Fig. 64. The free stream Reynolds number required to produce transition at x equal to (D/2) for a swept circular cylinder.

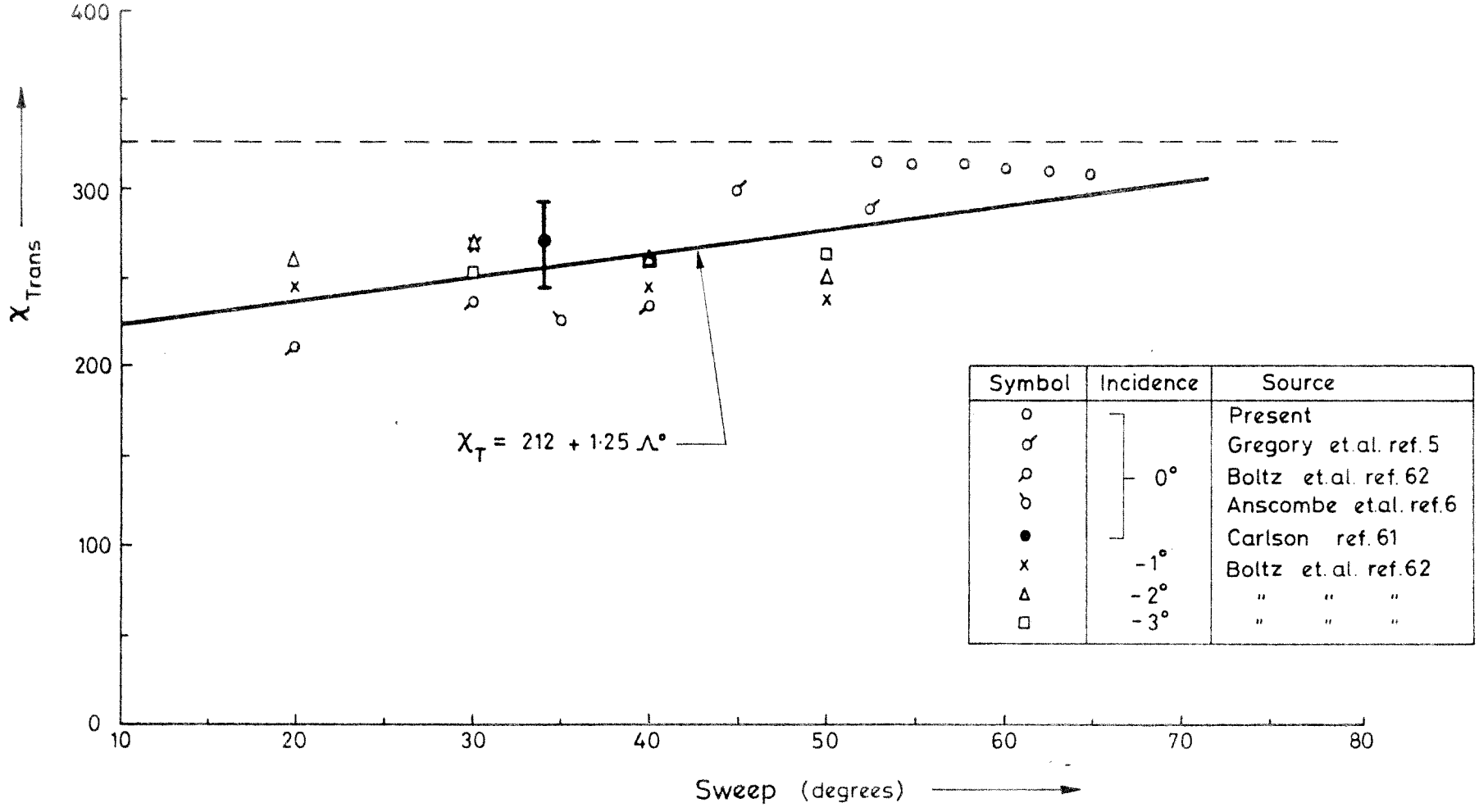

Fig.65. The value of χ required to produce transition at $\chi/C_o)_{\chi_{max.}}$ as a function of sweep angle.

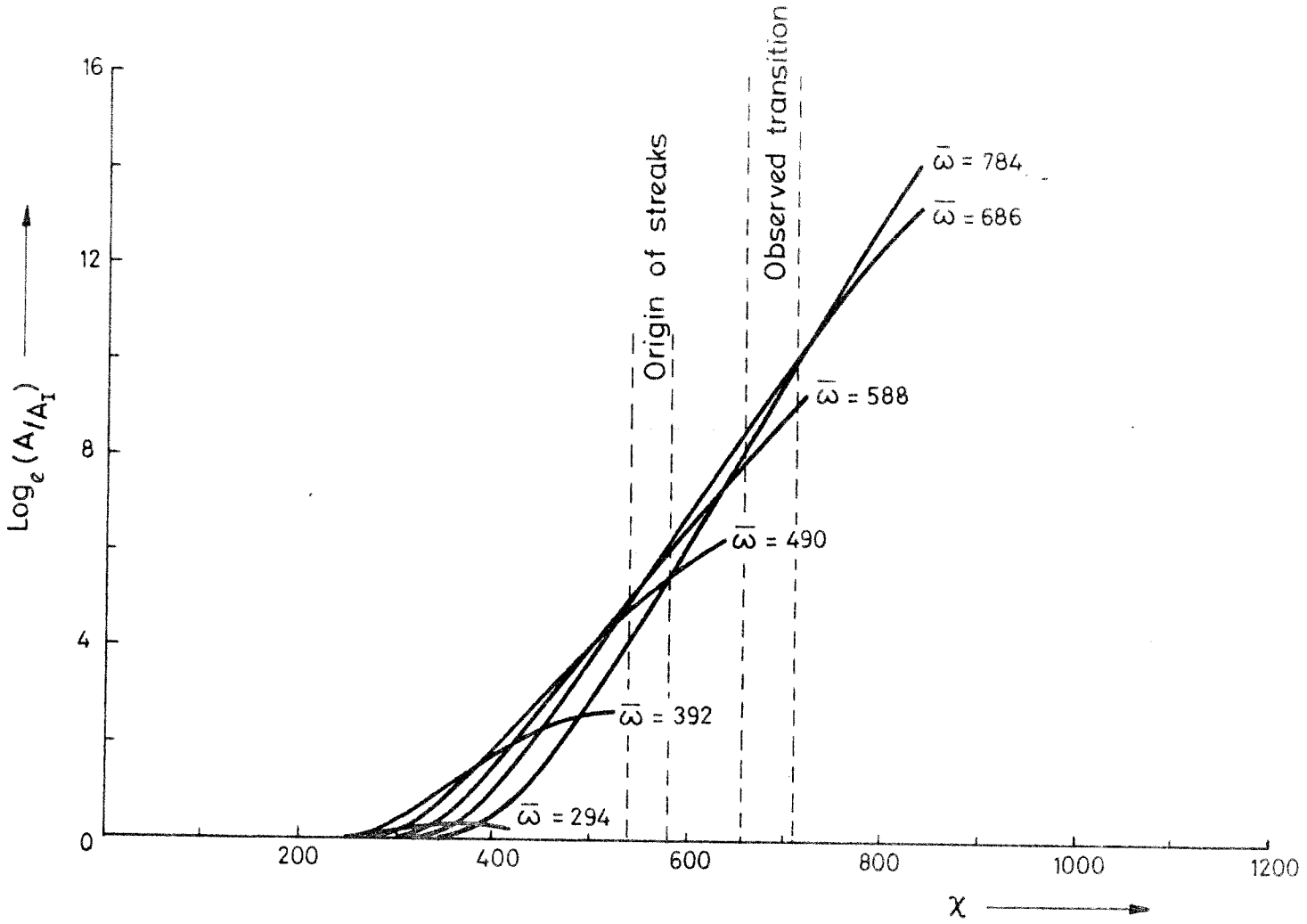

Fig. 66. The variation of theoretical disturbance amplitude ratio with Reynolds number for various frequencies in the rotating disc boundary layer.